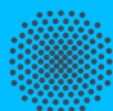


# Dissertation

Physikalische und chemische  
Wechselwirkungen in Gelatine-  
Methacryloyl-Lösungen und deren  
Vernetzung zu Hydrogelen als  
Trägerstruktur für Gelenkknorpel-  
Äquivalente

vorgelegt von  
**Lisa Rebers**



Universität Stuttgart



# Physikalische und chemische Wechselwirkungen in Gelatine-Methacryloyl-Lösungen und deren Vernetzung zu Hydrogelen als Trägerstruktur für Gelenkknorpel- Äquivalente

Von der Fakultät Energie-, Verfahrens- und Biotechnik  
der Universität Stuttgart zur Erlangung  
der Würde eines Doktors der Naturwissenschaften (Dr. rer. nat.)  
genehmigte kumulative Abhandlung

Vorgelegt von

**Lisa Rebers geb. Sewald**

aus Hameln

Hauptberichter: Prof. Dr. Günter E. M. Tovar

Mitberichterin: Prof. Dr. Christina Wege

Tag der mündlichen Prüfung:

11.05.2021

Institut für Grenzflächenverfahrenstechnik und Plasmatechnologie IGVP der  
Universität Stuttgart 2021



Gebe alles, was ich hab' für alles, was ich will  
Ich will 'ne ganze Menge, also geb' ich ganz schön viel

*Fynn Kliemann – Gebe alles was ich hab'*

# Danksagung

Mit der Fertigstellung dieser Arbeit endet eine besondere Zeit für mich. Ich möchte mich bei allen bedanken, die mich auf dieser Reise begleitet und unterstützt haben, ob für einen Umweg, eine Pause oder eine gemeinsame Etappe.

Mein besonderer Dank gilt...

...meinem Betreuer und Doktorvater **Prof. Dr. Günter E. M. Tovar**. Vielen Dank für deine Unterstützung von Beginn meiner Promotion über meine Elternzeit bis zum Ende meiner Arbeit. Durch dein Vertrauen und deine Anleitung hast du mir die Freiheit gegeben, eigene Ideen zu entwickeln.

...**Dr. Alexander Southan** und **Dr. Kirsten Borchers**, meinen fachlichen Betreuern. Vielen Dank für die vielen wöchentlichen Besprechungen in denen ihr mir gezeigt habt, wie man die richtigen Fragen stellt. Ihr habt mich immer unterstützt und mich zu einer Wissenschaftlerin gemacht. Ich habe viel von euch gelernt.

...**Prof. Dr. Christina Wege** für die Übernahme des Zweitgutachtens.

...der **Evonik Stiftung** für die Finanzierung meines Promotions-Stipendiums.

...**Dr. Michaela Müller**, **Dr. Thomas Schiestel** und **Jun.-Prof. Dr. Peter Loskill** für den Zugang zu euren Laboren und Geräten.

...den Gruppen **Chemisch-Physikalische Grenzflächen, Partikuläre Systeme und Formulierungen, MicroOrganoLab** und der Abteilung **Grenzflächentechnologie und Materialwissenschaft** für die Zusammenarbeit und die angenehme Arbeitsatmosphäre.

...meiner Freundin und Kollegin **Silke Keller**. Vielen Dank für deine Unterstützung und Hilfsbereitschaft, besonders während des letzten Jahres, das beste Büro und deine Freundschaft.

...meinen Kolleginnen **Melanie Dettling, Veronika Schönhaar, Sarah Schmidt, Regina Buck, Lisa Prestel, Ann-Sophie Schwemmler, Dr. Kirsten Borchers** und meinen Kollegen **Dr. Achim Weber** und **Dr. Alexander Southan**, die mit mir an der chemischen Biopolymer-Modifizierung gearbeitet haben und mich mit Synthesen unterstützt haben.

...“meinen Studentinnen und Studenten” **Lisa Böhler, Tobias Granse, Annina Hahn, Dominik Walz, Robin Stei, Gabriele Vacun, Lea Pfriendler** und **Sophia Regett** für eure Unterstützung im Labor und die Möglichkeit euch auf einem Teil eurer akademischen Ausbildung begleiten zu dürfen. Ich habe von und durch jeden von euch viel gelernt.

...meinen Doktoranden-Kolleginnen und -Kollegen, aus denen Freunde wurden. **Silke Keller, Dr. Isabel Jesswein, Tobias Götz, Dr. Julia Marzi, Aline Zbinden** und **Dr. Benjamin Riegger**, ihr ward die Quelle anregender (wissenschaftlicher) Diskussionen und habt Spaß in meinen Arbeitsalltag gebracht.

...“meine Co-Autorinnen und Co-Autoren” für die konstruktive Zusammenarbeit: **Dr. Alexander Southan, Dr. Kirsten Borchers, Tobias Götz, Raffael Reichsöllner, Dr. Stefan Baudis, Dr. Eva Hoch, Sandra Stier, Veronika Schönhaar, Dr. Christiane Claaßen, Dr. Marc H. Claaßen, Dr. Vincent Truffault, Sophia Regett, Tobias Granse, Dominik Walz** und **Prof. Dr. Günter E. M. Tovar**. Darüber hinaus möchte ich allen Mitarbeiterinnen und Mitarbeitern des Fraunhofer IGBs und IGVPs der Universität Stuttgart danken, die zu den Publikationen beigetragen haben.

...den **Käsefreunden** für eure Freundschaft und gemeinsamen Erlebnisse während dieser Zeit. Das gleiche gilt für **Seli, Bena** und **Lutz**, deren Freundschaft keine Entfernung kennt.

...**meinen Eltern** und **meinen Geschwistern**, ihr habt mich zu der gemacht, die ich bin, unterstützt mich in allen meinen Vorhaben und gebt mir die Sicherheit aufgefangen zu werden.

...**meiner Familie. Lauritz**, vielen Dank für deine bedingungslose Liebe und Unterstützung und für unser größtes Geschenk **Hannes**. Ihr vervollständigt mich.

# Inhaltsverzeichnis

Danksagung .....	I
1. Zusammenfassung und Abstract .....	1
1.1 Zusammenfassung.....	1
1.2 Abstract .....	5
2. Einleitung.....	9
2.1 Gelenkknorpel .....	9
2.1.1 Struktur und Zusammensetzung des Gelenkknorpels .....	9
2.1.2 Behandlungstherapien von Gelenkknorpeldefekten .....	12
2.1.3 Gelatine-Methacryloyl-Hydrogele als Trägermaterial für das Gelenkknorpel- <i>Tissue Engineering</i> .....	14
2.1.4 Zonales Gelenkknorpel- <i>Tissue Engineering</i> .....	16
2.2 Gelatine .....	19
2.2.1 Ursprung und Herstellung von Gelatine.....	19
2.2.2 Physikalische Gelierung von Gelatine .....	21
2.2.3 Standardcharakterisierung von Gelatine .....	23
2.3 Gelatine-Methacryloyl.....	26
2.3.1 Synthese und Charakterisierung von Gelatine-Methacryloyl .....	26
2.3.2 Chemisch vernetzte Gelatine-Methacryloyl-Hydrogele.....	29
2.3.3 Sequenziell vernetzte Gelatine-Methacryloyl-Hydrogele .....	32
3. Ziel und Hypothesen der Arbeit .....	35
3.1 Ziel der Arbeit.....	35
3.2 Hypothesen .....	35
4. Synthese und physikochemische Charakterisierung von Gelatine-Methacryloyl-Lösungen und -Hydrogelen .....	38
4.0 Erklärung meiner selbstständigen Leistung .....	38
4.1 Beyond the Modification Degree: Impact of Raw Material on Physicochemical Properties of Gelatin Type A and Type B Methacryloyls.....	39
4.1.1 Abstract .....	40



4.1.2	Introduction.....	40
4.1.3	Experimental Section .....	41
4.1.4	Results and Discussion .....	44
4.1.5	Conclusion .....	54
4.1.6	Acknowledgements.....	54
4.1.7	Supporting Information.....	55
5.	Sequenzielle Vernetzung von Gelatine-Methacryloyl-Hydrogelen.....	65
5.0	Erklärung meiner selbstständigen Leistung .....	65
5.0.1	Manuskript mit dem Titel <i>“Physical Interactions Strengthen Chemical Gelatin Methacryloyl Gels”</i> .....	65
5.0.2	Manuskript mit dem Titel <i>„Differentiation of Physical and Chemical Cross-Linking in Gelatin Methacryloyl Hydrogels“</i> .....	66
5.1	Physical Interactions Strengthen Chemical Gelatin Methacryloyl Gels .....	67
5.1.1	Abstract .....	68
5.1.2	Introduction.....	68
5.1.3	Results and Discussion .....	70
5.1.4	Conclusion .....	77
5.1.5	Materials and Methods.....	77
5.1.6	Acknowledgements.....	81
5.1.7	Supporting Information.....	83
5.2	Differentiation of Physical and Chemical Cross-Linking in Gelatin Methacryloyl Hydrogels .	84
5.2.1	Abstract .....	85
5.2.2	Introduction.....	85
5.2.3	Experimental .....	87
5.2.4	Results and Discussion .....	91
5.2.5	Conclusion .....	102
5.2.6	Acknowledgements.....	103
5.2.7	Author contributions.....	103
5.2.8	Funding.....	103

5.2.9	Competing interests .....	103
5.2.10	Supplementary Information .....	104
6.	Gelatine-Methacryloyl-Hydrogele mit einem Glykosaminoglykan-Gradienten als Biomaterial für das zonale Gelenkknorpel- <i>Tissue Engineering</i> .....	108
6.0	Erklärung meiner selbstständigen Leistung .....	108
6.1	Biomimetic Hydrogel Compositions and Zonal Structured Hydrogels for Reconstruction of Zonal Articular Cartilage Structure .....	110
6.1.1	Abstract .....	111
6.1.2	Introduction.....	111
6.1.3	Materials and Methods .....	113
6.1.4	Results .....	119
6.1.5	Discussion .....	125
6.1.6	Conclusion .....	132
6.1.7	Acknowledgements .....	132
6.1.8	Supporting Information.....	134
7.	Diskussion.....	141
7.1	Hypothese 1.....	141
7.2	Hypothese 2.....	144
7.3	Hypothese 3.....	147
8.	Schlussfolgerungen .....	150
9.	Ausblick .....	152
I.	Anhang .....	VII
I.I.	Erklärung über die Eigenständigkeit der Dissertation.....	VII
I.III.	Veröffentlichungen.....	VIII
I.III.I.	Veröffentlichungen in <i>peer-reviewed</i> Fachzeitschriften .....	VIII
I.III.II.	Vorträge auf Fachkonferenzen.....	IX
I.III.III.	Poster-Präsentationen auf Fachkonferenzen.....	X
II.	Abbildungsverzeichnis.....	XII
III.	Tabellenverzeichnis .....	XX

IV. Literaturverzeichnis..... XXIII

# 1. Zusammenfassung und Abstract

## 1.1 Zusammenfassung

Der Gelenkknorpel ist ein einfach wirkendes Gewebe, da er weder Blutgefäße noch Nerven enthält und nur aus Knorpelzellen (Chondrozyten) und extrazellulärer Matrix (EZM) besteht. Doch dieser Schein trügt, denn der Gelenkknorpel ist zonal strukturiert und somit komplex aufgebaut. Obwohl bekannt ist, dass diese zonale Strukturierung essenziell für die Materialeigenschaften des Knorpels ist, wird sie bisher kaum bei der Behandlung von Knorpeldefekten berücksichtigt. Daher besteht erheblicher Forschungsbedarf, um durch Adaption Biopolymer-basierter Biomaterialien Methoden zur Erstellung zonal strukturierter Knorpel-Äquivalente zu erarbeiten.

Die Verwendung von Biopolymer-basierten Biomaterialien für das Gelenkknorpel-*Tissue-Engineering* hat den Vorteil, dass diese Materialien beispielsweise Zell-Erkennungssequenzen beinhalten und die Biopolymere an sich biokompatibel sind. Das Biopolymer Gelatine wird durch Hydrolyse aus Kollagen-Proteinen gewonnen. Gelatine-Hydrogele werden als Biomaterial untersucht, da ihr kollagener Ursprung und der hohe Wasseranteil der extrazellulären Matrix (EZM) ähneln. Biomaterialien müssen jedoch bei Körpertemperaturen von etwa 37 °C stabil sein, weshalb rein physikalisch gelierte Gelatine-Hydrogele nicht geeignet sind. Neben der Möglichkeit Gelatine chemisch zu vernetzen, beispielsweise durch Enzyme oder Carbodiimide, werden methacryloylierte Gelatine (GM)-Derivate untersucht, die chemisch vernetzbare C=C-Doppelbindungen enthalten. Die GM-Polymere können radikalisch, beispielsweise in Anwesenheit eines Photoinitiators und durch die Bestrahlung mit UV-Licht, kovalent vernetzt werden. Eine im Rahmen dieser Arbeit durchgeführte Literaturrecherche zeigte jedoch, dass oft nur wenige oder keine Angaben zu dem bei der GM-Synthese verwendeten Gelatine-Rohmaterial gemacht werden. Da sich die Eigenschaften von Gelatinen durch deren Herstellungsprozess unterscheiden, wurde in dieser Arbeit zunächst der Einfluss des Rohmaterials auf die Eigenschaften der GM sowie GM-Lösungen und -Hydrogele untersucht.

In dieser Arbeit wurden fünf verschiedene GM-Derivate aus Gelatine Typ A ( $G_A$ ) und Gelatine Typ B ( $G_B$ ) mit unterschiedlicher Standardviskosität ( $G_A$  2.8 mPa s,  $G_B$  4.5 mPa s) und nahezu identischem Bloom-Wert ( $G_A$  233 g Bloom,  $G_B$  232 g Bloom) in Aminosäuren-Zusammensetzung, Modifizierungsgrad, isoelektrischen Punkt, hydrodynamischen Radius, Viskosität, Gelier- und Schmelzpunkt sowie Quellbarkeit und Speichermoduln der jeweiligen Hydrogele verglichen. Die Gelatine-Derivate wurden entsprechend des eingesetzten molaren Überschuss bezogen auf den Aminogruppen-Gehalt der Gelatine bezeichnet, beispielsweise wurde für GM2 ein zweifacher Überschuss an Methacrylsäureanhydrid verwendet und für GM2A8 zusätzlich ein achtfacher Überschuss an

Essigsäureanhydrid. Es konnte gezeigt werden, dass die Modifizierungsgrade der  $G_A$ - und  $G_B$  vergleichbar waren und mit der eingesetzten Menge an Methacrylsäure- und Essigsäureanhydrid zunahm (Methacryloylierungsgrad: GM2  $\sim 0,3 \text{ mmol g}^{-1}$ , GM10  $\sim 1,0 \text{ mmol g}^{-1}$ ; Acetylierungsgrad: GM2A8  $\sim 0,25 \text{ mmol g}^{-1}$ , GM5A5  $\sim 0,38 \text{ mmol g}^{-1}$ ) und alle untersuchten Eigenschaften vom Modifizierungsgrad der GMs abhängig waren.

Im Gegensatz dazu wurden in der dynamischen Viskosität sowie bei den Speichermoduln der Hydrogele der niedrig-modifizierten Derivate GM2 und GM5 signifikante Unterschiede zwischen beiden den GMs der zwei untersuchten Gelatine-Typen gefunden (Viskosität:  $G_{AM2}$   $0,0062 \text{ Pa s}$ ,  $G_{BM2}$   $0,0105 \text{ Pa s}$ ,  $G_{AM5}$   $0,0036 \text{ Pa s}$ ,  $G_{BM5}$   $0,0047 \text{ Pa s}$ ; Speichermodul: bspw.  $G_{AM2}$   $5 \text{ kPa}$ ,  $G_{BM2}$   $\sim 14 \text{ kPa}$ ). Diese wurden auf die unterschiedlichen Werte der Standardviskosität der Rohmaterialien zurückgeführt, wobei die verwendete Gelatine Typ B eine höhere Standardviskosität hatte und die entsprechenden Derivate auch eine höhere Viskosität und höhere Speichermoduln zeigten. Diese Ergebnisse verdeutlichten, dass die Angaben zum verwendeten Gelatine-Rohmaterial in jeder Studie vollständig angegeben und mindestens der Modifizierungsgrad quantitativ bestimmt werden sollte.

Um GM-Hydrogele weiter zu verfestigen und somit ihre Eignung als Biomaterial für das Gelenkknorpel-*Tissue-Engineering* zu erhöhen, wurde die sequenzielle Vernetzung von GM, bei der die GM-Hydrogelvorläuferlösungen vor der chemischen Vernetzung gekühlt werden, untersucht. Bei der sequenziellen Vernetzung werden. Es war bekannt, dass dadurch bereits der Kompressions-, Speicher- und Elastizitätsmodul der GM-Hydrogele erhöht wurde. Im Rahmen dieser Arbeit wurde überprüft, ob die sequenzielle Vernetzung von Hydrogelvorläuferlösung, für die bisher keine Gelierung zwischen  $10 \text{ }^\circ\text{C}$  und  $40 \text{ }^\circ\text{C}$  festgestellt wurde, mit höheren Druckspannungen belastet werden können als rein chemisch vernetzte GM-Hydrogele.

Die Untersuchung zeigte, dass auch die Druckfestigkeit von offensichtlich nicht-gelierenden Hydrogelvorläuferlösungen durch die sequenzielle Vernetzung erhöht wurde: Die rein chemisch vernetzten GM-Hydrogele versagten bei einer Druckspannung von  $\sim 570 \text{ kPa}$  (GM2),  $\sim 460 \text{ kPa}$  (GM10) und  $\sim 90 \text{ kPa}$  in den seitlich begrenzten Messungen und die sequenziell vernetzten GM-Hydrogele bei  $\sim 2650 \text{ kPa}$  (GM2),  $\sim 800 \text{ kPa}$  (GM10) und  $\sim 420 \text{ kPa}$  (GM2A8). Außerdem wurden für alle untersuchten 10 Gew.-% GM-Hydrogelvorläuferlösungen Gelpunkte während des Kühlprozesses der sequenziellen Vernetzung detektiert. Die GM2-Hydrogelvorläuferlösung gelierte nach 3 min Kühlung auf  $21 \text{ }^\circ\text{C}$ , die GM10-Hydrogelvorläuferlösung nach 20 min Kühlung auf  $21 \text{ }^\circ\text{C}$  und 4 min Kühlung auf  $4 \text{ }^\circ\text{C}$  und die GM2A8-Hydrogelvorläuferlösung nach 20 min Kühlung auf  $21 \text{ }^\circ\text{C}$  und 18 min Kühlung auf  $4 \text{ }^\circ\text{C}$ . Allerdings war die Speichermoduln der physikalischen GM10- und GM2A8-Hydrogele sehr gering (GM10  $\sim 2100 \text{ Pa}$ , GM2A8  $\sim 50 \text{ Pa}$ ) verglichen mit dem der gelierten GM2-Hydrogele ( $10600 \text{ Pa}$ ). Außerdem gelierte nur eine der drei untersuchten GM2A8-Hydrogelvorläuferlösung.

Anschließend wurde einerseits die Ausbildung hierarchischer Strukturen wie Tripel-Helices mit Hilfe von Circular dichroismus (CD)-Spektroskopie und dynamischer Differenzkalorimetrie (DSC) während der Kühlung der Hydrogelvorläuferlösungen zur Herstellung sequenzieller GM-Hydrogele untersucht wurde. Außerdem wurde der C=C-Doppelbindungsumsatz während der chemischen Vernetzung gemessen. Diese Untersuchungen zeigten, dass es in allen Hydrogelvorläuferlösungen zu einer Konformationsänderung der GM kam. Für GM2 und GM2A8 wurden im CD-Spektrum anhand einer negativen Bande bei ~200 nm und einer positiven Bande bei ~220 nm Tripel-Helices nachgewiesen. Für GM10 wurden Hinweise auf die rechtsgängige Poly-Prolin I-Konformation (negative Bande bei ~238 nm) gefunden. Außerdem wurden mittels DSC eine Renaturierung der physikalischen Wechselwirkungen der unmodifizierten Gelatine von 71 % für GM2, 4 % für GM2A8 und keine Renaturierung für GM10 gezeigt.

Kollegen an der Universität Wien untersuchten durch Echtzeit-Nahinfrarot-Spektroskopie-Photorheologie (RT-NIR-Photorheology) den Doppelbindungsumsatz während der chemischen Vernetzung von sequenziellen und rein chemischen GM-Hydrogelen. Es wurde gezeigt, dass die sequenzielle Vernetzung zu einem geringeren Doppelbindungsumsatz in den resultierenden Hydrogelen (58 % (GM2), 62 % (GM2A8) und 81 % (GM10) der zur Verfügung stehenden Doppelbindungen) führte als die rein chemische Vernetzung (86 % (GM2), 76 % (GM2A8) und 93 % (GM10) der zur Verfügung stehenden Doppelbindungen). Damit konnte gezeigt werden, dass der verfestigende Effekt der sequenziellen GM-Vernetzung auf die Konformationsänderung der GM-Polymere während der Kühlung vor dem chemischen Vernetzen und der damit einhergehenden Ordnung zurückgeführt werden konnte und nicht wie bisher vermutet auf einen höheren Doppelbindungsumsatz in den sequenziell vernetzten GM-Hydrogelen.

Die sequenziell vernetzten GM-Hydrogele wurden anschließend für deren Eignung als Gerüststruktur im zonalen Gelenkknorpel-*Tissue-Engineering* untersucht. Mithilfe einer dreiteiligen Hydrogelform konnten Hydrogele aus drei aufeinandergestapelten Zusammensetzungen dargestellt werden. Es wurden biomimetische Hydrogelzusammensetzungen aus GM, methacryloylierter Hyaluronsäure und methacryloyliertem Chondroitinsulfat untersucht und damit ein GM-basiertes Hydrogel mit einem biomimetischen Glykosaminoglykan-Gradienten erzeugt.

Die GM-basierten Hydrogele wurden auf deren Eignung als Biomaterial überprüft, wobei gezeigt wurde, dass der Herstellungsprozess der physikalisch gelierten und chemisch vernetzten sequenziellen GM-Hydrogele für Chondrozyten zytokompatibel war. Die Vitalität der in den GM-Hydrogelen verkapselten Chondrozyten nach bis zu 2 h Kühlung bei 4 °C war von der Vitalität von Chondrozyten, die ohne vorangegangene Kühlung in Hydrogelen verkapselt wurden, relativ nicht unterscheidbar ( $p > 0.05$ ). Die Hydrogele waren darüber hinaus teilweise bis vollständig innerhalb von sechs Wochen durch Kollagenase degradierbar: GM-Hydrogele waren nach 21 d vollständig abgebaut, von GM+CSM-

Hydrogele verblieben nach 42 d ~50 % des Gelgehalts, von GM+HAM-Hydrogelen ~75 %, von GM+HAM+CSM-Hydrogelen ~70 % und ~50 % von den zonalen Hydrogelen. Alle untersuchten Hydrogele wurden nicht von der eingesetzten Hyaluronidase degradiert.

Darüber hinaus wurden Relaxationsversuche unter Kompression mit den Hydrogelen durchgeführt. Für GM-Hydrogele wurde ein initialer Elastizitätsmodul ( $E_{ini}$ ) von 291,5 kPa und ein Elastizitätsmodul im Equilibrium ( $E_{eq}$ ) von 207,7 kPa gemessen, für GM+CSM 234,2 kPa ( $E_{ini}$ ) und 177,4 kPa ( $E_{eq}$ ), für GM+HAM 148,7 kPa ( $E_{ini}$ ) und 109,8 kPa ( $E_{eq}$ ), für GM+HAM+CSM 258,6 kPa ( $E_{ini}$ ) und 195,1 kPa ( $E_{eq}$ ) und für die zonalen Hydrogele 229,7 kPa ( $E_{ini}$ ) und 166,5 kPa ( $E_{eq}$ ). Diese Elastizitätsmoduln waren die höchsten bisher berichteten E-Moduln von GM-basierten Hydrogelen. In zonalen und reinen GM-Hydrogelen verkapselte Chondrozyten synthetisierten über vier Wochen Knorpel-spezifische EZM, sodass von einer Redifferenzierung der Zellen ausgegangen wurde. Die untersuchten zonalen Hydrogele könnten somit als *Scaffold* für das Gelenkknorpel-*Tissue Engineering* weiter untersucht werden.

## 1.2 Abstract

Articular cartilage appears simple since it contains neither blood vessels nor nerves and consists only of cartilage cells (chondrocytes) and extracellular matrix (ECM). However, this appearance is deceptive, because articular cartilage is zonally structured. This zonal structuring has hardly been considered in the treatment of cartilage defects up to now, although it is known to be essential for the material properties of cartilage. There is, therefore, a considerable need for research to develop methods for creating zonally structured cartilage equivalents by adapting biopolymer-based biomaterials.

An advantage of biopolymer-based biomaterials is that they e.g. contain cell recognition sequences and that the biopolymers themselves are biocompatible. The biopolymer gelatin is obtained by hydrolysis of collagen proteins. Gelatin hydrogels are investigated as biomaterials because their collagen origin and high water content is similar to the extracellular matrix (ECM). However, biomaterials must be stable at body temperature of about 37 °C, which is why purely physically gelled gelatin hydrogels are not suitable for the application as biomaterial. Thus, chemical cross-linking of gelatin is necessary. Besides chemical cross-linking of gelatin by enzymes or carbodiimides, methacryloylated gelatin (GM) derivatives are investigated which contain chemical cross-linkable C=C double bonds. The GM polymers can be covalently cross-linked by radicals, for example in the presence of a photoinitiator irradiated by UV light. However, a literature research, as part of this work, carried out that often little or even no information is given about the gelatin raw material used in GM synthesis. Since the properties of gelatin differ due to their production process, this thesis investigated firstly the impact of the raw material on the properties of GM as well as GM solutions and hydrogels.

Five different GM derivatives of gelatin type A ( $G_A$ ) and gelatin type B ( $G_B$ ) with different standard viscosities ( $G_A$  2.8 mPa s,  $G_B$  4.5 mPa s) and almost identical Bloom values ( $G_A$  233 g Bloom,  $G_B$  232 g Bloom) were compared regarding their amino acid compositions, degree of modification, isoelectric point, hydrodynamic radius, viscosity, gelling and melting point as well as swellability and storage modules of the respective hydrogels. The gelatin derivatives were designated according to the molar excess used in relation to the amino group content of the gelatin. For example, a twofold excess of methacrylic anhydride was used for GM2 and an additional eightfold excess of acetic anhydride for GM2A8. It could be shown that the degrees of modification of the  $G_A$  and  $G_B$  derivatives were comparable and increased with used amount of methacrylic and acetic anhydride (degree of methacryloylation: GM2  $\sim 0.3 \text{ mmol g}^{-1}$ , GM10  $\sim 1.0 \text{ mmol g}^{-1}$ ; degree of acetylation: GM2A8  $\sim 0.25 \text{ mmol g}^{-1}$ , GM5A5  $\sim 0.38 \text{ mmol g}^{-1}$ ). and all investigated properties depended on the degree of modification of the GMs.



In contrast to this, significant differences between both gelatin types were found in the standard viscosity as well as in the storage modules of the hydrogels of the low-modified derivatives GM2 and GM5 (viscosity:  $G_{AM2}$  0.0062 Pa s,  $G_{BM2}$  0.0105 Pa s,  $G_{AM5}$  0.0036 Pa s,  $G_{BM5}$  0.0047 Pa s; storage modulus: e.g.  $G_{AM2}$  5 kPa,  $G_{BM2}$  ~14 kPa). These differences were attributed to the differences in the standard viscosity of the raw materials, whereby the used gelatin type B had a higher standard viscosity and the corresponding derivatives showed a higher viscosity and higher storage modules. These results pointed out that the details of the gelatin raw material used should be given completely in each study and that at least the degree of modification should be determined quantitatively.

In order to further solidify GM hydrogels and thus increase their suitability as biomaterial for joint cartilage tissue engineering, sequential GM cross-linking, whereby, GM hydrogel precursor solutions are cooled prior to chemical crosslinking, was investigated. In sequential cross-linking. It was known that this leads to an increase in the mechanical properties of the GM hydrogels. In the context of this work, it was examined whether the sequential crosslinking of hydrogel precursor solutions for which no gelation between 10 °C and 40 °C has been detected so far, can be loaded with higher compressive stresses than purely chemically cross-linked GM hydrogels.

The investigation showed that the compressive strength of obviously non-gelling hydrogel precursor solutions was also increased by sequential cross-linking: The purely chemically cross-linked GM hydrogels failed in the laterally limited measurements at a compressive stress of ~570 kPa (GM2), ~460 kPa (GM10) und ~90 kPa in the confined measurements and the sequentially cross-linked GM-hydrogels at ~2650 kPa (GM2), ~800 kPa (GM10) und ~420 kPa (GM2A8). In addition, gelation were detected during the cooling process of sequential crosslinking for all investigated 10 wt-% GM hydrogel precursor solutions. The GM2 hydrogel precursor solution gelled after 3 min cooling to 21 °C, the GM10 hydrogel precursor solution after 20 min cooling to 21 °C and 4 min cooling to 4 °C and the GM2A8 hydrogel precursor solution after 20 min cooling to 21 °C and 18 min cooling to 4 °C. However, the storage moduli of the physical GM10 and GM2A8 hydrogels were very low (GM10 ~2100 Pa, GM2A8 ~50 Pa) compared to the gelled GM2 hydrogels (10600 Pa). Furthermore, only one of the three investigated GM2A8 hydrogel precursor solutions gelled.

Subsequently, on the one hand the formation of hierarchical structures such as triple helices using circular dichroism (CD) spectroscopy and dynamic differential calorimetry (DSC) during cooling of the hydrogel precursor solutions, on the other hand, the double bond conversion during chemical cross-linking. These investigations showed that there was a conformational change of GM in all hydrogel precursor solutions. For GM2 and GM2A8, triple helices were detected in the CD spectrum with a negative band at ~200 nm and a positive band at ~220 nm. For GM10, indications of the right-handed poly-proline I conformation (negative band at ~238 nm) were found. Furthermore, a renaturation of

the physical interactions of the unmodified gelatin of 71 % for GM2, 4 % for GM2A8 and no renaturation for GM10 was shown by DSC.

Colleagues at the University of Vienna used real-time near-infrared spectroscopy photorheology (RT-NIR photorheology) to investigate the double bond conversion during the chemical crosslinking of sequential and purely chemical GM hydrogels. It was shown that sequential crosslinking of the available double bonds lead to a lower double bond turnover in the resulting hydrogels (58 % (GM2), 62 % (GM2A8) and 81 % (GM10) than purely chemical crosslinking (86 % (GM2), 76 % (GM2A8) and 93 % (GM10) of the available double bonds). Thus, it could be shown that the solidifying effect of sequential GM crosslinking could be attributed to the conformational change of the GM polymers during cooling prior to chemical crosslinking and the associated order and not, as previously assumed, to a higher double bond conversion in the sequentially cross-linked GM hydrogels.

The sequentially cross-linked GM hydrogels were then investigated for their suitability as scaffolding structure in zonal articular cartilage tissue engineering. Using a three-part hydrogel form, hydrogels from three compositions stacked on top of each other could be visualized. Biomimetic hydrogel compositions consisting of GM, methacryloylated hyaluronic acid and methacryloylated chondroitin sulfate were investigated to generate a GM-based hydrogel with a biomimetic glycosaminoglycan gradient.

The GM-based hydrogels were tested for their suitability as biomaterial. It was shown that the manufacturing process of the physically gelled and chemically cross-linked sequential GM hydrogels was cytocompatible for chondrocytes. The vitality of the chondrocytes encapsulated in the GM hydrogels after up to 2 h cooling at 4 °C was relatively indistinguishable from the vitality of chondrocytes encapsulated in hydrogels without prior cooling ( $p > 0.05$ ). Furthermore, the hydrogels were partially to completely degradable by collagenase within six weeks: GM hydrogels were completely degraded after 21 d, for GM+CSM hydrogels ~50 % of the gel content remained after 42 d, for GM+HAM hydrogels ~75 %, for GM+HAM+CSM hydrogels ~70 % and ~50 % for the zonal hydrogels. All investigated hydrogels were not degraded by the hyaluronidase used.

Furthermore, relaxation experiments under compression with the hydrogels were performed. For GM hydrogels, an initial elastic modulus ( $E_{ini}$ ) of 291.5 kPa and an elastic modulus in the equilibrium ( $E_{eq}$ ) of 207.7 kPa were measured, for GM+CSM 234.2 kPa ( $E_{ini}$ ) and 177.4 kPa ( $E_{eq}$ ), for GM+HAM 148.7 kPa ( $E_{ini}$ ) and 109.8 kPa ( $E_{eq}$ ), for GM+HAM+CSM 258.6 kPa ( $E_{ini}$ ) and 195.1 kPa ( $E_{eq}$ ) and for the zonal hydrogels 229.7 kPa ( $E_{ini}$ ) and 166.5 kPa ( $E_{eq}$ ). These elastic moduli were the highest moduli of elasticity of GM-based hydrogels reported so far. Chondrocytes encapsulated in zonal and pure GM hydrogels synthesized cartilage-specific ECM over four weeks, so that a redifferentiation of the cells

was assumed. The zonal hydrogels studied could thus be further investigated as scaffolds for articular cartilage tissue engineering.

## 2. Einleitung

### 2.1 Gelenkknorpel

Der Gelenkknorpel ist ein Teil des Bewegungsapparats und bedeckt die knöchernen Bestandteile der Gelenke. Er wird somit durch Druck- und Scherbelastung beansprucht. Das Knorpelgewebe wird allgemein in drei Subtypen unterteilt den hyalinen, elastischen und Faserknorpel. Der Gelenkknorpel gehört zum hyalinen Knorpel, in dem das am häufigsten vertretene Kollagen das Kollagen Typ II ist. Alle Knorpel-Subtypen sind frei von Gefäßen und Nerven, was deren limitierte Selbstheilungskapazität bedingt. Im Folgenden wird die komplexe Struktur und Zusammensetzung des Gelenkknorpels sowie Strategien und Materialien für die Erzeugung von Knorpelgewebe-Äquivalenten zur Behandlung von Knorpeldefekten beschrieben.

#### 2.1.1 Struktur und Zusammensetzung des Gelenkknorpels

Die Zusammensetzung und Struktur des Gelenkknorpels ermöglicht ein reibungsfreies Gleiten der Gelenkbestandteile und absorbiert und verteilt die auftretenden Lasten gleichmäßig auf den darunterliegenden Knochen. [1, 2] Der Gelenkknorpel besteht aus den Knorpelzellen (Chondrozyten), die in die extrazelluläre Matrix (EZM) eingebettet sind, und dem im Gewebe eingelagerten Wasser. Die EZM wird von den Chondrozyten auf- und umgebaut. [3]

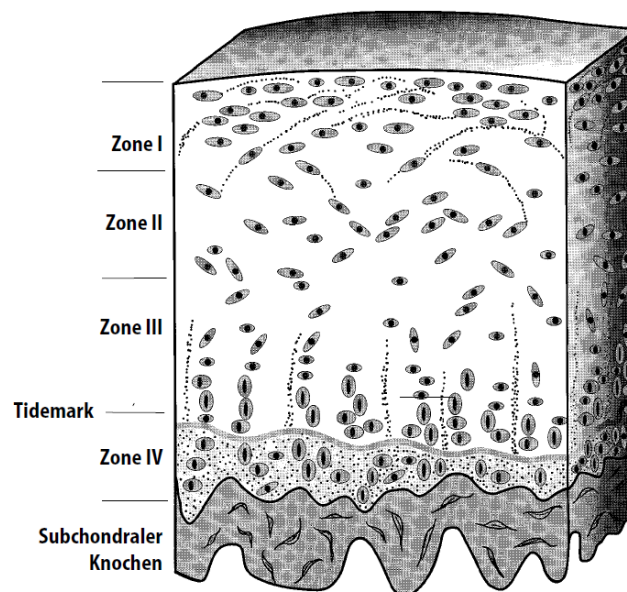


**Abbildung 1:** Zonale Struktur des Gelenkknorpels. Der nicht-kalzifizierte Knorpel wird von der Gelenkoberfläche Richtung Knochen in die Zonen I, II und III unterteilt. Die Zone III wird durch die Tidemark von Zone IV getrennt, die wiederum an den subchondralen Knochen anschließt. Nachdruck mit Genehmigung von Springer Nature: Springer-Verlag, Knorpelregeneration und Knorpelersatz, M. Rudert und C. J. Wirth, © 1998. [4]

Der Gelenkknorpel ist in den folgenden Eigenschaften zonal strukturiert (siehe **Abbildung 1**): EZM-Zusammensetzung, Chondrozyten-Morphologie sowie -Organisation [3] und Kollagen-Organisation [5]. Der nicht-kalzifizierte Knorpel wird von der Gelenkoberfläche Richtung Knochen in Zone I, Zone II und Zone III unterteilt, die auch als Tangentialfaserzone, Übergangszzone und Radiärzone bezeichnet werden. [2, 4] Der kalzifizierte Knorpel (Zone IV) schließt an den subchondralen Knochen an und wird durch die Tidemark von Zone III getrennt.

Kollagen Typ II ist der Hauptbestandteil der Biopolymere der EZM des Gelenkknorpels [2], dies entspricht 10-30 Gew.-% des Nassgewichts [6]. Der hohe Kollagen-Anteil verleiht dem Gelenkknorpel-Gewebe seine Zug- und Scherfestigkeit [6]. Neben Kollagen Typ II, das 90-95 % der Kollagene im Knorpel ausmacht [4], kommen die Typen VI, IX, X und XI in der Gelenkknorpel-EZM vor [7]. Knorpel-typische Kollagen-Fibrillen bestehen aus Kollagen Typ II, IX und XI und strukturellen Makromolekülen [8]. Chondrozyten synthetisieren primäre Fibrillen, die dann im extrazellulären Raum zu Knorpel-Fibrillen fusionieren. Im Vergleich zu Kollagen Typ I-Fibrillen, die einen Durchmesser von 50 nm-100 nm haben [9], sind Kollagen Typ II-Fibrillen mit einem Durchmesser von 10 nm-20 nm [10] deutlich dünner. Außerdem bindet Kollagen Typ II 50-100 % mehr Wasser als Kollagen Typ I [11] und besitzt mehr Hydroxylisin-gebundene Zucker, die wahrscheinlich mit Proteoglykanen interagieren [12]. Diese Kollagen Typ II-Fibrillen sind über den Knorpelquerschnitt arkadenartig angeordnet, siehe **Abbildung 2**. [5] In Zone III verlaufen die Fibrillen senkrecht und in Zone I parallel zur Gelenkoberfläche. Darüber hinaus spalten sich die Fibrillen in Zone I in ihre primären Fibrillen auf. Der Kollagengehalt ist über alle Zonen konstant.

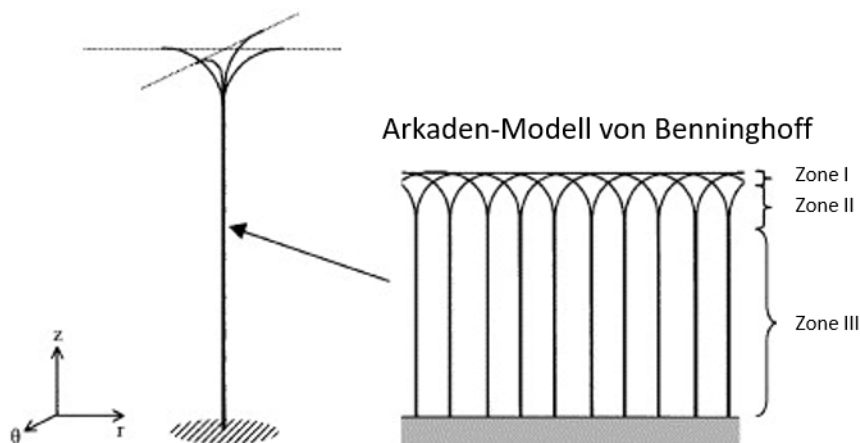


**Abbildung 2:** Arkaden-Modell der Kollagen-Organisation im Gelenkknorpel von Benninghoff [5]. Nachdruck mit Genehmigung von Elsevier: Elsevier Ltd., Stresses in the local collagen network of articular cartilage: a poroviscoelastic fibril-reinforced finite element study, W. Wilson *et al.*, © 2004. [13] Anmerkung: Die Beschriftungen in der Abbildung wurden übersetzt und die Bezeichnung der Zonen verändert.

Am zweit-häufigsten kommen Proteoglykane in der Knorpel-EZM vor und machen 3-10 Gew.-% des Nassgewichts aus [6]. Der Gehalt an Proteoglykanen nimmt von Zone I zu Zone III zu [4]. Proteoglykane sind Proteine, die post-translational mit Glykosaminoglykanen (GAGs) modifiziert werden. [14] Die

GAGs Chondroitinsulfat (CS), Heparansulfat und Keratansulfat kommen an Proteoglykanen gebunden vor. GAGs sind lineare Kohlenhydrat-Polymere mit unterschiedlich zusammengesetzten spezifischen Disaccharid-Einheiten.

Das Proteoglykan Aggrecan kommt hauptsächlich im Knorpel vor und besteht aus einem zentralen, langen Kernprotein und daran gebundene CS und Keratansulfate. Die GAG-Ketten machen etwa 90 Gew.-% des Aggrecans aus [3, 15]. Das Aggrecan hat einen Flaschenbürsten-artigen Aufbau und wird wiederum über das Link-Protein nicht-kovalent an dem GAG Hyaluronsäure (HA) gebunden. [4, 14] Dadurch entstehen große Aggregate, die bis zu 100 Proteoglykane beinhalten. [3, 4] Diese Aggregate sind so groß, dass sie im Kollagenetzwerk der Knorpel-EZM immobilisiert werden, siehe **Abbildung 3**. Zusätzlich werden Kollagen- und Proteoglykannetzwerk durch kleine Proteoglykane und Glykoproteine miteinander verbunden. [14] Die hohe Dichte an negativ geladenen Gruppen der GAGs zieht Kationen und Wasser an und führt dadurch zu einem inneren hydrostatischen Druck. Dieser hydrostatische Druck verleiht dem Knorpelgewebe seine Druckfestigkeit [16].

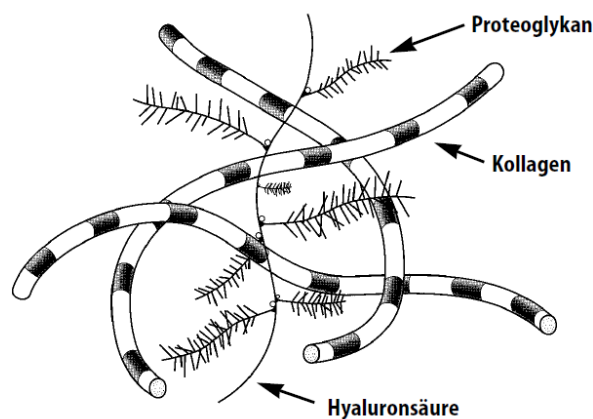


**Abbildung 3:** Extrazelluläre Matrix des Knorpelgewebes. Die Proteoglykan-Aggregate sind im Kollagenetzwerk immobilisiert. Die Aggregate bestehen aus einer Hyaluronsäure, an die über das Link-Protein Proteoglykane gebunden sind. Diese Proteoglykane haben eine flaschenbürsten-artige Struktur und bestehen aus einem zentralen Kernprotein, an das Glykosaminoglykane gebunden sind. Nachdruck mit Genehmigung von Springer Nature: Springer-Verlag, Knorpelregeneration und Knorpelersatz, M. Rudert und C. J. Wirth, © 1998. [4]

Der hohe Wassergehalt ist außerdem essentiell für die Versorgung der Chondrozyten. [3] Denn die Versorgung der Chondrozyten erfolgt aufgrund der Avaskularität des Knorpelgewebes über Diffusion der niedermolekularen Nährstoffe, beispielsweise Sauerstoff und Glukose, aus der Gelenkflüssigkeit. [17] Andere hochmolekulare Stoffe wie Serumalbumin werden über die Flüssigkeitsbewegung während der Belastung durch das Gewebe transportiert.

Die Dichte an gewebespezifischen Zellen im Knorpel ist im Vergleich zu anderen Geweben, wie beispielsweise dem Epithelgewebe, niedrig. Es wurde geschätzt, dass die Chondrozyten nur etwa 10 Gew.-% des Knorpelgewebes ausmachen. [6] Außerdem unterscheidet sich die Verteilung der Chondrozyten in den drei Zonen des Gelenkknorpels, wobei die höchste Dichte in Zone I und die geringste Dichte in Zone III zu finden ist. Dieser inverse Zusammenhang zwischen Zelldichte und

Knorpeltiefe kann durch die Avaskularität des Gewebes erklärt werden: Die Versorgung mit Nährstoffen durch Diffusion limitiert die Zellzahl besonders in den tiefen Zonen (Zone II und Zone III). Außerdem unterscheiden sich die Chondrozyten in den drei Zonen hinsichtlich ihrer Morphologie und Organisation (siehe **Abbildung 1**) [3, 4]: In Zone I liegen die Chondrozyten länglich, einzeln und parallel zur Gelenkoberfläche vor. In Zone II zeigen die Chondrozyten eine rundliche Morphologie und sind zufällig verteilt und in Zone III haben sie eine sphärische Morphologie und sind säulenartig aufeinandergestapelt. Außerdem wurden unterschiedliche Protein-Expressionen der Chondrozyten in den drei Zonen nachgewiesen, sodass von zonal unterschiedlichen Chondrozyten-Phänotypen gesprochen wird. Beispielsweise wird in Zone I Proteoglykan 4 (auch bekannt als *superficial zone protein*, SZP) [18] und Clusterin [19] exprimiert, in Zone II und Zone III hingegen *cartilage oligomeric matrix protein* [20] und *cartilage intermediate layer protein* [21].

### 2.1.2 Behandlungstherapien von Gelenkknorpeldefekten

Knorpelschäden werden durch degenerative Krankheiten wie Arthrose oder Traumata verursacht und führen zu Gelenkschmerzen. Diese Gelenkschmerzen sind weltweit eine der häufigsten Ursachen für die Einschränkung der Lebensqualität der Betroffenen im Alltag [22]. In einer Befragung des Robert Koch-Instituts aus dem Jahr 2017 litten 29,3 % aller befragten Frauen und 24,4 % der befragten Männer an akuten, also im Laufe des letzten Tages verspürten, Gelenkschmerzen [23]. Aufgrund der bereits erläuterten Avaskularität des Knorpels ist dessen Selbstheilungskapazität stark limitiert. [24] Deshalb werden Knorpeldefekte oft mit chirurgisch rekonstruktiven, Gelenk-erhaltenen Therapien (Stimulation des Knochenmarks, osteochondrale Transplantation, (Matrix-assoziierte) autologe Chondrozyten Transplantation (ACT)) behandelt, oder durch den teilweisen oder vollständigen Ersatz des Gelenks mit einer Endoprothese therapiert. Die Haltbarkeit eines solchen Gelenkersatzes ist allerdings zeitlich begrenzt, sodass vor dem Ersatz mögliche regenerative Therapien eingesetzt werden.

Das Prinzip der autologen Chondrozyten Transplantation ist in **Abbildung 4** dargestellt und wird im Folgenden erläutert. Dem Patienten wird in einer ersten Operation ein gesundes Stück Knorpel entnommen. [25] Dieses Knorpelstück wird dann enzymatisch verdaut um die Chondrozyten zu isolieren. Dabei werden einige hunderttausend Chondrozyten erhalten, die anschließend in Zellkulturschalen zweidimensional kultiviert werden um die Zellen zu expandieren, bis etwa zehn Millionen Zellen zur Verfügung stehen. Diese Chondrozyten werden in eine Suspension überführt und in einer zweiten Operation direkt in den Knorpeldefekt injiziert. Der befüllte Defekt wird dann mit Knochenhaut der Tibia verschlossen.

Während der Expansionskultivierung dedifferenzieren die Chondrozyten, das heißt sie verlieren ihre gewebespezifischen Eigenschaften. Diese Dedifferenzierung ist notwendig, damit die Chondrozyten

sich teilen. Jedoch verlieren die Knorpelzellen durch die Dedifferenzierung ihren differenzierten Zustand, was an ihrer veränderten Morphologie und Genexpression zu erkennen ist: Während die Chondrozyten im Knorpel sphärisch vorliegen, zeigen sie nach der Dedifferenzierung eine elongierte Morphologie, die der Morphologie von Fibroblasten ähnelt. [26] Diese Morphologie wird durch die Aktin-Myosin-Fibrillenbündel aufrechterhalten, die im differenzierten Zustand der Chondrozyten nicht nachweisbar sind. Des Weiteren exprimieren die Knorpelzellen Kollagen Typ I anstatt Kollagen Typ II. [27] Kollagen Typ I ist typisch für Faserknorpel, allerdings nicht für Gelenkknorpel. Somit werden bei der ACT dedifferenzierte Knorpelzellen in den Defekt injiziert. [28] Dies ist wahrscheinlich der Ursprung für den häufig entwickelten Faserknorpel nach einer ACT-Behandlung in den Defekten.

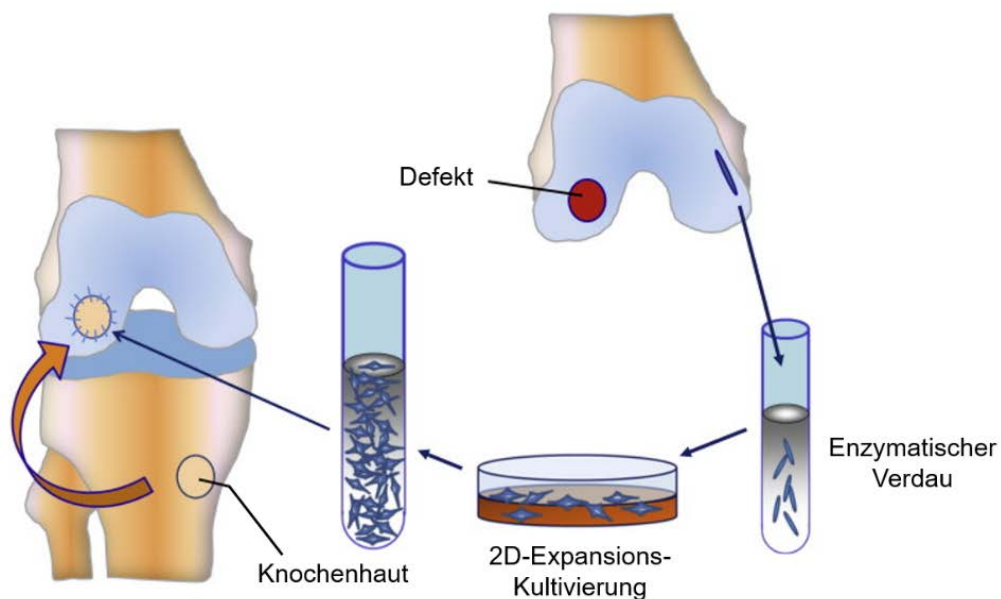


**Abbildung 4:** Prinzip der autologen Chondrozyten Transplantation. Außerhalb der Knorpelläsion wird ein Stück gesunder Knorpel entnommen und enzymatisch verdaut um die Chondrozyten zu isolieren. Die Chondrozyten werden zur Expansion zweidimensional kultiviert. Nach der Expansion wird eine Chondrozyten-Suspension in die Läsion injiziert und mit einem Stück Knochenhaut verschlossen. Nachdruck mit Genehmigung von Elsevier: Elsevier Ltd., An educational review of cartilage repair: precepts & practice – myths & misconceptions – progress & prospects, E. B. Hunziker *et al.*, © 2015. [25] Anmerkung: Die Beschriftungen in der Abbildung wurden übersetzt.

Es wurde gezeigt, dass die dreidimensionale Kultivierung von dedifferenzierten Chondrozyten zu deren Redifferenzierung führt [29, 30]. Deshalb wurde die ACT zur Matrix-assoziierten ACT (MACT) weiterentwickelt, bei der zuerst eine Gerüststruktur aus Kollagen mit den dedifferenzierten Chondrozyten besiedelt wird, die dann anschließend in den Defekt implantiert wird [31]. Das Behandlungsprinzip der MACT leitet in das Prinzip des Gelenkknorpel-*Tissue Engineerings* (TE) über, das sich noch im Forschungsstadium befindet und im folgenden Kapitel erläutert wird.



### 2.1.3 Gelatine-Methacryloyl-Hydrogele als Trägermaterial für das Gelenkknorpel-*Tissue Engineering*

Beim Gelenkknorpel-TE werden den Patienten, ähnlich wie bei der MACT, Chondrozyten entnommen, diese zweidimensional vermehrt, auf eine Trägerstruktur (*Scaffold*) gesät und dem Patienten in den Knorpeldefekt implantiert [32]. Dabei gelten Hydrogele als vielversprechende Biomaterialien für den Einsatz als Trägerstruktur. [32] Ein Hydrogel wird als ein nicht-flüssiges kolloidales (Polymer)Netzwerk definiert, das durch kovalente chemische Vernetzung oder physikalische Aggregation der Polymerketten entsteht und mit Wasser durchdrungen ist. [33] Für das Gelenkknorpel-TE werden Hydrogele aus Biopolymeren, die einen natürlichen Ursprung haben, und aus synthetischen Polymeren untersucht. Dabei hat die Verwendung von Biopolymeren, die in der natürlichen Knorpel-EZM vorkommen, den Vorteil, dass sie das Zellverhalten (beispielsweise Migration und Proliferation) regulieren können.

Eine Strategie im Knorpel-TE ist es den *Scaffold* so zu gestalten, dass er dem Knorpelgewebe möglichst ähnlich ist. Da die EZM des Knorpels hauptsächlich aus Kollagen Typ II besteht, wird Kollagen als Biomaterial für *Scaffolds* untersucht. Allerdings ist die Verarbeitung von Kollagen aufwendig, sodass häufig auf dessen Hydrolysat Gelatine zurückgegriffen wird. Denn im Gegensatz zu Kollagen ist Gelatine bei neutralem pH wasserlöslich, die Hydrogele schrumpfen nicht und durch Abkühlen wässriger Gelatine-Lösungen bilden sich physikalische Hydrogele (siehe 2.2). Gelatine kann von Kollagenasen degradiert werden, da sie die entsprechenden Matrix-Metalloproteasen Erkennungssequenzen besitzt [34] und enthält Arginin-Glycin-Asparaginsäure (RGD)-Peptid, an das Zellen Integrin-vermittelt adhären können [35]. Gelatine wird zwar aus Kollagen Typ I-reichen Geweben wie Knochen und Haut gewonnen, allerdings wird sie trotzdem als erste Näherung als *Scaffold* für das Knorpel-TE untersucht.

Physikalische Gelatine-Hydrogele sind jedoch nicht für die Anwendung als Gerüststruktur im TE geeignet, da sie oberhalb von etwa 30 °C schmelzen und somit bei Körpertemperatur flüssig wären (vergleiche Kapitel 2.2.2). Deshalb ist eine kovalente, chemische Vernetzung der Gelatine-Moleküle notwendig um Hydrogele darzustellen, die als *Scaffold* bei physiologischen Bedingungen geeignet sind. Da die Gelatine selbst funktionelle Gruppen in den Seitenketten ihrer Aminosäuren trägt, können diese Gruppen auch zur Vernetzung genutzt werden. Beispielsweise vernetzten Carbodiimide die Carboxylgruppen von Asparagin- und Glutaminsäure mit den Aminogruppen von Lysin und Hydroxylysin, wodurch eine Amid-Bindung entsteht [36, 37]. Außerdem können Enzyme verwendet werden, um chemisch vernetzte Gelatine-Hydrogele herzustellen [38-40]. Diese Vernetzungsreaktionen sind allerdings schwer zu kontrollieren, weshalb es schwierig ist, Materialeigenschaften mit diesen Methoden gezielt einzustellen und zu verändern.

Eine weitere Möglichkeit ist es andere chemisch vernetzbare Gruppen in die Gelatine einzubringen, die dann durch einen externen Stimulus vernetzt werden können, wodurch Materialeigenschaften eingestellt werden können. Das am häufigsten für das TE verwendete, chemisch-modifizierte Gelatine-Derivat ist Gelatine-Methacryloyl (GM). Typischer Weise werden während der chemischen Modifizierung die Amino- und Hydroxylgruppen der Gelatine mit Methacrylsäureanhydrid zu Methacrylamiden und Methacrylaten umgesetzt. Diese Methacryloylgruppen können dann radikalisch polymerisiert werden, dafür wird meist ein Photoinitiator und ultraviolettes (UV) Licht verwendet. Dieses Vorgehen wurde vor etwa 25 Jahren von Nazarova *et al.* publiziert [41], jedoch wird vor allem die Publikation von Van den Bulcke *et al.* aus dem Jahr 2000 zitiert [42]. Diese Publikationen sind die Grundlage für die Untersuchung von GM als Biomaterial. Die Herstellung und Charakterisierung von GM-Lösungen und -Hydrogelen wird in Kapitel 2.3 ausführlich dargestellt. Literaturübersichten wurden zur Anwendung von GM-Hydrogelen im TE allgemein von Yue *et al.* [35] und im Speziellen für das Gelenkknorpel-TE von Sun *et al.* [43] aufgestellt.

Die Arbeitsgruppe um Dietmar W. Hutmacher und Travis J. Klein an der Universität von Queensland untersucht und entwickelt GM-basierte Hydrogele für das Gelenkknorpel-TE [44-53]. Der Fokus der Forschung dieser Arbeitsgruppe liegt auf Hydrogelen aus GM und methacryloylierter Hyaluronsäure (HAM). Sie haben beobachtet, dass Hybrid-Hydrogele aus GM und HAM die sphärische Morphologie der Chondrozyten begünstigen und diese Zellen mehr Kollagen Typ II als Kollagen Typ I exprimierten. [52] Der Kompressionsmodul der GM-Hydrogele mit HAM war höher als der von reinen GM-Hydrogelen und wurde zusätzlich durch die neu synthetisierte EZM der Chondrozyten verstärkt, sodass nach acht Wochen ein Kompressionsmodul von etwa 150 kPa vorlag. In dieser Studie wurden auch Hydrogele aus GM, HAM und methacryloyliertem Chondroitinsulfat untersucht. Diese hatten vergleichbare Eigenschaften wie die GM-HAM-Hydrogele.

In einer anschließenden Studie untersuchte die Gruppe von Hutmacher und Klein Hydrogele aus GM und HAM mit einem Gesamtpolymergehalt von 10 Gew.-%, wobei der Anteil an HAM von 0-2 Gew.-% variierte. [46] Während die Kompressionsmoduln aller GM-HAM-Hydrogele nach einem Tag ähnlich waren (~50-60 kPa), wurde nach acht Wochen Kultivierung ein signifikanter Einfluss des HAM-Gehalts auf die mechanischen Eigenschaften der Hydrogele (Kompressionsmodul, Gleichgewichtsmodul, Dynamischer Modul und Bruchfestigkeit) festgestellt. Dabei nahmen die untersuchten mechanischen Eigenschaften mit der HAM-Konzentration der Hydrogele zu. Außerdem war die von den verkapselten Chondrozyten sekretierte EZM in GM-HAM-Hydrogelen gleichmäßiger verteilt als in reinen GM-Hydrogelen. Der Gehalt an GAGs, die durch die verkapselten Chondrozyten sekretiert wurden, aller untersuchten Hydrogel-Zusammensetzungen war jedoch nicht unterscheidbar und korrelierte damit nicht mit den mechanischen Eigenschaften. Deshalb wurde die Hypothese aufgestellt, dass die

gleichmäßigere EZM-Verteilung in GM-HAM-Hydrogelen zu höheren Kompressions-, Gleichgewichts- und dynamischen Moduln sowie zur erhöhten Bruchfestigkeit führte.

In einer der jüngsten Publikationen aus der Gruppe von Klein und Hutmacher wurde der Einfluss des für die GM-Synthese eingesetzten Gelatine-Typs (vergleiche 2.2.1) und des verwendeten Photoinitiators auf die Redifferenzierung von dedifferenzierten Chondrozyten untersucht. [51] Gelatine Typ B, im Vergleich zu Gelatine Typ A, stellten sich als Rohmaterial für die GM-Synthese in Kombination mit Irgacure 2959 (0,25 Gew.-%) , im Vergleich zu Lithium Phenyl-2,4,6-trimethylbenzoylphosphinat (LAP, 0,15 Gew.-%), als Photoinitiator zum Vernetzen der Hydrogele als besonders geeignet heraus um dedifferenzierte Knorpelzellen zu redifferenzieren. Die mRNA-Expression von COL2A1 (Gen, das  $\alpha$ -1-Typ-II-Kollagen codiert) in mit Irgacure 2959 vernetzten Hydrogelen war signifikant höher als in mit gleicher UV-Dosis und LAP vernetzten Hydrogelen. Diese Studien verdeutlichen, dass methacryloylierte Derivate von Gelatine, Hyaluronsäure und Chondroitinsulfat geeignet sind, um mechanisch belastbare Hydrogele darzustellen. Außerdem können dedifferenzierte Chondrozyten in den Hydrogelen kultivieren werden und redifferenzieren, sodass Knorpel-typische EZM in den Hydrogelen nachgewiesen werden kann. Außerdem wird der Bedarf an systematischer Charakterisierung von GM und GM-Hydrogelen um deren Anwendung im TE in der Zukunft zu verwirklichen aufgezeigt.

#### 2.1.4 Zonales Gelenkknorpel-*Tissue Engineering*

Das anfängliche Ziel des Gelenkknorpel-TE war es, ein homogenes Gewebe zu erzeugen, das die Eigenschaften des gesamten Knorpels widerspiegelt [54, 55]. Dabei wird jedoch die zonale Struktur, die wie bereits in Kapitel 2.1.1 erläutert, essenziell für die Eigenschaften und der Funktion des Gelenkknorpels ist, vernachlässigt. Deshalb wird im zonalen Gelenkknorpel-TE versucht die zonale Strukturierung des Knorpels zu imitieren. Die Ansätze des zonalen Gelenkknorpel-TE können in vier Herangehensweisen unterteilt werden [44], siehe **Abbildung 5**: *Scaffold*- und Matrix-freie, Matrix-basierte, *Scaffold*-basierte und Hybride-Ansätze.

In allen Herangehensweisen bis auf den *Scaffold*-basierten Ansatz werden typischerweise zonale Chondrozyten-Phänotypen verwendet. Die Isolierung der zonalen Chondrozyten-Phänotypen ist aufwendig und ineffektiv, da nur solche Teilstücke des Knorpels genutzt werden, die man sicher einer Zone des Gelenkknorpels zuordnen kann. [56] Die anderen Knorpelstücke werden verworfen, vergleiche **Abbildung 6**. Deshalb wurden in einigen Studien bereits statt drei zonalen Phänotypen nur zwei verwendet, wobei die Chondrozyten aus Zone II und Zone III als Mischpopulation verwendet wurden [57]. Im Folgenden werden Beispiele für die vier Ansätze des zonalen Gelenkknorpel-TE erläutert.

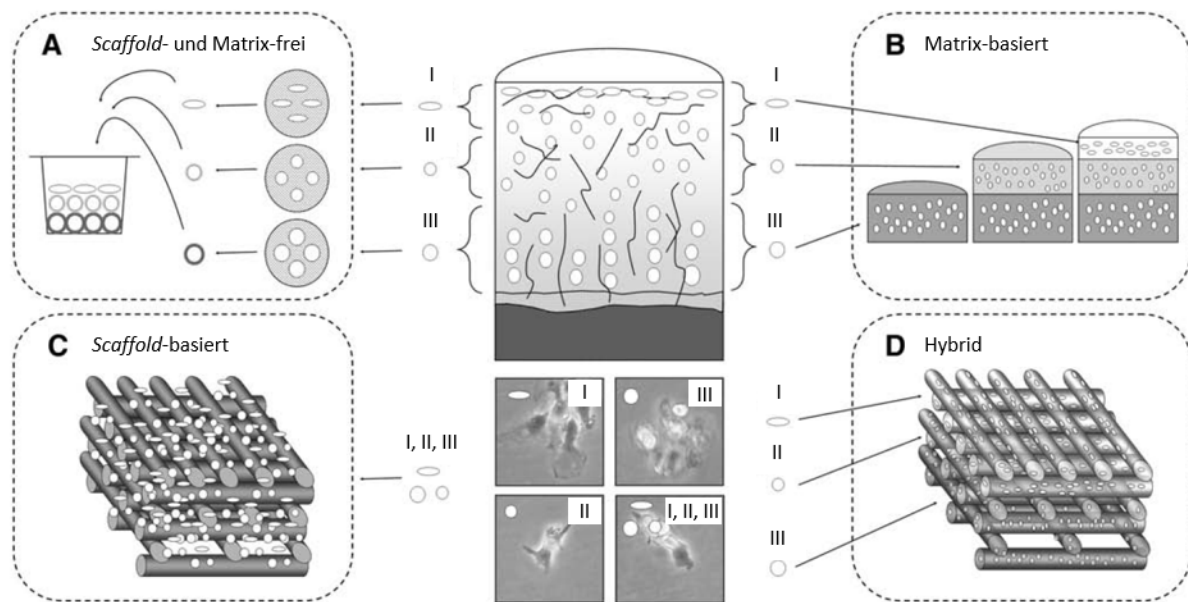


**Abbildung 5:** Strategien des zonalen Gelenkknorpel-Tissue Engineerings. **A** Bei der Scaffold- und Matrix-freien Strategie werden die Chondrozyten aus den Zonen I, II und III getrennt und ohne Scaffold verwendet, und produzieren ihre eigene Matrix. **B** Bei der Matrix-basierten Strategie werden Hydrogele aufeinander geschichtet die jeweils einen zonalen Chondrozyten Phänotyp der Zonen I-III beinhalten. **C** Im Scaffold-basierten Ansatz wird eine Mischpopulation aus Chondrozyten der Zonen I-III auf eine zonal strukturierte Gerüststruktur gesät. **D** Für den Hybrid-Ansatz wird mit zellhaltigen Materialien mittels additiver Fertigungsverfahren eine zonale Struktur aufgebaut. Nachdruck mit Genehmigung von Mary Ann Liebert: Mary Ann Liebert, Inc., Tissue Engineering of Articular Cartilage with Biomimetic Zones, T. J. Klein *et al.*, © 2009. [44] Anmerkung: Die Beschriftungen in der Abbildung wurden übersetzt und die Bezeichnung der Zonen verändert.

Die Scaffold- und Matrix-freie Herangehensweise soll die ontogenetische Entwicklung des Knorpels nachahmen, indem Chondrozyten aus unterschiedlichen Zonen des Gelenkknorpels, Stamm- oder Vorläuferzellen ohne 3D-Trägermaterial aufeinander kultiviert werden. [44] Eine weitere Studie von Klein *et al.* kann dieser Strategie zur Erzeugung zonal strukturierten Gelenkknorpel-Äquivalenten zugeordnet werden. [57] In dieser Studie wurden Chondrozyten aus Zone I und eine Mischpopulation aus Zone II und III zunächst separat in Alginate expandiert, anschließend das Alginate entfernt und die zwei Zellpopulationen ohne zusätzliche Matrix in hoher Dichte aufeinander kultiviert (S/M-Konstrukt). Zum Vergleich wurden außerdem Hohe-Dichte-Kulturen durchgeführt, die nur aus Chondrozyten aus Zone I (S-Konstrukt) bzw. Zone II/III (M-Konstrukt) bestanden. Alle Konstrukte wurden zwei Wochen lang kultiviert und anschließend unter anderem in Bezug auf ihren GAG- und Kollagen-Gehalt sowie der Expression von SZP untersucht. Es wurde gezeigt, dass die M-Konstrukte den höchsten GAG- und Kollagen-Gehalt hatten, während die Gehalte von S- und S/M-Konstrukten nicht unterscheidbar waren. Jedoch konnte in den S/M-Konstrukten eine Strukturierung in der GAG-Färbung beobachtet werden. Die Färbung war für den Bereich der Zellen aus Zone II/III im Vergleich zu dem Bereich der Zellen aus Zone I stärker. Das SZP wurde an der Oberfläche aller Konstrukte stärker nachgewiesen als im Inneren der Konstrukte. In den S/M-Konstrukten konnte jedoch zusätzlich noch ein Verlauf in der SZP-Expression nachgewiesen werden: Von der Oberfläche zu den Zellen aus den Zonen II/III nahm die Expression ab. Solch ein Gradient wurde für die anderen Konstrukte nicht beobachtet.

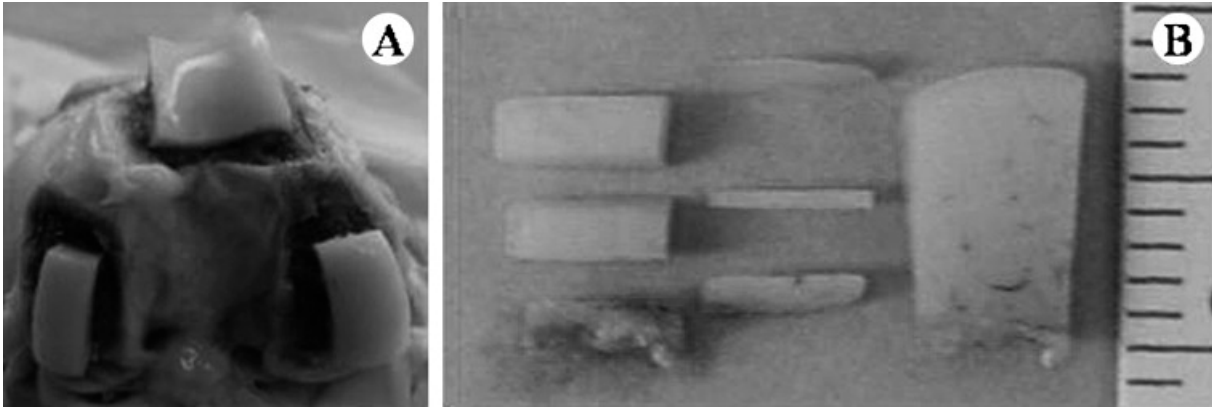


**Abbildung 6:** Präparation von Knorpelgewebe für die Isolierung der zonalen Phänotypen aus Zone I, II und III (A). Nur die oberen, mittleren und unteren 10 % des Knorpels wurden für die Isolierung verwendet (B). Nachdruck mit Genehmigung von Elsevier: Elsevier Ltd., Experimental Model for Cartilage Tissue Engineering to Regenerate the Zonal Organization of Articular Cartilage, T.-K. Kim *et al.*, © 2003. [56]

In der Matrix-basierten Strategie zur Herstellung zonal strukturierter Biomaterialien für das Gelenkknorpel-TE werden Hydrogele einer Zusammensetzung, die zonale Chondrozyten-Phänotypen beinhalten, aufeinander geschichtet vernetzt [44], siehe **Abbildung 5-B**. Ein Beispiel für diese Strategie ist die Studie von Kim *et al.*, in der zonale Chondrozyten-Phänotypen zusammen mit mesenchymalen Stammzellen (MSC) in Hydrogelen aus HAM verkapselt und aufeinander geschichtet wurden. [55] Es wurde gezeigt, dass die Zellen über eine Dauer von 16 Wochen vital waren und Kollagen Typ II, Chondroitinsulfat und Proteoglykane akkumuliert wurden. Allerdings war die Synthese von diesen EZM-Bestandteilen an den Rändern des dreidimensionalen Konstrukts höher als in der Mitte des Konstrukts. Diese unterschiedliche EZM-Akkumulation wurde durch eine nicht-ausreichende Versorgung mit Nährstoffen und mangelndem Abtransport von Abfallstoffen begründet. Deshalb wurde für eine bessere Versorgung der Zellen durch Diffusion ein Kanal mittig in das Hydrogel eingesetzt. Dies resultierte in einer gleichmäßigen Akkumulation von Kollagen Typ II und Chondroitinsulfat im gesamten drei-lagigen Hydrogel. Jedoch wurde dadurch die EZM-Synthese insgesamt nicht erhöht und der Elastizitätsmodul blieb gleich (~150 kPa nach 8 Wochen Kultivierung und ~600 kPa nach 16 Wochen Kultivierung).

In der *Scaffold*-basierten Strategie für den Aufbau von zonal strukturierten Gelenkknorpel-Äquivalenten wird die Gerüststruktur genutzt, um mechanische Festigkeit und eine Organisation vorzugeben [58]. Camarero-Espinosa *et al.* untersuchten ein drei-lagiges Gerüst aus Polylactid und Cellulose-Nanokristallen, um die Kollagen-Orientierung im nativen Gelenkknorpel zu imitieren. [59] Die Gerüststruktur wurde durch thermisch induzierte Phasenseparation mit anschließender Gefriertrocknung hergestellt und dann mit Chondrozyten besiedelt. Über die Dauer der vierwöchigen Kultivierung wurde eine Zunahme an Kollagen in der Gerüststruktur nachgewiesen. Allerdings wurde mehr Kollagen Typ I als Kollagen Typ II von den Chondrozyten sekretiert, was sich auch in der lang gestreckten Morphologie der Zellen widerspiegelte und einen Hinweis auf einen dedifferenzierten Zustand der Zellen gibt. Somit konnte während des untersuchten Zeitraums im verwendeten 3D-Gerüst

keine Redifferenzierung der dedifferenzierten Chondrozyten erreicht werden und es gab keinen offensichtlichen Einfluss der zonal unterschiedlichen Struktur des Gerüsts auf das Zellverhalten.

In der vierten Strategie, der Hybrid-Strategie (siehe **Abbildung 5-D**), wird das *Bioprinting* eingesetzt, um zonale Chondrozyten-Phänotypen und das Biomaterial orts aufgelöst abzulegen und so heterogene Knorpelgewebe-Äquivalente aufzubauen [44]. Cohen *et al.* entwickelten ein *Bioprinting*-Verfahren und untersuchten dessen Eignung für die Herstellung von strukturierten Gelenknorpel-Äquivalenten. [60] Es wurde gezeigt, dass das Fertigungsverfahren geeignet war, um in Alginat verkapselte Chondrozyten zytokompatibel und steril zu prozessieren. Darüber hinaus konnten zwei Alginat-Komponenten zu einem Konstrukt verarbeitet werden, sodass die Möglichkeit des Aufbaus von heterogenen Materialien demonstriert wurde. Die erzeugten Zell-Matrix-Konstrukte waren über 20 Wochen formstabil und die Chondrozyten synthetisierten GAGs.

Der Einsatz von zonalen Chondrozyten Phänotypen ist aufwendig und zeigte bisher keine eindeutigen Vorteile, deshalb wird die Verwendung dieser Subpopulationen kritisch diskutiert [48]. Die Beispiele für die verfolgten Strategien im zonalen Gelenknorpel-TE zeigen, dass die Entwicklung der Gerüststrukturen komplex ist. Außerdem wurde bisher nur in Einzelfällen ein Einfluss der zonalen Struktur auf die EZM-Sekretion der verkapselten Chondrozyten beobachtet.

## 2.2 Gelatine

Arthur Veis definierte Gelatine mit dem folgenden Wortlaut: "Gelatine ist das wasserlösliche Produkt der Auflösung, Desorganisation und des Abbaus von [...] wasserunlöslichen Kollagenfasern" [61]. Um Gelatine und ihre Eigenschaften einordnen und verstehen zu können, ist es somit wichtig zunächst dessen Ursprungprotein Kollagen zu betrachten. Im Folgenden werden der Aufbau von Kollagen Typ I, aus dem Gelatine hergestellt wird, die verschiedenen Herstellungsprozesse von Gelatine aus Kollagen, die physikalische Gelierung und die Standardcharakterisierung von Gelatine beschrieben.

### 2.2.1 Ursprung und Herstellung von Gelatine

Die Klasse der Kollagene ist die am häufigsten auftretende Proteinklasse in Geweben [61, 62]. Bis heute sind 28 Kollagen-Typen bekannt [63]. Kollagen Typ I kommt in nahezu allen Geweben vor, vor allem in Sehnen, Knochen und Haut. [64] Kollagen Typ II kommt fast ausschließlich im Knorpel vor und der Kollagen Typ III-Gehalt sinkt mit dem Alter der Haut. Die anderen Kollagen-Typen kommen nur in geringen Mengen vor und sind meist gewebespezifisch. Die molekulare Struktur von Kollagen ist komplex und besteht aus einer Primär-, Sekundär-, Tertiär- und Quartärstruktur [64, 65]. Im Folgenden wird die molekulare Struktur von Kollagen Typ I beschrieben, da Gelatine typischerweise aus Knochen

oder Haut gewonnen wird und in diesen Geweben hauptsächlich Kollagen Typ I vorkommt. Im Vergleich zu Kollagen Typ II haben die Kollagen Typ I-Fibrillen einen größeren Durchmesser und binden weniger Wasser [9-11].

Die Primärstruktur von Kollagen Typ I besteht aus zwei Polypeptidkette, die als  $\alpha$ -Ketten bezeichnet werden. [64] Jede  $\alpha$ -Kette besteht aus 334 sich wiederholenden Einheiten (Glycin-X-Y), wobei Prolin und Hydroxyprolin am häufigsten an der X-Position stehen, und hat ein Molekulargewicht von etwa 100 kDa [64, 65]. Die Drehung der Sekundärstruktur entsteht durch die in der Primärstruktur abwechselnden neutralen und polaren Aminosäuren-Sequenzen [62], sowie Prolin und Hydroxyprolin, die die Rotation der Polypeptidkette begrenzen. Dadurch ist die  $\alpha$ -Kette linksgängig, wobei drei Aminosäuren eine Drehung bilden [64]. Ramachandran und Kartha beschrieben als erste die rechtsgängige Tertiärstruktur, auch Superhelix oder Tropokollagen genannt, als drei umeinander gedrehte  $\alpha$ -Ketten [66-68]. Im Fall von Kollagen Typ I handelt es sich um ein Heterotrimer, das aus zwei  $\alpha$ -1-Ketten und einer  $\alpha$ -2-Kette besteht. Vier bis acht dieser Superhelices stapeln sich aufeinander und bilden so die Kollagen-Fibrillen, die Quartärstruktur von Kollagen. [64, 65] Diese Struktur wird zusätzlich durch kovalente Bindungen stabilisiert und verstärkt [64]. Kollagen denaturiert zwischen 37 °C und 40 °C in zwei Schritten [69]: Zuerst wird die Tertiärstruktur aufgebrochen und als zweites die Verstrickung der Sekundärstrukturen gelöst. Die Denaturierung von Kollagen hängt von dem pH und der Salzkonzentration der verwendeten Lösung sowie den verwendeten Denaturierungsreagenzien ab [62].

Gelatine wird hauptsächlich aus tierischen Knochen und Häuten gewonnen, die reich an Kollagen Typ I sind. Dabei werden an den Herstellungsprozess von Gelatine vier Anforderungen gestellt [62]: (1) Verunreinigungen müssen entfernt werden. (2) Kollagen-Fragmente mit einer geeigneten Größe müssen durch Aufschluss der Quervernetzungen und/oder kovalenten Bindungen entstehen. (3) Die Gelierkraft der resultierenden Gelatine muss erhalten bleiben. (4) Stabilisierende Wasserstoffbrückenbindungen müssen aufgelöst werden um die Kollagen-Fragmente wasserlöslich zu machen. Es gibt zwei Herstellungsprozesse, die kommerziell angewendet werden: Die saure und die alkalische (auch als "*Liming*" bekannt) Behandlung. Diese Prozesse werden in zwei Schritten durchgeführt. [64] Der erste Schritt wird Konditionierungsprozess genannt, dabei werden die kovalente Querverbindungen im Kollagen teilweise zerstört. In dem zweiten, sogenannten Extraktionsprozess wird die Gelatine durch thermische Hydrolyse ausgeschmolzen. In dem gesamten Prozess können die Dauer und die Temperatur als Variablen verändert werden. Die Hydrolyse während des Konditionierungsprozesses kann chemisch oder durch Enzyme durchgeführt werden, wobei Enzyme nicht kommerziell eingesetzt werden. Der saure Konditionierungsprozess führt zu Gelatine Typ A ( $G_A$ ) und der alkalische zu Gelatine Typ B ( $G_B$ ). Diese zwei Gelatine-Typen  $G_A$  und  $G_B$  unterscheiden sich in

ihrer Aminosäuren-Zusammensetzung, ihrem isoelektrischen Punkt (IEP) und ihrer Molekulargewichtsverteilung.

Der saure Gelatine-Herstellungsprozess hat den Vorteil, dass er verhältnismäßig kurz (10 h-48 h) und somit auch verhältnismäßig günstig ist [62]. Jedoch kann dieser Herstellungsprozess nur für Gewebe verwendet werden, die weniger stark vernetzt sind wie z. B. Haut und junger oder demineralisierter Knochen. [61, 62] Für den sauren Konditionierungsprozess wird das Rohmaterial, also das tierische Gewebe, gewaschen und anschließend in verdünnter, wässriger Säure eingeweicht. Das Gewebe wird solange in der verdünnten Säure getränkt, bis es den maximalen Quellgrad erreicht. Anschließend wird das konditionierte Rohmaterial gewaschen, bis der pH der Waschlösung höher als vier ist und kann dann für die thermische Extraktion weiterverwendet werden.

Bei dem alkalischen Konditionieren wird das gewaschene Rohmaterial in hydratisiertem Kalk (2-5 %) getränkt. [62] Typischerweise werden Natriumhydroxid oder Natriumkarbonat für das sogenannte Schärfen verwendet, um den Prozess zu katalysieren. Ohne dieses Schärfen würde der Konditionierungsprozess drei bis zehn Monate dauern [61], mit dem Schärfen dauert es nur acht bis zwölf Wochen [62]. Während dieser Zeit wird die Lösung gerührt und die Temperatur unterhalb von 20 °C gehalten. Außerdem wird während der alkalischen Konditionierung Ammoniak von den Glutamin- und Asparagin-Resten des Kollagens freigesetzt, was zu deren Umsetzung zu Glutamin- und Asparaginsäure führt [61, 62, 64]. Nach dem Konditionierungsprozess wird das Rohmaterial zunächst gewaschen, bis das Waschwasser einen pH-Wert von neun bis zehn besitzt und danach in einer Säurelösung und schließlich in destilliertem Wasser gewaschen [61, 62]. Nach diesem Waschvorgang kann das Rohmaterial extrahiert werden.

Die Aminosäuren-Zusammensetzung hängt vom ursprünglichen Kollagen und der Art der Gelatine-Herstellung ab [62]. Da die Aminosäuren-Zusammensetzung in den Kollagenen der Säugetiere nahezu konstant ist [62], beeinflusst der Konditionierungsprozess die Gelatine-Materialeigenschaften am stärksten, wie es bereits von Ames im Jahr 1952 beschrieben wurde [70].

### 2.2.2 Physikalische Gelierung von Gelatine

Die bekannteste Eigenschaft von Gelatine-Lösungen ist die Fähigkeit zu gelieren. Obwohl die physikalische Gelierung einfach erscheint, handelt es sich um einen komplexen Vorgang, der bis heute nicht vollständig verstanden wurde. Im Folgenden wird die Konformation von Gelatine-Molekülen in wässrigen Lösungen und physikalischen Gelen sowie der reversible Gelierprozess beschrieben.

Typischerweise wird Gelatine bei Temperaturen um 50 °C in Wasser gelöst. Diese wässrigen Gelatine-Lösungen haben bei Temperaturen oberhalb von 40 °C einen Newtonschen Charakter [61]. Die



Konformation von Gelatine in wässrigen Lösungen wurde beispielsweise mittels Circular dichroismus (CD)-Spektroskopie untersucht [71-74]. Die CD-Spektren von wässrigen Gelatine-Lösungen sind denen von sauren, wässrigen Kollagen-Lösungen ähnlich: Bei etwa 200 nm wurde eine charakteristische negative Bande beobachtet. Diese negative Bande wurde der ungeordneten Polypeptid-Kette (poly-L-Lysin) zugeordnet [71].

Wenn wässrige Gelatine-Lösungen unter 40 °C gekühlt werden erhöht sich ihre Viskosität und die Lösung verhält sich nicht länger wie ein Newtonsches Fluid. [61] Während des Kühlens verändert sich die Konformation der Gelatine in wässrigen Lösungen. In CD-spektroskopischen Untersuchungen der Konformationsänderung während des Kühlens wurde gezeigt, dass die negative Bande bei 200 nm ausgeprägter wird und eine positive Bande bei 220 nm auftritt [72, 73]. Diese Charakteristika waren mit denen von gekühlten Kollagen-Lösung vergleichbar, wobei die Banden der CD-Spektren von Kollagen ausgeprägter waren als die von Gelatine [71, 73]. Außerdem wurde eine negative Bande bei 238 nm detektiert, die nur bei der Kühlung von Gelatine-Lösungen auftrat [74]. Es wurde geschlussfolgert, dass die Kühlung von Gelatine-Lösungen zu einer teilweisen Regeneration des CD-Spektrums von Kollagen führt, wobei die positive Bande bei 220 nm die Tripel-Helices repräsentiert, in der die einzelnen Helices eine linksgängige Poly-Prolin-II-Helix(-trans)-Konformation haben [73]. Die Gelatine-spezifische negative Bande bei 238 nm korrelierte mit der positiven Bande bei 220 nm [74]: Je stärker die positive Bande ausgeprägt war, desto weniger stark war die negative Bande ausgeprägt und anders herum. Wetzel *et al.* ordneten die negative Bande bei 238 nm den einzelnen Helices mit einer stabilen Poly-Prolin-I(-cis)-Konformation zu [74], denn es wurde gezeigt, dass die Einzel-Helices in der Poly-Prolin-I-Konformation stabiler als in der Poly-Prolin-II-Konformation sind [75]. Folglich geht die Regeneration der Triple-Helix während der Kühlung von Gelatine-Lösungen mit einer cis-trans-Umwandlung der einzelnen Helices einher und ist ein bestimmender Schritt der Proteinfaltung [76].

Die Viskosität der Gelatine-Lösung steigt während der Kühlung bis sich, aufgrund der Konformationsänderungen bei der sich aus Einzel-Helices Tripel-Helices bilden, ein physikalisches Hydrogel ausbildet [77]. Die Gelierung von Gelatine-Lösungen durch Kühlen wird als ein mehrphasiger Prozess verstanden [61, 62, 78-80]. Das derzeitige Verständnis der Gelierung basiert auf Studien von Djabourov, Leblond and Papon [78, 79] sowie Bohidar und Jena [80]. Djabourov, Leblond und Papon zeigten, dass der bestimmende Prozess während der Gelierung die Konformationsänderung der Gelatine-Moleküle ist. [78] Zuerst bildet sich ein lockeres Netzwerk, wobei es entlang jedes einzelnen Gelatine-Moleküls zu mehreren Helix-Keimbildungen kommt. Diese Helices aggregieren dann zu enger verstrickten Tripel-Helices, wobei ein Gelatine-Molekül noch in mehreren Triple-Helices verstrickt ist. Die Entstehung dieses lockeren Netzwerks wurde mit dem ersten schnellen Wachstum an Tripel-Helices während der Gelierung korreliert, das in CD-spektroskopischen und dynamischen Differenzkalorimetrie (DSC)- [81] sowie in Ultraschall-Absorptions-Untersuchungen gezeigt wurde [82]. Anschließend werden

in einem langsameren Prozess neue Helices ausgebildet. [78] Dabei re-arrangieren sich die Helices in eine finale Gleichgewichts-Konfiguration mit unabhängigen Tripel-Helices, ähnlich wie natives Tropo-Kollagen in wässrigen Lösungen.

Die temperaturabhängige Gelierung von wässrigen Gelatine-Lösungen zu physikalischen Hydrogelen und deren Schmelzen, das wieder in wässrigen Gelatine-Lösungen resultiert, kann durch viele Methoden beobachtet werden. Eine Möglichkeit, die Gelier- und Schmelztemperatur von Gelatine-Lösungen zu bestimmen, ist die temperaturabhängige Messung von Speicher- und Verlustmodul ( $G'$ ,  $G''$ ) mit einem Rheometer. [64, 83] Dabei entspricht die Temperatur am Schnittpunkt von  $G'$  und  $G''$  der Schmelztemperatur der Heizkurven ( $G'=G''$ ) und die Geliertemperatur dem Schnittpunkt der Kühlkurven ( $G''=G'$ ). Es muss beachtet werden, dass die beobachteten Gelier- und Schmelztemperaturen von der Gelatine-Lösung (Konzentration, Gelatine, Lösungsmittel) sowie den Messeinstellungen (Kühl-/Heizrate, Amplitude, Frequenz) abhängt. Eine andere Methode ist die Messung der Enthalpie während des Kühlens und Heizens der Gelatine-Lösung mittels DSC [80, 81, 84]. Wie bereits beschrieben kommt es während des Gelierens einer wässrigen Gelatine-Lösung zur Ausbildung von Tripel-Helix-Bereichen, die einen kristallinen Charakter besitzen. Da kristalline Substanzen einen Schmelzpunkt ( $T_m$ ) in DSC-Messungen zeigen, kann diese Methode genutzt werden, um die Umwandlung der Triple-Helices in Polypeptidketten zu bestimmen und die Änderung der Enthalpie zu quantifizieren. Der Schmelzpunkt zeichnet sich durch eine sprunghafte endotherme Änderung der Enthalpie aus, die mit der Denaturierung der Tripel-Helices assoziiert wird [85, 86].

Die physikalische Gelierung von Gelatine wird durch unterschiedliche Faktoren beeinflusst. Dabei spielt besonders die vorangegangene Temperaturbehandlung (*thermal history*) eine besondere Rolle. Ein Beispiel dafür ist die Hysterese von Gelatinelösungen: Schmelz- und Geliertemperatur sind nicht deckungsgleich, da der Schmelzvorgang mehr Energie benötigt. Außerdem nimmt die Stabilität der physikalischen Gele mit der Dauer der Kühlung unterhalb des Schmelzpunktes zu [71, 73, 81]. Der pH und die in der Lösung vorliegende Ionen beeinflussen zusätzlich die Konformationsänderungen der Gelatine und somit der Gelierung [71, 73]. Beispielsweise hemmen Calciumchlorid und Natriumchlorid die Regeneration von Tripel-Helices [73]. Ein weiterer Faktor ist das Molekulargewicht [72] und der Extraktionsprozess [74] der verwendeten Gelatine.

### 2.2.3 Standardcharakterisierung von Gelatine

Gelatine wird industriell in vielen Anwendungen eingesetzt, beispielsweise in der Lebensmittelindustrie, Photographie und Pharmazie. [62] Da Gelatine ein Biopolymer ist, das aus Kollagen gewonnen wird, sind die Materialeigenschaften abhängig von dessen Ursprung und Herstellungsprozess. Deshalb ist es wichtig die physikalischen Eigenschaften von Gelatine-Lösungen

und Gelatine-Gelen zu charakterisieren, um die Reproduzierbarkeit des finalen Produkts zu garantieren. Dies gilt besonders für die potenzielle Anwendung im TE. Die Standardcharakterisierung zur Untersuchung von Gelatine wurden in der ersten Hälfte des 20. Jahrhunderts etabliert. Im Folgenden werden Standard-Viskosität, Bloom Wert (stellvertretend für die Gel-Festigkeit), isoelektrischer Punkt (IEP) sowie Methoden für deren experimentelle Bestimmung beschrieben.

Die Gel-Festigkeit der physikalischen Hydrogele war die erste Gelatine-Eigenschaft, die standardmäßig untersucht wurde [62]. Die Methode zur Untersuchung der Gel-Festigkeit, die von Oscar T. Bloom im Jahr 1925 entwickelt und patentiert wurde, ist noch heute der geltende Standard. [87] Die Methode beinhaltet eine standardisierte Herstellung einer Gelatine-Lösung sowie ein standardisiertes Kühlen der Lösungen zur physikalischen Gelierung [62]: 7.5 g Gelatine werden mit 105 mL destilliertem Wasser in einer Bloom-Flasche ( $59 \pm 1$  mm Durchmesser) vermischt und in einem Wasserbad auf  $65\text{ }^{\circ}\text{C}$  erwärmt, bis sich die Gelatine löst. Anschließend wird die Lösung in einem  $10\text{ }^{\circ}\text{C}$  kaltem Wasserbad für 17 h gekühlt und anschließend die Gelstärke des physikalischen Hydrogels mit dem von Oscar T. Bloom entwickelten Gelometer gemessen. Während dieser Messung wird ein Stempel mit einem Durchmesser von 0,5 Zoll (das entspricht 1,27 cm) in das physikalische Hydrogel gedrückt. Das Gewicht, das notwendig ist, um die Oberfläche des Gels um 4 mm zu komprimieren wird gemessen und ist das Ergebnis der Gel-Festigkeits-Messung und wird in "g Bloom" oder "Bloom" angegeben. Kommerzielle Gelatinen sind in einem Bereich zwischen 50 g Bloom und 300 g Bloom erhältlich, wobei ein höherer Bloom-Wert eine höhere Gel-Festigkeit repräsentiert. [64] Außerdem gelieren und schmelzen physikalische Hydrogele aus Gelatinen mit einem hohen Bloom-Wert bei höheren Temperaturen und gelieren schneller als Gelatinen mit einem niedrigem Bloom-Wert.

Die Standard-Viskosität von Gelatine ist die zweit-wichtigste Eigenschaft von Gelatine. [62, 64] Für die Bestimmung der Viskosität wird eine Gelatine-Lösung auf die gleiche Art wie für die Messung des Bloom-Wertes hergestellt und nach dem Lösen auf  $60\text{ }^{\circ}\text{C}$  temperiert. [64] Außerdem wird eine kalibrierte Pipette, die sogenannte Bloom-Pipette, im Einklang mit DIN 53 260 verwendet [88]. Das Ergebnis der Auslaufzeit von 100 mL Gelatine-Lösung aus der Bloom-Pipette mit einer geeichten Kapillare wird in mPa s ausgedrückt [64]. Grundsätzlich hängt die Viskosität von Gelatine-Lösungen von der Gelatine-Konzentration, dem Lösungsmittel, den enthaltenen Salzen, dem pH-Wert und der Temperatur ab. [62] Je höher die Gelatine-Konzentration der Lösung ist, desto weniger Einfluss haben die anderen Faktoren. Dies wird durch die Annäherung deutlich, dass die Viskosität von Gelatine-Lösungen eine exponentielle Funktion der Gelatine-Konzentration ist. Die Viskosität konzentrierter Gelatine-Lösungen wird ausschließlich durch die hydrodynamischen Interaktionen zwischen den Gelatine-Molekülen bestimmt, da eine höhere Konzentration die Moleküle räumlich näher zusammenbringt. Außerdem wurde eine Korrelation zwischen der Viskosität und dem Anteil an hochmolekularen Komponenten der Gelatine beobachtet, wobei eine höhere Viskosität mit einem

hohen Anteil hochmolekularer Komponenten einhergeht [64]. Darüber hinaus wurde gezeigt, dass die Viskosität von Gelatine-Lösungen am IEP der verwendeten Gelatine am geringsten ist [62].

Die Definition des IEPs lautet "der pH-Wert, bei dem die elektrische Nettoladung einer Elementarentität null ist" [33]. Der IEP ist ein entscheidendes Charakteristikum von Proteinen, welche aus positiv und negativ geladenen Aminosäuren bestehen und deshalb Polyampholyte sind. Die Ladung der Aminosäuren entsteht durch deren saure oder basische funktionelle Gruppen. Der IEP von Gelatine ist für deren Anwendung, beispielsweise in der Pharmazie, entscheidend. Der IEP wird durch eine chromatographische Ionen-Austausch-Methode bestimmt, die von Janus, Kenchington und Ward im Jahr 1951 entwickelt wurde. [89] Bei dieser Methode werden Mischbettt-Ionen-Austauscher-Harze verwendet, um eine Gelatine-Lösung bei 30 °C zu deionisieren. Der pH-Wert der deionisierten Gelatine-Lösung entspricht dem isoionischen Punkt der Gelatine, welcher nahezu identisch mit deren IEP ist. Andere Methoden zur IEP-Bestimmung sind beispielsweise die isoelektrische Fokussierung oder pH-abhängige Messungen der Trübung der Lösung [90]. Wenn die Aminosäuren-Zusammensetzung bekannt ist, kann der IEP auch abgeschätzt werden [91]. Im Fall von Gelatine ist der Herstellungsprozess für den IEP entscheidend. [61, 62, 64, 70] Wie bereits beschrieben wurde, wird während der alkalischen Konditionierung Ammoniak aus Glutamin und Asparagin frei, sodass sie zu Glutamin- und Asparaginsäure werden. Diese Zunahme an Carboxyl-Gruppen in der Gelatine führt zu einem reduzierten IEP von  $G_B$  (IEP bei pH 5-6) verglichen mit  $G_A$  und deren Ursprungs-Protein Kollagen (IEP bei pH 8-10).

Die Molekulargewichtsverteilung von Gelatine ist ebenfalls abhängig von der Art des Herstellungsprozesses, und somit vom Gelatine-Typen, sowie der Intensität des Herstellungsprozesses. [61, 64] Gelatine ist das Produkt der Kollagen-Hydrolyse und besteht somit aus Polypeptid-Ketten mit unterschiedlichen Längen. Allerdings ist dieser hydrolytische Abbau von Kollagen während des Gelatine-Herstellungsprozesses nicht rein zufällig. Typischerweise wird Größenausschluss-Chromatographie verwendet, um die Molekulargewichtsverteilung zu untersuchen. [64] Dabei wird das Polymer in einem definierten Lösemittel gelöst. Diese Lösung wird dann in eine Chromatographie-Säule mit einem definierten Porengrößengradienten injiziert. Bei Polyampholyten wie Gelatine muss deren IEP und die Ladung der verwendeten Säule beachtet werden. Das Polymer durchläuft die Säule in Abhängigkeit von seinem Molekulargewicht, wobei kleine Polymere mehr mit der Säule interagieren als große Polymere und deshalb längere Retentionszeiten haben. Das mittlere Molekulargewicht von  $G_A$  (70-90 kDa [61]) ist ähnlich zu der Primärstruktur von Kollagen Typ I (~100 kDa [64]), wohingegen das mittlere Molekulargewicht von  $G_B$  niedriger ist (50-70 kDa [62]). Nach Schrieber und Garais entspricht die Fraktion mit einem Molekulargewicht von ~100 kDa den  $\alpha$ -Ketten, die für die Gelierkraft entscheidend sind und die Fraktion mit ~200-400 kDa den Ketten die die

Viskosität bestimmen [64]  $G_B$  besitzt mehr  $\alpha$ -Ketten als  $G_A$  und  $G_A$  hat eine breitere Molekulargewichtsverteilung als  $G_B$ .

Es gibt mehr Standardcharakterisierungen für Gelatine als die hier beschriebenen, zum Beispiel Wassergehalt, Leitfähigkeit, Gehalt an anorganischen Komponenten und der pH [64]. Bei der Verwendung von Gelatine muss beachtet werden, dass sich einige Materialeigenschaften gegenseitig beeinflussen. Deshalb muss die Herstellung von Gelatine-Lösungen und -Hydrogelen genau und gewissenhaft durchgeführt werden. Darüber hinaus müssen Gelatine-Typ, verwendete Konzentration, thermische Geschichte und pH der Lösungen und der verwendeten Puffer für jede Untersuchung angegeben werden um aussagekräftige Ergebnisse zu kommunizieren.

## 2.3 Gelatine-Methacryloyl

Gelatine-Methacryloyl (GM) wird seit der Publikation von Van den Bulcke *et al.* im Jahr 2000 [42] als Biomaterial untersucht. GM besitzt wie das Rohmaterial Gelatine noch Erkennungssequenzen, um von Matrix-Metalloproteasen, wie beispielsweise den Kollagenasen, degradiert werden zu können [34]. Des Weiteren enthält GM das Arginin-Glycin-Asparaginsäure (RGD)-Peptid, an das Zellen Integrin-vermittelt adhären können [35]. Es wurde gezeigt, mechanische Signale über RGD-abhängige Integrine von Chondrozyten aufgenommen werden [92]. Im Folgenden wird die Synthese und Charakterisierung von GM und deren Vernetzung zu Hydrogelen erläutert. **Synthese und Charakterisierung von Gelatine-Methacryloyl**

Während der GM-Synthese werden sowohl Amino- als auch Hydroxylgruppen, typischerweise mit Methacrylsäureanhydrid, umgesetzt. [93] Dabei ist die Reaktivität von Aminogruppen während der Methacryloylierung höher als die von Hydroxylgruppen [50, 94]. Obwohl in der Veröffentlichung von Nazarova *et al.* [41] GM bereits als „Methacryloyl Derivat“ bezeichnet wurde, wurde GM nach der Publikation von Van den Bulcke *et al.* [42] als „Gelatine-Methacrylamid“ benannt. Diese Benennung wurde dann erneut zu „Gelatine Methacryloyl“ geändert, sodass Methacrylamide und Methacrylate in der Benennung berücksichtigt werden.

Um den Stand der Wissenschaft zu Synthese und Charakterisierung von GM darzustellen, wurde eine Literaturrecherche durchgeführt, bei der alle Publikationen berücksichtigt wurden, in denen die Publikation von Van den Bulcke *et al.* [42] zitiert ist, GM synthetisiert wurde und die vor Juni 2019 publiziert wurden. Ausgeschlossen von dieser Literaturrecherche wurden die Publikationen, die im Rahmen dieser Dissertation veröffentlicht wurden ([95-97]). Aus diesen 223 Publikationen [35, 42, 45-47, 49-53, 94, 98-309], in denen 231 Synthese-Vorgehen beschrieben werden, wurden die Angaben zur Synthese und der Charakterisierung von GM gesammelt und im Folgenden dargestellt. In **Abbildung 7**

ist die Anzahl der berücksichtigten Publikationen, in denen GM synthetisiert wurde, von 2000 bis Juni 2019 kumulativ aufgetragen. Von 2000 bis einschließlich 2010 wurden nur 11 Publikationen veröffentlicht, das entspricht 5 % aller berücksichtigten Veröffentlichungen. Zwischen 2011 und 2016 wurden insgesamt 79 Publikationen veröffentlicht (30 %) und somit 144 (65 %) zwischen 2016 und Juni 2019. Diese Entwicklung verdeutlicht, dass GM als (Bio)-Material zunehmend an Bedeutung gewinnt und als solches untersucht wird.

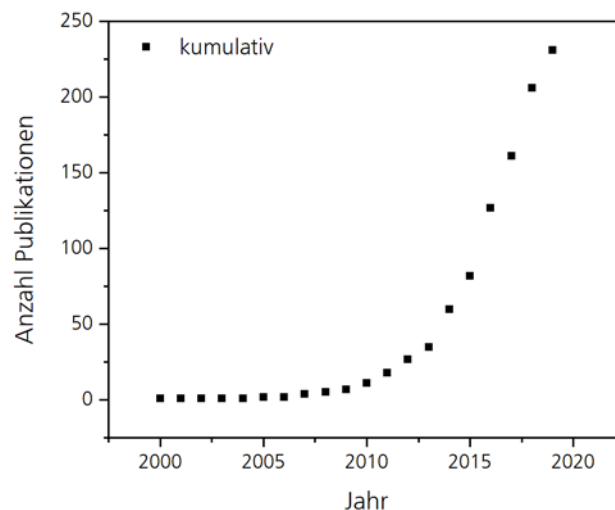


**Abbildung 7:** Kumulative Darstellung der Publikationen, die zwischen 2000 und Juni 2019 veröffentlicht, GM synthetisiert wurde und die Publikation von Van den Bulcke *et al.* [42] zitiert wurde [35, 42, 45-47, 49-53, 94, 98-309].

Der Herstellungsprozess der Gelatine bestimmt, wie in Kapitel 2.2 bereits erläutert, den Gelatine-Typ und weitere Eigenschaften. Jedoch wurden in den überprüften Publikationen meist nur wenige, bis hin zu gar keinen Angaben zu der verwendeten Gelatine gemacht. Der prozentuale Anteil an Publikationen, die die jeweiligen Angaben machten, ist im Folgenden in Klammern angegeben: Hersteller (86 %), Gelatine-Typ (77 %), tierischer Ursprung (71 %), Bloom Wert (42 %), IEP (7 %), Aminogruppen-Gehalt (2 %) und Standard-Viskosität (1 %). Nur in der Publikation von Van den Bulcke *et al.* wurden alle Materialeigenschaften genannt [42].

In **Tabelle 1** ist aufgeschlüsselt, welche unterschiedlichen Gelatine-Typen und tierischen Ursprünge der Gelatine in den betrachteten Veröffentlichungen verwendet wurden. Am häufigsten (53,2 %) wurde  $G_A$  verwendet, während  $G_B$  nur in 23,4 % aller GM-Synthesen verwendet wurde. In 23,4 % der beschriebenen GM-Synthesen wurde der Gelatine-Typ nicht genannt. Als tierischer Ursprung wurde am häufigsten Gelatine porciner Herkunft verwendet (48,5 %), gefolgt von boviner Herkunft (19,0 %) und Gelatine aus Fisch (2,6 %). Eine GM-Synthese wurde mit rekombinanter Gelatine beschrieben [100] und in 29,4 % der Veröffentlichungen wurde keine Angabe zum tierischen Ursprung gemacht.

**Tabelle 1:** Gegebene Information über Gelatine-Typ und tierischen Ursprung der für die GM-Synthese verwendeten Gelatine von 2000 bis Juni 2019 publizierten Studien, in denen GM synthetisiert wurde und in denen die Publikation von Van den Bulcke *et al.* [42] zitiert wurde [35, 42, 45-47, 49-53, 94, 98-309]. In den berücksichtigten 223 Veröffentlichungen wurden 231 GM-Synthesen beschrieben.

<b>Gelatine-Typ</b>	<b>Tierischer Ursprung</b>	<b>Anzahl Studien absolut</b>	<b>Anzahl Studien relativ</b>
Typ A	Porcine Haut	93	40,3%
	Porcin	3	1,3%
	Bovine Haut	2	0,9%
	Keine Spezifizierung	25	10,8%
Typ B	Bovine Haut	23	10,0%
	Bovine Knochen	9	3,9%
	Bovin	6	2,6%
	Porcine Haut	4	1,7%
	Keine Spezifizierung	12	5,2%
Keine Spezifizierung	Bovin	1	0,4%
	Bovine Haut	3	1,3%
	Kalt-löslich, porciner Ursprung	1	0,4%
	Kaltwasserfisch-Haut	5	2,2%
	Fisch	1	0,4%
	Porcine Haut	11	4,8%
	Rekombinant	1	0,4%
	Keine Spezifizierung	31	13,4%

Für die GM-Synthese wurden Gelatinen mit Bloom-Werten zwischen 70-300 Bloom verwendet, wobei die meisten Gelatinen einen Bloom-Wert von 300 besaßen (23,8 %) [49, 50, 98, 102, 104, 106, 118, 122, 127, 131, 134, 135, 140, 143, 146, 166, 169, 170, 173, 175, 179, 180, 182, 185, 186, 188, 189, 202, 208-213, 215, 220, 225, 227, 229, 235, 242, 244, 249, 254, 259, 264, 273, 278, 279, 281-283, 288, 291, 293] und nur zwei Synthesen wurden mit einer Gelatine mit einem Bloom-Wert, der geringer als 130 war, durchgeführt [232, 234]. In den übrigen GM-Synthesen wurden Gelatinen mit Bloom-Werten zwischen 160 und 260 Bloom (38 %) verwendet [42, 94, 99, 101, 103, 110-112, 120, 124, 125, 132, 136, 148, 151, 157, 160, 162, 163, 177, 184, 194, 196, 198, 221, 231, 233, 265, 268, 271, 275, 294, 295, 300, 301, 305, 309, 310]. Die Standardviskosität der verwendeten Gelatinen wurde nur in zwei Publikationen angegeben und lag bei 4,88 mPa s [42, 112]. In vier Publikationen wurde darüber hinaus der Aminogruppen-Gehalt experimentell bestimmt, dieser lag typischerweise zwischen 0,3 und 0,4 mmol g<sup>-1</sup> [42, 94, 124], nur ein Aminogruppen-Gehalt lag mit 0,075 mmol g<sup>-1</sup> außerhalb dieses Bereichs [184]. In vielen Veröffentlichungen wurde der Aminogruppen-Gehalt von 0,35 mmol g<sup>-1</sup>, der von Van den Bulcke *et al.* [42] publiziert wurde, zitiert.

Die GM-Synthese-Durchführung in allen Publikationen ist sehr ähnlich. Das Rohmaterial wird typischerweise in destilliertem Wasser oder phosphatgepufferter Salzlösung gelöst. Anschließend wird Methacrylsäureanhydrid hinzugegeben und bei Temperaturen zwischen 37 °C und 60 °C für 1-6 h oder in Einzelfällen 12-72 h [140, 142, 144, 230, 256, 265] gerührt. In einigen Studien wurde der pH-Wert der Lösung während dieser Zeit nachjustiert, sodass der pH der Lösung neutral oder leicht basisch war [94, 100, 108, 120, 123-125, 177, 189, 221, 229, 242, 299]. Anschließend wird die Reaktionslösung für 1-7 d gegen destilliertes Wasser bei max. 50 °C dialysiert, um das Nebenprodukt Methacrylsäure zu entfernen. Die Lösung wird gefriergetrocknet und bei Raumtemperatur, 4 °C oder -20 °C gelagert.

Der Aminogruppen-Gehalt des Rohmaterials für die GM-Synthese ist insofern interessant, dass lange davon ausgegangen wurde, dass nur die Aminogruppen während der Methacryloylierung umgesetzt werden. Deshalb wurde der Methacryloylierungsgrad (englisch *degree of methacryloylation*, DM) relativ als Anteil der modifizierten Aminogruppen angegeben. Die noch zugänglichen Aminogruppen wurden beispielsweise mit dem Trinitrobenzolsulfonsäure (TNBS)-Assay nach Habeeb quantifiziert [311], oder durch das reduzierte Signal der  $\epsilon$ -Methylengruppen der Lysine im  $^1\text{H-NMR}$ -Spektrum bei  $\sim 2,8\text{-}2,95$  ppm. Inzwischen wurden neue Methoden zur Quantifizierung des DMs entwickelt, die auch die Methacrylate berücksichtigen und ein differenzieren von Methacrylamid- und Methacrylat-Gruppen ermöglichen [50, 94]. Obwohl diese Methoden zur Verfügung standen, haben nur drei Veröffentlichungen diese angewendet, um den DM zu bestimmen [94, 271, 295]. Weitere vier Veröffentlichungen nutzen andere Methoden, um den DM in  $\text{mmol g}^{-1}$  Gelatine und nicht bezogen auf den Aminogruppen-Gehalt angeben zu können [175, 242, 281, 294]. In 118 Studien (48 %) wurde der DM als substituierte Aminogruppen in % angegeben und in allen übrigen 107 der überprüften Publikationen wurde kein DM angegeben, das entspricht 45 %.

Auch alle anderen Standard-Methoden zur Charakterisierungen von Gelatine wurden bisher bei der Charakterisierung von GM vernachlässigt. Wenige Autoren bestimmten die Viskosität von GM-Lösungen in Abhängigkeit von der Polymerkonzentration und der Temperatur und ermittelten so auch Gel- und Schmelzpunkt der Lösungen [42, 120, 125, 146, 298]. Auch die Molekulargewichtsverteilung der GM wurde nur in sechs Publikationen untersucht [100, 124, 154, 208, 255, 303]. Der IEP von GMs wurde bisher beispielsweise nicht untersucht. Die vollständige Charakterisierung der GM-Derivate ist jedoch notwendig, um Ergebnisse vergleichen zu können und die systematische und kontrollierte Anwendung von GM als Biomaterial zu ermöglichen.

### 2.3.2 Chemisch vernetzte Gelatine-Methacryloyl-Hydrogele

Während der GM-Synthese werden Methacryloyl-Gruppen in die Gelatine eingebracht. Diese Methacryloyl-Gruppen besitzen C=C-Doppelbindungen, die dann durch einen Radikalstarter



polymerisiert werden können. Durch Polymerisierung der C=C-Doppelbindungen werden die GM-Moleküle kovalent miteinander vernetzt. Diese chemische Vernetzung der GM-Moleküle führt zu einem Polymernetzwerk, sodass sich die GM-Lösung verfestigt und ein Hydrogel entsteht. Die Verwendung von Photoinitiatoren für die Vernetzung von GM hat die Vorteile, dass die Vernetzung zeitlich und räumlich gesteuert werden kann. [312] Darüber hinaus hat der Einsatz von Photoinitiatoren Vorteile bei der Verkapselung von Zellen, da die Vernetzung schnell und ohne hohe Temperaturen oder extreme pH-Wert-Änderungen verläuft.

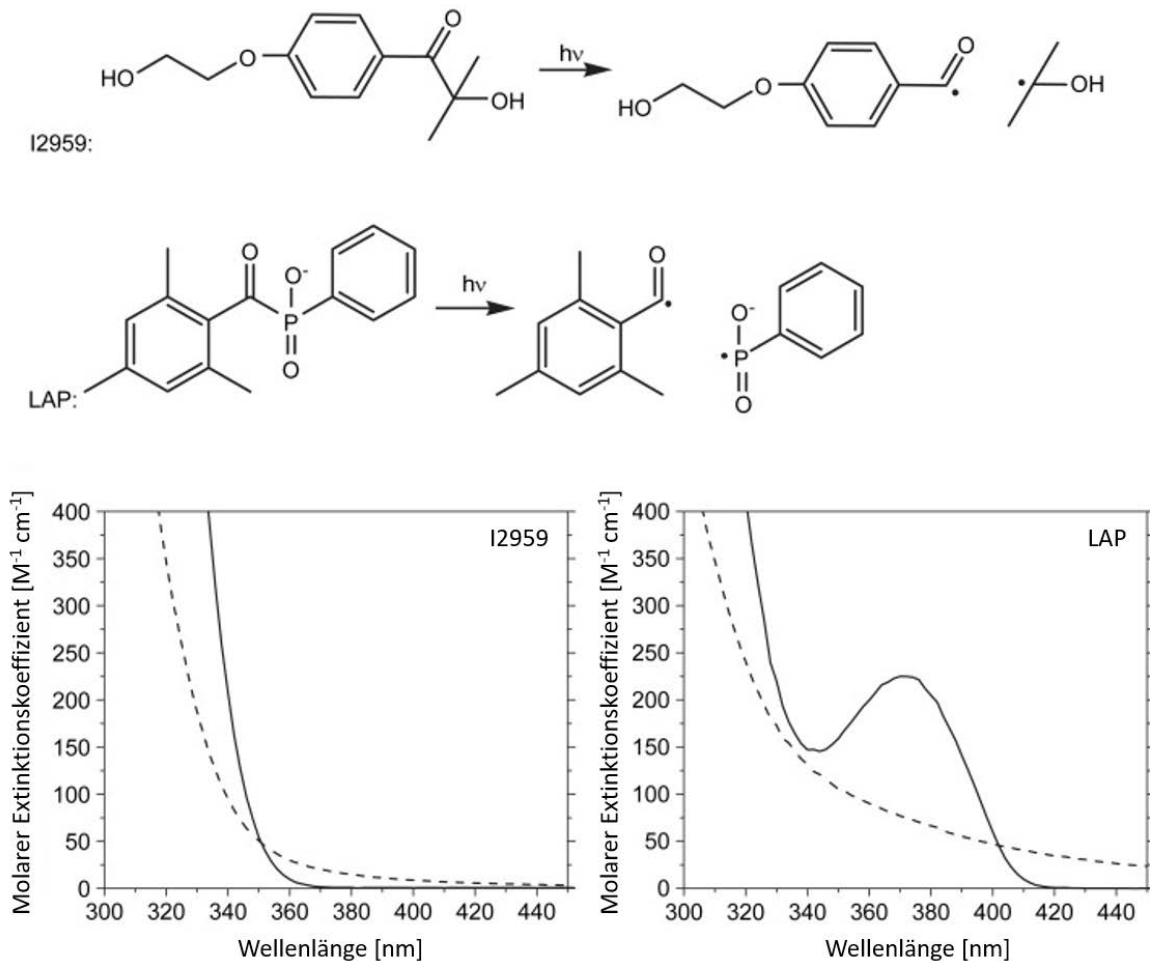


**Abbildung 8:** Oben: Chemische Struktur und Spaltung der zwei Photoinitiatoren 1-[4-2(Hydroxyethoxy)-phenyl]-2-hydroxy-2-methyl-1-propanon (I2959) und Lithiumphenyl-2,4,6-trimethylbenzoylphosphinat (LAP). Unten: Molare Absorption der Photoinitiatoren (durchgezogene Linie) und deren Spaltungsprodukten (gestrichelte Linie). Nachdruck mit Genehmigung von Elsevier: Elsevier Ltd., Photoinitiated polymerization of PEG-diacrylate with lithium phenyl-2,4,6-trimethylbenzoylphosphinate: polymerization rate and cytocompatibility, B. D. Fairbanks *et al.*, © 2009. [313] Anmerkung: Die Beschriftungen in der Abbildung wurden übersetzt.

Für die radikalische Vernetzung von zellhaltigen Hydrogelen wird typischerweise 1-[4-2(Hydroxyethoxy)-phenyl]-2-hydroxy-2-methyl-1-propanon (I2959) als Photoinitiator verwendet [313]. Die Strukturformel und der Zerfall von I2959 ist in **Abbildung 8** dargestellt. Der I2959 wird für die Zellverkapselung verwendet, da er in Konzentrationen bis max. 2 Gew.-% wasserlöslich ist [314]. Wie an dem Absorptionsspektrum von I2959 zu sehen ist (**Abbildung 8**, unten links), ist der molare

Extinktionskoeffizient für Wellenlängen größer 350 nm jedoch sehr gering bzw. gleich null. Da Proteine und Desoxyribonukleinsäuren bei 280 nm bzw. 260 nm Strahlung absorbieren, werden für die Verkapselung von Zellen möglichst längere Wellenlängen um 365 nm eingesetzt, um phototoxische oder mutagene Effekte zu vermeiden [315-317]. Die Vernetzung von zellhaltigen GM-Hydrogelen mit I2959 bei 365 nm ist somit relativ ineffizient, weshalb verhältnismäßig hohe I2959-Konzentrationen und lange UV-Bestrahlungen für die Vernetzung von GM zu Hydrogelen notwendig sind, die wiederum zytotoxisch sein können.

Ein anderer, bisher weniger häufig eingesetzter Photoinitiator für die Vernetzung von zellhaltigen GM-Hydrogelen ist Lithiumphenyl-2,4,6-trimethylbenzoylphosphinat (LAP). Die Synthese sowie die Wasserlöslichkeit bis 8,5 Gew.-% von LAP wurde von Majima *et al.* publiziert [318]. In **Abbildung 8** ist die chemische Struktur und der Zerfall von LAP sowie das Absorptionsspektrum dargestellt. LAP hat bei 365 nm einen molaren Extinktionskoeffizienten von etwa  $175 \text{ M}^{-1} \text{ cm}^{-1}$ . In einer Studie, die die Vernetzung von Polyethylenglycol-Diacrylat mit I2959 und LAP verglich, konnten Fairbanks *et al.* zeigen, dass die Vernetzung mit LAP deutlich effizienter war als die Vernetzung mit I2959. [313] LAP vernetzte die Hydrogele in weniger als einem Zehntel der Zeit, die bei der Vernetzung mit I2959 benötigt wurde. Bei der Vernetzung mit LAP bei 405 nm konnten außerdem UV-Strahlung und Initiator-Konzentration reduziert werden. Außerdem konnte die Zytokompatibilität des LAPs für die Verkapselung von Fibroblasten gezeigt werden. Andere Studien wiesen die Zytokompatibilität von LAP für die Verkapselung von Adipozyten [319] und aus Fettgewebe gewonnenen Stammzellen [320] in GM-Hydrogelen nach.

Zur Herstellung von GM-Hydrogelen werden meist wässrige Lösungen mit einem GM-Gehalt von 5-20 Gew.-% verwendet [100, 104, 120]. Die Hydrogelvorläuferlösung beinhaltet typischerweise 0,05-0,10 Gew.-% I2959 [102, 119, 127] und ist zwischen 37 °C und 60 °C warm [45, 131, 138, 140]. Die zur Vernetzung eingesetzten Wellenlängen, Intensität sowie die Vernetzungsdauer variieren zwischen 276-515 nm [106, 109, 137, 150], 2,6-17,5  $\text{mW cm}^{-2}$  [42, 52, 121, 140, 143] und 5 s-120 min [46, 52, 101, 107, 109, 135]. Leider wird die Vernetzung der GM-Hydrogele meist nur unzureichend erläutert, sodass die aufgeführten Angaben oft nicht gemacht werden. Deshalb war auch kein Vergleich der verwendeten UV-Dosen möglich.

Auch die mechanische Charakterisierung der erzeugten GM-Hydrogele wird oft vernachlässigt. Es wird häufig der Speichermodul  $G'$  oder der Kompressionsmodul untersucht, wobei Speichermoduln von 0,09-133 kPa [100, 102, 120, 154] und Kompressionsmoduln von 1-180 kPa [45, 127, 141, 297, 298] berichtet wurden. Betrachtet man die Anwendung von GM-Hydrogelen als *Scaffold* im TE ist die mechanische Charakterisierung essenziell, um diese als Einflussfaktor auf das Zellverhalten zu berücksichtigen. Deshalb gilt auch für die GM-Hydrogele, dass deren vollständige Charakterisierung

notwendig ist, um Ergebnisse vergleichen zu können und somit die Anwendung von GM-Hydrogelen als Biomaterial zu ermöglichen.

### 2.3.3 Sequenziell vernetzte Gelatine-Methacryloyl-Hydrogele

Neben der rein chemischen Vernetzung, bei der die GM-Moleküle über die Polymerisierung der C=C-Doppelbindungen vernetzt werden, wurde die sequenzielle Vernetzung von GM-Hydrogelen untersucht. Während der sequenziellen Vernetzung werden die Hydrogelvorläuferlösung zunächst abgekühlt, sodass ein physikalisches Hydrogel entsteht und anschließend chemisch vernetzt. Durch die sequenzielle Vernetzung wurde der Kompressionsmodul [45, 302], Speichermodul [303] und Elastizitätsmodul [298] im Vergleich zu rein chemisch vernetzten GM-Hydrogelen erhöht. Durch diese Verfestigung gelten sequenziell vernetzte GM-Hydrogele als besonders geeignet für den Einsatz als Gerüststruktur für das *Tissue Engineering* von lasttragenden Geweben.

Die erste Studie, die physikalisch gelierte und anschließend chemisch vernetzte GM-Hydrogele verglich, war die Studie von Schuurman *et al.* im Jahr 2013. [45] Es wurden GM-Hydrogele mit 10 Gew.-% und 20 Gew.-% GM (DM:  $75 \pm 9$  % der potenziell vorhandenen Aminogruppen) hergestellt, wobei die Hydrogelvorläuferlösungen entweder bei 37 °C, oder nach einer 15-minütigen Kühlung auf 25 °C chemisch vernetzt wurden. Während dieser Kühlung gelierten die GM-Hydrogelvorläuferlösungen und bildeten physikalische Hydrogele, die dann chemisch vernetzt wurden. Es konnte gezeigt werden, dass das sequenzielle Vernetzen der Hydrogelvorläuferlösung den Kompressionsmodul der resultierenden Hydrogele signifikant steigerte: Der Kompressionsmodul der rein chemischen Hydrogele lag bei  $\sim 30$  kPa (10 Gew.-%) bzw.  $\sim 175$  kPa (20 Gew.-%) und der der sequenziellen Hydrogele bei  $\sim 55$  kPa (10 Gew.-%) und  $\sim 270$  kPa (20 Gew.-%). Diese Verfestigung wurde auf die während der physikalischen Gelierung ausgebildeten Tripel-Helices zurückgeführt. Der Kompressionsmodul wurde somit durch das sequenzielle Vernetzen um mehr als das eineinhalbfache gesteigert und war unabhängig von der Temperatur während des Messens. Damit wurde gezeigt, dass die thermo-responsiven Eigenschaften der GM durch die chemische Vernetzung verloren gingen. Das wies darauf hin, dass die Polymerketten in der Form fixiert werden, in der sie chemisch vernetzt werden, entweder zufällig oder in einer hierarchischen Konformation und dass die Ausbildung von hierarchisch organisierten Helices die Druckstabilität steigert.

In einer späteren Studie von Bartnikowski *et al.* im Jahr 2015 wurde unter anderem der Einfluss unterschiedlicher Kühlprotokolle vor der chemischen Vernetzung auf den Elastizitätsmodul untersucht. [298] Die Hydrogelvorläuferlösungen (10 Gew.-% GM, DM: 76,2 % der potenziell vorhandenen Aminogruppen) wurden entweder bei 37 °C chemisch vernetzt, nach 20 min Kühlung bei Raumtemperatur oder nach 10 min Kühlung bei 4 °C. Der ermittelte Elastizitätsmodul der rein chemisch

vernetzten Hydrogele war 74 kPa. Der Elastizitätsmodul der mit zwei unterschiedlichen Kühlprotokollen hergestellten physikalisch gelierten und anschließend chemisch vernetzten GM-Hydrogele war nicht unterscheidbar, aber signifikant höher als der der rein chemisch vernetzten GM-Hydrogele (104 kPa). Dieser Effekt wurde wie zuvor von Schuurman *et al.* [45] auf die Ausbildung von Tertiärstrukturen während des Kühlprozesses zurückgeführt. Darüber hinaus wurden Vorteile der sequenziellen Vernetzung von GM-Hydrogelen für die Verkapselung von Zellen formuliert [298]: Durch die physikalische Gelierung können Zellen gleichmäßiger im Hydrogel verteilt werden, da sie aufgrund der Gelierung nicht absinken können, sondern an der jeweiligen Stelle fixiert werden. Außerdem wird der Einfluss der Kühlung während der UV-Vernetzung der auftritt, falls die UV-Bestrahlungskammern nicht temperiert werden, auf die Eigenschaften der GM-Hydrogele minimiert.

Rizwan *et al.* benannten sequenzielle GM-Hydrogele in ihrer Veröffentlichung von 2016 als erste als „sequenzielle“ Hydrogele. [302] Es wurden durch die Vernetzung der Hydrogelvorläuferlösung bei 37 °C rein chemische GM-Hydrogele (10 Gew.-%, 20 Gew.-% und 30 Gew.-%, DM: 39 % der potenziell vorhandenen Aminogruppen) hergestellt und sequenzielle GM-Hydrogele, die vor der chemischen Vernetzung für eine Stunde bei 4 °C gekühlt wurden. Der Kompressionsmodul der sequenziellen Hydrogele war wiederum signifikant höher als der der rein chemischen GM-Hydrogele und nahm mit der verwendeten GM-Konzentration zu: Die Moduln der rein chemischen Hydrogele lagen bei ~7 kPa (10 Gew.-%), ~35 kPa (20 Gew.-%), ~50 kPa (30 Gew.-%) und die der sequenziellen Hydrogele bei ~28 kPa (10 Gew.-%), ~100 kPa (20 Gew.-%) und ~228 kPa (30 Gew.-%). Darüber hinaus wurde die Mikrostruktur der Hydrogele mittels Rasterelektronenmikroskopie untersucht und gezeigt, dass sequenzielle Hydrogele im getrockneten Zustand kleinere durchschnittliche Porendurchmesser besaßen und homogener strukturiert waren. Außerdem wurden unterschiedlich hergestellten GM-Hydrogele mittels Fourier-Transform-Infrarotspektroskopie (FTIR) untersucht und gezeigt, dass nur für rein chemisch vernetzte GM-Hydrogele eine Schulter bei 1634 cm<sup>-1</sup> beobachtet wurde, was auf C=C-Doppelbindungen hinweist. Deshalb wurde geschlossen, dass die sequenzielle Vernetzung zu einem höheren C=C-Doppelbindungsumsatz führte und somit zu einer effizienteren chemischen Vernetzung, was neben der Möglichkeit der Stabilisierung durch Helix-Bildung die festeren Hydrogele erklären könnte. Mittels Circular dichroismus (CD)-Spektroskopie wurde dann durch eine positive Bande bei ~220 nm nachgewiesen, dass die verwendeten GM-Lösungen bei 4 °C, wie ihr Rohmaterial, Tripel-Helices ausbilden. [302] Deshalb wurde die Verfestigung der GM-Hydrogele durch die sequenzielle Vernetzung auf die Ausbildung von Tripel-Helices zurückgeführt, die möglicherweise zu einem höheren C=C-Doppelbindungsumsatz und einer höheren Homogenität führte. Außerdem wurden durch Rizwan *et al.* die Ergebnisse von Bartnikowski *et al.* [298] bestätigt, dass die mechanischen Eigenschaften der Hydrogele temperaturunabhängig waren.

Van Hoorick *et al.* untersuchten 2018 erstmals den Einfluss der sequenziellen Vernetzung auf GM-Hydrogele aus GMs mit einem hohen DM, indem neben den primären Aminen auch die Hydroxylgruppen der Carbonsäuren methacryloyliert wurden. [303] Es wurden Hydrogele aus GM mit einem DM von  $0,37 \text{ mmol g}^{-1}$  (97 % Umsetzung der Aminogruppen, gel-MOD) und  $0,99 \text{ mmol g}^{-1}$  (gel-MOD-AEMA) verglichen. Dynamische-Differenzkalorimetrie-Messungen zeigten, dass gel-MOD noch  $\sim 95$  % aller physikalischen Interaktionen des Rohmaterials eingehen konnte, wobei gel-MOD-AEMA nur noch  $\sim 30$  % ausbilden konnte und die Geliertemperatur mit zunehmendem DM abnahm. Die chemische Vernetzung wurde *in situ* anhand des Speichermoduls gemessen und gezeigt, dass bei der sequenziellen Vernetzung der Speichermodul zunächst während der Kühlung zunimmt und dann stärker während der chemischen Vernetzung. Die resultierenden Speichermoduln zeigten erneut, dass sequenzielle GM-Hydrogele signifikant höhere Speichermoduln besaßen als rein chemische GM-Hydrogele.

Die dargestellten Studien zeigten, dass die zuerst physikalisch gelierten und anschließend chemisch vernetzten GM-Hydrogele höhere Speicher- und Kompressionsmoduln besaßen als rein chemisch vernetzte GM-Hydrogele. Mithilfe von CD-Spektroskopie und dynamischer Differenzkalorimetrie konnte gezeigt werden, dass es während der Kühlung zu physikalischen Wechselwirkungen in GM-Lösungen kommt die zu Tripel-Helices und zur Gelierung der Lösung führen. Es wird vermutet, dass die physikalische Gelierung dazu führt, dass sich vernetzbare Methacryloyl-Gruppen akkumulieren und es so bei der chemischen Vernetzung zu einem effizienteren C=C-Doppelbindungsumsatz kommt als bei der Vernetzung von ungekühlten GM-Lösungen. Diese Hypothese wird bisher jedoch nur durch die Ergebnisse der qualitativen FTIR-Messung von Rizwan *et al.* [302] untermauert. Auch das physikalische Netzwerk, das während der Kühlung ausgebildet wird, scheint zur Verfestigung der sequenziellen Hydrogele beizutragen, da sich dadurch die Vernetzungsdichte erhöht.

Um die Mechanismen hinter der Verfestigung durch die sequenzielle Vernetzung von GM-Hydrogelen wurde aufzuklären, sollte der Einfluss der physikalischen Gelierung und chemischen Vernetzung differenziert werden. Dafür könnten hoch-modifizierte GM-Derivate verwendet werden, die einen sehr niedrigen Gelpunkt haben. Dadurch könnte auch überprüft werden, ob die sequenzielle Vernetzung auch Hydrogele aus diesen hoch-modifizierten GM-Derivaten (Methacryloylierung von Amino- und Hydroxylgruppen) verfestigt werden. Außerdem wäre für die Erforschung von GM-Hydrogelen als Biomaterialien interessant, den Gehalt an nicht-vernetzten C=C-Doppelbindungen zu kennen, somit ist eine quantitative Analyse der chemischen Vernetzung erstrebenswert.

## 3. Ziel und Hypothesen der Arbeit

### 3.1 Ziel der Arbeit

Das Ziel dieser Arbeit war es, Gelatine-Methacryloyl (GM) und deren Vernetzung zu Hydrogelen für die potenzielle Anwendung im *Tissue Engineering* systematisch zu charakterisieren und ein *proof-of-concept* eines GM-basierten zonalen Gelenkknorpel-Äquivalent zu erbringen. Hierfür sollte zunächst der Einfluss des für die GM-Synthese verwendeten Gelatine-Typs auf die resultierenden Eigenschaften der GM, ihrer Lösungen und Hydrogele untersucht werden. Anschließend wurde die sequenzielle Vernetzung, bei der die Hydrogelvorläuferlösungen vor der chemischen Vernetzung gekühlt werden, untersucht, da sie zur Verfestigung von GM-Hydrogelen führt und deshalb besonders geeignet zu sein scheint, um zellhaltige Hydrogele als *Scaffold* für das Gelenkknorpel-*Tissue-Engineering* aufzubauen. Mithilfe der sequenziellen Vernetzung sollte ein zonales Hydrogel mit einem biomimetischen Glykosaminoglykan-Gradienten zytokompatibel dargestellt werden. Die Eignung des zonalen Hydrogels als *Scaffold* für das Gelenkknorpel-*Tissue-Engineering* sollte anhand der Redifferenzierung dedifferenzierter, im Hydrogel verkapselter, Chondrozyten gezeigt werden.

Dieser Dissertation unterliegen wissenschaftliche Fragen, die als Hypothesen formuliert wurden. Diese drei Hypothesen werden im Folgenden erläutert. Anschließend werden die Ergebnisse zu den Untersuchungen der Hypothesen in den Kapiteln 4, 5 und 6 dargestellt und diskutiert. Des Weiteren werden die Ergebnisse im Zusammenhang in Kapitel 7 zusammenfassend diskutiert. Die Arbeit wird von den Schlussfolgerungen und dem Ausblick (Kapitel 8 und 9) abgeschlossen.

### 3.2 Hypothesen

#### **Hypothese 1**

In der Biomaterialforschung wird die Anwendung von GM umfassend untersucht, beispielsweise als Biotinte für das *Bioprinting* und als Gerüststruktur für künstliche Gewebe. Jedoch wird der Einfluss des verwendeten Gelatine-Rohmaterials bisher ignoriert, sodass in einigen Publikationen keine Angaben zum Gelatine-Typen oder zum Hersteller gemacht werden. Die folgende Hypothese wurde aufgestellt:

*Die Wahl des Gelatine-Rohmaterials und der Modifizierungsgrad beeinflussen die physikochemischen Eigenschaften von Gelatine Methacryloyl und den resultierenden Hydrogelen.*

In diesem Kontext wurden fünf Gelatine-Methacryloyl (-Acetyl)-Derivate mit Gelatine Typ A und Gelatine Typ B mit dem gleichen Vorgehen synthetisiert. Die Derivate wurden charakterisiert und

verglichen, wobei der Methacryloylierungsgrad, Acetylierungsgrad, Viskosität, Gelier- und Schmelztemperatur, isoelektrischer Punkt, hydrodynamischer Radius sowie Speicher- und Verlustmodul der resultierenden Hydrogele untersucht wurden. Diese Studie wurde in der *peer-reviewed* Fachzeitschrift *Macromolecular Bioscience* mit dem Titel *“Beyond the Modification Degree: Impact of Raw Material on Physicochemical Properties of Gelatin Type A and Type B Methacryloyls”* veröffentlicht [96].

## **Hypothese 2**

Die sequenzielle Vernetzung von GM-Hydrogelvorläuferlösungen führt zu einer Verfestigung der GM-Hydrogele im Vergleich zu rein chemisch vernetzten GM-Hydrogelen. Bei dieser Strategie wird vor der chemischen Vernetzung die physikalische Gelierung der GM-Hydrogelvorläuferlösung herbeigeführt, siehe 2.3.3. Es gab bisher erst eine Studie, in der sequenzielle Hydrogele mit GM-Derivaten, die einen hohen Methacryloylierungsgrad ( $0.99 \text{ mmol g}^{-1}$ ) besaßen, hergestellt und untersucht wurden [303]. Diese Hydrogele wurden zwar durch die sequenzielle Vernetzung verfestigt, zeigten aber auch einen Gelpunkt bei  $\sim 28 \text{ }^\circ\text{C}$ . Außerdem ist die Beteiligung der chemischen Vernetzung und physikalischen Gelierung an der Verfestigung der sequenziellen Hydrogele noch ungeklärt.

*Die sequenzielle Vernetzung von hoch-modifizierten GM(A) Derivaten, für die kein Gelpunkt oberhalb von  $10 \text{ }^\circ\text{C}$  gemessen wurde, verfestigt die resultierenden Hydrogele im Vergleich zu rein chemisch vernetzten Hydrogelen nicht. Die Beteiligung der chemischen Vernetzung und physikalischen Gelierung an der Verfestigung der sequenziellen Hydrogele kann differenziert werden.*

Es wurden Kompressionsversuche an rein chemisch und sequenziell vernetzten GM(A)-Hydrogelen aus GM(A)-Derivaten mit hohem Modifizierungsgrad durchgeführt. Darüber hinaus wurde der physikalische Gelierprozess während des verwendeten Kühlprotokolls vor der chemischen Vernetzung untersucht. Diese Untersuchung wurde in der *peer-reviewed* Fachzeitschrift *gels* mit dem Titel *„Physical Interactions Strengthen Chemical Gelatin Methacryloyl Gels“* veröffentlicht [95].

Anschließend wurde zusammen mit Kollegen der Technischen Universität Wien der Doppelbindungsumsatz (englisch *double bond conversion*, DBC) während der Vernetzung der GM(A)-Hydrogelvorläuferlösungen mittels Echtzeit-Nahinfrarot-Spektroskopie-Photorheologie untersucht. Außerdem wurde die physikalische Gelierung während des Kühlens vor der chemischen Vernetzung mittels Circular dichroismus-Spektroskopie und dynamischer Differenzkalorimetrie untersucht. Diese Studie wurde mit dem Titel *„Differentiation of physical and chemical cross-linking in gelatin methacryloyl hydrogels“* der *peer-reviewed* Fachzeitschrift *scientific reports* veröffentlicht [321].

### **Hypothese 3**

Sequenzielle GM-Hydrogele sind durch ihre Verfestigung, im Vergleich zu rein chemischen GM-Hydrogelen, besonders für die Anwendung als *Scaffold* im Gelenkknorpel-*Tissue-Engineering* geeignet. Jedoch sind extrazelluläre Matrix (EZM) und Chondrozyten auf mehreren Ebenen zonal strukturiert. Die folgende Hypothese wurde überprüft:

*Ein zonal strukturiertes GM-basiertes, sequenziell vernetztes Hydrogel aus drei unterschiedlichen Zusammensetzungen ist als Scaffold für das Gelenkknorpel-Tissue-Engineering geeignet.*

Um der physiologischen Belastung des Gelenkknorpels nahezukommen, wurden die untersuchten, sequenziellen, GM-basierten Hydrogele im Hinblick auf ihr Relaxationsverhalten unter Kompression untersucht. Außerdem wurde die Zytokompatibilität der sequenziellen Hydrogel-Vernetzung untersucht. Die Bioaktivität der GM-basierten Hydrogele wurde anhand der enzymatischen Degradation und Redifferenzierung dedifferenzierter Chondrozyten überprüft. Die Ergebnisse sind für die Veröffentlichung in einer *peer-reviewed* Fachzeitschrift vorbereitet.



## 4. Synthese und physikochemische Charakterisierung von Gelatine-Methacryloyl-Lösungen und -Hydrogelen

Die Ergebnisse und die Diskussion zu Hypothese 1 sind als Manuskript mit dem Titel *“Beyond the Modification Degree: Impact of Raw Material on Physicochemical Properties of Gelatin Type A and Type B Methacryloyls”* dargestellt. Dieses Manuskript wurde in der *peer-reviewed* Fachzeitschrift *Macromolecular Bioscience* veröffentlicht. Darüber hinaus wird die Hypothese 1 im Kapitel 7.1 zusammenfassend diskutiert.

Hinweis: Das Layout des Manuskripts wurde an das Layout der Abhandlung angepasst. Diese Überarbeitungen haben den Inhalt der Veröffentlichung nicht verändert.

### 4.0 Erklärung meiner selbstständigen Leistung

Ich habe die Studie zum größten Teil eigenständig konzipiert und ihre wissenschaftliche Methodik ausgearbeitet. Außerdem habe ich den Großteil der praktischen Arbeiten durchgeführt, dies beinhaltet konkret:

- Die Synthese von 15 der 36 verwendeten GM(A) Derivate ( $G_A M_2$  (2 von 3),  $G_B M_2$  (4 von 5),  $G_B M_5$  (2 von 4),  $G_B M_{10}$  (2 von 4),  $G_B M_{2A8}$  (3 von 5),  $G_B M_{5A5}$  (2 von 4)). Die Synthese der anderen GM(A)-Derivate erfolgte unter meiner Anleitung (4 Synthesen), sowie durch erfahrene Kollegen (10 Synthesen) und die Co-Autorin Christiane Claaßen (7 Synthesen).
- Die rheologischen Messungen zur Bestimmung der dynamischen Viskosität sowie die Gelier- und Schmelztemperatur von 10 Gew.-% GM(A)-Lösungen erhoben.
- Die Herstellung aller Hydrogele sowie die rheologische Messung deren Speichermoduln und der gravimetrischen Bestimmung deren Quellbarkeit.
- Die 30 von 40 Messung des isoelektrischen Punktes ( $G_A M_2$  (3 von 3),  $G_A M_5$  (3 von 3),  $G_A M_{10}$  (3 von 3),  $G_A M_{2A8}$  (3 von 3),  $G_A M_{5A5}$  (3 von 3),  $G_B$  (1 von 3),  $G_B M_2$  (3 von 5),  $G_B M_5$ ,  $G_B M_{10}$  (2 von 4),  $G_B M_{2A8}$  (3 von 4),  $G_B M_{5A5}$  (3 von 3). Alle anderen Messungen (10 von 40) des isoelektrischen Punktes wurde unter meiner Anleitung durchgeführt.

Alle erhobenen Daten, bis auf die der NMR-Spektroskopie und der Aminosäuren-Analyse, wurden von mir ausgewertet. Der weitaus größte Teil des *peer-reviewed* Fachartikels wurde von mir geschrieben, konkret habe ich den Original-Entwurf des Manuskripts konzipiert und geschrieben und federführend die Änderungsvorschläge meiner Co-Autoren harmonisiert und eingearbeitet.

## 4.1 Beyond the Modification Degree: Impact of Raw Material on Physicochemical Properties of Gelatin Type A and Type B Methacryloyls

Lisa Sewald<sup>1</sup>, Christiane Claaßen<sup>1</sup>, Tobias Götz<sup>1</sup>, Marc H. Claaßen<sup>2</sup>, Vincent Truffault<sup>2</sup>, Günter E. M. Tovar<sup>1,3</sup>, Alexander Southan<sup>1</sup> and Kirsten Borchers<sup>1,3,\*</sup>

<sup>1</sup> Institute of Interfacial Process Engineering and Plasma Technology IGVP, University of Stuttgart, Nobelstraße 12, 70569 Stuttgart, Germany.

<sup>2</sup> Max Planck Institute for Developmental Biology, Max-Planck-Ring 5, 72076 Tübingen. Germany.

<sup>3</sup> Fraunhofer Institute for Interfacial Engineering and Biotechnology IGB, Nobelstraße 12, 70569 Stuttgart, Germany.

\*Corresponding Author: E-Mail: [kirsten.borchers@igb.fraunhofer.de](mailto:kirsten.borchers@igb.fraunhofer.de)

**Published in the peer-reviewed journal *Macromolecular Bioscience***

Publisher: Wiley-VCH Verlag GmbH & Co. KGaA

DOI: <https://doi.org/10.1002/mabi.201800168>

Volume: 18, Page 1800168

©2018 WILEY-VCH Verlag GmbH & Co. KGaA. With kind permission of John Wiley and Sons.

Received May 4, 2018

Revised: August 28, 2018

Published online: October 4, 2018

### 4.1.1 Abstract

Gelatin methacryloyl (acetyl) (GM(A)) is increasingly investigated for various applications in life sciences and medicine, for example, drug release or tissue engineering. Gelatin type A and type B are utilized for  $G_A M(A)$  and  $G_B M(A)$  preparation, but the impact of gelatin raw material on modification reaction and resulting polymer properties is rather unknown so far. Therefore, the degrees of modification (DMA) and physicochemical properties of five  $G_A M(A)$  and  $G_B M(A)$  derivatives are compared: The degrees of methacryloylation ( $0.32\text{--}0.98\text{ mmol g}^{-1}$ ) are indistinguishable for  $G_A M(A)$  and  $G_B M(A)$  as are the sol-gel temperatures. Isoelectric points, solution viscosities, and hydrodynamic radii which are distinct for  $G_A$  and  $G_B$ , converge with increasing DMA. Interestingly, differences are measured for the storage moduli and equilibrium degrees of swelling of respective  $G_A$  and  $G_B$  derivative-based hydrogels, in spite of their comparable DMA. This underlines the importance of GM(A) characterization beyond the modification degree.

### 4.1.2 Introduction

Gelatin is considered to be a highly suitable base material for biomaterials due to its inherent biocompatibility and bioactivity. [47, 309] Gelatin is produced by denaturation and disintegration of collagen type I. Many extracellular matrix-mimicking properties such as the Arg-Gly-Asp (RGD) motif, mediating cell attachment [35], and other motifs sensitive for biodegradation via matrix metalloproteinases [34] are preserved during hydrolysis, making gelatin a frequently investigated candidate for scaffolds in regenerative medicine. [64, 322, 323]

A common strategy to obtain gelatin hydrogels, which are stable under physiological conditions, is the functionalization of gelatin with methacryl groups (gelatin methacryloyl, GM) and its subsequent photo-induced cross-linking reaction as originally introduced by van den Bulcke *et al.* [42] in 2000. The GM preserves many beneficial properties of gelatin and additionally offers the possibility to tailor material properties of cross-linked GM hydrogels by adjusting the degree of methacryloylation (DM) of GM. [42, 120, 125] Additional modification of gelatin with inert acetyl functions (GMA) has been introduced by our group to tune viscosity and gelation of aqueous GM solutions independently from its cross-linking potential. [125] Formulations of GM(A) with adjusted properties are also increasingly used for sophisticated fabrication techniques such as inkjet-printing [125], robotic dispensing [93, 320, 324, 325], fused deposition modeling [163], or two-photon polymerization [108, 303]. Differences in mechanical properties of resulting GM hydrogels and tissue-specific additives are utilized to emulate most diverse tissues such as bone [304, 320], cartilage [177, 301], adipose tissue [319], cardiac tissue [326], and as matrix for formation of capillary structures [305]. GM hydrogels with different cross-linking densities were also utilized for drug delivery applications [299, 327].

There are two general processes leading to gelatin: An acidic conditioning process applied for weakly interconnected collagen, for example, pig skin, results in gelatin type A ( $G_A$ ), whereas gelatin type B ( $G_B$ ) is obtained by an alkaline conditioning process of densely interconnected collagen, for example, from bovine bone. [322] The difference in the production process of  $G_A$  and  $G_B$  causes a difference in amino acid composition: Asparagine and glutamine from collagen are converted to aspartic acid and glutamic acid for  $G_B$ , whereas they are preserved in  $G_A$ . [64] Therefore,  $G_A$  (isoelectric point (IEP) = 8 to 9 [64]) and  $G_B$  (IEP = 4.8 to 5.5 [64]) are oppositely charged at physiological pH.  $G_A$  and  $G_B$  were used to prepare  $G_{AM}$  [49, 106, 109, 121, 122, 296, 306] or  $G_{BM}$  [42, 105, 163, 177, 303, 328, 329] derivatives. However, in spite of the fact that the two different processes of hydrolysis affect the gelatin raw materials' properties, it was not studied so far if and to what extent the used raw  $G_A$  or  $G_B$  material defines the properties of the prepared GMs. To the best of our knowledge, the only study addressing this point was published by Lee *et al.* [300], who investigated  $G_{AM}$  and  $G_{BM}$  for bioink application and observed a higher DM of  $G_{BM}$  compared to  $G_{AM}$  and higher storage moduli of resulting hydrogels as well.

In this study, we prepared a set of five GM(A)s from  $G_A$  and  $G_B$ , using different molar excesses of methacrylic anhydride (MAAnh) and acetic anhydride (AcAnh). We determined the resulting DMs, degrees of acetylation (DA), total degrees of modification (DMA), and properties of GM(A) solutions and cross-linked hydrogels. Besides determination of viscosities, gelation and melting points of GM(A) solutions, we were particularly interested in the molecular weight distribution and IEP of GM(A)s, storage modulus, and swelling of cross-linked hydrogels. Based on the results, we hypothesized that standard viscosity, amino acid composition, and Bloom value of the raw gelatin affect material properties of GM(A)s, even if the degree and type of modification are comparable.

### 4.1.3 Experimental Section

#### Materials

The following materials were purchased from Sigma-Aldrich (Germany): AcAnh, disodium hydrogen phosphate ( $\text{Na}_2\text{HPO}_4$ ), Dulbecco's phosphate buffered saline with  $\text{MgCl}_2$  and  $\text{CaCl}_2$  (PBS+), and MAAnh. Sodium 3-trimethylsilyl-propionate-2,2,3,3-d4 (TMSP) and mixed-bed ion exchanger Amberlite IRN150 were bought from Merck (Germany). Other reagents were purchased from the following sources (given in parentheses): Deuterium oxide ( $\text{D}_2\text{O}$ ) (Deutero; Germany),  $G_A$  (MedellaPro, pig skin North America, 233 g Bloom, viscosity: 2.8 mPa s, Gelita, Germany),  $G_B$  (Limed, bovine bone, 232 g Bloom, viscosity: 4.5 mPa s, Gelita, Germany), Whatman filter paper (grade 589/1, VWR, Germany). Dialysis membranes (molecular weight cutoff: 12–14 kDa) were purchased from Medicell International Ltd. (UK). The radical

photoinitiator 1-[4-(2-hydroxyethoxy)phenyl]-2-hydroxy-2-methyl-1-propan-1-one (Irgacure 2959) was a kind gift from Bodo Möller Chemie GmbH (Germany).

### Synthesis of Gelatin Derivatives

GM was prepared as previously described [94] and the procedure was the same for G<sub>A</sub> and G<sub>B</sub>. GM derivatives were prepared with twofold (GM2), fivefold (GM5), and tenfold (GM10) molar excess of MAAnh with respect to a nominal amino group content of 0.35 mmol g<sup>-1</sup> (described by van den Bulcke *et al.* [42]). Twofold functionalized GMA derivatives were prepared with a twofold molar excess of MAAnh and an eightfold molar excess of AcAnh (GM2A8) or a fivefold molar excess of MAAnh and AcAnh (GM5A5), respectively.

### NMR Spectroscopy of Gelatin Derivatives

NMR samples were prepared by dissolving ≈15 mg biopolymer in 600 μL D<sub>2</sub>O with TMSP as internal standard (1 mg mL<sup>-1</sup>). The DM was determined from <sup>1</sup>H-NMR spectra from a Bruker Avance 500 spectrometer (500 MHz, room temperature), the DA was quantified from <sup>1</sup>H-<sup>13</sup>C-HSQC (heteronuclear single quantum coherence)-spectra from a Bruker Avance-III spectrometer (800 Hz, 37 °C) as reported previously by our group[94]. The DMA was calculated by summing up DM and DA.

### Dynamic Viscosity and Gelation of Gelatin (Derivative) Solutions

A Physica Modular Compact MCR301 rheometer from Anton Paar (Germany) equipped with cone-plate system (d = 40 mm) was used for investigation of the dynamic viscosity of 10 % (w/w) solutions of (chemically modified) gelatin in PBS+, pH 7.4 at constant shear. The gained values were averaged from 2.5 min lasting measurements (50 s<sup>-1</sup>, 37 °C, 3 s per measuring point). The gelation temperature  $T_{gel}$  and melting temperature  $T_{melt}$  of gelatin (derivatives) were analyzed by determination of storage modulus  $G'$  and loss modulus  $G''$  of solutions (10 % w/w) or the respective gels between 10 and 40 °C at a fixed cooling/heating rate (1 °C min<sup>-1</sup>), amplitude (5 %), and frequency (1 s<sup>-1</sup>).  $T_{gel}$  was determined from the cooling curve and  $T_{melt}$  from the heating curve at  $G' = G''$ . Since usually the temperature where  $G' = G''$  is not measured exactly, the first temperature where  $G' > G''$  (cooling curve,  $T_{gel}$ ) or  $G' < G''$  (heating curve,  $T_{melt}$ ) was used.

### Determination of the Isoelectric Point

IEP determination of gelatin with the use of a mixed bed deionization was introduced by Janus *et al.* [89] in 1951. This method was modified for the investigation of gelatin derivatives as follows: G<sub>A</sub> and G<sub>B</sub> as well as their derivatives were dissolved in ultrapure water (5 % w/v) at 60 °C (G<sub>A</sub> and G<sub>B</sub>) or 40 °C (GM(A)) and shaking. Afterward, 2 g mixed bed ion exchanger Amberlite IRN150 was added to the solution and shaken at 60 or 40 °C, respectively, for additional 30 min. The pH and conductivity of filtered gelatin (derivative) solutions were measured at 30 °C. Deionization of gelatin was assumed in

the case of a conductivity  $<50 \mu\text{S cm}^{-1}$ . In the case of conductivity  $>50 \mu\text{S cm}^{-1}$ , the treatment was repeated at altered ratio of resin and gelatin using 4 g mixed bed ion exchanger or a 2.5 % (w/v) gelatin solution. As the isoionic and isoelectric points of gelatin are equal if deionized in this way, the pH of the deionized gelatin solution was equivalent to its IEP [89].

The hypothetical IEPs of gelatin (derivatives) were also calculated using the ExPASy Proteomics tools site as described before. [91, 330] We used the amino acid analysis results (see **Table S 1**, 4.1.7 Supporting Information) and corrected the data for  $G_A$  regarding the asparagine and glutamine content with data from reference [64]. The amino acid composition was changed for IEP calculation of gelatin derivatives such that lysine and hydroxylysine were replaced by glycine to simulate the proposed derivatization of all amino groups.

### Size Exclusion Chromatography

The hydrodynamic radii of  $G_A$  and  $G_B$  as well as their derivatives were investigated using size exclusion chromatography (SEC). We used the “1260 Infinity GPC-SEC Analysis System” (Agilent Technologies, USA) equipped with refractive index detector and the “Suprema Linear S” column (PSS, Germany) with a nominal separation range of  $10^2$ – $10^5$  Da. Measurements (1 mg mL<sup>-1</sup> sample concentration, 50  $\mu\text{L}$  injection volume, 0.5 mL min<sup>-1</sup> flow rate) were performed at 40 °C with 11.88 g L<sup>-1</sup> Na<sub>2</sub>HPO<sub>4</sub> (pH = 9.2) as eluent.

### Preparation of Hydrogels

Hydrogels with initial protein concentrations of 10 % (w/w) were prepared by photo-initiated radical cross-linking as described by our group before [120]. Briefly, GM(A) was dissolved in PBS+ containing 0.05 % Irgacure 2959 with regard to biopolymer content, poured into a cylindrical cast (1 × 30 mm), and covered by a quartz glass pane. Samples were cured by exposure to UVA light ( $\approx 18.2 \text{ mW cm}^{-2}$ ) for 2.5 min.

### Equilibrium Degree of Swelling of Hydrogels

The following procedure was used to investigate the equilibrium degree of swelling (*EDS*): Hydrogel samples were washed immediately after cross-linking in 10 mL ultrapure water (37 °C) for at least 5 h, while water was changed every hour. Afterward the gels were swollen in PBS+ at 37 °C overnight. The swollen gels were weighed [ $w(\text{swollen})$ ], vacuum-dried, and weighed again [ $w(\text{dried})$ ]. The *EDS* was calculated in percentage utilizing Equation 1.

$$EDS = \frac{w(\text{swollen}) - w(\text{dried})}{w(\text{dried})} \times 100 \% \quad (1)$$

Hydrogel cylinders with 8 mm diameter were punched out of the swollen hydrogels and were used for further experiments.

## Rheological Characterization of Hydrogels

The viscoelastic properties of the cross-linked, washed, and swollen hydrogels were characterized by modifying a procedure given by Hoch *et al.* [120]. The oscillatory dynamic measurements were performed with a Physica Modular Compact MCR301 Rheometer from Anton Paar (Germany) using a parallel-plate model (8 mm, 37 °C, 0.32 N load). Oscillatory strain amplitude sweeps ( $0.01\% \leq \gamma \leq 100\%$ ) were performed at  $1\text{ s}^{-1}$  to establish the range of linear viscoelasticity ( $G'_{LVER}$ ).

## Statistical Analysis

A two-side Student t-test was used for statistical analysis. Statistical significance was considered for  $p$ -values  $< 0.05$ , significance levels were marked as follows: \* $p < 0.05$ ; \*\* $p < 0.01$ ; \*\*\* $p < 0.001$ . Presented data show the mean  $\pm$  standard deviation of at least three independently repeated experiments using three different batches of each gelatin derivative.

### 4.1.4 Results and Discussion

#### Methacryloylation and Acetylation Degree of $G_A$ and $G_B$ Derivatives

We prepared five derivatives of  $G_A$  and  $G_B$ , whereby both gelatin raw materials had nearly identical Bloom values ( $G_A$ : 233 g Bloom,  $G_B$ : 232 g Bloom), but different standard viscosities given by the manufacturer as 2.8 mPa s ( $G_A$ ) and 4.5 mPa s ( $G_B$ ). The two gelatin raw materials were reacted with various amounts of MAAnh to obtain cross-linkable derivatives with different degrees of methacryloylation (GM2, GM5, and GM10), or with MAAnh and AcAnh to obtain cross-linkable derivatives and simultaneously mask amino- and hydroxyl-functions and thus reduce physical interaction of gelatin through insertion of inert acetyl functions (GM2A8 and GM5A5). We applied standardized molar excesses of the anhydrides, whereby the numbers in our nomenclature denote the used excess in relation to a nominal amino group content per gram gelatin ( $0.35\text{ mmol g}^{-1}$ ) as reported by van den Bulcke *et al.* [42].

We characterized the  $G_A$  and  $G_B$  raw material by amino acid analysis (methods and results are given in **Table S 1**, 4.1.7 Supporting Information). It was shown recently by 2D-NMR [94] and liquid chromatography tandem-mass spectrometry (LC-MS/MS) [50] that besides amino acids bearing amino groups also hydroxyl group containing amino acids were chemically modified during GM(A) synthesis. The amount of amino group containing amino acids (lysine and hydroxylysine,  $G_A$ :  $0.33\text{ mmol g}^{-1}$ ,  $G_B$ :  $0.31\text{ mmol g}^{-1}$ ) and of hydroxyl group containing amino acids (serine, threonine, tyrosine, hydroxyproline, and hydroxylysine,  $G_A$ :  $1.47\text{ mmol g}^{-1}$ ,  $G_B$ :  $1.50\text{ mmol g}^{-1}$ ) was almost the same for the used  $G_A$  and  $G_B$ .

We then used  $^1\text{H-NMR}$  with TMSP as an internal standard to quantify the DM and  $^1\text{H-}^{13}\text{C-HSQC-NMR}$  in combination with the TMSP method to quantify the DA according to a method previously introduced by our group [94]. The general appearance of the  $^1\text{H-NMR}$  spectra of  $G_A$  derivatives and  $G_B$  derivatives was very similar, spectra of  $G_B$  and its derivatives are shown in **Figure S 1** (4.1.7 Supporting Information): Methacryloyl groups gave signals at 5.0–6.5 ppm and 1.9 ppm, and acetyl groups an additional signal at 2.1 ppm; both signals intensities increased with increasing amounts of applied MAAnh and AcAnh. The  $\epsilon$ -methylene group signal of lysine (2.8–2.95 ppm) was absent in the spectra of all derivatives indicating that the amount of remaining free lysine after modification was below the detection threshold.

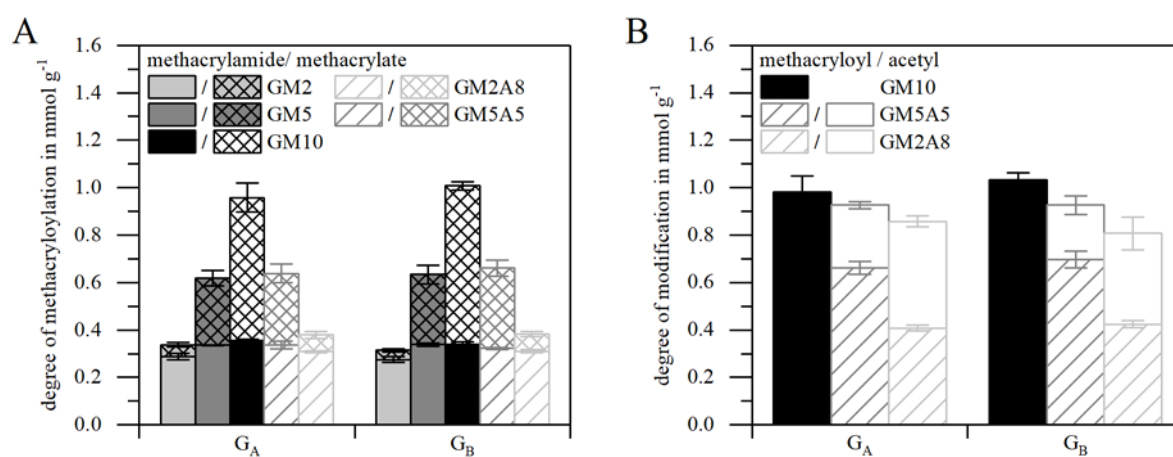


**Figure 1 A)** DM, broken down to methacrylate (filled bars) and methacrylamide (criss-crossed upper bars) in  $\text{mmol g}^{-1}$  of  $G_A$  and  $G_B$  derivatives determined by integration of  $^1\text{H-NMR}$ -spectra with the TMSP-method.[37] The particular DMs were indistinguishable for  $G_A$  and  $G_B$ . The DM increased with the molar excess of MAAnh used. **B)** DMA in  $\text{mmol g}^{-1}$  for derivatives prepared with tenfold excess of anhydride, broken down to methacryloyl and acetyl modification. All corresponding values and statistical analysis results of two-sided Student t-tests are given in **Table S 3** and **Table S 3**, 4.1.7 Supporting Information. The data for  $G_A$  derivatives were published in ref. [37] before.

The results of DM calculations broken down into methacrylamide and methacrylate content are shown in **Figure 1-A** (all corresponding values see **Table S 2**, 4.1.7 Supporting Information), the DMA divided into methacryloylation and acetylation are shown in **Figure 1-B**. The degrees of modification (DM, DA, and DMA) of each comparable pair of  $G_A$  and  $G_B$  derivative (GAM2/GBM2, GAM5/GBM5, GAM10/GBM10, GAM2A8/GBM2A8, GAM5A5/GBM5A5) were not significantly different in any case. This meets with the expectation according to the very similar amounts of reactive amino and hydroxyl group of the raw materials.

The DM increased significantly for both gelatin raw materials from  $\approx 0.32 \text{ mmol g}^{-1}$  (GM2) to  $\approx 0.98 \text{ mmol g}^{-1}$  (GM10) with increasing molar excess of MAAnh applied, consistent with previous reports.[9,10,28,37] The same was true for the DA: The DA of GM2A8 ( $\approx 0.4 \text{ mmol g}^{-1}$ ) was significantly higher than the DA of GM5A5 ( $\approx 0.25 \text{ mmol g}^{-1}$ ), consistent with our previous study [94]. The DMs of GM and GMA prepared with the same amount of MAAnh (GM2/GM2A8 or GM5/GM5A5) were comparable for both types of gelatin, thus also consistent with data shown before for  $G_A$  [94]. The



methacrylamide amount remained almost constant in all gelatin derivatives, while the amount of methacrylate groups rose with increasing excess of MAAnh. This observation was in good agreement to the absence of the lysine signal in all gelatin derivatives spectra and particularly reflects the elevated reactivity of amino functions compared to hydroxyl functions, as described before [50, 94]. The trend of declining DMA with increasing ratio of AcAnh for all derivatives that were reacted with a tenfold excess of anhydride (GM10, GM5A5, GM2A8) can be attributed to elevated hydrolysis sensitivity of AcAnh compared to MAAnh and thus less available anhydride in the course of the modification reaction when AcAnh was applied instead of MAAnh.

Our results are generally in accordance with results reported by Lee *et al.* [300], who also compared the DM of  $G_A$  and  $G_B$  methacryloyls: Their highest feed ratio of 0.1 mL MAAnh per 1 g gelatin corresponded roughly to our twofold molar excess (GM2). Like us, they observed a nearly quantitative conversion of amino groups and no difference in the DM between  $G_A$  and  $G_B$  derivatives at this feed ratio of MAAnh. In addition, the authors investigated  $G_A$  and  $G_B$  methacryloyls with lower feed ratios of MAAnh and found higher DMs for  $G_B$ M compared to  $G_A$ M. In summary, this suggests that differences in the physicochemical nature of the raw material (e.g., IEPs) do influence the reaction kinetics in the initial stages of methacrylamide formation, while distinctions are leveled out after quantitative conversion of amino functions and thus at higher degrees of modification as investigated in this study.

### **Isoelectric Points of $G_A$ , $G_B$ , and Their Derivatives**

The IEP is defined as “the pH value at which the net electric charge of an elementary entity is zero.”[33] It is a characteristic of ampholytes-like proteins. The different IEPs of unmodified  $G_A$  and  $G_B$  have been shown to affect the release of proteins out of gelatin-based hydrogels substantially due to electrostatic interactions between protein and hydrogel [310, 331]. However, no IEPs were reported for modified gelatins in recent reports, for example, on controlled release applications [299, 327, 332]. Due to the reaction of free amino groups upon reaction with anhydrides, it can be expected that the IEPs of  $G_A$ M(A) and  $G_B$ M(A) derivatives decrease upon modification. The IEP can be determined for example by isoelectric focusing gel electrophoresis [90] or estimation of turbidity with respect to the solution pH [90, 333]. In this study the IEP was determined according to the deionization method described by Janus *et al.* [89] Additional to experimental determination of the IEP, we theoretically estimated the IEPs of  $G_A$ ,  $G_B$ , and derivatives using the ExPASy Proteomics tools site [91].

The results of experimental IEP determination are shown in **Figure 2**. As illustrated in **Figure 2-A**, gelatin derivatives precipitated during the deionization process, indicating the method as appropriate, since the solubility of the elementary entity is minimal at its IEP.  $G_A$  (IEP = 8.8) and  $G_B$  (IEP = 4.9) showed the well-known difference in IEP due to the conditioning processes of gelatin [64]. As shown in **Figure 2-B** IEPs of gelatin derivatives were significantly lower compared to their corresponding unmodified

raw materials and IEPs of respective  $G_A$  ( $\approx 4.5$ ) and  $G_B$  ( $\approx 4.1$ ) derivatives were significantly different ( $p < 0.01$ ).

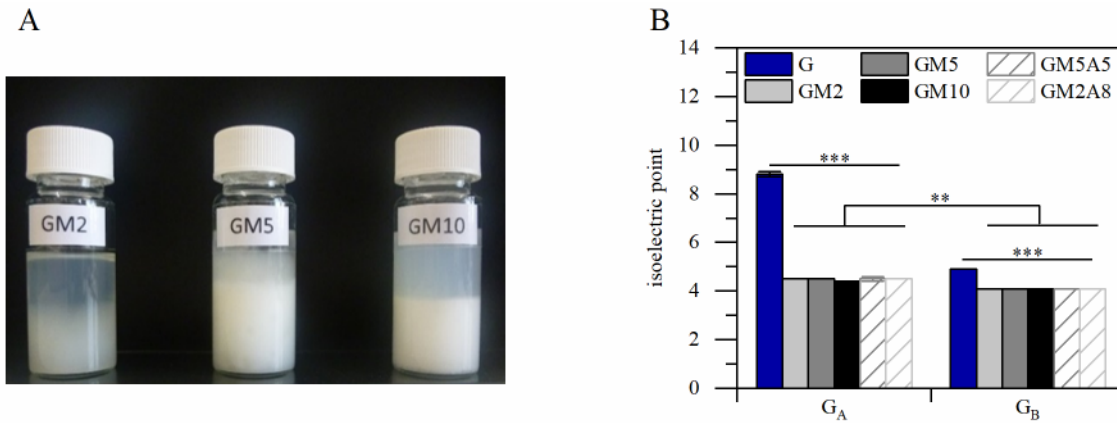


**Figure 2: A)** Solutions of deionized gelatin derivatives. Gelatin derivatives precipitated following the deionization process. **B)** IEP of  $G_A$  (8.8),  $G_B$  (4.9), and derivatives  $G_A M(A)$  ( $\approx 4.5$ ),  $G_B M(A)$  ( $\approx 4.1$ ). The IEP of modified gelatins were different compared to the respective unmodified gelatin. Additionally, the IEPs of  $G_A$  derivatives were higher compared to the corresponding  $G_B$  derivatives. Significant differences were calculated using a two-sided Student t-test, and significance levels were marked as follows:  $**p < 0.01$ ,  $***p < 0.001$ .

The experimental results could be roughly predicted by calculated IEP values for the raw materials, yielding 9.1 for  $G_A$  and pH 4.7 for  $G_B$ . Theoretical estimation of the IEP of GM(A)s was achieved by replacement of lysine and hydroxylysine by glycine according to the nearly quantitative conversion of amino groups due to chemical modification and resulted in 4.7 for  $G_A$  derivatives and 4.2 for  $G_B$  derivatives. Theoretical and experimental results reflect the elevated amount of carboxyl functions in  $G_B$  compared to  $G_A$ : During modification reactions the basic amino groups, which contribute to the positive charges, were consumed while the acidic carboxyl groups, which contribute to negative charge are not converted. The reaction of anhydrides with hydroxyl groups could be neglected because only charged amino acids influence the IEP. Thus, the general decrease of IEPs toward acidic pH upon modification met with the expectation. This shift was less pronounced for  $G_B$  because an excess of negative charges existed already before modification[64]. The elevated content in acidic side chains in  $G_B$  compared to  $G_A$  at equal amounts of remaining alkaline amino acids (histidine, arginine) also accounts for the persistent difference of IEPs between  $G_A M(A)$  and  $G_B M(A)$  after conversion of free amino groups.

In this study, we investigated GM(A) derivatives with rather high DM with almost complete conversion of free amino functions. Notably, such derivatives were all negatively charged at physiological pH, whether made from  $G_A$  or  $G_B$  raw material. Theoretical estimation predicts that  $G_A M(A)$  derivatives will be positively charged at pH 7.4 only up to a conversion of 10 % of free amino functions (Figure S 2, 4.1.7 Supporting Information). The resulting IEP after derivatization of gelatins should thus be considered, explicitly when the polymer charge is crucial, for example in drug delivery systems, for stabilization of emulsions [64], or when impact of charges has to be expected such as in

cell culture. Viscosity [334] and gelation time [335] of gelatins are also correlated with and are lowest at the IEP. Therefore, we investigated see gelation behaviour and 3.5 dynamic viscosity at pH 7.4 in this study, and thus from afar the IEPs of the various derivatives.

### Hydrodynamic Radii of $G_A$ and $G_B$ and Their Derivatives

We used SEC to investigate the hydrodynamic radii of  $G_A$  and  $G_B$  and their derivatives after chemical modification. The pH of the aqueous solutions was adjusted to 9.2 and thus all samples were negatively charged. The elugram of unmodified  $G_B$  showed a shoulder at higher elution volumes and therefore at lower hydrodynamic radii, which was not visible for  $G_A$  (**Figure 3**). This initial difference probably reflects the differences in molecular weight distribution of  $G_A$  compared to  $G_B$  [64]. The elugram shapes of the derivatives of both types of gelatin were very similar. With increasing degree of modification, the curves shifted toward higher elution volumes and the double-functionalized GMA derivatives (GM2A8 and GM5A5) were eluted even later than GM10 for both types of gelatin. In general,  $G_A$  derivatives were eluted at slightly higher elution volumes than  $G_B$  derivatives while the effect became less pronounced with increasing degree of modification (**Figure S 3**, 4.1.7 Supporting Information).

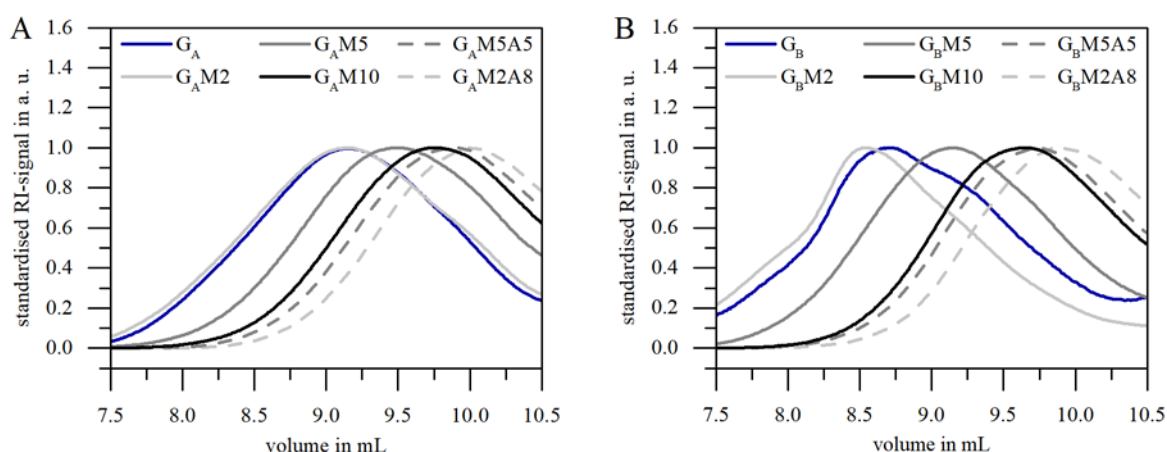


**Figure 3:** A) SEC elugrams of  $G_A$  and its derivatives B) as well as of  $G_B$  and its derivatives. GMs were eluted at higher elution volumes compared to the raw materials. Increasing DMs lead to increasing elution volumes. GMAs were eluted at even higher elution volumes, which further increased with the DA. Elution volumes smaller than 7.5 mL and greater than 10.5 mL were outside the separation range of the used SEC column.

The shift of elugrams with increasing DM was recently observed for  $G_B M$  derivatives by van Hoorick *et al.* as well [303]. They associated the increase in elution volume with hydrolytic degradation during their synthesis procedure. However, since SEC measurements provide no direct information on the molecular weight of GM(A)s due to the lack of a calibration reference, we tend to a different interpretation of the data. The macromolecules are separated according to their hydrodynamic radii, but due to the mild reaction conditions applied and dialysis at room temperature, we assume no direct evidence for pronounced hydrolysis in this study. [64, 336] In addition, the magnitude of shift was distinct for various derivatives, whereas the reaction conditions (and thus potential hydrolysis) were

equal in all syntheses. Instead, we suggest that the delayed elution times with increasing DM and DA could be ascribed to an alteration of chain conformation in aqueous solution. The reduction of charged groups and proton acceptors and donors is expected to strongly affect the formation of secondary, tertiary, and supramolecular structures of the protein, that is,  $\beta$ -chains and helical structures which are stabilized via hydrogen bonds [337], and can thus result in smaller hydrodynamic radii after modification.

The elution of double-functionalized GMAs later than GM10 could be due to fact that acetyl groups have a smaller size compared to methacryloyl groups what in turn might have additionally reduced the hydrodynamic radii of GMAs compared to GMs. Conformational changes in GM(A) derivatives toward smaller hydrodynamic radii just like decreasing molecular weight are expected to also affect dynamic viscosity and gelation temperatures (**Figure 4, Table 1**) due to reduced intermolecular interactions and significantly decreased contact areas of adjacent polymer chains.

### **Melting and Gelling Temperatures of G<sub>A</sub>, G<sub>B</sub>, and Their Derivatives**

Physical gel formation is characteristic for aqueous gelatin solutions. [64] Upon cooling, they solidify at a certain gelation temperature  $T_{gel}$ , whereas upon heating they liquefy at a certain melting temperature  $T_{melt}$ , also denoted as sol-gel- or gel-sol-point. In order to assess the impact of modification on gelation of aqueous solutions (10 % (w/w)) of various G<sub>A</sub> and G<sub>B</sub> derivatives, the solutions were characterized by temperature-dependent oscillatory rheology at pH 7.4.  $T_{gel}$  and  $T_{melt}$  were determined at the equilibrium of  $G'$  and  $G''$  in the cooling curve or heating curve, respectively. Such curves are never congruent since the melting process is at a higher energy level and thus they show a hysteresis. The values for  $T_{gel}$  and  $T_{melt}$  for all G<sub>A</sub> and G<sub>B</sub> derivatives are listed in **Table 1**, the corresponding cooling and heating curves are shown in **Figure S 4** and **Figure S 5**, 4.1.7 Supporting Information).

$T_{gel}$  was approximately 5 °C below  $T_{melt}$  for all samples, which is commonly denoted to be the standard correlation between the two transition temperatures. [64] This trend was not impaired through modification. Both transition temperatures significantly decreased upon modification ( $p < 0.01$  for GM2 and  $p < 0.001$  for GM5) and no gel formation at all was detected for highly modified derivatives GM5A5, GM2A8, and GM10 in the investigated temperature range between 10 and 40 °C.

Again, we assign the reduction in gel forming properties to the integration of methacryloyl and acetyl residues along the gelatin chains. Masking of amino and hydroxyl functions, steric hindrance, or reduced molecular radii may be involved.

$T_{gel}$  as well as  $T_{melt}$  were indistinguishable for the investigated unmodified G<sub>A</sub> and G<sub>B</sub> and the respective derivatives thereof. This result suggested that the sol-gel points of gelatin might rather be represented by the Bloom value (which was equal for both gelatin raw materials G<sub>A</sub>: 233, G<sub>B</sub>: 232), than

by the standard viscosity (which was different for both raw materials  $G_A$ : 2.8 mPa s;  $G_B$ : 4.5 mPa s), however, various investigations showed that it is not possible to define simple relationships between such empirical features of gelatins due to the immense complexity of the interactions of influencing conditions [338]. Therefore, these characteristic numbers have to be determined for each specific material.

**Table 1:** Gelation temperatures ( $T_{gel}$ ) and melting temperatures ( $T_{melt}$ ) of solutions (10 % w/w, pH 7.4) of unmodified  $G_A$ ,  $G_B$  and derivatives thereof.  $T_{gel}$  and  $T_{melt}$  of the raw materials decreased after chemical modification. No  $T_{gel}$  and  $T_{melt}$  could be determined (CND) for derivatives with high degrees of modification (GM10, GM5A5, GM2A8) above 10 °C GM10. No significant differences between sol-gel points of  $G_A$  and  $G_B$  as well as their respective derivatives were detected.

gelatin derivative	dynamic viscosity in Pa s
$G_A$	$0.0103 \pm 0.0003$
$G_{AM2}$	$0.0062 \pm 0.0022$
$G_{AM5}$	$0.0036 \pm 0.0007$
$G_{AM10}$	$0.0030 \pm 0.0002$
$G_{AM5A5}$	$0.0024 \pm 0.0002$
$G_{AM2A8}$	$0.0030 \pm 0.0007$
$G_B$	$0.0222 \pm 0.0000$
$G_{BM2}$	$0.0105 \pm 0.0009$
$G_{BM5}$	$0.0047 \pm 0.0004$
$G_{BM10}$	$0.0037 \pm 0.0014$
$G_{BM5A5}$	$0.0025 \pm 0.0002$
$G_{BM2A8}$	$0.0029 \pm 0.0000$

Gelatin solutions with different sol-gel points or no  $T_{gel}$  can be convenient for different processes. Highly modified derivatives should be chosen if solution properties need to be mostly independent from the surrounding temperature, or low viscosity is required, for example, for drop-on-demand techniques like inkjet printing [125] (see further discussion below). If gelling of GM(A)s is desired, for example for strengthening of chemical networks [302], low modified GMs should be used.

#### Dynamic Viscosity of Solutions of $G_A$ , $G_B$ , and Their Derivatives

The viscosity of gelatin solution is primarily defined by the manufacturing process of gelatin[64]. We investigated the effect of raw material and chemical modification on the dynamic viscosity of GM(A) solutions (10 % w/w) using rotational rheology (**Figure 4**; corresponding values are provided in **Table S 4** and **Table S 5**, 4.1.7 Supporting Information). Measurements were taken above  $T_{melt}$  at 37 °C in PBS+ at pH 7.4.

The dynamic viscosity of solutions of unmodified  $G_B$  was 0.022 Pa s and significantly higher ( $p < 0.001$ ) compared to solutions of unmodified  $G_A$ , which was 0.010 Pa s. This trend was in accordance with the viscosity specifications given by the manufacturer ( $G_A$ : 0.0028 Pa s,  $G_B$ : 0.0045 Pa s) which

were determined at standard conditions using a calibrated pipette and 6.67 % gelatin solutions at 60 °C [64].

Obviously, the viscous properties of the solutions changed in correlation with the degree of modification. The dynamic viscosity of the gelatin derivatives decreased with increasing DMA for both,  $G_A$  and  $G_B$  derivatives, as observed before [120, 125]. The lowest dynamic viscosities ( $\approx 0.003$  Pa s) were observed for GMs with high DMA (GM10, GM5A5, and GM2A8) and at such high degrees of modification significant differences between  $G_A$  and  $G_B$  derivatives were no longer existent ( $p > 0.05$ ). At lower degrees of modification (GM2, GM5), the dynamic viscosities of  $G_B$  derivatives were still higher than the respective  $G_A$  derivatives ( $p < 0.05$ ). The reason for viscosity decrease was presumably found in the progression of chemical masking of amino acid side chains leading to reduced hydrophilic interactions between polymer chains. In addition we propose that the viscosity is also reduced due to stronger compaction of the molecules at higher DM(A)s as suggested with regard to the decrease in hydrodynamic radii and consequently less intermolecular interactions.

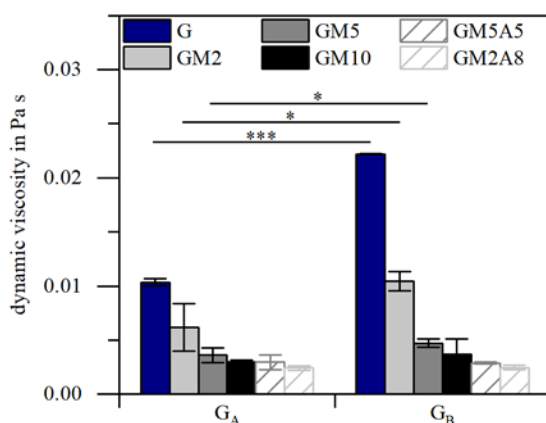


**Figure 4:** Dynamic viscosity of 10 % (w/w)  $G_A$  and  $G_B$  (derivative) solutions determined at  $50 \text{ s}^{-1}$ , pH 7.4, and  $37 \text{ }^\circ\text{C}$ . All corresponding values are entitled in **Table S 4**, 4.1.7 Supporting Information. The viscosity of unmodified  $G_B$  was significantly higher compared to unmodified  $G_A$ . This was also true for relatively low methacryloylated derivatives GM2 and GM5. Viscosities of highly modified derivatives GM10, GM5A5, and GM2A8 were indistinguishable. Significant differences were determined using a two-sided Student t-test, and significance levels were marked as follows: \* $p < 0.05$ ; \*\*\* $p < 0.001$ .

The control of viscosity by the total degree of modification DM(A) at given flexibility of cross-linking capacity by the ratio of methacryloyl and acetyl functions is of interest with regard to handling of gelatin solutions. For example, for electrospinning viscosities in the range of 0.3–0.7 Pa s are preferred [339], drop-on-demand techniques, i.e. inkjet printing, can process maximum viscosities of 0.01 Pa s [340], and dispensing of stable structures requires viscosities above 0.03 Pa s [341]. According to their viscosity, the solutions of all gelatin derivatives theoretically were within the inkjet printable range at  $37 \text{ }^\circ\text{C}$ , in contrast to solutions of unmodified  $G_B$ . Yet, we observed before that in fact only such highly modified derivatives qualified for inkjet printing, that possessed sufficiently low viscosities also at  $25 \text{ }^\circ\text{C}$  [125], because accelerated evaporation resulted in clogging of the nozzles at  $37 \text{ }^\circ\text{C}$ . Based on the double-functionalization technique (control of the ratio of methacryloyl and acetyl functions), such

derivatives can also be provided with various amounts of cross-linkable functions per gram polymer [125].

From the results on IEP mentioned above, hydrodynamic radius, and viscosity of dissolved gelatin derivatives we derive the hypothesis that in general the impact of the raw material properties decreases with increasing degree of modification. However, it is important to note that differences remain for some parameters even at high modification levels, that is, higher hydrodynamic radii, and lower IEPs for  $G_B$  derivatives.

### Storage modulus and Equilibrium Degree of Swelling of Cross-Linked Hydrogels

We compared the storage modulus in the linear viscoelastic range ( $G'_{LVER}$ ) as well as the *EDS* for radically cross-linked hydrogels from  $G_A$  and  $G_B$  derivatives to further complete the material characterizations (**Figure 5**, **Table S 6**, **Table S 7**, 4.1.7 Supporting Information).  $G'_{LVER}$  was indistinguishable for respective  $G_A$  and  $G_B$  derivatives with high levels of modification (GM10, GM2A8, GM5A5), but higher  $G'_{LVER}$  was found for low modified  $G_B$  derivatives ( $G_B$ M2,  $G_B$ M5) than for  $G_A$  derivatives ( $G_A$ M2,  $G_A$ M5) (**Figure 5-A**,  $p < 0.01$ ). Additionally,  $G'_{LVER}$  of gelatins with lower levels of modification (GM2, GM5) were generally much higher than that of their complements with higher levels of modification (GM2A8, GM5A5), although the amount of cross-linkable groups was very similar. In fact, there was no significant difference of  $G'_{LVER}$  determined between GM2, GM5, and GM10 although the DM significantly increased.

We assign the high storage moduli of GM2 and GM5 to synergistic effects of physical interaction (e.g., helix formation) and chemical cross-linking. Other authors have also described the observation that GM hydrogel stiffness was increased when physical gelation was allowed prior to chemical cross-linking of GMs. [17,54,58,59] In our study, GM2 and GM5 were able to form physical gels, while GM10, GM2A8, and GM5A5 were not, due to high level of modification. Therefore, in the former case the chemical cross-linking most probably locked the gel structure when triple helices had already developed, while in the latter case, the material was not able to form helices and was linked as random polymer chains. Due to chemical cross-linking, the physical gel structure is fixed and thus, temperature-dependent melting was assumed to be impeded. Indeed, we measured storage moduli of GM2-based hydrogels at 4 °C (below  $T_{melt}$ ) and at 37 °C (above  $T_{melt}$ ) and found no difference in the storage moduli (**Table S 7**, 4.1.7 Supporting Information). Studies of Schuurman *et al.* [45] and Rizwan *et al.* [302] also showed that the mechanical stiffness was not temperature-dependent, when physical gels were fixed by chemical cross-linking.

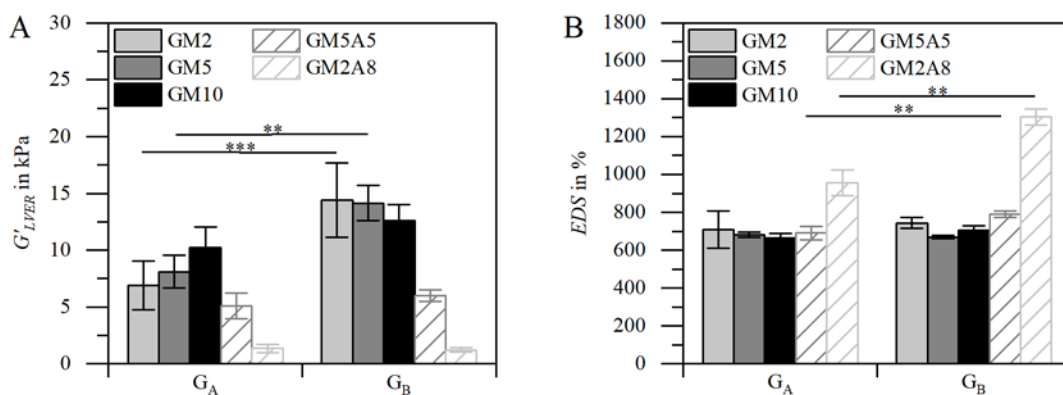


**Figure 5:** **A)**  $G'_{LVER}$  (at 37 °C) and **B)** EDS of GM(A) hydrogels prepared from 10 % (w/w) solutions.  $G'_{LVER}$  of GM-hydrogels were higher compared to GMA hydrogels with identical DM, and  $G_B$ M hydrogels had higher  $G'_{LVER}$  than  $G_A$ M hydrogels. All corresponding values and statistical analysis results of two-sided Student t-tests are given in and **Table S 7**, 4.1.7 Supporting Information). EDSs of hydrogels were approximately the same for all derivatives (700–800 %), except for GM2A8 which possessed significantly higher EDS and significant differences between  $G_A$  and  $G_B$ . Significant differences were calculated using a two-sided Student t-test, and significance levels were marked as follows: \*\* $p < 0.01$ ; \*\*\* $p < 0.001$ .

The indistinguishability of mechanical stiffness of GM2, GM5, and GM10 hydrogels (10 % w/w) for both raw materials is also in accordance with the concept of superposition of physical and chemical cross-linking within GM gels with low DM. Although the chemical cross-linking density increased with increasing amounts of cross-linkable methacrylic functions (compare  $G'_{LVER}$  of the derivatives GM2A8, GM5A5, GM10), stabilization of the gel structure through physical interaction obviously compensated the reduced chemical cross-linking in the derivatives with lower DM (GM2, GM5). Considering physical interactions, it seems also sensible to expect stronger gels in the case of low modified  $G_B$  derivatives than in the case of low modified  $G_A$  derivatives, as was indeed observed for  $G_B$ M2,  $G_B$ M5 compared with  $G_A$ M2,  $G_A$ M5, because  $G_B$  exhibited higher viscosities.

Nevertheless, other studies on GM derivatives from lower to similar DMs than in this study, found that the mechanical stiffness of GM hydrogels increased in direct correlation with the DM. [42, 300] In conclusion, we suggest that physical and chemical cross-linking complement each other in gels that are capable of both such as GM2 and GM5, and that an optimum can be achieved in terms of elastic gel stiffness, which can be predicted to be in the range of GM2 or GelMa2.2 as introduced in ref. [300]. Both derivatives were generated by similar MAA<sub>nh</sub> concentrations, and the  $G'_{LVER}$  of both materials has been determined accordingly to be in the range of 10 kPa (10 % gels) in the respective study.

Finally, it is interesting to note the EDS (**Figure 5-B**): Typically, the EDS is negatively correlated with the mechanical stiffness of hydrogels and consequently, higher EDS was expected for  $G_A$ M than for  $G_B$ M and comparable results for GMA derivatives. In contrast, the EDS of  $G_A$ M and  $G_B$ M were indistinguishable, and  $G_B$ MA gels took up more water than  $G_A$ MA. We consider the difference in chemical composition, namely the higher amount of acidic groups present in  $G_B$  than in  $G_A$  due to the extraction process, to cause the unexpected higher swelling capability of  $G_B$  derivatives.



#### 4.1.5 Conclusion

Gelatins are available from various sources and the extraction processes yield materials with various qualities, for example, in terms of IEP, viscosity, and gel strength. We raised the question how such primary properties still affect cross-linkable derivatives after chemical modification, since such materials are increasingly used with a view to medical application and thus comprehensive knowledge and control of material properties are required. We used one  $G_A$  and one  $G_B$  with equal gel strengths and different viscosities. The applied modification protocol resulted in full conversion of all accessible amino functions and raising conversion of hydroxyl functions of the gelatin. We revealed that at such high levels of modification, the degrees of modification (DM, DA, DMA) were indistinguishable for all respective  $G_A$  and  $G_B$  derivatives. Importantly, in spite of this apparent equality, differences associated with distinct physicochemical properties of the raw materials remained detectable in  $G_A$ - and  $G_B$ -based derivatives for almost all investigated parameters, that is, IEP, hydrodynamic radius, viscosity,  $G'_{LVER}$ , and  $EDS$  of resulting hydrogels, although variances leveled out with increasing  $DM(A)$ .

#### 4.1.6 Acknowledgements

The authors kindly thank Birgit Claasen (IOC, University of Stuttgart) for the  $^1H$ -NMR measurements and Christoph Simon (Gelita AG, Eberbach, Germany) for scientific assistance regarding the IEP determination, and Lisa Böhler (University of Stuttgart) for assistance in the lab. L.S. thanks the Evonik Stiftung (Essen) for financial support. C.C. and K.B. thank the Deutsche Forschungsgemeinschaft (grant ID BO 4252/1-1) for financial support. T.G. thanks the Baden Württemberg Stiftung (Stuttgart) for financial support within the project BioMatS-011. A.S. and G.E.M.T. thank the Carl Zeiss Foundation and the University of Stuttgart for financial support within the *Projekthaus NanoBioMater*.

#### 4.1.7 Supporting Information

**Table S 1:** Amino acid composition of non-modified G<sub>A</sub> and G<sub>B</sub>. The results from the amino acid analysis and information given in [64] were used to perform the theoretical IEP estimation for G<sub>A</sub>. (Source: Encyclopedia of Polymer Science and Engineering, Volume 3, p. 488–513 (1987). Copyright Wiley & Sons. Reproduced with permission from John Wiley & Sons Ltd. Data taken from [64]: “Gelatin Handbook: Theory and Industrial Practice” Reinhard Schrieber, Herbert Gareis, ISBN: 978-3-527-31548-2. Reproduced with permission.)

Amino acid	Gelatin Type A			Gelatin Type B		
	Literature Values [64]	Determined Values		Literature Values [64]	Determined Values	
	[per 1000 residues]	[per 1000 residues]	[mmol g <sup>-1</sup> ]	[per 1000 residues]	[per 1000 residues]	[mmol g <sup>-1</sup> ]
aspartic acid	29	30*	0.286*	46	45	0.427
asparagine	16	16**	0.158**	-	-	-
threonine	18	15	0.144	18	16	0.154
serine	35	34	0.328	33	32	0.306
glutamic acid	48	49*	0.469*	72	74	0.701
glutamine	25	25**	0.245**	0	-	-
glycine	330	343	3.314	335	341	3.248
alanine	112	107	1.037	117	116	1.104
cysteine	-	-	-	-	-	-
valine	26	21	0.206	22	21	0.201
methionine	3.6	6	0.060	3.9	5	0.05
isoleucine	10	10	0.094	11	12	0.111
leucine	24	23	0.223	24.3	25	0.238
tyrosine	2.6	3	0.033	1.2	1	0.010
phenylalanine	14	13	0.126	14	12	0.116
histidine	4	5	0.048	4.2	4	0.038
lysine	27	27	0.259	28	27	0.253
hydroxylysine	6.4	7	0.066	4.3	6	0.061
arginine	49	50	0.483	48	48	0.462
proline	132	122	1.180	124	113	1.075
hydroxyproline	91	93	0.902	93	102	0.971

\*values are calculated as the difference of the amino acid analysis and the values for the corresponding amides from reference [64]

\*\*values from reference [64] were used

The University of Hohenheim, Germany, performed the amino acid analysis of  $G_A$  and  $G_B$  according to the European Commission (EC) Regulation No 152/2009 III F. The results of this analysis are shown in **Table S 1**. In short, hydrochloric acid was used to hydrolyze gelatin and the resulting amino acids were separated via ion chromatography. These separated amino acids were converted in a post-column derivatization using ninhydrin and were detected using a photometric detector. Amino acids standards were used for quantification.

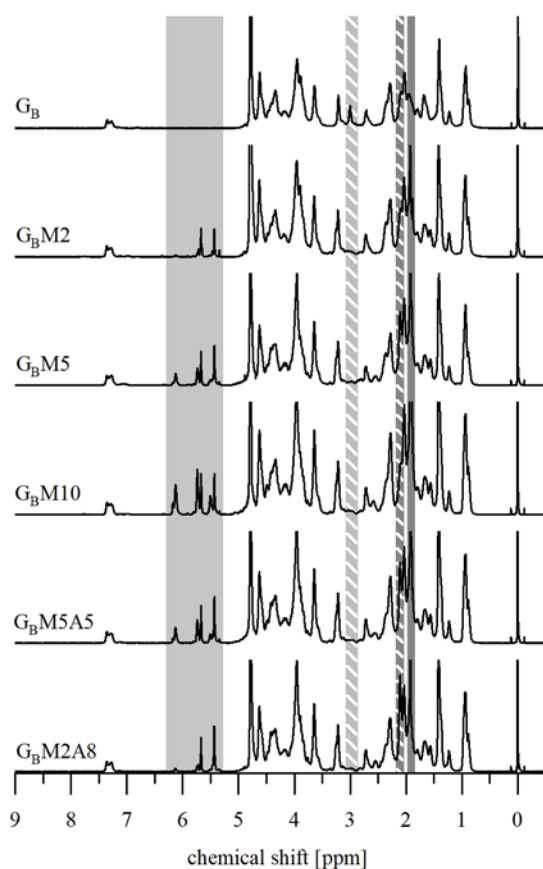


**Figure S 1:**  $^1\text{H-NMR}$  of  $G_B$  and its derivatives. Acrylic protons of methacryl groups were highlighted light grey, non-modified lysine residues criss-crossed light grey, methyl protons of acetyl groups criss-crossed dark grey and methyl protons of methacryl groups dark grey.

**Table S 2:** Degree of methacryloylation (DM) of G<sub>A</sub> and G<sub>B</sub> derivatives in mmol g<sup>-1</sup> split up in methacrylamide and methacrylate.

Gelatin derivative	DM [mmol g <sup>-1</sup> ]	
	methacrylamide	methacrylate
G <sub>A</sub> M2	0.29 ± 0.01	0.05 ± 0.01
G <sub>A</sub> M5	0.34 ± 0.01	0.28 ± 0.03
G <sub>A</sub> M10	0.36 ± 0.01	0.60 ± 0.06
G <sub>A</sub> M5A5	0.34 ± 0.02	0.30 ± 0.04
G <sub>A</sub> M2A8	0.31 ± 0.01	0.07 ± 0.02
G <sub>B</sub> M2	0.28 ± 0.01	0.04 ± 0.01
G <sub>B</sub> M5	0.34 ± 0.01	0.30 ± 0.04
G <sub>B</sub> M10	0.34 ± 0.01	0.67 ± 0.02
G <sub>B</sub> M5A5	0.32 ± 0.01	0.34 ± 0.03
G <sub>B</sub> M2A8	0.31 ± 0.01	0.07 ± 0.01

**Table S 3:** Entitled differences of degree of methacryloylation (DM) of G<sub>A</sub> and G<sub>B</sub> derivatives. Significances are tagged as follows: \*= $p < 0.05$ , \*\*= $p < 0.01$ , \*\*\*= $p < 0.001$ , n. s. = not significant.

	G <sub>A</sub> M2	G <sub>A</sub> M5	G <sub>A</sub> M10	G <sub>A</sub> M5A5	G <sub>A</sub> M2A8	G <sub>B</sub> M2	G <sub>B</sub> M5	G <sub>B</sub> M10	G <sub>B</sub> M5A5	G <sub>B</sub> M2A8
G <sub>A</sub> M2		***	**	***	n. s.	n. s.				
G <sub>A</sub> M5	***		**	n. s.	**		n. s.			
G <sub>A</sub> M10	**	**		*	**			n. s.		
G <sub>A</sub> M5A5	***	n. s.	*		***				n. s.	
G <sub>A</sub> M2A8	n. s.	**	**	***						n. s.
G <sub>B</sub> M2	n. s.						**	***	***	*
G <sub>B</sub> M5		n. s.				**		**	n. s.	*
G <sub>B</sub> M10			n. s.			***	**		***	***
G <sub>B</sub> M5A5				n. s.		***	n. s.	***		**
G <sub>B</sub> M2A8					n. s.	*	*	***	**	

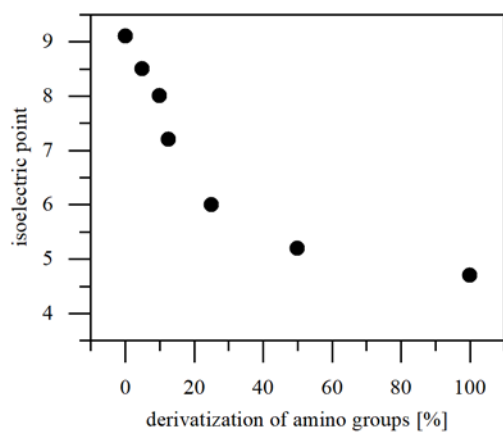


**Figure S 2:** Calculated isoelectric points of  $G_A$  regarding different degrees of derivatization of amino groups (method see main manuscript).

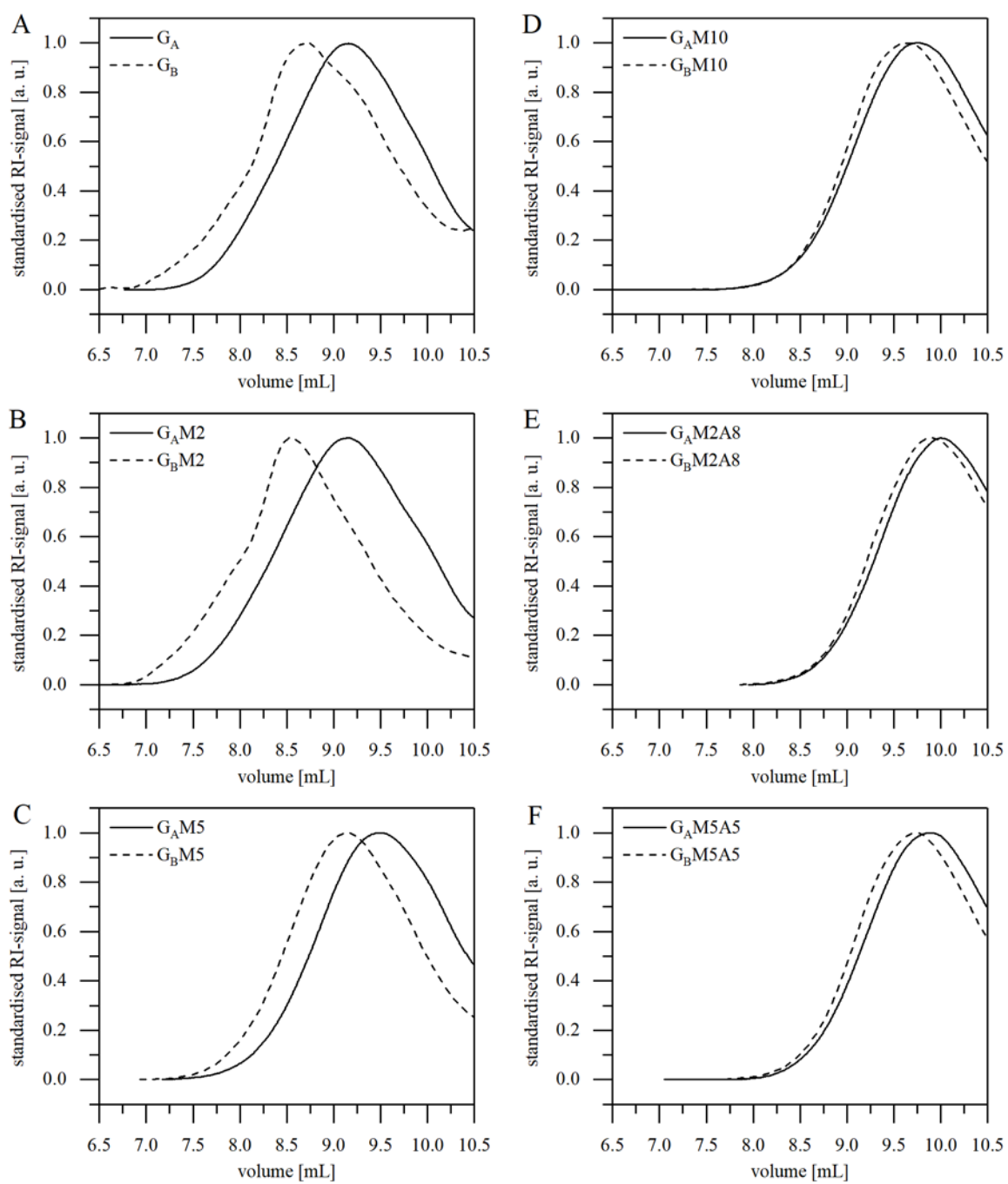


**Figure S3:** SEC elugrams of  $G_A$  and  $G_B$  (A) and derivatives (B-F).

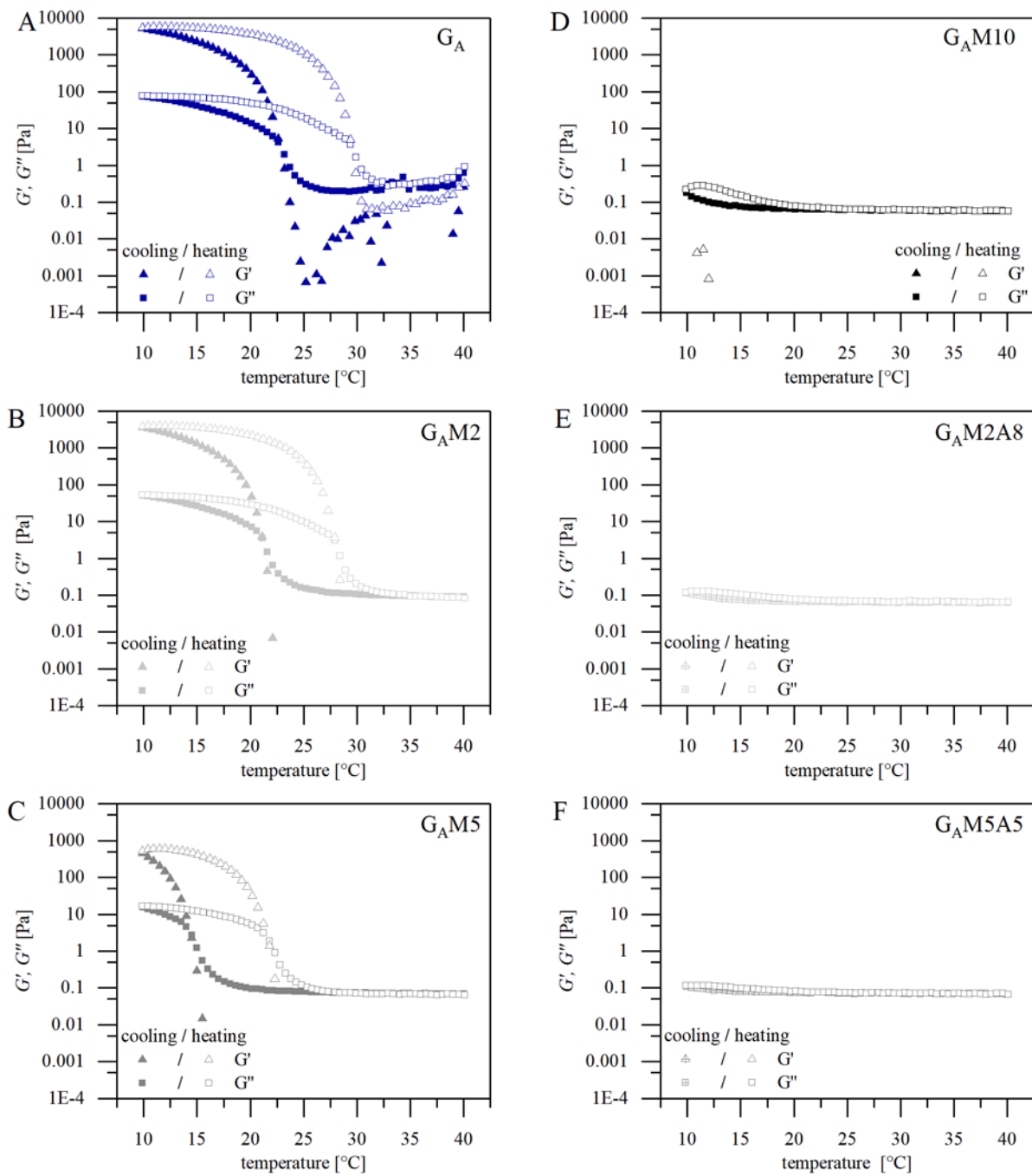


**Figure S 4:** Gelling behavior of  $G_A$  (A) and its derivatives  $G_{AM2}$  (B),  $G_{AM5}$  (C),  $G_{AM10}$  (D),  $G_{AM2A8}$  (E),  $G_{AM5A5}$  (F) in terms of  $G'$  and  $G''$ .

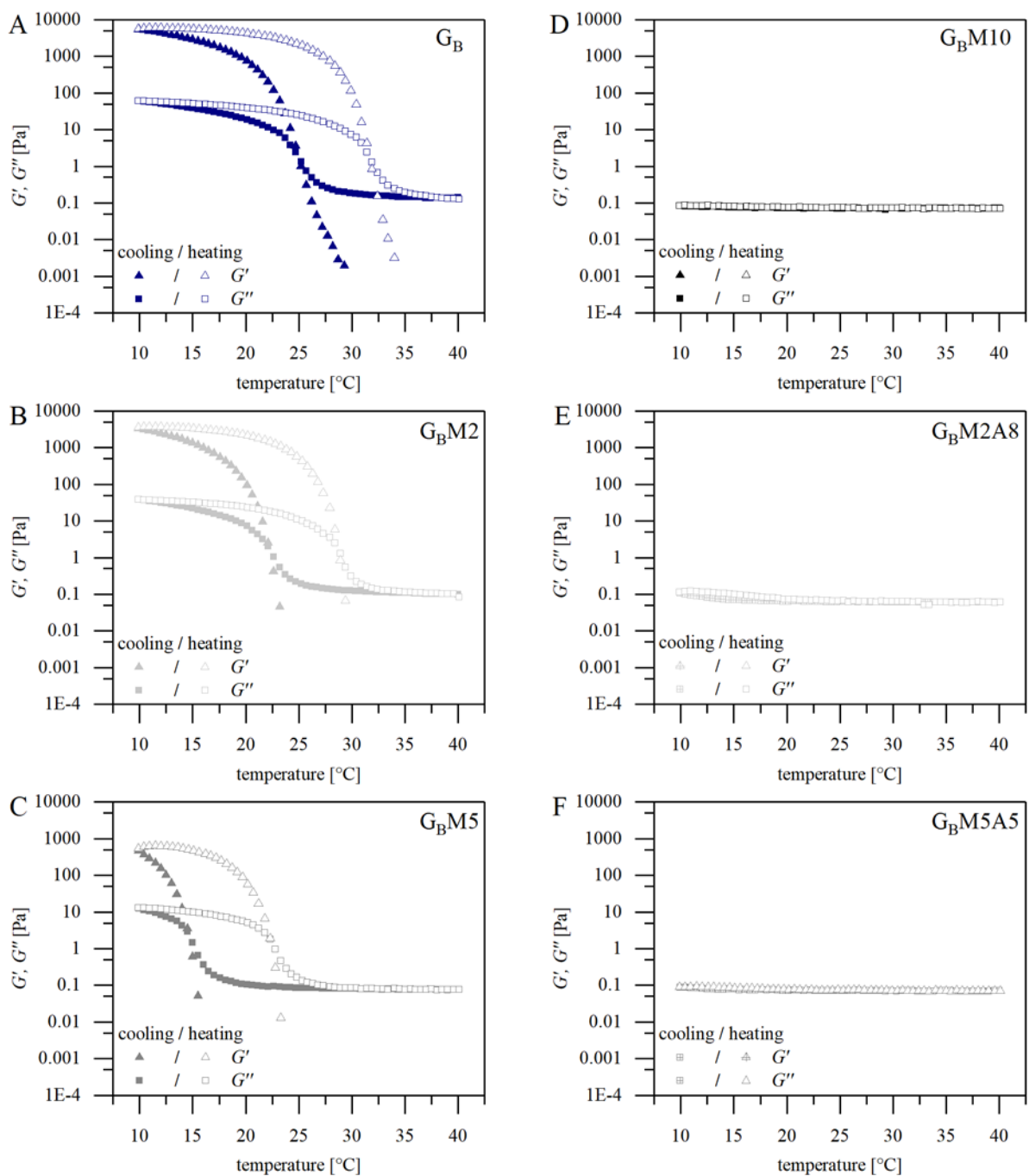


**Figure S 5:** Gelling behavior of  $G_B$  (A) and its derivatives  $G_{B}M2$  (B),  $G_{B}M5$  (C),  $G_{B}M10$  (D),  $G_{B}M2A8$  (E),  $G_{B}M5A5$  (F) in terms of  $G'$  and  $G''$ .



**Table S 4:** Dynamic viscosity of G<sub>A</sub> and G<sub>B</sub> derivatives' solutions (10 % (w/w) in PBS) in Pa s.

Gelatin derivative	Dynamic viscosity [Pa s]
G <sub>A</sub>	0.0103 ± 0.0003
G <sub>A</sub> M2	0.0062 ± 0.0022
G <sub>A</sub> M5	0.0036 ± 0.0007
G <sub>A</sub> M10	0.0030 ± 0.0002
G <sub>A</sub> M5A5	0.0024 ± 0.0002
G <sub>A</sub> M2A8	0.0030 ± 0.0007
G <sub>B</sub>	0.0222 ± 0.0000
G <sub>B</sub> M2	0.0105 ± 0.0009
G <sub>B</sub> M5	0.0047 ± 0.0004
G <sub>B</sub> M10	0.0037 ± 0.0014
G <sub>B</sub> M5A5	0.0025 ± 0.0002
G <sub>B</sub> M2A8	0.0029 ± 0.0000

**Table S 5:** Entitled differences of viscosity of 10 % (w/w) solutions. Significances are tagged as follows: \*=p<0.05, \*\*=p<0.01, \*\*\*=p<0.001, n. s. = not significant.

	G <sub>A</sub> M2	G <sub>A</sub> M5	G <sub>A</sub> M10	G <sub>A</sub> M5A5	G <sub>A</sub> M2A8	G <sub>B</sub> M2	G <sub>B</sub> M5	G <sub>B</sub> M10	G <sub>B</sub> M5A5	G <sub>B</sub> M2A8
G <sub>A</sub> M2		*	***	***	***	***	***			
G <sub>A</sub> M5	*		n. s.	n. s.	n. s.	*		*		
G <sub>A</sub> M10	***	n. s.		n. s.	n. s.	*			*	
G <sub>A</sub> M5A5	***	n. s.	n. s.		n. s.	*				n. s.
G <sub>A</sub> M2A8	***	n. s.	n. s.	n. s.		n. s.				
G <sub>B</sub> M2	***	*	*	*	n. s.					
G <sub>B</sub> M5	***							**	***	***
G <sub>B</sub> M10		*						**	**	**
G <sub>B</sub> M5A5			*					***	**	n. s.
G <sub>B</sub> M2A8				n. s.				***	**	n. s.

**Table S 6:** Storage modulus in the linear viscoelastic range ( $G'_{LVER}$  in kPa) and equilibrium degree of swelling ( $EDS$  in % of the polymer dry mass applied) of GM(A) hydrogels (10 % (w/w)).

Gelatin derivative	$G'_{LVER}$ [kPa]	$EDS$ [%]
G <sub>A</sub> M2	6.92 ± 2.14	709.9 ± 96.9
G <sub>A</sub> M5	8.10 ± 1.45	682.2 ± 14.2
G <sub>A</sub> M10	10.21 ± 1.85	664.5 ± 22.3
G <sub>A</sub> M5A5	5.01 ± 1.11	691.1 ± 35.6
G <sub>A</sub> M2A8	1.35 ± 0.37	955.3 ± 67.3
G <sub>B</sub> M2	14.40 ± 3.29	743.5 ± 28,7
G <sub>B</sub> M5	14.15 ± 1.54	669.5 ± 8.7
G <sub>B</sub> M10	12.60 ± 1.48	704.7 ± 24.6
G <sub>B</sub> M5A5	5.99 ± 0.50	790.1 ± 15.6
G <sub>B</sub> M2A8	1.22 ± 0.19	1303.3 ± 42.7

**Table S 7:** Entitled differences of  $G'_{LVER}$  of hydrogels from utilized gelatin derivatives. Significances are tagged as follows: \*= $p < 0.05$ , \*\*= $p < 0.01$ , \*\*\*= $p < 0.001$ , n. s. = not significant.

	G <sub>A</sub> M2	G <sub>A</sub> M5	G <sub>A</sub> M10	G <sub>A</sub> M5A5	G <sub>A</sub> M2A8	G <sub>B</sub> M2	G <sub>B</sub> M5	G <sub>B</sub> M10	G <sub>B</sub> M5A5	G <sub>B</sub> M2A8
G <sub>A</sub> M2		n. s.	*	n. s.	***	***				
G <sub>A</sub> M5	n. s.		n. s.	*	**		**			
G <sub>A</sub> M10	*	n. s.		*	**			n. s.		
G <sub>A</sub> M5A5	n. s.	*	*		*				n. s.	
G <sub>A</sub> M2A8	***	**	*	*						n. s.
G <sub>B</sub> M2	***						n. s.	n. s.	***	***
G <sub>B</sub> M5		**				n. s.		n. s.	**	n. s.
G <sub>B</sub> M10			n. s.			n. s.	n. s.		*	**
G <sub>B</sub> M5A5				n. s.		***	**	*		***
G <sub>B</sub> M2A8					n. s.	***	n. s.	**	***	

**Table S 8:** Entitled differences of *EDS* of hydrogels from utilized gelatin derivatives. Significances are tagged as follows: \*= $p<0.05$ , \*\*= $p<0.01$ , \*\*\*= $p<0.001$ , n. s. = not significant.

	G <sub>A</sub> M2	G <sub>A</sub> M5	G <sub>A</sub> M10	G <sub>A</sub> M5A5	G <sub>A</sub> M2A8	G <sub>B</sub> M2	G <sub>B</sub> M5	G <sub>B</sub> M10	G <sub>B</sub> M5A5	G <sub>B</sub> M2A8
G <sub>A</sub> M2		n. s.	n. s.	n. s.	**	n. s.				
G <sub>A</sub> M5	n. s.		n. s.	n. s.	*		n. s.			
G <sub>A</sub> M10	n. s.	n. s.		n. s.	**			n. s.		
G <sub>A</sub> M5A5	n. s.	n. s.	n. s.		**				**	
G <sub>A</sub> M2A8	**	*	**	**						**
G <sub>B</sub> M2	n. s.						*	n. s.	*	***
G <sub>B</sub> M5		n. s.				*		n. s.	***	***
G <sub>B</sub> M10			n. s.			n. s.	n. s.		**	***
G <sub>B</sub> M5A5				**		*	***	**		***
G <sub>B</sub> M2A8					**	***	***	***	***	

## 5. Sequenzielle Vernetzung von Gelatine-Methacryloyl-Hydrogelen

Die Ergebnisse und die Diskussion zu Hypothese 2 werden in diesem Kapitel dargestellt. Die Untersuchungen zu Hypothese 2.1 sind als Manuskript mit dem Titel *“Physical Interactions Strengthen Chemical Gelatin Methacryloyl Gels”* dargestellt. Dieses Manuskript wurde in der *peer-reviewed* Fachzeitschrift *gels* veröffentlicht. Die Studie zu Hypothese 2.2 ist als Manuskript mit dem Titel *„Differentiation of Physical and Chemical Cross-Linking in Gelatin Methacryloyl Hydrogels“* wiedergegeben. Dieses Manuskript wurde in der *peer-reviewed* Fachzeitschrift *Scientific Reports* veröffentlicht. Die Hypothese 2 wird im Kapitel 7.2 zusammenfassend diskutiert.

### 5.0 Erklärung meiner selbstständigen Leistung

#### 5.0.1 Manuskript mit dem Titel *“Physical Interactions Strengthen Chemical Gelatin Methacryloyl Gels”*

Ich habe die Studie zum größten Teil eigenständig konzipiert und ihre wissenschaftliche Methodik ausgearbeitet. Außerdem habe ich den Großteil der praktischen Arbeiten durchgeführt oder angeleitet, dies beinhaltet konkret:

- Die Synthese von 5 der 9 verwendeten GM(A)-Derivate (GM2 (2 von 3), GM2A8 (3 von 3)). Die Synthesen der anderen 4 GM(A)-Derivate erfolgten unter meiner Anleitung.
- Die quantitative Bestimmung des Methacryloylierungsgrades aller GM(A)-Synthesen.
- Die Temperatur-abhängigen rheologischen Messungen zur Bestimmung des Gelierpunktes.
- Die Herstellung aller Hydrogele sowie deren Charakterisierung mithilfe von Kompressionsversuchen wurden unter meiner Anleitung von Tobias Granse im Rahmen seiner von mir betreuten Masterarbeit durchgeführt.

Alle erhobenen Daten wurden von mir ausgewertet. Der weitaus größte Teil des *peer-reviewed* Fachartikels wurde von mir geschrieben, konkret habe ich den Original-Entwurf des Manuskripts konzipiert und geschrieben und federführend die Änderungsvorschläge meiner Co-Autoren harmonisiert und eingearbeitet.

### 5.0.2 Manuskript mit dem Titel „*Differentiation of Physical and Chemical Cross-Linking in Gelatin Methacryloyl Hydrogels*“

Ich habe die Studie zum größten Teil eigenständig konzipiert und ihre wissenschaftliche Methodik ausgearbeitet. Außerdem habe ich den Großteil der praktischen Arbeiten durchgeführt oder angeleitet, dies beinhaltet konkret:

- Die Synthese von 6 der 9 verwendeten GM(A)-Derivate (GM2 (3 von 3), GM10 (3 von 3)). Die Synthesen der anderen 3 GM(A)-Derivate erfolgten unter meiner Anleitung.
- Die quantitative Bestimmung des Methacryloylierungsgrades aller GM(A)-Synthesen.
- Die Anleitung der dynamischen Differenzkalorimetrie- und Circularidchroismus-Spektroskopie-Messungen. Die Messungen wurden von Sophia Regett nach einem von mir vorgegebenen Methodik durchgeführt.

Alle erhobenen Daten der dynamischen Differenzkalorimetrie-Messungen und der Circularidchroismus-Spektroskopie wurden von mir ausgewertet. Der weitaus größte Teil des *peer-reviewed* Fachartikels wurde von mir geschrieben, konkret habe ich den Original-Entwurf des Manuskripts konzipiert und geschrieben und federführend die Änderungsvorschläge meiner Co-Autoren harmonisiert und eingearbeitet.

## 5.1 Physical Interactions Strengthen Chemical Gelatin Methacryloyl Gels

Lisa Rebers<sup>1</sup>, Tobias Granse<sup>1,2</sup>, Günter E. M. Tovar<sup>1,2,\*</sup>, Alexander Southan<sup>1</sup> and Kirsten Borchers<sup>1,2,\*</sup>

<sup>1</sup> Institute of Interfacial Process Engineering and Plasma Technology IGVP, University of Stuttgart, Nobelstraße 12, 70569 Stuttgart, Germany.

<sup>2</sup> Fraunhofer Institute for Interfacial Engineering and Biotechnology IGB, Nobelstraße 12, 70569 Stuttgart, Germany.

\*Corresponding Authors: E-Mail: guenter.tovar@igvp.uni-stuttgart.de,  
kirsten.borchers@igb.fraunhofer.de

**Published in the peer-reviewed journal *gels***

Publisher: Multidisciplinary Digital Publishing Institute (MDPI)

DOI: <https://doi.org/10.3390/gels5010004>

Volume: 5, Page 4

©2019 by the authors.

Received October 20, 2018

Revised: January 10, 2019

Accepted: January 12, 2019

Published online: January 19, 2019

### 5.1.1 Abstract

Chemically cross-linkable gelatin methacryloyl (GM) derivatives are getting increasing attention regarding biomedical applications. Thus, thorough investigations are needed to achieve full understanding and control of the physico-chemical behavior of these promising biomaterials. We previously introduced gelatin methacryloyl acetyl (GMA) derivatives, which can be used to control physical network formation (solution viscosity, sol-gel transition) independently from chemical cross-linking by variation of the methacryloyl-to-acetyl ratio. It is known that temperature dependent physical network formation significantly influences the mechanical properties of chemically cross-linked GM hydrogels. We investigated the temperature sensitivity of GM derivatives with different degrees of modification (GM2, GM10), or similar degrees of modification but different methacryloyl contents (GM10, GM2A8). Rheological analysis showed that the low modified GM2 forms strong physical gels upon cooling while GM10 and GM2A8 form soft or no gels. Yet, compression testing revealed that all photo cross-linked GM(A) hydrogels were stronger if cooling was applied during hydrogel preparation. We suggest that the hydrophobic methacryloyl and acetyl residues disturb triple helix formation with increasing degree of modification, but additionally form hydrophobic structures, which facilitate chemical cross-linking.

### 5.1.2 Introduction

Gelatin is a collagen-derived biopolymer forming physical hydrogels due to the occurrence of secondary and tertiary structures and triple helix formation [322]. Physical gelling of the gelatin solutions is temperature dependent: Upon cooling, solutions gel at the gelation temperature and liquefy at the melting temperature [64]. Due to their inherent biocompatibility and bioactivity, gelatin-based hydrogels are frequently investigated for medical applications. For this purpose, hydrogels usually must be mechanically stable at body temperature, e.g., for drug release or tissue engineering [331, 342], which is not fulfilled by physical gelatin hydrogels. Hence, thermally stable covalent cross-links are needed in gelatin hydrogels. This can be achieved for example with the use of carbodiimides, such as 1-ethyl-3-(3-dimethylaminopropyl)carbodiimide (EDC) [310] for cross-linking of unmodified gelatin, or by chemical modification of gelatin with cross-linkable groups such as methacryloyl groups, resulting in gelatin methacryloyl (GM, also known as GelMA) as originally introduced by van den Bulcke *et al.* [42].

GM is a gelatin derivative, which is widely investigated in the field of regenerative medicine [35, 93]. It is usually synthesized by the reaction of methacrylic anhydride (MAAnh) with amino and hydroxyl functions of gelatin [50, 94]. The molar ratio of the reactive groups of gelatin and applied MAAnh excess during synthesis adjusts the content of methacryloyl groups in the resulting GM [42, 94, 96, 120]. The

resulting methacrylamide and methacrylate functions can be radically cross-linked by application of a radical initiator. Typically, a photo-initiator (e.g., Irgacure 2959, or lithium phenyl-2,4,6-trimethylbenzoylphosphinate (LAP, Li-TPO-L)) is added and cross-linking is induced by UVA-irradiation.

Increasing the degree of modification of gelatin generally results in a decrease of the physical interactions between the macromolecules [96, 125, 302, 303] and thus results e.g., in lower solution viscosities and lower sol-gel transition temperatures. In our group, we provide GM derivatives with various, well defined amounts of reactive methacryloyl functions (e.g., GM2, GM5, GM10). Furthermore, we developed GM derivatives with additional acetyl functions, which are not reactive (GMA, e.g., GM2A8, GM5A5). The suffixes denote the molar excess of MAA<sub>nh</sub> or acetic anhydride (AcAnh) which was applied during modification reaction, with regard to the amount of free amino groups in gelatin [42, 94, 96, 120, 125]. Thereby, it is possible to tune the chemical cross-linking potential, tunable by the degree of methacryloylation (DM), and the physical interaction potential, tunable by the total degree of modification, independently from each other.

Gelatin derivatives with a high degree of modification, e.g., generated by application of high amounts of MAA<sub>nh</sub> or AcAnh (GM10, GM2A8, GM5A5) [94, 96, 125], or by additional modification of the carboxylic functions of gelatin [303], show no physical gel formation at room temperature. These low viscous and non-gelling gelatin derivatives were described to be well suited for special 3D structuring methods such as inkjet-printing[125] and two photon polymerization [108, 303].

On the other hand, the total degree of modification also influences the mechanical properties of chemically cross-linked GM hydrogels beyond the degree of methacryloylation: We observed recently that the storage moduli ( $G'$ ) of chemically cross-linked GM hydrogels with low degrees of modification were unexpectedly high [96]. In particular, there was no difference detected between  $G'$  of chemically cross-linked GM2, GM5, and GM10 hydrogels. In contrast,  $G'$  increased as expected with increasing DM, if the total degree of modification was kept constantly high, as it is the case for GM2A8, GM5A5 and GM10. Based on these rheological data we assumed that GM2 and GM5 hydrogels were additionally stabilized by physical network formation due to their lower degree of modification compared to GM10, GM2A8, and GM5A5. These findings are supported by other studies, which took advantage of the physical gelling ability of GM hydrogel precursor solutions [45, 302, 303]: In these studies, compression moduli or storage moduli of GM hydrogels were increased dramatically, if physical network formation was first initiated by cooling of the GM solutions and UV-initiated chemical cross-linking was done afterwards. Similar effects were described for hydrogels out of unmodified gelatin that were cross-linked with enzymes [343-345] or a chemical cross-linker [346, 347].

However, it is unknown thus far whether adequate thermal protocols can also be used to strengthen GM(A) hydrogels with high degrees of modification such as GM10 or GM2A8 which show



no sol-gel transition above 10 °C due to strongly reduced physical interactions. In this study, we applied a cooling protocol to GM2, GM10 and GM2A8 hydrogel precursor solutions prior to chemical cross-linking and tested the compressive strength of resulting hydrogels. Since rheological data of GM(A) hydrogels are already heavily published, we chose compression testing as material characterization method. An advantage of this method is the possibility to apply higher stresses to the material compared to rheology. Thus, we developed an experimental set-up to determine the material response to compression at 37 °C in a swollen state.

### 5.1.3 Results and Discussion

In this study, we used GMs with different chemical modification degrees: GM2, GM10, and GM2A8, see **Figure 6**. These derivatives were chosen because GM2 and GM2A8 have similar DMs (see **Figure 6**), but different total degrees of modification due to the acetylation of GM2A8 while GM10 and GM2A8 have similar total degrees of modification, but different DMs.

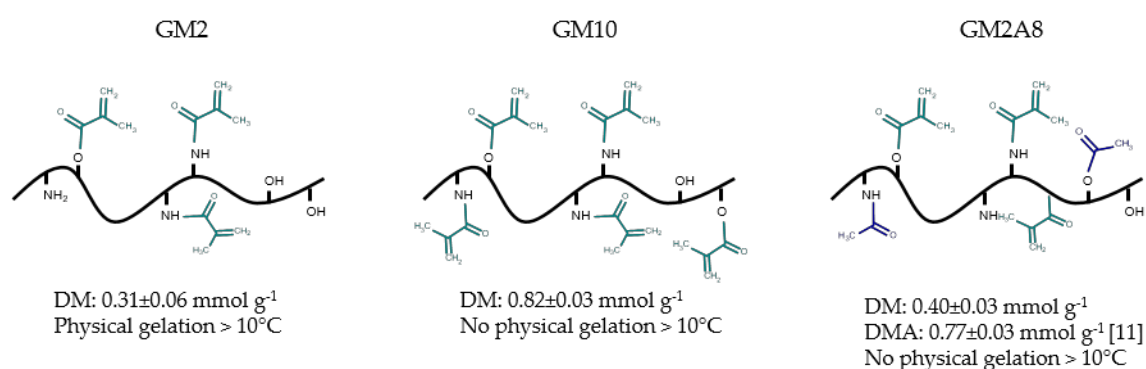


**Figure 6:** Schematic presentation of different gelatin derivatives used in this study. The suffix denotes the molar excess of anhydrides (MAAnh and AcAnh) used during synthesis procedure. Methacryloyl groups are marked green and acetyl groups blue. Furthermore, the degree of methacryloylation (DM), the total degree of modification (DMA, i.e., DM + degree of acetylation) and the capability to form physical gels [96] are given.

Furthermore, two hydrogel preparation procedures were compared: Immediate chemical cross-linking of hydrogel precursor solutions after dissolution of the respective gelatin derivative at 37 °C (denoted with a “-” in this study) and chemical cross-linking after cooling (20 min at 21 °C followed by 40 min at 4 °C) of the hydrogel precursor solution (denoted with a “+” in this study, also called sequential cross-linking in the literature). The chemical cross-linking was induced by 365 nm irradiation of the GM(A) solutions in alumina molds covered with quartz glass in presence of LAP as photo-initiator. All hydrogel precursor solutions were liquid in the molds when the photo-induced cross-linking was started immediately after transferring the warm solutions to the pre-warmed molds (-). GM2A8 were still liquid, when cross-linking was initiated after cooling during the sequential cross-linking procedure

(+), as occasionally indicated by floating air bubbles. GM2 formed physical gels during the sequential cross-linking procedure.

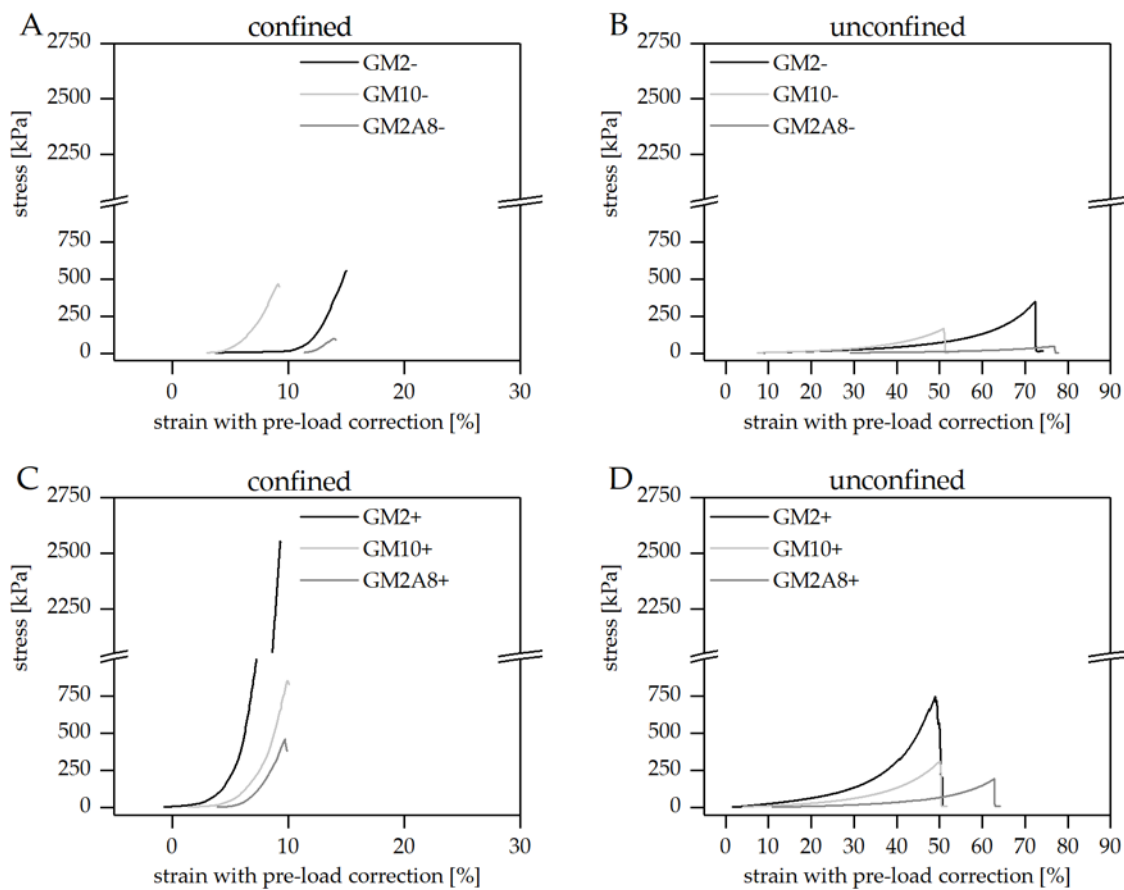


**Figure 7:** Stress-strain diagrams of gelatin methacryloyl acetyl (GM(A)) hydrogels made without (-) (A,B) and with cooling (C,D) cross-linking and measured in confined (A,C) and unconfined (B,D) set-up. The utilized the gels to different extents; therefore we determined the respective deformation and added it to the measured strains, which shifted the curves to the right to the corrected, effectively applied overall strains, resulting in different initial strains for the various specimens. Material failure resulted in complete drop of stress in the unconfined set-up (B,D). In the confined set-up the first drop of stress was interpreted to indicate material failure and curves are only displayed up to the corresponding strain (A,C).

After chemical cross-linking, all hydrogels were tested in compression tests using a custom-made set-up for the measurement of hydrogels in a physiological setting (swollen state, phosphate buffered saline (PBS+), 37 °C), either in a confined or unconfined mode. Representative stress-strain diagrams for both measurement set-ups are shown in **Figure 7**.

The stress-strain curves of all hydrogels were generally of a comparable shape, regardless of the hydrogel preparation procedure and the measurement set-up: The hydrogels showed relatively low stress responses at low strains, resulting in low slopes. The slopes generally increased upon increasing deformation indicating strain stiffening of the hydrogels until material failure. Similar behavior has been described for hydrogels before [348, 349]. It has to be noted that the pre-load of 0.2 N, which was applied to avoid artefacts due to incomplete contact of the indenter with the specimens, resulted in relevant deformations especially of the softer hydrogels. This initial compression was taken into account and added to the strains applied during the measurement (see **Figure 7**). The compressive

strains at break ( $\epsilon_b$ ) and the respective compressive stresses at break ( $\sigma_b$ ) were extracted from such corrected stress-strain curves (**Figure 8, Table 2**).

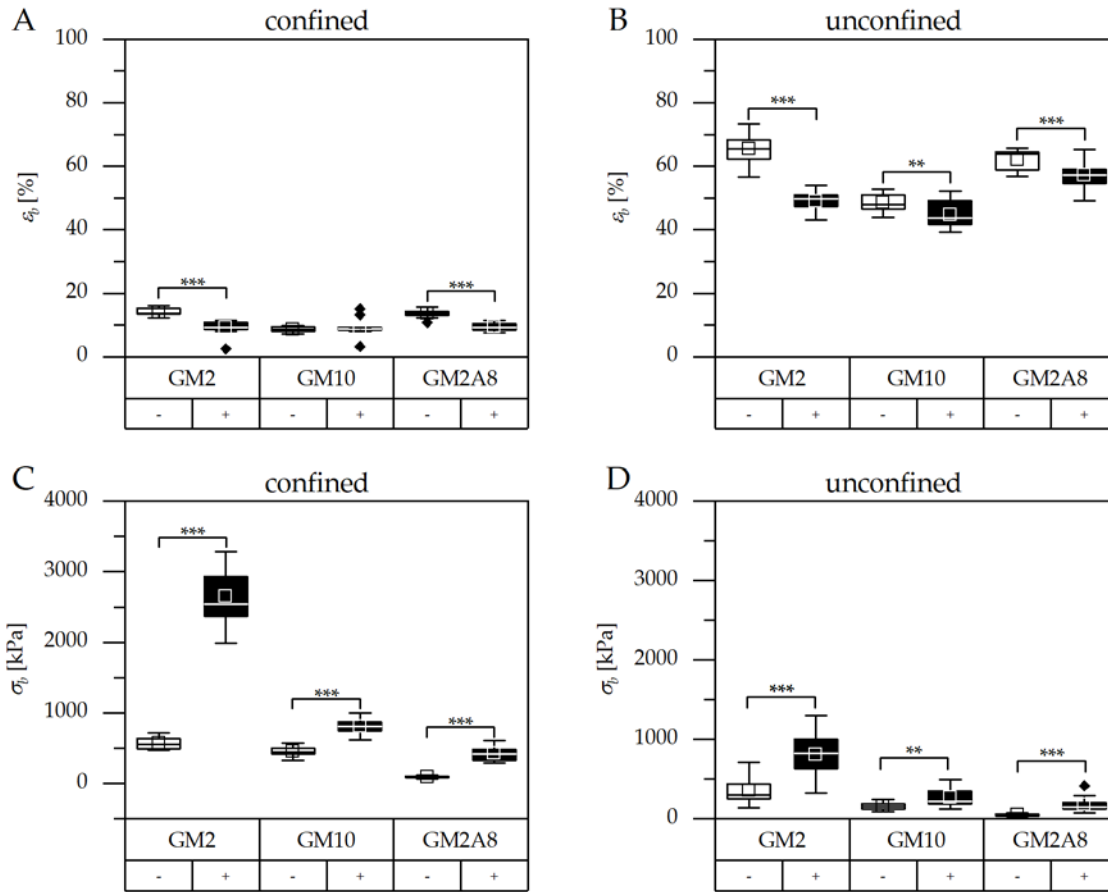


**Figure 8:** Compressive strains at break ( $\epsilon_b$ ) measured in the confined (**A**) or unconfined (**B**) set-up and the respective compressive stresses at break ( $\sigma_b$ ) (**C,D**). Hydrogels were prepared with (+) or without (-) cooling. The 25<sup>th</sup> and 75<sup>th</sup> percentiles of all specimen determine the boxes. The whiskers mark the inner fence (1.5-fold interquartile range). Data points beyond the inner fence are outliers and shown as black diamonds. The line in the box represents the median and the center of the square the mean. Significant differences are marked as follows: \*\* $p < 0.01$ , \*\*\* $p < 0.001$ .

Hydrogels are not able to extend laterally in the confined measuring set-up. Therefore, the effective vertical strains were generally smaller compared to the unconfined set-up, in particular the compressive strains at break ( $\epsilon_b$ ). Correspondingly, the stress and in particular the compressive strength at break ( $\sigma_b$ ) was greater in the confined set-up than in the unconfined set-up. Furthermore, the relative impact of cooling on  $\epsilon_b$  and  $\sigma_b$  was also different in the confined and unconfined measurement set-ups (e.g.,  $\sigma_b(\text{GM2}(+))/\sigma_b(\text{GM2}(-))=4.6$  in the confined measurement, or  $\sigma_b(\text{GM2}(+))/\sigma_b(\text{GM2}(-))=2.2$  in the unconfined measurement;  $\sigma_b(\text{GM10}(+))/\sigma_b(\text{GM10}(-))=1.8$  in the confined measurement, or  $\sigma_b(\text{GM10}(+))/\sigma_b(\text{GM10}(-))=1.6$  in the unconfined measurement). This makes it obvious that data from the confined and unconfined measurements must not be mixed up for comparison, not even for relative correlation. Consequently, standardized procedures for hydrogel characterization are required

in order to enable generation and publication of comprehensive and informative data sets which can then be compared across laboratory borders.

**Table 2:** Compressive strain at break ( $\epsilon_b$ ) and the respective compressive stresses at break ( $\sigma_b$ ) of GM(A) hydrogels measured in a confined or an unconfined setting. Each GM(A) hydrogel was investigated without cooling (-) and with cooling (+) before chemical cross-linking.

gelatin derivative		confined		unconfined	
		$\sigma_b$ [kPa]	$\epsilon_b$ [%]	$\sigma_b$ kPa]	$\epsilon_b$ [%]
GM2	-	570.6 ± 31.6	14.0 ± 0.4	358.6 ± 117.4	65.4 ± 4.0
	+	2647.7 ± 42.9	9.2 ± 2.1	805.8 ± 96.3	48.9 ± 0.6
GM10	-	457.2 ± 24.9	8.7 ± 0.6	159.4 ± 45.7	48.5 ± 2.8
	+	801.4 ± 67.5	9.2 ± 1.1	251.6 ± 59.2	44.8 ± 2.6
GM2A8	-	91.0 ± 8.6	13.7 ± 0.9	47.3 ± 8.6	62.1 ± 1.4
	+	423.3 ± 56.6	9.5 ± 0.7	180.9 ± 21.7	57.1 ± 1.5

Firstly, we consider the hydrogels which were prepared without cooling:  $\epsilon_b$  of GM2A8(-) was significantly higher than that of GM10(-), and simultaneously  $\sigma_b$  of GM2A8(-) was lower than that of GM10(-), as it was expected due to the differences in the DM. In contrast, the compressive properties of GM2(-) were exceptional. GM2(-) gels were as compressible as GM2A8(-) gels, but simultaneously the compressive strength at break of GM2(-) was higher than GM2A8(-) and even higher than GM10(-). This confirmed our prior observations from rheological characterizations, that GM2A8 hydrogels had a lower  $G'$  compared to GM10 hydrogels, and that  $G'$  of GM2(-) hydrogels were also significantly higher compared to GM10 and GM2A8 hydrogels [96].

The lower storage modulus  $G'$  and compressive strength  $\sigma_b$  of GM10(-) and GM2A8(-) compared to GM2(-) can be assigned to the known effect that elevated degrees of modification restrain the ability of GM materials to form triple helices[125, 303]. It can be derived from the presented data that it was mainly the different amounts of chemical bonds of GM2A8(-) and GM10(-) which defined the compressive strengths of such hydrogels, while physical network formation additionally contributed to strengthening of GM2(-). This was the case, although none of the hydrogel precursor solutions was cooled below the gelation temperature  $T_{gel}$  but all were cross-linked in the liquid state. Obviously, some beneficial presorting of the GM2 took place, although gelling was not visually observed.

As a consequence, we wondered whether cooling of the hydrogel precursor solutions could also induce strengthening of hydrogels made of highly modified GM(A)s, which do not show gel transition above 10 °C. Therefore, we used a cooling procedure (20 min at 21 °C followed by 40 min at

4 °C) prior to chemical cross-linking to impose temperature-dependent physical interactions. The results are shown in **Figure 7** and **Figure 8** graphically. The measured  $\sigma_b$  and  $\varepsilon_b$  are given in **Table 2** for an easier access. The compressibility of all (+) hydrogels was significantly reduced by cooling, i.e., hydrogels were less compressible (**Figure 8-A, B**,  $p < 0.01$ ; except for GM10 hydrogels measured in the confined set-up where  $\varepsilon_b$  remained unchanged). Simultaneously, the  $\sigma_b$  values increased significantly for all (+) hydrogels ( $p < 0.01$ , **Figure 8-C, D**).

This was expected for GM2(+) gels, because GM2 solutions obviously formed physical hydrogels upon cooling. Physical gelling has been correlated with triple helix formation of gelatin and GM derivatives in several studies [45, 302, 303]. It was suggested that these quaternary structures are then fixed by covalent cross-links such that both, physical and chemical networks contribute to the elastic stability of the hydrogel and temperature-related melting was hindered [45, 96, 302]. It is discussed that the helices could act as templates for a more effective cross-linking of the C=C double bonds of gelatin methacryloyl. Indeed, unreacted C=C double bonds were still detectable by Fourier transform infrared spectroscopy of GM gels that were UV-cured at 37 °C, but not in gels made from the same material after incubation at 4 °C to allow physical gelling before UV-curing [302].

Additionally, the presented results in this study show that strengthening by cooling was also effective in GM2A8(+) and GM10(+) hydrogels with high degrees of modification. This was rather unexpected, as we proofed in earlier studies that physical interactions are strongly reduced in GM2A8 and GM10 solutions, resulting e.g., in decreased viscosity and absent physical gelation for temperatures above 10 °C [96]. Therefore, we further investigated GM2, GM10, and GM2A8 hydrogel precursor solutions rheologically during the thermal protocol in order to learn more about the gelation process during cooling (**Table 3**, and **Figure S 6**, 5.1.7 Supporting Information ). GM2 solutions gelled (i.e.,  $G' \geq G''$ ) after 3 min at 21 °C as expected. Additionally, we detected  $G' \geq G''$  for GM10 solutions after approx. 4 min at 4 °C. GM2A8 solutions showed gelling just for one out of three batches after 18 min at 4 °C, while no gelling was observed at all during 40 min at 4 °C for two out of three batches. At the end of the thermal protocol  $G'$  of physical GM2 gels was the highest (10,633±514 Pa, n=3),  $G'$  of GM10 gels was lower (2112±1264 Pa, n=3) than that, and  $G'$  of gelled GM2A8 was extremely low (24 Pa, n=1).

The ratio of  $G''$  and  $G'$  (loss factors  $\tan(\delta)$ , see **Table 3**) of the cooled solutions accentuate the  $G'$  data:  $\tan(\delta)$  of GM2A8 (0.165, single measurement) was higher than  $\tan(\delta)$  of GM10 (~0.013) and GM2 (~0.008). The approx. 100 times higher  $G'$  than  $G''$  points out that GM2 and GM10 both formed networks with elastic properties, although the physical GM2 gels were much stronger than physical GM10 gels, as revealed by the absolute values of  $G'$ . Physical GM2A8 gels showed a rather viscous behavior. This was confirmed by the fact, that just one out of three measured hydrogel precursor solutions showed a gelation point.

**Table 3:** Rheological analysis of GM(A) solutions (10% (w/w)) during cooling (20 min 21°C + 40 min 4°C). Gelation was determined when the storage modulus  $G'$  became larger than the loss modulus  $G''$  ( $G' \geq G''$ ). Furthermore, the storage moduli of the physical hydrogels measured at the end of the thermal protocol (after 60 min), before chemical cross-linking, is given ( $G'$ ). The loss factor of physical hydrogels is determined as ratio of  $G''$  and  $G'$  ( $\tan \delta$ ).

	GM2 (n=3)	GM10 (n=3)	GM2A8*
$G' \geq G''$	3 min/21°C	20 min/21°C + 4 min/4°C	20 min/21°C + 18 min/4°C
$G'$ [Pa]	10633 ± 514	2112 ± 1264	48
$\tan(\delta)$ ( $G''/G'$ )	0.008 ± 0.000	0.013 ± 0.003	0.165

\* To be noted: A gelation point  $G' \geq G''$  was singularly detected for one batch out of three, the other two solutions showed no sign of gelling, therefore no standard deviations were determined.

If the formation of strong physical GM2(+) gels was due to the formation of triple-helical regions, conversely, the low or very low  $G'$  suggested reduced or no helix formation in GM10(+) and GM2A8(+) solutions. In native triple helices 30 amino acids per strand are associated in one triple helix turn [350]. We calculated the theoretical mean distance between two methacryloyl- or acetyl-modified amino acids in the GM(A) derivatives as the reciprocal of the total degree of modification (see **Table S 9**, 5.1.7 Supporting Information). We assumed an average molecular weight of amino acids (based on the amino acid composition of the raw material published in [96]) of 122 g mol<sup>-1</sup> to calculate the theoretical number of amino acids between two chemical modifications. According to this estimation, one chemically modified amino acid occurs statistically every 26 amino acids in GM2, while in GM10 and GM2A8 one modification occurs every 10 amino acids. Thus, theoretically in GM2 one amino acid per triple helix turn is chemically modified, while in GM10 and GM2A8 there are three modified amino acid per triple helix turn. In fact, GM2 is mainly modified at lysine residues [94, 96]. Regarding the lysine distribution in the triple-helical region of the collagen-chain (bovine collagen type I, according to Uniprot database), 83 % of lysines in this region are separated by more than 30 other (not lysine) amino acids. Thus, it seems plausible, that triple-helix formation and thus significant stiffening of the gels can occur in GM2 solutions, but not in GM10 and GM2A8 solutions, since in GM10 and GM2A8 other hydroxyl containing amino acids are modified additionally.

In this context we want to consider additional factors which could be responsible for the strengthening of the GM10(+) and GM2A8(+) hydrogel network besides the assembly of triple helices, i.e., re-arrangement of GM(A) polymer chains by hydrophobic interactions of methacryloyl and acetyl groups. Methacryloyl and acetyl groups are rather hydrophobic and might form hydrophobic domains in an aqueous environment. Thereby, a polymer network with few open loops might form and the hydrophobic methacryloyl groups might be oriented in favor of higher conversions during chemical

cross-linking. Cooling would help to stabilize such hydrophobic domains and consequently the density of elastically active chemical cross-links would be enhanced compared to solutions that are cross-linked at higher temperatures. In this way, the insertion of methacryloyl and acetyl groups might have a structure-forming effect apart from hindering the formation of triple-helices.

Indeed, we observed before that the hydrodynamic radius of gelatin derivatives decreased with increasing degrees of modification [96]. We assigned this to the masking of the hydroxyl groups of hydroxyproline in the amino acid sequence by insertion of hydrophobic methacryloyl or acetyl-residues. The resulting loss of hydrogen bindings can be expected to de-stabilize the native, elongated-helix conformation of single collagen or gelatin molecules, and to promote the (more globular) random coil conformations with shielded hydrophobic domains to exclude water. The hydrodynamic radius was even smaller in derivatives with higher acetyl portions, possibly because less volume was needed by acetyl than by methacryloyl-groups [96]. We hypothesize an impact of the type and size of the inserted methacryloyl and acetyl functions: Finally, such differences in the hydrodynamic radius might influence the degree of entanglement of GM(A) molecules and account for the unexpected rheological difference of GM10 and GM2A8 (**Table 3**) in spite of the very similar degrees of modification of the two derivatives.

To summarize, we suggest that hydrophobic interactions contribute to the formation of dense protein domains and by that to physical networks in gelatin methacryloyl hydrogels. Cooling stabilizes such hydrophobic domains and thus radical cross-linking of the methacryloyl groups becomes more effective resulting in stronger hydrogels at lower temperatures. In gelatin derivatives with low degrees of modification the formation of triple helices occurs in parallel to formation of hydrophobic domains. Thus, the resulting hydrogels are stronger than hydrogels based on gelatin derivatives with a high degree of modification, where hydrophobic domains are the dominant structure while formation of stiff triple helical regions is hindered.

This hypothesis is supported by significant differences in the temperature sensitivity of cross-linked GM(A) hydrogels and hydrogels which are generated by chemical cross-linking of unmodified gelatin with a chemical cross-linker [346] or enzymatically [343]: Other authors [45, 302] and ourselves [96] have observed that the mechanical properties of chemically cross-linked GM(A) hydrogels were not temperature-dependent, no matter whether they had been cross-linked in the gelled or in the liquid state. The compression tests in this study were conducted at 37 °C. Although this is above the melting temperature for all GM(A)s [96], the mechanical differences between gels that had been cross-linked in the liquid state or the (quasi-)gelled state were conserved: The interactions that additionally strengthened the hydrogels were not lost upon heating. This indicates that in the macromolecular network of chemically cross-linked GM(A) hydrogels triple helices and other physical interactions neither form nor melt. In contrast, authors who performed cross-linking of unmodified gelatin hydrogels with bis(vinylsulfonyl)methane [346, 347] observed temperature-sensitivity of the

hydrogels: Helices were reversibly formed by a temperature switch after the chemical cross-linking reaction had been stopped. The same was observed for enzyme catalyzed cross-linking of gelatin with transglutaminase. We postulate that the superimposed hydrophobic structure, which is then fixed by covalent cross-linking, might be the reason for the distinct temperature stability of GM gels, which is not fully achieved by chemical cross-linking of unmodified gelatin. Consequently, the hydrophobic nature of the inserted methacryloyl-functions and acetyl-functions enables formation of gelatin hydrogels with elevated strength.

#### 5.1.4 Conclusion

The compressive strength of chemically cross-linked gelatin methacryloyl gels can be increased by cooling whether physical gel formation is visually observed or not. This indicated that temperature dependent physical interactions can be used to strengthen cross-linked GM(A) hydrogels, e.g., hydrophobic interactions in the case of highly modified gelatin derivatives. On the other hand, it also emphasizes the need to tightly control the thermal history of GM(A) solutions even if physical gelation is not an obvious issue. Furthermore, quaternary structures based on hydrophobic interactions may facilitate the radical cross-linking of GM(A) and result in hydrogels, which are temperature independent and stable at 37 °C, other than enzymatic or chemical cross-linking of unmodified gelatin. This can make a relevant difference regarding possible biomedical application.

#### 5.1.5 Materials and Methods

##### **Materials**

The following materials were purchased from Sigma Aldrich (Darmstadt, Germany): Acetic anhydride (AcAnh), sodium hydrogen phosphate ( $\text{Na}_2\text{HPO}_4$ ), Dulbecco's phosphate buffered saline with  $\text{MgCl}_2$  and  $\text{CaCl}_2$  (PBS+), methacrylic anhydride (MAAnh) as well as sodium hydroxide (NaOH). Sodium 3-trimethylsilyl-propionate-2,2,3,3-d<sub>4</sub> (TMSP) was bought from Merck (Darmstadt, Germany). Other reagents were purchased from the following sources (given in parentheses): Deuterium oxide (D<sub>2</sub>O) (Deutero; Kastellaun, Germany), Gelatin (type B, Limed, bovine bone, 232 Bloom, standard viscosity=4.5 mPa s; Gelita; Eberbach, Germany). Dialysis membranes (MWCO 12 kDa–14 kDa) were purchased from Medicell International Ltd. (London, UK). The photoinitiator lithium phenyl-2,4,6-trimethylbenzoylphosphinate (LAP, also known as Li-TPO-L, TMPPL) was synthesized according to Fairbanks *et al.*[313]. <sup>1</sup>H-NMR spectroscopy (500 MHz, D<sub>2</sub>O, d) proofed adequate shifts and integrals, i.e., 7.74 (m, 2 H), 7.56 (m, 1 H), 7.46 (m, 2 H), 6.87 (s, 2 H), 2.22 (s, 3 H), 2.04 (s, 6 H).



## Synthesis of Gelatin Methacryloyl (GM2, GM10) and Gelatin Methacryloyl Acetyl (GM2A8)

Gelatin methacryloyl (GM) was prepared as previously described [94]. In short, gelatin (25.01 g) was dissolved in deionized water (250 mL) at 37 °C and its pH was adjusted to 7.3 with the use of an automatic titration device. Within 30 min 2.70 g/13.49 g of MAAnh were added, which corresponds to a two-fold (GM2) or ten-fold (GM10) molar excess relative to an amino group content of gelatin (0.35 mmol g<sup>-1</sup> [6]). In case of GM2A8 synthesis, after 2 h of methacryloylation reaction 7.15 g of acetic anhydride (AcAnh) were added dropwise within 30 min, resulting in an eight-fold (GM2A8) molar excess relative to the content of amino-groups of gelatin [42]. The reaction mixture was stirred vigorously for 5 h in total, keeping its pH constantly between 7.0 and 7.4. The reaction mixture was filtrated subsequently and its pH was adjusted to 9.5. After leaving the mixture at 4 °C for 2 days, the solution was dialyzed for 4 days against deionized water at room temperature. Afterwards, the pH was adjusted to 8.5 and the solution was freeze-dried. The degree of methacryloylation (DM) was determined using <sup>1</sup>H-NMR spectroscopy as described by Claaßen *et al.* [94]. The mean and the standard deviation of the three syntheses of each derivative used in this study are given in **Figure 6**.

### Preparation of GM(A) Hydrogels

Hydrogels with initial GM(A) concentration of 10 % (w/w) were prepared either by immediate photo-initiated radical cross-linking or by cooling of the precursor solution and subsequent chemical cross-linking. In detail, GM(A) was dissolved in PBS+ containing 0.2 % (w/w) LAP with regard to biopolymer content for 2 h at 37 °C. Afterwards, the solution was poured into a cylindrical mold (25 mm diameter, 5 mm depth) and covered by a quartz glass pane. If physical gelation of hydrogel precursor solution was desired, the mold was left at 21 °C for 20 min and afterwards for 40 min at 4 °C. Then, chemical cross-linking was done by exposure to UVA light (approx. 365 nm, 18.2 mW cm<sup>-2</sup>) for 2.5 min. If physical gelation was not desired, the hydrogel precursor solution was cured immediately after pouring into the mold. After curing, the quartz glass pane was removed and the cross-linked hydrogels were taken out of the mold. Hydrogels were washed for 5 h in PBS+ at 37 °C, exchanging the PBS+ every hour. Afterwards, the hydrogels were swollen in PBS+ for 19 h at 37 °C.

### Measurement Set-Up for Hydrogel Compression Testing

We used the material testing machine Allround-Line Z005 equipped with a 2.5 kN Xforce HP load cell (Zwick, Ulm, Germany) for compression testing of GM(A) hydrogels. The appropriate software “testXpert II” was utilized for execution of the measurements and analysis of the data. Furthermore, a measurement set-up was established to enable measurement of hydrogels at 37 °C in a swollen state (**Figure 9**): A measuring chamber made from polyether ether ketone (PEEK) was used with an inflow and outflow. A hose pump pumped PBS+ through the measuring chamber in a closed circuit. The PBS+

was warmed to 37 °C on a stirrer/hotplate, which was controlled by a temperature sensor in the chamber.

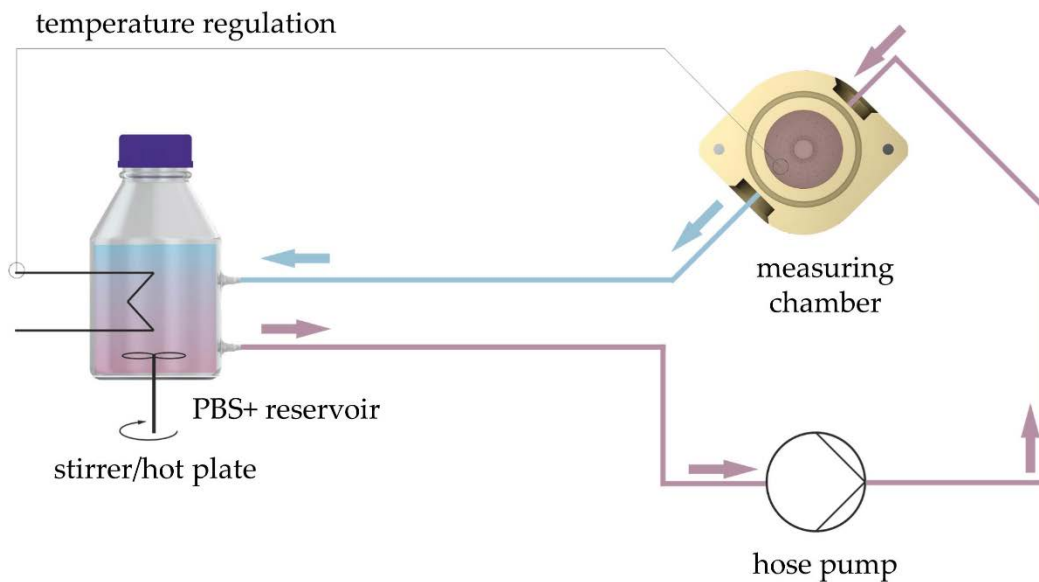


**Figure 9:** Experimental set-up for compression tests of hydrogels in a swollen state at 37 °C. The measuring chamber was flushed with 37 °C warm PBS+ throughout the measurements. The PBS+ was warmed on a magnetic stirrer/hotplate and pumped in a closed circuit through the measuring chamber by the hose pump.

To ensure PBS+ exchange within the measuring chamber without uncontrolled movement of the hydrogel we constructed a perforated inlet with a platform, see **Figure 10-B, C**. The hydrogels were placed on that platform for measurements and were covered completely with PBS+. We constructed an adapter for the Z005 tool holder of the testing machine and a measuring head with a diameter of 15 mm, see **Figure 10-A**. The adapter was fixed at the Z005 tool holder using four M5 screws. The measuring head was screwed into the adapter by its M8 thread. A M3 grub screw was used to cinch the screwed measuring head.

### Compression Testing of GM(A) Hydrogels

Cylindrical hydrogel samples ( $\varnothing$  8 mm) were punched out of the washed and swollen hydrogel in quadruplicates for compression testing. Samples were stored in 37 °C warm PBS+ until the measurement. The geometry of the hydrogel samples is crucial for the output data, since for calculation a perfect cylindrical sample shape is assumed. Therefore, the height of every sample before compression testing was determined with a caliper.

Failure testing of hydrogels was performed at 37 °C in a swollen state using a pre-load of 0.2 N and 0.5 % s<sup>-1</sup> as test speed. For unconfined measurements, the hydrogel was placed into the measurement chamber without any lateral limitation and a measuring head with a diameter of 15 mm was used. A compression chamber with a filter disk as bottom and a standard indenter with a diameter of 8 mm were utilized for confined measurements.

For the measurements, the hydrogel sample was placed in the middle of the inlet platform and the measuring head was positioned 5.5 mm above the inlet of the measuring chamber. After 4 min waiting in this position, the measuring head sloped with  $0.1 \text{ mm s}^{-1}$  to the hydrogel sample until a pre-load of 0.2 N was achieved. After reaching this pre-load, the height of the test specimens was recorded ( $h_{0.2N}$ ) and the measurement started automatically with a constant strain rate of  $0.5 \% \text{ s}^{-1}$  relative to the initial test specimen's height until destruction.

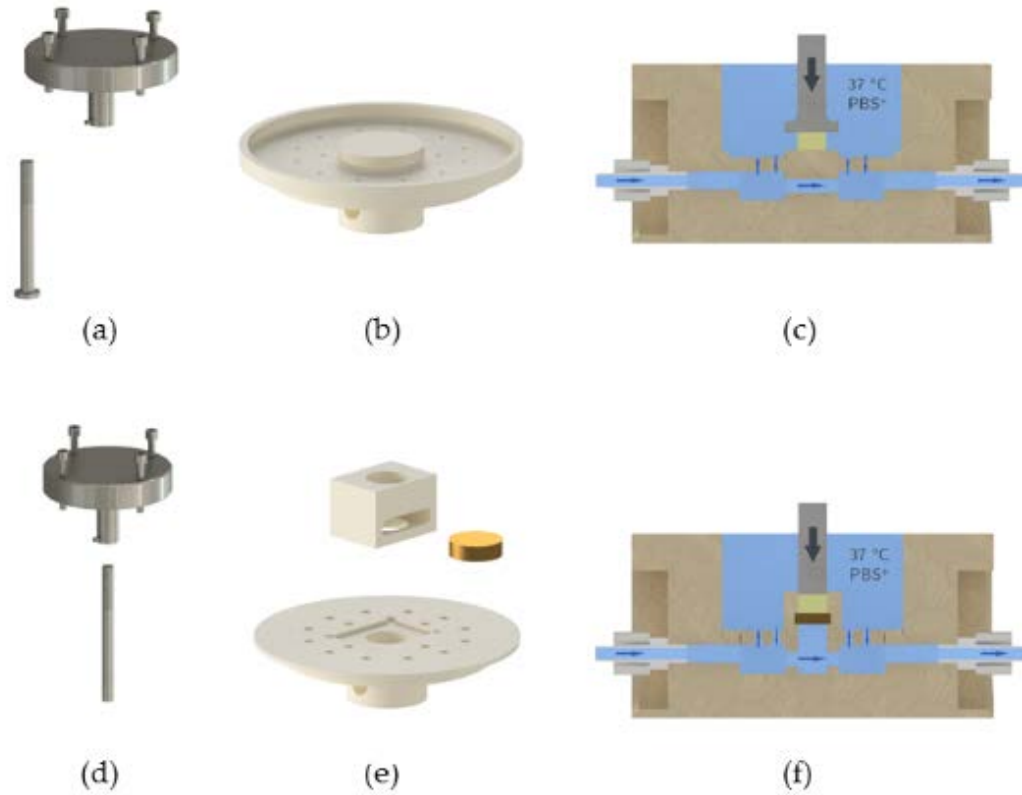


**Figure 10:** Technical drawing of the measurement components for unconfined (a–c) and confined (d–f) measurements: (a/d) Self-designed measuring head for the material testing machine Z005, consisting of an adapter and the measuring head. The diameter was 15 mm (a) and 8 mm (d). (b/e) Technical drawing of the inlet of the measuring chamber. Due to the perforation of the inlet the exchange of the PBS+ surrounding the hydrogel was ensured. For confined testing a chamber with a filter disk ensuring PBS+ exchange was utilized. (c/f) Transverse section of the measuring chamber.

### Data Analysis of Compression Testing

The stress–strain relationship resulting out of compression testing was analyzed. Since hydrogels have a progressive stress–strain relationship like elastomers, the compression strength and compressive stress at break were the same and we named it  $\sigma_b$ . The compressive strain at break or compressive Strain at compressive strength is named  $\varepsilon_b$  in this study. We programmed the software “testXpert II” to register the compressive strength at break ( $\sigma_b^{reg}$ ) and the compressive strain at break ( $\varepsilon_b^{reg}$ ) in confined measurements automatically after a strength drop of 50 kPa. In unconfined measurements the maximum registered stress was defined to be  $\sigma_b$ , the corresponding compressive strain was defined to be  $\varepsilon_b^{reg}$ .

Furthermore, we recognized a significantly reduced height ( $h_{0.2N}$ ) for soft gels at the chosen pre-load of 0.2 N. Consequently, we had to correct the registered values for the compressive strains at break  $\varepsilon_b^{reg}$ , because the machine regarded  $h_{0.2N}$  as reference height instead of the original heights of the gels  $h_0$ . We measured the original heights of hydrogels ( $h_0$ ) manually with a caliper. The corrected values for  $\varepsilon$  were then calculated using Equation 2. Specifically, the height at break  $h_b$  was determined as the measured height at  $\sigma_b^{reg}$ . The corrected  $\varepsilon_b$  was calculated using Equation 3.

$$\varepsilon = \frac{h_0 - h}{h_0} \times 100 \% \quad (2)$$

$$\varepsilon_b = \frac{h_0 - h_b}{h_0} \times 100 \% \quad (3)$$

### Temperature Depending Rheological Measurements

A Physica Modular Compact MCR301 rheometer from Anton Paar (Ostfildern, Germany) equipped with cone-plate system (d=40 mm) was used to investigate  $G'$  and  $G''$  of the hydrogel precursor solutions as a function of temperature.  $G'$  and  $G''$  were determined at a fixed amplitude (5 %) and frequency ( $1 \text{ s}^{-1}$ ).

To reproduce the utilized gelation procedure, we performed the following temperature changes during rheological measurements: The  $37 \text{ }^\circ\text{C}$  warm hydrogel precursor solution was put into the measuring gap and the measurement was started. The first 5 min the temperature was  $37 \text{ }^\circ\text{C}$ , afterwards the bottom plate of the rheometer was cooled to  $21 \text{ }^\circ\text{C}$  for 20 min followed by a further cooling to  $4 \text{ }^\circ\text{C}$  for 40 min.  $T_{gel}$  was determined from the cooling curve  $G'=G''$ . Since usually the temperature where  $G'=G''$  is not measured exactly, the first temperature where  $G'>G''$  (cooling curve,  $T_{gel}$ ) was used.

### Statistics and Box-Plots

The presented data include hydrogels out of three independent synthesis per gelatin derivative. Furthermore, we did compression testing on quadruples of each hydrogel. For statistical analysis, a t-test was utilized. We chose modified box-plots for data presentation. The boxes represent 75 % of the data; the line within the box marks the mean and the square the median. Whiskers tag the 1.5-fold interquartile range, statistical outliers are represented as hash outside the whiskers.

#### 5.1.6 Acknowledgements

L.R. thanks the Evonik Stiftung (Essen, Germany) for financial support. A.S. and G.E.M.T. thank the Carl Zeiss Foundation (Stuttgart, Germany) and the University of Stuttgart for financial support within the *Projekthaus NanoBioMater*. The authors thank Veronika Schönhaar (Fraunhofer IGB) for

synthesis of the photoinitiator LAP and Birgit Claasen (IOC, University of Stuttgart) for  $^1\text{H-NMR}$  measurements and Okan Avci, Fraunhofer IPA for helpful discussions.

### 5.1.7 Supporting Information

**Table S 9:** Degree of modification of gelatin derivatives. The mean distance of two chemically modified amino acids was calculated as the reciprocal of the degree of modification. The amount of amino acids between the two chemically modified amino acids was estimated assuming an average molecular weight of amino acids of  $122 \text{ g mol}^{-1}$  calculated out of the amino acid composition of the used gelatin type B (composition can be found in ref. [96]).

	Degree of Modification [mmol g <sup>-1</sup> ]	Mean distance between two chemical modified amino acids [g mol <sup>-1</sup> ]	Mean number of amino acids between two chemical modified amino acids
GM2	0.31	3158	26
GM10	0.82	1194	10
GM2A8	0.77	1271	10

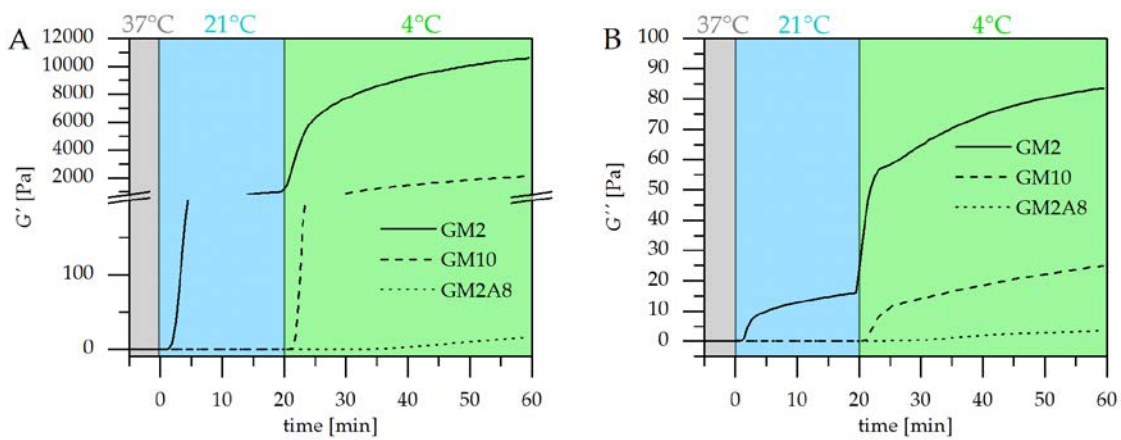


**Figure S 6:** Rheological evaluation of GM(A) gelling behavior during the chosen thermal protocol: **(A)** Storage moduli ( $G'$ ) and **(B)** loss moduli ( $G''$ ). Note the interruption of the y-axis the associated change of scales. Due to this interruption the curves of GM10 and GM2A8 both end at 200 Pa and start again at 800 Pa.

## 5.2 Differentiation of Physical and Chemical Cross-Linking in Gelatin Methacryloyl Hydrogels

Lisa Rebers<sup>a,#</sup>, Raffael Reichsöllner<sup>b,#</sup>, Sophia Regett<sup>a</sup>, Günter E. M. Tovar<sup>a,c,\*</sup>, Kirsten Borchers<sup>a,c</sup>, Stefan Baudis<sup>b</sup> and Alexander Southan<sup>a,\*</sup>

<sup>a</sup> Institute of Interfacial Process Engineering and Plasma Technology IGVP, University of Stuttgart, Stuttgart, Germany.

<sup>b</sup> Christian Doppler Laboratory for Advanced Polymers for Biomaterials and 3D Printing, Institute of Applied Synthetic Chemistry, TU Wien, Vienna, Austria.

<sup>c</sup> Fraunhofer Institute for Interfacial Engineering and Biotechnology IGB, Stuttgart, Germany.

# These authors contributed equally.

\*Corresponding Authors: E-Mail: [alexander.southan@igvp.uni-stuttgart.de](mailto:alexander.southan@igvp.uni-stuttgart.de), [guenter.tovar@igvp.uni-stuttgart.de](mailto:guenter.tovar@igvp.uni-stuttgart.de)

**Published in the peer-reviewed journal *Scientific Reports***

Publisher: Nature Research

DOI: <https://doi.org/10.1038/s41598-021-82393-z>

Volume: 11, Page 3256

©2021 by the authors.

Received November 25, 2020

Accepted: January 18, 2021

Published online: February 5, 2021

### 5.2.1 Abstract

Gelatin methacryloyl (GM) hydrogels have been investigated for almost 20 years, especially for biomedical applications. Recently, strengthening effects of sequential cross-linking procedure, whereby GM hydrogel precursor solutions are cooled before chemical cross-linking, were reported. It was hypothesized that physical and enhanced chemical cross-linking of the GM hydrogels contribute to the observed strengthening effects. However, a detailed investigation is missing so far. In this contribution, we aimed to reveal the impact of physical and chemical cross-linking on strengthening of sequentially cross-linked GM and gelatin methacryloyl acetyl (GMA) hydrogels. We investigated physical and chemical cross-linking of three different GM(A) derivatives (GM10, GM2A8 and GM2), which provided systematically varied ratios of side-group modifications. GM10 contained the highest methacryloylation degree (DM), reducing its ability to cross-link physically. GM2 had the lowest DM and showed physical cross-linking. The total modification degree, determining the physical crosslinking ability, of GM2A8 was comparable to that of GM10, but the chemical cross-linking ability was comparable to GM2. At first, we measured the double bond conversion (DBC) kinetics during chemical GM(A) cross-linking quantitatively in real-time via near infrared spectroscopy-photorheology and showed that the DBC decreased due to sequential cross-linking. Furthermore, results of circular dichroism spectroscopy and differential scanning calorimetry indicated gelation and conformation changes, which increased storage moduli of all GM(A) hydrogels due to sequential cross-linking. The data suggested that the total cross-link density determines hydrogel stiffness, regardless of the physical or chemical nature of the cross-links.

### 5.2.2 Introduction

Gelatin methacryloyl (GM, GelMA) hydrogels are considered as promising biomaterials. They are commonly investigated for biomedical applications such as scaffolds for tissue engineering or drug delivery [35, 351]. Properties of GM solutions, *e.g.* viscosity and temperature of physical gelation, as well as characteristics of the cross-linked hydrogels, *e.g.* water content and mechanical properties, can be tuned by rather simple experimental adjustments: commonly accepted methods include varying the GM concentration and/or the degree of methacryloylation (DM) before cross-linking [42, 96, 120], adjusting the irradiation dose used during photo-cross-linking, or combining other (photo-cross-linkable) materials with GM [351]. These approaches focus mainly on the ability of GM to form chemical cross-links and neglect the physical interactions of gelatin molecules, which are less pronounced after methacryloylation than in unmodified gelatin, but can still be sufficient to form physical cross-links and gels, respectively.



Several studies investigated in how far the formation of both, physical and chemical cross-links, in GM hydrogels can act synergistically to improve mechanical properties. To this end, a sequential cross-linking procedure of GM hydrogels was applied by several authors, which increased the maximum strength [95], compressive modulus [45, 302], storage modulus [303, 352] and E-modulus distinctly [298]. During this sequential cross-linking procedure, the hydrogel precursor solutions were held at rather low temperatures, *e.g.* 4 °C, and were chemically cross-linked afterwards. The observed strengthening effect was usually not temperature-dependent after chemical cross-linking [45, 95, 302, 303] – in contrast to gelatin hydrogels chemically cross-linked with bis(vinylsulfonyl)methane [346, 347]. However, a recent study suggests that the former must not always be the case [353]. The impact of the sequential cross-linking procedure on the mechanical properties is plausible because it increases the total cross-link density in GM-hydrogels [45, 95, 302, 303, 353].

It must be assumed that the underlying effects differ depending on the degree of modification of the GM. In GMs with a low DM, approx. 0.3 mmol g<sup>-1</sup>, complete modification of accessible amino groups of the raw material occurs, but little to no modification of hydroxyl groups (*e.g.* GM2 [94, 96]). Such derivatives form physical hydrogels above 10 °C upon cooling similar to unmodified gelatin [96]. This indicates that effective physical cross-linking can take place, presumably by the formation of triple helices, in spite of the methacryloylation [45, 95, 302, 303, 353].

In contrast to this, solutions prepared from GMs with much higher DMs, *e.g.* 0.8 mmol g<sup>-1</sup> [95] or 0.99 mmol g<sup>-1</sup> [303], are unable to form obvious hydrogels at temperatures above 10 °C [95, 303]. Therefore, it can be hypothesized that physical cross-linking is largely suppressed by the modification of amino and hydroxyl groups. In this case, the strengthening effect might be due to a more efficient chemical cross-linking of methacryloyl functions due to closer packaging of GM coils [302, 303] or the formation of hydrophobic methacryloyl domains induced by the initial cooling step [95]. Thus, the chemical cross-linking would result in a higher double bond conversion (*DBC*) while cross-linking of physical gels would rather reduce the *DBC* comparatively.

Rizwan *et al.* did Fourier transform infrared spectroscopy with solely chemically cross-linked and sequentially cross-linked GM hydrogels and found first qualitative indications of a higher *DBC* in sequentially cross-linked GM hydrogels [302]. Van Vlierberghe *et al.* introduced a method using high-resolution magic angle spinning (HR-MAS) NMR spectroscopy to investigate the final *DBC* and found *DBC*s lower than 40 % [354]. Billiet *et al.* used the same method and implicated a non-linear relationship between qualitative methods, such as swelling measurements, and quantitative methods predicating cross-linking efficiencies [124].

In this study, we aimed to shed further light into the participation of physical and chemical cross-links on the mechanical properties of GM hydrogels prepared either by the sequential cross-linking

procedure or the classical cross-linking procedure omitting the initial cooling step. Therefore, we used three different GM derivatives for hydrogel preparation, which differed in their ability to form either chemical or physical cross-links: (1) GM2, a GM derivative with a relatively low DM of  $0.29 \text{ mmol g}^{-1}$ , thus with a low density of chemically cross-linkable groups, but a high physical cross-linking potential. (2) GM2A8, a methacryloylated and acetylated gelatin (GMA) derivative with a DM of  $0.36 \text{ mmol g}^{-1}$  which was comparable to GM2, but with the low physical cross-linking potential due to the high total degree of modification. (3) GM10, a GM derivative with a DM of  $0.95 \text{ mmol g}^{-1}$ , thus also having a low tendency to form physical cross-links but with a high density of chemically cross-linkable groups.

By real time-near infrared spectroscopy combined with photorheology, we aimed to measure the DBC and gelation kinetics during cooling and during the photo-induced cross-linking reaction of methacryloyl functions of GM *in situ* for the first time. Both cross-linking methods, either the classical method at  $37 \text{ }^\circ\text{C}$  or sequential cross-linking including an initial cooling step, were in the focus of this investigation. Additionally, the formation of hierarchical structures such as triple helices at cross-linking conditions were investigated qualitatively by circular dichroism spectroscopy and quantitatively by differential scanning calorimetry.

Putting the data on chemical and physical cross-linking into context, we hope to contribute to understanding the processes underlying the formation of GM hydrogels.

### 5.2.3 Experimental

#### Materials

Acetic anhydride (AcAnh), Dulbecco's phosphate buffered saline with  $\text{MgCl}_2$  and  $\text{CaCl}_2$  (PBS), methacrylic anhydride (MAAnh) as well as sodium hydroxide (NaOH) were purchased from Sigma Aldrich (Darmstadt, Germany). Sodium 3-trimethylsilyl-propionate-2,2,3,3-d<sub>4</sub> (TMSP) was bought from Merck (Darmstadt, Germany). Other reagents were purchased from the following sources (given in parentheses): deuterium oxide ( $\text{D}_2\text{O}$ , Deutero; Kastellaun, Germany for  $^1\text{H-NMR}$  measurements, Eurisotop; Saarbrücken, Germany for NIR-Photorheology), Gelatin (type B, limed, bovine bone, 232 Bloom, standard viscosity =  $4.5 \text{ mPa s}$ ; Gelita; Eberbach, Germany). Dialysis membranes (MWCO 12 kDa–14 kDa) were purchased from Medicell International Ltd. (London, UK). The photoinitiator lithium phenyl-2,4,6-trimethylbenzoylphosphinate (LAP) was synthesized according to Fairbanks *et al.* [313]. The  $^1\text{H-NMR}$  spectrum (500 MHz,  $\text{D}_2\text{O}$ ) was in accordance with the literature, *i.e.*, 7.74 (m, 2H), 7.56 (m, 1H), 7.46 (m, 2H), 6.87 (s, 2H), 2.22 (s, 3H), 2.04 (s, 6H).

#### Gelatin Methacryloyl (Acetyl) (GM(A)) Synthesis Procedure

Gelatin methacryloyl (GM) and gelatin methacryloyl acetyl (GMA) derivatives GM2, GM10, and GM2A8 were prepared as described previously [94]. Briefly, gelatin (25.01 g) was dissolved in deionized water (250 mL) at 37 °C and the solution pH was adjusted to 7.3 using an automatic titration device. Within 30 min, 2.70 g or 13.49 g of MAA<sub>nh</sub> were added, respectively, for GM2 or GM10, which corresponds to a two-fold or ten-fold molar excess of MAA<sub>nh</sub> relative to the amino groups present in gelatin (0.35 mmol g<sup>-1</sup>) [42]. For GM2A8 synthesis, 7.15 g of acetic anhydride (AcAnh) were added dropwise after 2 h of methacryloylation reaction within 30 min, resulting in an eight-fold AcAnh molar excess relative to the amino-groups present in gelatin [42]. In all cases, the reaction mixture was stirred vigorously for 5 h in total, keeping its pH constantly between 7.0 and 7.4. The reaction mixture was filtrated subsequently and its pH was adjusted to 9.5. After 2 days storage at 4 °C, the solution was dialyzed for 4 d against deionized water, the first 3 d at room temperature and the last day at 40 °C. After that, the solution pH was adjusted to 8.5 and freeze-dried.

The degree of methacryloylation (DM) was determined using the TMSP-method as described by Claaßen *et al.* [94] utilizing <sup>1</sup>H-NMR spectroscopy. The used GM-batches had the following DMs: 0.29 mmol g<sup>-1</sup> (GM2), 0.95 mmol g<sup>-1</sup> (GM10) and 0.36 mmol g<sup>-1</sup> (GM2A8). The degree of acetylation of GM2A8 was reported before as 0.76 ± 0.03 mmol g<sup>-1</sup> [96]. Thus, the total modification degree of GM2A8 was assumed to be ~1.12 mmol g<sup>-1</sup>. The <sup>1</sup>H-NMR spectra of GM(A) derivatives are given in the Supporting Information (**Figure S 7**).

### **Circular Dichroism (CD) Spectroscopy**

For CD spectroscopy, 0.1% (w/w) gelatin or gelatin derivative solutions were prepared as follows: 2 mg gelatin or gelatin derivative were dissolved in 1998 mg PBS over night at 37 °C. The solutions were kept at 37 °C until they were filled into the quartz glass measuring cuvette (cell length 0.1 mm) and transferred directly into the 37 °C pre-warmed CD spectrometer (Jasco J-815, Pfungstadt, Germany). Firstly, CD spectra at 37 °C were recorded: Fifty spectra accumulations were collected between 200 - 260 nm, whereby the temperature was kept constant (± 0.1 °C).

Afterwards, the gelatin or gelatin derivative solutions were removed from the CD spectrometer, stored at 21 °C and the temperature was maintained for 20 min, followed by cooling to 4 °C and maintaining the temperature for 40 min. Subsequently, CD-spectra were collected in the 4 °C pre-cooled CD spectrometer as described above. According to Martin and Schilstra [355] the mean of CD between 250 and 260 nm was subtracted from CD spectra to correct the vertical drift. CD spectra of PBS were recorded as baseline at 4 °C and 37 °C and subtracted from the gelatin and gelatin derivative CD spectra to obtain pure sample CD spectra. Three independent measurements of each solution were done.

Measured values are expressed as mean residue ellipticity  $\theta$ . For calculation of  $\theta$ , a mean molar mass per amino acid residue of  $90.68 \text{ g mol}^{-1}$  was used, based on the amino acid composition of the unmodified gelatin published by Sewald *et al.* [96] For gelatin derivatives, we corrected the mean molar mass per amino acid residue due to inserted functional groups with DMs determined in this study and degree of acetylation determined in this study [96]:  $92.75 \text{ g mol}^{-1}$  (GM2),  $94.91 \text{ g mol}^{-1}$  (GM2A8) and  $97.46 \text{ g mol}^{-1}$  (GM10).

### Differential Scanning Calorimetry (DSC)

For preparation of quantitative DSC measurements, a temperature and enthalpy calibration of the differential scanning calorimeter (Netzsch, DSC 200 F3 Maia, Selb, Germany) was done as described by the manufacturer with hermetically sealed high purity standards of bismuth, indium, zinc, tin, caesium chloride and rubidium nitrate with a temperature rate of  $5 \text{ }^\circ\text{C s}^{-1}$ .

Gelatin or gelatin derivative solutions in PBS were prepared as follows: 100 mg gelatin or gelatin derivative was dissolved in 800 mg PBS at  $37 \text{ }^\circ\text{C}$ . A defined amount of gelatin or gelatin derivative solution was weighed into a crucible, which was subsequently hermetically sealed. Afterwards, DSC measurements were performed from  $-10 \text{ }^\circ\text{C}$  to  $80 \text{ }^\circ\text{C}$  at  $5 \text{ }^\circ\text{C s}^{-1}$  in three cycles with three independent samples for gelatin and each gelatin derivative. The renaturation level ( $X_{DSC}$ ) determined by DSC was calculated according to Bigi *et al.* [356] utilizing Equation 4, whereby  $\Delta H_m$  was the denaturation enthalpy of the sample and  $\Delta H_{G,m}$  the denaturation enthalpy of the unmodified gelatin.

$$X_{DSC} = \Delta H_m / \Delta H_{G,m} \quad (4)$$

## Real Time-Near (RT) Infrared Spectroscopy (NIR)-Photorheology

Real time (RT)-near infrared spectroscopy (NIR)-photorheology is a hyphenated technique of a rheological measurement during *in situ* photo-cross-linking of a formulation, coupled with RT-NIR spectroscopy in reflection mode of the respective sample. The setup consists of an Anton Paar (Graz, Austria) MCR302 WESP rheometer, a Bruker (Billerica, USA) Vertex 80 IR spectrometer and an Excelitas (Waltham, USA) Omnicure S2000 UV source (320–500 nm), as described in Gorsche *et al.* [357]. The rheometer had a glass base plate with a covering hood (both with a Peltier element) and was used with a PP08 tool (plate-plate geometry, 8 mm plate diameter, aluminium).

For sample preparation, a LAP stock solution was prepared by dissolving 10 mg of LAP in 990  $\mu\text{L}$  of  $\text{D}_2\text{O}$ . GM2, GM10 or GM2A8 hydrogel precursor solutions were prepared by dissolving 100 mg of the respective gelatin derivative in 780  $\mu\text{L}$  of  $\text{D}_2\text{O}$  and 20  $\mu\text{L}$  of LAP stock solution. A solution of unmodified gelatin was prepared in the same way. Hydrogel precursor solutions were pre-warmed to 37 °C before RT-NIR-photorheology measurements for decreased viscosity and prevention of premature physical gelation. Each GM hydrogel precursor solution was measured with two different temperature settings. During these temperature settings the storage modulus ( $G'$ ) of gelatin (derivative) solutions was measured to investigate the physical cross-linking. Firstly, the hydrogel precursor solutions were cross-linked following the classical method and the double bond conversion ( $DBC$ ) was monitored at constant 37 °C. Secondly, a temperature profile (see **Figure S 8** in the Supporting Information) was investigated, representing the sequential cross-linking method. The measurements at 37 °C were performed in quadruples and the sequential cross-linking method was performed in triplicates. The sequential cross-linking method contained three temperature levels: during the first minute of the measurement, the temperature was held at 37 °C. Then, the temperature was decreased to 21 °C and held at 21 °C for the following 20 min. Afterwards, the temperature was further decreased to 4 °C and held at 4 °C for 40 min. From this point on, the  $DBC$  monitoring and chemical cross-linking reaction for the temperature profile were started. **Figure S 8** in the Supporting Information precisely illustrates the time points and durations of cooling steps, the NIR-data collection, and the chemical cross-linking, respectively.

Rheological data were measured throughout the experiments in oscillation mode with a constant frequency of 1  $\text{s}^{-1}$ , a constant strain of 1 %, a gap size of 1 mm, and a gap filling of 53  $\mu\text{L}$ . The measuring gap was filled in the measuring position and water evaporation was prevented with a surrounding paraffin ring around the sample cylinder. Rheological data was recorded with a frequency of 5 data point  $\text{s}^{-1}$  before UV cross-linking and 1 data point  $\text{s}^{-1}$  during UV cross-linking with the help of the software RHEOPLUS/32 V3.62.

For chemical cross-linking, UV light was guided from a UV source via a bifurcated light guide through the glass base plate of the rheology setup. The UV intensity was measured at the surface of

the glass plate with a spectrophotometer (Ocean Optics USB2000+, Ostfildern, Germany) and was adjusted to 10 mW cm<sup>-2</sup>. Samples were cured for 5 min to ensure a steady state of chemical cross-linking.

NIR spectra were taken in transmission mode with a spectral resolution of 4 cm<sup>-1</sup>, leading to a time resolution (scanning speed) of about 2 spectra s<sup>-1</sup>. Contrary to the published RT-NIR-rheology method [357], background measurements were taken with a gelatin solution, which was prepared as stated above. NIR spectra data acquisition was started 5 s prior to initiation of the chemical cross-linking by UV irradiation for later calculation of methacryloyl signal integrals before irradiation (*Integral* (*t* = 0)). NIR spectra were recorded with the software OPUS 7.0. Method "F" was used for integration of methacryloyl signals, which determines the local baseline at the relevant spectral range. Furthermore, this method was adjusted for each of the principal measurements and was the same for measurement repetitions. The methacryloyl C=C double bond signal was integrated in the wavenumber range of 6220-6110 cm<sup>-1</sup>.

The *DBC* was calculated in % from the integrals with the following Equation 5:

$$DBC [\%] = \left(1 - \frac{Integral(t)}{Integral(t=0)}\right) \cdot 100 \quad (5)$$

*Integral(t=0)* was determined via averaging of integrals of a 5 s window before the initiation of the chemical cross-linking reaction. The final *DBC* was determined via averaging of calculated *DBC*s over the last 10 s of the measurement.

## Statistical Analysis

The results are presented as mean values of at least three independently performed measurements with the respective standard deviation. Statistical significances were determined by a one-tailed ANOVA. Significant differences were defined for *p* values lower than  $\alpha = 0.05$ ,  $\alpha = 0.01$  and  $\alpha = 0.001$ .

## 5.2.4 Results and Discussion

### Physical interactions in modified gelatin derivatives

We first aimed at a detailed characterization of the state that is obtained after the initial cooling step in a sequential cross-linking procedure, before taking a closer look at the chemical cross-linking process of the studied gelatin derivatives. For this purpose, we used CD spectroscopy and DSC to investigate conformations of gelatin (derivatives) in aqueous solution. In this context, the ability of GM(A) derivatives to form typical gelatin triple helices as well as unordered polypeptide chains, at 37 °C and after cooling procedure, is of special interest. CD spectroscopy is highly sensitive towards conformation changes and thus gives some information about specific protein conformations. DSC was

used to quantify physical interactions by measuring the enthalpy change upon heating. CD spectra are given in **Figure 11** and **Figure S 11** in the Supporting Information, DSC curves are shown in **Figure 12**.

The CD spectra of all solutions recorded at 37 °C were negative from 200 nm to roughly 250 nm. The gelatin and GM(A) solutions showed a negative CD band around 200 nm, which was more pronounced for gelatin than for GM(A). Apart from that, the spectra at 37 °C had no distinct features. The CD spectra of all gelatin (derivative) solutions changed due to the cooling procedure, indicating strong conformation changes: the negative band around 200 nm was more pronounced for all solutions compared to the spectra recorded at 37 °C. Furthermore, a clear positive CD band around 221 nm was observed for gelatin (3070.3 deg cm<sup>2</sup> dmol<sup>-1</sup>), GM2 (1629.5 deg cm<sup>2</sup> dmol<sup>-1</sup>) and GM2A8 (344.8 deg cm<sup>2</sup> dmol<sup>-1</sup>). For GM10, a slightly negative CD value was observed (-57.2 deg cm<sup>2</sup> dmol<sup>-1</sup>) at 221 nm. In addition, a negative band between 230 and 250 nm stood out for highly modified GM2A8 and GM10. A more detailed graphic of this band is shown in **Figure S 11** in the supporting information.

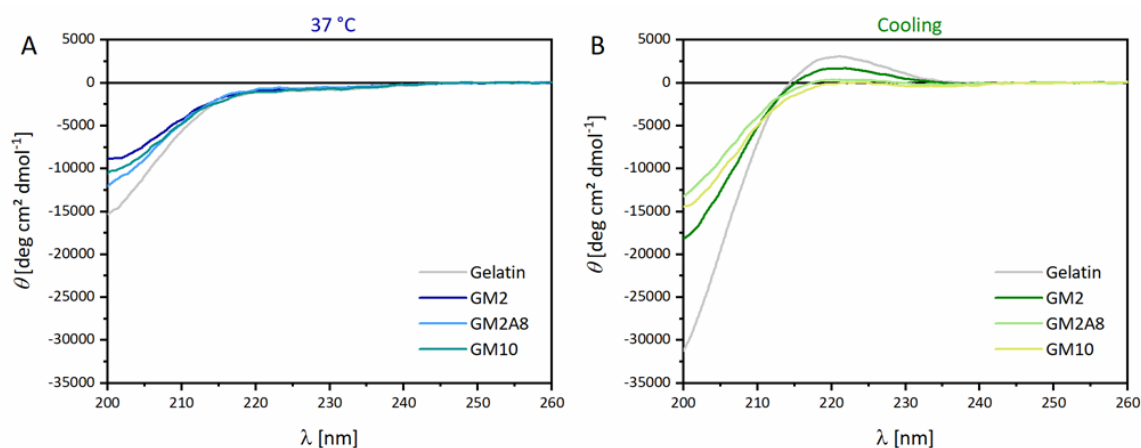


**Figure 11:** Molar ellipticity  $\theta$  of unmodified gelatin, GM2, GM2A8, and GM10. The spectra were recorded at 37 °C (**A**) or after the temperature protocol, whereby the 37 °C warm solution was cooled to 21 °C for 20 min followed by cooling to 4 °C for 40 min (**B**, Cooling). For gelatin and GM2 a clear positive signal around 220 nm was detected after cooling, which suggested the presence of alpha helices. The signal was absent for all solutions measured at 37 °C, and the negative molar ellipticity of all solutions around 200 nm emphasized the presence of random coil structures. The figure was created with Origin 2019b (<http://www.originlab.com/2019b>).

These temperature-dependent changes in CD spectra can be ascribed to temperature-sensitive conformation changes of gelatin (derivatives) in solution. A negative band in CD spectra of warm gelatin and collagen solutions around 200 nm was shown to be connected to random polypeptide chains [71], whereby the positive band around 220 nm in combination with an intense negative band around 200 nm in cooled solutions is characteristic for triple helices [72, 73, 358]. The triple helix CD spectra resemble that of polyproline II helices (trans form of polyproline), implying that the three single left-handed helices of the triple helix are in the same conformation as *trans* polyproline. [74] This conformation is solely stabilized in the triple helix structure [359]. That is why we inferred that all gelatin (derivative) solutions had a random polypeptide chain conformation at 37 °C. Furthermore, GM2 and GM2A8 solution showed pronounced triple helix conformations after cooling. This was in

accordance with results of other studies investigating sequential GM hydrogels [271, 295, 302] in which a 0.2 mg mL<sup>-1</sup> solution in distilled water was cooled for 2 h at 4 °C [271, 295] or a 0.1 % (w/v) solution was cooled for 1 h at 4 °C [302].

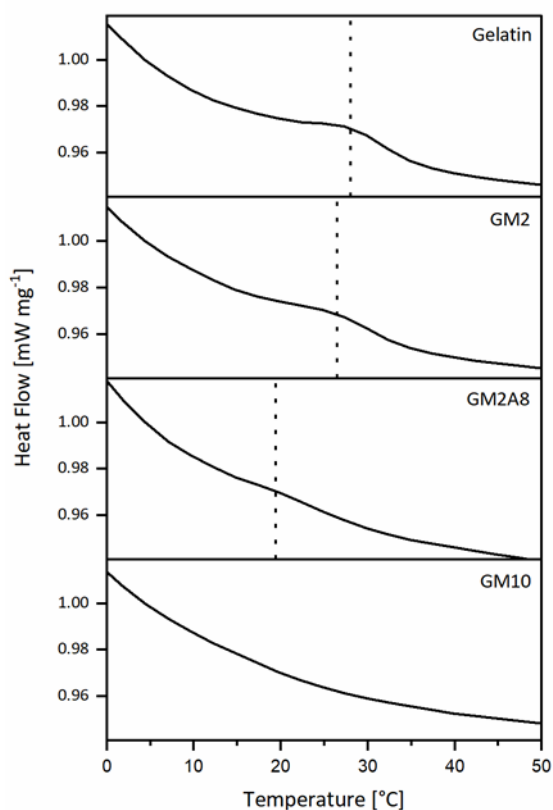


**Figure 12:** Differential scanning calorimetry (DSC) curves of unmodified gelatin, GM2, GM2A8, and GM10. Vertical dotted lines indicate the melting temperatures. The figure was created with Origin 2019b (<http://www.originlab.com/2019b>).

In addition, the amount of triple helices after the cooling procedure decreased with increasing degree of modification (gelatin > GM2 > GM2A8 > GM10). These results were consistent with another CD study of GMs of Zhu *et al.* showing that an increasing DM increased the random polypeptide chain conformation and decreased the triple helix conformation [295]. Furthermore, Zhu *et al.* investigated GM with a DM of ~0.32 mmol g<sup>-1</sup> (DS\_100), which was very close to the GM2 we used in this study (DM = 0.29 mmol g<sup>-1</sup>). They detected just a very slight positive band of DS\_100 at 222 nm, whereas we detected a clear positive band at 221 nm for GM2. This might be explained by experimental differences: our cooling period was shorter, our GM concentration five times higher and we used PBS instead of deionized water. It was shown before that all these differences impact triple helix renaturation [71, 73].

Negative bands at wavelength > 230 nm with a maximum at ~238 nm of gelatin and collagen were previously correlated with a right-handed helical poly-proline I conformation [74]. This poly-proline II conformation of single chains contains cis peptide bonds and thereby is the cis-peptide form of poly-proline. The helical pitch of the right-handed poly-proline I helix is smaller (5.6 Å turn<sup>-1</sup>, 3.3 residues turn<sup>-1</sup>) than the pitch of the left-handed poly-proline II conformation (9.3 Å turn<sup>-1</sup>,



3.0 residues turn<sup>-1</sup>), making it more compact [360]. It was shown that the poly-proline I conformation stabilized single chains [75] and is preferred in organic solvents [361]. Furthermore, a correlation with the positive band at ~220 nm was found: the smaller the positive band at ~220 nm, the bigger the negative band at ~238 nm. Thus, the destruction of triple helices into single helices due to high temperatures might be correlated with a trans-cis-transition of peptide bonds in single helices [74]. That is why we assigned the negative band at > 230 nm, which was measured for all GM(A) solutions, to single chains, which did not associate to triple helices during cooling. The molar ellipticity  $\theta$  at 238 nm after the cooling procedure was lowest for GM10 (-319.9 deg cm<sup>2</sup> dmol<sup>-1</sup>), followed by GM2A8 (-203.1 deg cm<sup>2</sup> dmol<sup>-1</sup>), GM2 (-127.7 deg cm<sup>2</sup> dmol<sup>-1</sup>) and gelatin (-38.9 deg cm<sup>2</sup> dmol<sup>-1</sup>). Thus, in GM10 the most single helices were built up and did not form critical nucleus structures to form triple helices, as proposed by Guo *et al.* [362].

The CD spectroscopy findings were generally supported by the DSC measurements (**Figure 12**). An endothermic peak was detected for all gelatin (derivative) solutions during heating except for GM10. The respective temperatures were interpreted as melting temperatures  $T_m$ . The obtained  $T_m$ , melting enthalpies  $\Delta H_m$  and  $X_{DSC}$  are given in **Table 4**.  $T_m$ ,  $\Delta H_m$  as well as  $X_{DSC}$  generally decreased with increasing degree of modification up to the point that no values were obtained for GM10.

This observation was in accordance with previous findings measured by temperature-dependent rheology for GM10, which showed no gelation or melting temperature between 10 °C and 40 °C [96]. However, in the previous experiments also for GM2A8 no physical gelation was detected. The results of GM2 were in accordance with previous DSC studies of GM derivatives with DMs of 89 % [302] and 97 % [303], where the percentage describes the relative amount of methacryloylated amino groups. In concert with the CD spectra, the endothermic peaks of the DSC curves for gelatin, GM2 and GM2A8 were assigned to triple helix denaturation [303, 356, 363], thereby again indicating the existence of triple helices in all cooled solutions except for GM10 solutions.

**Table 4:** Melting temperatures  $T_m$  and melting enthalpies  $\Delta H_m$  obtained from the DSC curves shown in **Figure 12** as well as renaturation levels  $X_{DSC}$  calculated from DSC measurements. GM10 did not show any signal in the DSC measurements or the signal was too shallow to be analysed, so no values were found (n.f.). The measured melting enthalpies were significantly different from each other [ $p < 0.05$  (gelatin, GM2),  $p < 0.001$  (gelatin, GM2A8; GM2, GM2A8)].

	$T_m$ (°C)	$\Delta H_m$ (J g <sup>-1</sup> )	$X_{DSC}$ (%)
<b>Gelatin</b>	28.0 ± 0.7	0.69 ± 0.11	100
<b>GM2</b>	26.5 ± 0.7	0.46 ± 0.06	71.0
<b>GM2A8</b>	19.4 ± 1.0	0.03 ± 0.02	4.3
<b>GM10</b>	n.f.	n.f.	n.f.

The effect of methacryloylation on gelatin triple helix formation was discussed already in the early publication on GM by van den Bulcke *et al.* [42]. It was shown in different studies that the

modification of gelatin impacts solution viscosities [96, 120, 125, 300] and melting temperature [42, 96, 125], which was correlated with the helix content of the GM solutions. However, there was also evidence that there is not necessarily a correlation between melting temperature and helix content [72]. The impact of methacryloylation on triple helix renaturation was explained by reduced interchain or intrachain hydrogen bindings within the triple helices by chemical functionalization of amino and hydroxyl groups, on the one hand [295]. On the other hand, peptide sequences such as the glycine-proline-hydroxyproline tripeptide, which are known to participate in the triple helix formation [364], are chemically modified especially in the highly modified derivatives, potentially hindering the (complete) formation of triple helices [272].

The presented data strongly indicate conformational changes in all investigated GM(A) solutions due to cooling procedure: for all solutions a more pronounced band of random polypeptide chains was detected. Furthermore, for GM2 and GM2A8 triple helices were evidenced by CD spectroscopy and DSC measurements, but not for GM10. However, more single helices were detected in GM10 than in gelatin, GM2 and GM2A8 solutions.

### Physical gelation of gelatin and respective derivatives

The effect of the conformational changes induced by the cooling procedure during sequential cross-linking on the physical gelation ability of the gelatin raw material and its derivatives was analyzed by measuring  $G'$  of the solutions by rheology, see **Figure 13**.

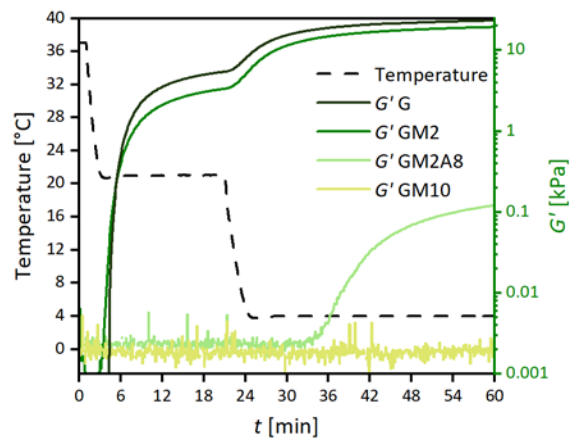


**Figure 13:** Evolution of storage modulus  $G'$  during the initial cooling protocol of the sequential cross-linking procedure for the tested gelatin derivatives and the raw material gelatin (G). Note that the data on the subsequently performed chemical cross-linking of the samples shown here is depicted in **Figure 14** and discussed in the next section. The figure was created with Origin 2019b (<http://www.originlab.com/2019b>).

Information about physical gelation speed  $k_{g,p}$  and the physical gelation delay time  $t_{d,p}$  were extracted and are collected in **Table 5**. The values were defined such that  $k_{g,p}$  is the slope of the initial linear part of the  $G'(t)$  curves (for unmodified gelatin and GM2 at 21 °C and 4 °C, for GM2A8 at 4 °C) and  $t_{d,p}$  is the intersection of the corresponding linear fit line with the baseline [357]. In accordance with

the CD spectroscopy and DSC data discussed above and findings reported by Rebers *et al.* [95] before, physical gelation was observed during sequential cross-linking (**Table 5**). Just gelatin and GM2 solutions formed physical gels during the period at 21 °C. This meets with the expectations based on the determined melting temperatures (**Table 4**), although the latter are commonly higher than the corresponding gelation temperatures.

More specifically, delay times of the gelation events of GM2 and gelatin were in the same range. Unmodified gelatin gelled at 21 °C with a stiffness increase of  $10.0 \pm 1.0 \text{ Pa s}^{-1}$  and the final  $G'$  after 20 min at 21 °C was  $5.40 \pm 0.50 \text{ kPa}$ . Gelatin gelation at 4 °C resulted in a 2.5 times faster stiffness increase than for the 21 °C step and a  $G'$  of  $23.59 \pm 1.93 \text{ kPa}$ . For GM2, the increase of  $G'$  at 21 °C was comparably slower ( $5 \pm 0.1 \text{ Pa s}^{-1}$ ), resulting in a  $G'$  of  $3.33 \pm 0.07 \text{ kPa}$  when starting to cool to 4 °C. After cooling was complete, the increase of  $G'$  was accelerated so that for GM2, a final  $G'$  of  $19.4 \pm 0.01 \text{ kPa}$  was reached at the end of the cooling protocol. In contrast to GM2, physical GM2A8 gels were formed only at 4 °C with a rather slow increase of  $G'$ , resulting in a low final value of  $0.124 \pm 0.02 \text{ kPa}$  and GM10 solutions did not show any measurable response to cooling.

**Table 5:** Parameters describing the physical gelation of gelatin derivative solutions using the sequential cross-linking protocol: physical gelation delay time  $t_{d,p}$ , initial increase rate  $k_{g,p}$  of storage modulus  $G'$  upon cooling, and  $G'$  after cooling to 21 °C for 20 min and 4 °C for 40 min, respectively.

	Physical Gelation					
	21 °C			4 °C		
	$t_{d,p}$ (s)	$k_{g,p}$ (Pa s <sup>-1</sup> )	$G'$ at end of period (kPa)	$t_{d,p}$ (s)	$k_{g,p}$ (Pa s <sup>-1</sup> )	$G'$ at end of period (kPa)
<b>Gelatin</b>	$251.1 \pm 13.9$	$10.0 \pm 1.0$	$5.40 \pm 0.50$	$79.5 \pm 1.8$	$24.8 \pm 2.0$	$23.59 \pm 1.93$
<b>GM2</b>	$226.7 \pm 5.4$	$5 \pm 0.1$	$3.33 \pm 0.07$	$101.6 \pm 0.6$	$21 \pm 0.2$	$19.4 \pm 0.01$
<b>GM2A8</b>	-	-	-	$981.0 \pm 124.0$	$0.11 \pm 0.01$	$0.124 \pm 0.022$
<b>GM10</b>	-	-	-	-	-	-

The results from physical gelation experiments of gelatin and GM(A) derivatives confirmed a tight correlation of gelation behaviour and degree of modification. While gelatin and GM2 formed gels even at 21 °C, GM2A8 only forms gels when cooled to 4 °C and GM10 did not gel even at 4 °C. Furthermore, this correlation could be qualitatively expanded towards the mechanical properties of physically cross-linked hydrogels as final storage moduli of gels after the 4 °C treatment decreased (gelatin > GM2 > GM2A8, no gels for GM10) with increasing degree of modification. In combination with the results from CD spectroscopy the data suggested a correlation between the helix content and  $G'$  of the mixtures.

## Chemical cross-linking kinetics of modified gelatin derivatives

In the next step, the chemical cross-linking kinetics depending on the chemical gelatin modification as well as the cross-linking protocol were studied. For this purpose, we used real time-near infrared (RT-NIR) spectroscopy hyphenated with photorheology. This allows the simultaneous measuring of time-dependent changes in the storage modulus  $G'$  and in the double bond conversion  $DBC$  when using the classical photo-cross-linking method at 37 °C or sequential cross-linking including an initial cooling step. The results of time-dependent  $G'$  and  $DBC$  measurements are shown in **Figure 14**. The parameters describing the initial increase of  $G'$  ( $k_{g,c}$ ) as well as the initial increase of  $DBC$  ( $k_{DBC}$ ) were calculated with the  $G'(t)$  and  $DBC(t)$  curves, respectively (**Table 6**), similarly to how it was described above for  $k_{g,p}$ . Additionally, extracted reaction rates of double bond conversion are shown in **Figure S 12**.

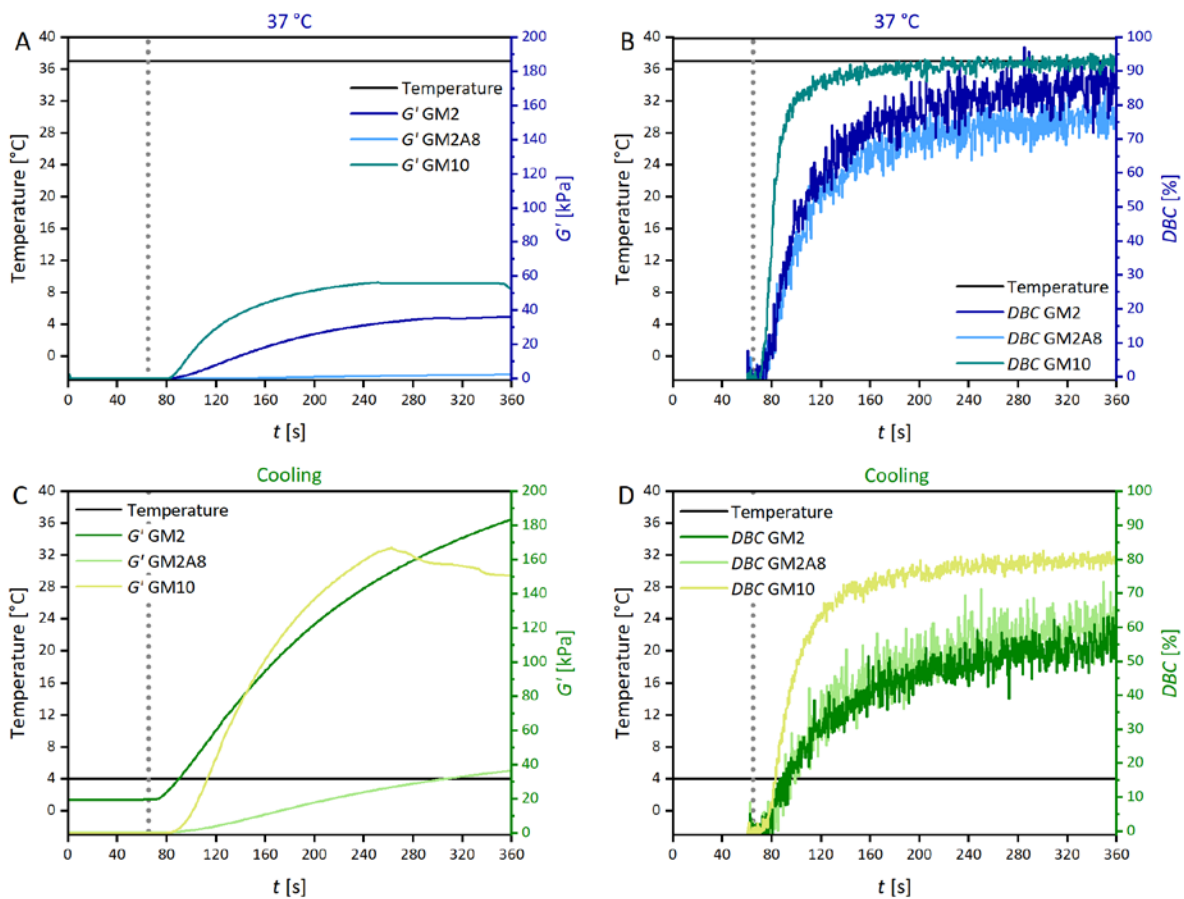


**Figure 14:** Real time-near infrared spectroscopy-photorheology data of GM2, GM2A8 and GM10 solutions. The storage moduli ( $G'$ ) and double bond conversions ( $DBC$ ) measured for chemical cross-linking at 37 °C (classical method) are shown in (A, B).  $G'$  and  $DBC$  measured during the sequential cross-linking procedure (cooling) are shown in (C, D), respectively. Note that the data in (C, D) were obtained directly after physical cross-linking shown in **Figure 13** using the same samples. The time axes in this figure therefore refer to the chemical cross-linking period only. Sequential cross-linking resulted in higher  $G'$  after chemical cross-linking and lower  $DBC$ s for all three gelatin derivatives. The grey dotted line indicates the start of UV-initiated cross-linking. The figure was created with Origin 2019b (<http://www.originlab.com/2019b>).

The baseline for calculation of  $k_{DBC}$  was set to zero, for cross-linking at 37 °C, or to the final  $G'$  of the physical gel for sequential cross-linking procedure (20 min at 21 °C and 40 min at 4 °C).

Furthermore, the chemical gelation delay time ( $t_{d,c}$ ), measured from the start of UV-irradiation, and the final  $DBC$ s in  $\text{mmol g}^{-1}$  time are given in the Supporting Information (**Table S 10** for the classical method, **Table S 11** for sequential cross-linking).

The  $DBC$  increased rapidly for all derivatives and cross-linking conditions directly after starting UV irradiation,  $G'$  increased slightly delayed, compare **Figure 14-A** and **Figure 14-B** as well as **Figure 14-C** and **Figure 14-D**, respectively. At 37 °C, the  $DBC$  rates  $k_{DBC}$  were indistinguishable for GM2 and GM2A8 ( $p > 0.05$ ), while  $k_{DBC}$  of GM10 was roughly 9.5 times as high when expressed as amount of converted double bonds per second. The  $k_{DBC}$  was generally lower for sequential cross-linking than for the classical method, but relative differences between the derivatives were similar in both cross-linking conditions. The results showed that both, increasing DM as well as elevated temperature, accelerated the absolute  $DBC$  kinetics (**Figure S 12** and **Figure S 13**). These findings were expected and gave the following order  $DBC$  kinetics: GM10 > GM2A8 > GM2, following the order of DM of the derivatives.

However, interestingly there was no clear correlation between  $k_{DBC}$  and  $k_{g,c}$  of  $G'$  (**Figure S 13**), especially because of exceptionally low  $k_{g,c}$  of GM2A8. At both cross-linking conditions,  $k_{g,c}$  decreased in the order of GM10 > GM2 >> GM2A8  $k_g$  and the resulting  $G'$  were significantly higher for all gelatin derivatives in the sequential cross-linking protocol when UV irradiation was carried out at 4 °C ( $p < 0.001$ ). A similar observation was already described by van Hoorick *et al.*, who performed time-dependent photorheology measurements on a highly modified gelatin derivative with a total DM of 0.99  $\text{mmol g}^{-1}$  and a GM with a lower DM of 0.37  $\text{mmol g}^{-1}$  [303]. They also followed a sequential cross-linking protocol (5 °C for 10 min prior to chemical cross-linking), but did not quantify the effect of the cooling step on the  $DBC$  kinetics. These results showed that the time-dependent evolution of mechanical properties of all GM(A) hydrogels was strongly influenced by the thermal history of the gelatin derivative solution.

The data on  $G'$  and the  $DBC$  in our present study now allow the conclusion that  $DBC$  causes an increase of  $G'$ , whether a physical gel was initially formed or not. The conversion rate  $k_{DBC}$  was reduced at 4 °C compared to 37 °C, also independently from the physical state of the solution. The observed strengthening effect of sequential cross-linking (i.e. elevated  $G'$  compared to gels that were photo-cross-linked at 37 °C) occurred for all gelatin derivatives no matter whether with rather strong (GM2), or with only weak (GM2A8), or without prior physical gelation (GM10). Particular interesting seems the fact, that GM10 hydrogels showed elevated  $G'$  if cross-linked after cooling at 4 °C instead of 37 °C ( $p < 0.001$ ), although no physical gel formation occurred and the  $DBC$  at 4 °C was obviously lower than 37 °C ( $p < 0.001$ ).

**Table 6:** Parameters describing the chemical cross-linking of gelatin derivative solutions with the classical method at 37°C or with the sequential cross-linking method: Initial increases  $k_{g,c}$  and  $k_{DBC}$  of  $G'$  and  $DBC$ , respectively, chemical gelation delay

time  $t_{d,c}$  upon UV irradiation, final storage modulus  $G'$ , and final  $DBC$ . The data given in % are relative to the degree of methacryloylation (DM) of the respective gelatin derivative.

	Chemical Cross-Linking									
	Classical method (37 °C)					Sequential cross-linking (4 °C)				
	$k_{g,c}$ (Pa s <sup>-1</sup> )	$k_{DBC}$ (% s <sup>-1</sup> )	$k_{DBC}$ ( $\mu\text{mol g}^{-1} \text{s}^{-1}$ )	$G'$ (kPa)	$DBC$ (%)	$k_{g,c}$ (Pa s <sup>-1</sup> )	$k_{DBC}$ (% s <sup>-1</sup> )	$k_{DBC}$ ( $\mu\text{mol g}^{-1} \text{s}^{-1}$ )	$G'$ (kPa)	$DBC$ (%)
<b>GM2</b>	273 ± 14	1.9 ± 0.4	5.4 ± 1.1	36.0 ± 1.9	86.2 ± 1.2	926 ± 28	0.7 ± 0.1	1.9 ± 0.3	180.9 ± 3.3	58.1 ± 2.1
<b>GM2A8</b>	15 ± 1	1.7 ± 0.2	5.9 ± 0.8	2.3 ± 0.2	75.6 ± 1.2	173 ± 9	1.0 ± 0.3	3.5 ± 1.0	35.6 ± 1.9	62.1 ± 6.3
<b>GM10</b>	887 ± 24	5.4 ± 0.1	51.2 ± 1.3	55.6 ± 4.4	93.1 ± 0.1	1770 ± 236	2.2 ± 0.1	20.7 ± 0.8	165.1 ± 15.0	80.8 ± 0.8

Given that  $G'$  increases with an increasing density of elastically active chains, the sequential cross-linking protocol seems to enhance the number of elastically active chains formed per converted acrylic group during UV irradiation, and it is conceivable that this is connected to diverse physical interactions and conformation changes during the cooling protocol described above.

#### Correlation between stiffness and double bond conversion

The data on the physical interactions and chemical cross-linking of the gelatin derivatives, described in the previous sections, indicated a complex interplay between physical and chemical cross-links affecting the stiffness of the hydrogels. To further understand the correlation between the hydrogel stiffness given by  $G'$  and the  $DBC$ , the time-dependent data on  $G'$  and  $DBC$  from **Figure 14** were combined in **Figure 15**. The values of final  $G'$  and final  $DBC$  relative to the respective DM are collected in **Table 6**. These results showed that the cross-linking of GM(A) is much more complex than usually assumed. The stiffness of GM(A) hydrogels can be adjusted by the DM, as it is often stated [42, 96, 120], but a higher DM does not necessarily lead to stiffer hydrogels.

The  $DBC$  correlated in a positive sense with the number of methacryloyl functions (DM) present in the respective GM(A) derivative (GM2 ~ GM2A8 < GM10). Nevertheless, there was no systematic correlation between final  $DBC$  and final  $G'$ : as expected,  $G'$  of each derivative was much higher if chemical cross-linking was performed after cooling compared with chemical cross-linking at 37 °C. However, the final  $DBC$  of each derivative was lower for chemical cross-linking compared with sequential cross-linking. This was unexpected.

As **Figure 15** shows, in all cases, a non-linear increase of  $G'$  with increasing  $DBC$  was found. The impact of  $DBC$  on  $G'$  was less in GM2A8 and GM10 hydrogel precursor solutions than in GM2 hydrogel precursor solutions. Furthermore, differences in the effect of  $DBC$  on  $G'$  were observed between the two investigated cross-linking procedures and are described in the following.

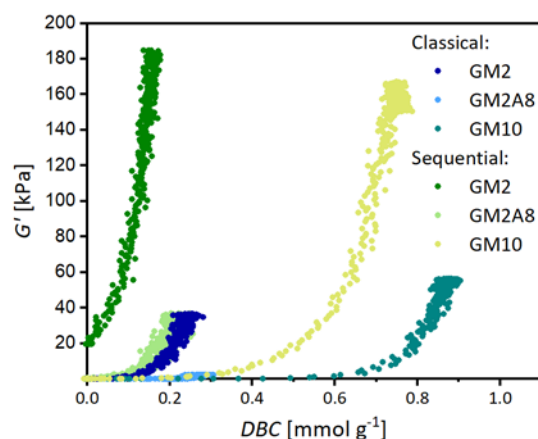


**Figure 15:** Increase of storage modulus  $G'$  with the double bond conversion ( $DBC$ ) for the three gelatin derivatives GM2, GM2A8, and GM10 using the classical or the sequential cross-linking procedure, respectively. Note that the light blue triangles representing the data obtained for GM2A8 with the classical cross-linking procedure are visible close to the abscissa at  $DBC$ s below  $0.3 \text{ mmol g}^{-1}$ . The figure was created with Origin 2019b (<http://www.originlab.com/2019b>).

For chemical cross-linking at  $37^\circ\text{C}$ ,  $DBC$  data for GM2A8 and GM10 were very similar up to the final  $DBC$  of GM2A8 ( $0.272 \text{ mmol g}^{-1}$ ) and only rather low  $G'$  values were found. At higher  $DBC$  of GM10,  $G'$  starts to increase stronger at  $DBC$  of roughly  $> 0.6 \text{ mmol g}^{-1}$ , reaching its final value at  $55.6 \text{ kPa}$  with a  $DBC$  of  $93.1\%$ . For GM2, an increase of  $G'$  at much smaller  $DBC$ s ( $\sim 0.1 \text{ mmol g}^{-1}$ ) was found. In all three GM(A) hydrogels, the majority of double bonds were converted during UV irradiation. However, it was interesting that GM2 performed different from GM10 and especially from GM2A8 also at  $37^\circ\text{C}$  although gel formation or triple helix formation was not detected for any of the derivatives.

Concerning the  $DBC$  in GM hydrogels, only very limited data existed so far [124, 154, 197, 354]. Unfortunately, none of these studies gave any details about temperature control during curing, which would be crucial in the light of the findings reported here. All investigations used hydrogel precursor solutions out of GMs with a DM between  $0.23$  and  $0.33 \text{ mmol g}^{-1}$ , which is similar to the DM of GM2 investigated in this study, containing the photoinitiator Irgacure 2959. However, in these studies different  $DBC$ s varying from  $0.09 \text{ mmol g}^{-1}$  up to  $0.29 \text{ mmol g}^{-1}$  ( $40\text{-}95\%$ ) were reported. Summarizing, a wide range of final  $DBC$ s was found in different studies and the reason is unclear so far. It is obvious that due to the multitude of experimental parameters (GM concentration, DM of GM, photoinitiator, photoinitiator concentration, solvent, UV irradiation time, UV lamp emission spectrum, sample thickness, thermal history, etc.) the comparison of datasets from different studies is difficult, especially if not all relevant experimental parameters were described in detail. Therefore, future studies should investigate the impact of experimental parameter on the  $DBC$ . Thereby, GM hydrogels without remaining reactive C=C-double bonds could be established, which are of special interest for application as biomaterials.

For chemical cross-linking at  $4^\circ\text{C}$  (sequential protocol), effects of the  $DBC$  on  $G'$  were observed immediately after starting the chemical cross-linking at  $0 \text{ mmol g}^{-1} DBC$  for GM2, at  $0.1 \text{ mmol g}^{-1} DBC$

for GM2A8, and at  $0.3 \text{ mmol g}^{-1} \text{ DBC}$  for GM10. This means that the contribution of the formed chemical cross-links to  $G'$  was much more effective for all derivatives if the solutions were cooled. However, it was unexpected that GM10 hydrogel precursor solutions performed as GM2 and GM2A8 solutions, since there was gel-formation and triple helix formation detected upon cooling for GM2 and GM2A8, but not for GM10. Thus, for GM10, right-handed single helices as postulated from the CD spectra could be the reason for the elevated effect of  $\text{DBC}$  on  $G'$  as well as the random polypeptide chain conformation, which was increased in all GM(A) solutions due to cooling.

Concerning the  $\text{DBC}$  at which  $G'$  starts to increase, the physical interactions and conformation changes caused by the cooling protocol apparently shift the  $G'$ - $\text{DBC}$  curve to the left, see **Figure 15**. This confirmed our hypothesis that  $G'$  of hydrogels is not solely dependent on the degree of chemical cross-linking [95, 96], and chemical cross-links might support physical cross-links stiffening sequentially cross-linked hydrogels [95, 303, 365, 366]. However, the general shape of all  $G'$ - $\text{DBC}$  curves were quite similar (**Figure 15**). This suggests that it is irrelevant if a cross-link was based on physical or chemical interactions and that, only the cross-link density itself determines the modulus, in accordance with the theory of rubber elasticity. The data suggest that an acrylic group converted in a network with already a rather high concentration of cross-links leads to larger increase of elastically active chains than in a network with a lower concentration of cross-links. Therefore,  $G'$  of sequentially cross-linked GM2 increased as soon as UV irradiation was started because it contained the highest density of physical cross-links (**Table 4, Figure 11**), whereas  $G'$  of all other gelatin derivatives went through an induction period determined by the starting concentration of physical cross-links and interactions.

The lower final  $\text{DBC}$  and  $k_{\text{DBC}}$  in sequentially cross-linked GM(A) hydrogels refuted the hypothesis that sequential cross-linking increases the efficiency of chemical cross-linking, established in earlier studies [95, 303, 353, 365, 366]. A possible explanation could be that methacryloyl groups lose mobility and get inaccessible by gelation and network organization due to the cooling procedure, as mentioned by Park *et al.* [353]. The increase of  $G'$  at lower  $\text{DBC}$ s after cooling indicate that such obstacles as the physical gelation hinder chemical cross-linking already in an earlier phase of the chemical cross-linking reaction, ultimately limiting the achievable  $\text{DBC}$ s. The fact that the  $\text{DBC}$  of GM2 was most affected by the restrictions caused by physical gelation is consistent with this explanation, as also indicated by the higher  $\text{DBC}$  of GM2A8 compared to GM2.

Interestingly, our observation of smaller  $\text{DBC}$ s after sequential cross-linking seems to contradict findings by Rizwan *et al.* [302]. They reported a decrease in unreacted double bonds in 30 % GM hydrogels prepared from a GM with a DM of  $0.31 \text{ mmol g}^{-1}$  due to their sequential hydrogel preparation procedure ( $4 \text{ }^\circ\text{C}$  for 1 h) compared to cross-linking at  $37 \text{ }^\circ\text{C}$ , measured by qualitative Fourier transform infrared spectroscopy (FTIR). Therefore, it cannot be ruled out that differences in experimental conditions have strong impact on the development of material properties. This is known from



unmodified gelatin as well and strict compliance to standard protocols is required if standard parameters like viscosity, gel strength etc. are determined for commercial products.

Concerning the final  $G'$ , the observed effects in this study are in agreement with previous reports [45, 95, 298, 302, 303], and we confirmed the stiffening effect of sequential cross-linking even for GM hydrogel precursor solutions, which do not form physical networks [95, 303]. The seemingly reasonable assumption that physical interactions do not play any role when cross-linking above the physical gel melting temperature of gelatin, *e.g.* at 37 ° was disproved, especially by the remarkable difference in stiffness of GM2 and GM2A8 hydrogels at comparable  $DBC$ s when using the classical cross-linking procedure: also at 37 °C, differences in physical interactions significantly alter hydrogel properties.

Summarizing, with the sequential cross-linking method, three main differences were observed compared to the classical method for a given gelatin derivative: (1) The final  $DBC$  was generally lower, (2) the final  $G'$  was generally higher, and (3)  $G'$  increased at lower  $DBC$  values. Since we measured in this study lower  $DBC$ s during sequential cross-linking than during chemical cross-linking, we concluded that the physical interactions and conformation changes induced by the cooling protocol (see **Figure 11** and **Figure 12**) were effective for stiffening all sequentially cross-linked hydrogels. However, the individual contributions for each GM derivative seem to depend on the DM and total degree of modification. The data in this study were obtained without including GMs with lower DMs, and there might be an optimum DM with an optimum sequential cross-linking procedure leading to the maximum hydrogel stiffness. Lower DMs, however, cause too shallow absorption bands in the NIR spectra and would be difficult to analyse. Further insight will be necessary to find out if additional effects have to be considered to be responsible for the observed correlations between  $DBC$  and  $G'$ .

In any case, it cannot be emphasized enough that the experimental conditions must be controlled as precise as possible and the conditions applied need to be described in detail to reproduce experiments. We have to remark that the final  $G'$  values in this study were measured for hydrogels in their relaxed state and not in their swollen state. Therefore, a direct comparison with hydrogels swollen to equilibrium is not possible [303].

### 5.2.5 Conclusion

The stiffness of gelatin methacryloyl (GM) hydrogels was increased dramatically by sequential cross-linking including an initial cooling step. We refuted the previously established hypothesis that a more effective double bond conversion ( $DBC$ ) leads to this stiffening: cooling before chemical cross-linking in fact caused lower  $DBC$ s in all GM hydrogels. Triple helix formation was detected for GM2 and GM2A8, and single helices with *cis*-peptide bonds (right-handed single helices) were detected in GM10

and GM2A8 solutions upon cooling. Therefore, we propose that these physical interactions, which lead to ordered conformational structures, caused the steep increase of the stiffness with low *DBC*s, possibly resulting in higher total numbers of physical and chemical crosslinks. Consequently, the combination of conformational structures based on physical interactions, and chemical cross-links is necessary to obtain gelatin derivative hydrogels with high structural strength. These findings are important e.g. in applications of GM hydrogels in cartilage tissue engineering where strong hydrogels are desired while keeping the degree of modification at a low level.

### 5.2.6 Acknowledgements

L.R. thanks the Evonik Stiftung (Essen, Germany) for financial support. The authors thank Birgit Claasen and her group (Institute of Organic Chemistry, University of Stuttgart) for <sup>1</sup>H-NMR measurements, Veronika Schönhaar (Fraunhofer Institute for Interfacial Engineering and Biotechnology IGB) for photoinitiator synthesis and Albert Jeltsch (Institute of Biochemistry and Technical Biochemistry, University of Stuttgart) for the possibility to carry out CD spectroscopy measurements. Furthermore, we thank Andre Michele (IGVP, University of Stuttgart) and Felix Markus (Institute of Polymer Chemistry, University of Stuttgart) for the help with DSC sample preparation. Funding by the Christian Doppler Research Association (Christian Doppler Laboratory for Advanced Polymers for Biomaterials and 3D Printing), the Austrian Federal Ministry for Digital and Economic Affairs, and the National foundation for Research, Technology and Development are gratefully acknowledged.

### 5.2.7 Author contributions

L.R., R.R., S.B. and A.S. conceptualized the study. L.R., R.R. and S.R. did the investigations. L.R., R.R., S.B. and A.S. elaborated the methodology. L.R., R.R. and A.S. made the visualizations. A.S., S.B., K.B. and G.E.M.T. supervised the study. L.R., R.R., K.B. and A.S. wrote the original draft. S.R., S.B. and G.E.M.T. reviewed and edited the original draft.

### 5.2.8 Funding

Open Access funding enabled and organized by Projekt DEAL.

### 5.2.9 Competing interests

The authors declare no competing interests.

## 5.2.10 Supplementary Information

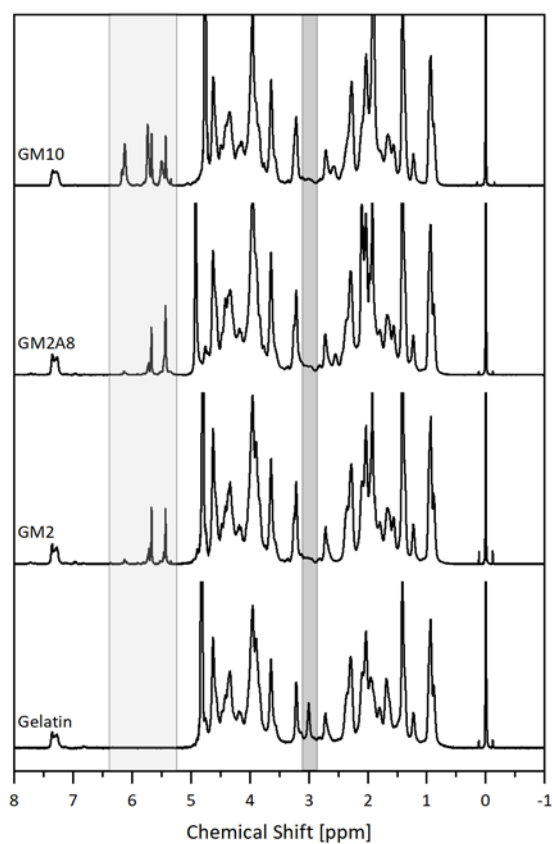


**Figure S 7:** <sup>1</sup>H-NMR spectra of gelatin used for methacryloylation (GM) (and acetylation (GMA)) and its derivatives. Unmodified lysine groups, only present in the spectrum of the unmodified gelatin, were highlighted in dark grey, acrylic protons of methacryloyl groups in light grey. The figure was created with Origin 2019b (<http://www.originlab.com/2019b>).

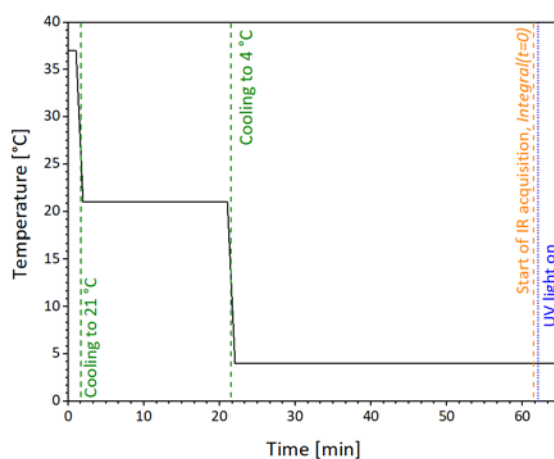


**Figure S 8:** Utilized temperature profile for physical gelation prior to chemical cross-linking. The 37 °C warm GM-solutions were cooled for 20 min to 21 °C followed by cooling to 4 °C 40 min (green dotted lines). Afterwards, infrared spectroscopy (IR) acquisition was started (orange dotted line) and the UV light was turned on 5 s later (blue dotted line). The figure was created with Origin 2019b (<http://www.originlab.com/2019b>).

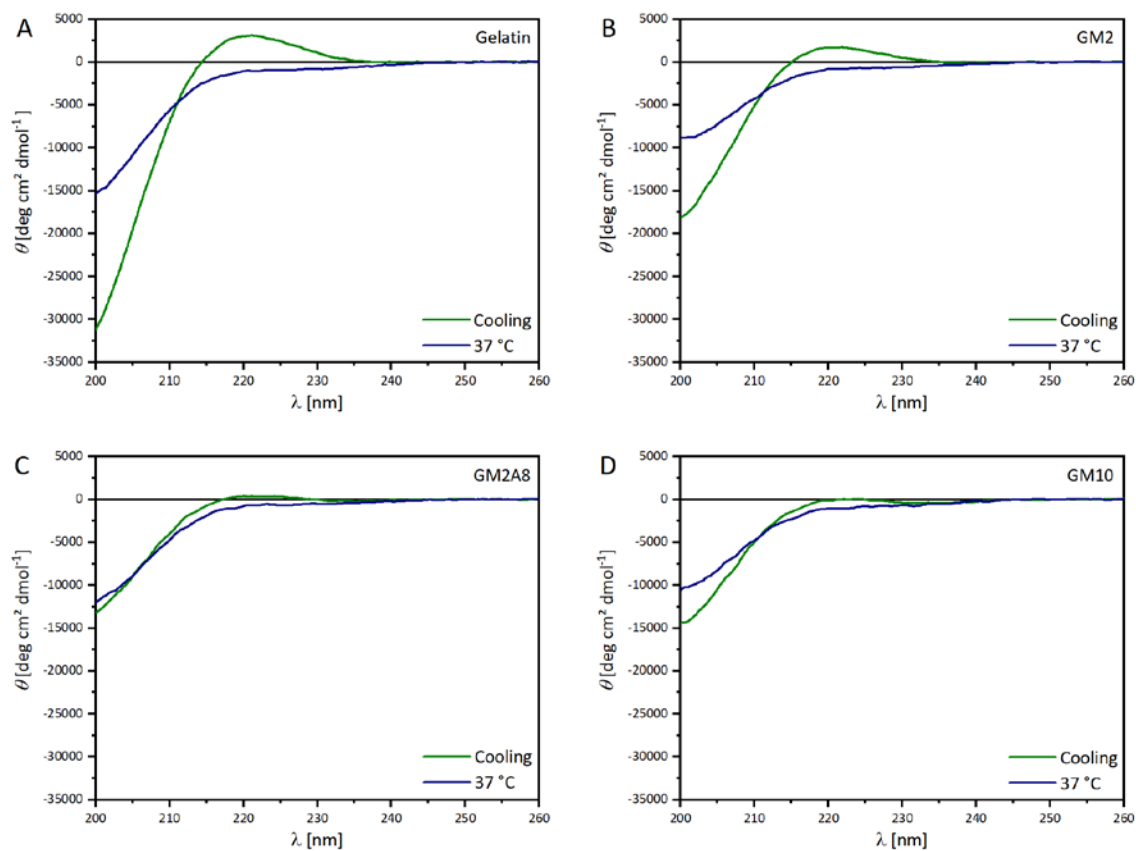


**Figure S 10:** Circular dichroism (CD) spectra of gelatin (A), GM2 (B), GM2A8 (C) and GM10 (D). CD spectra were recorded at 37 °C or after cooling procedure (37 °C to 21 °C for 20 min followed by cooling to 4 °C for 40 min). The figure was created with Origin 2019b (<http://www.originlab.com/2019b>).

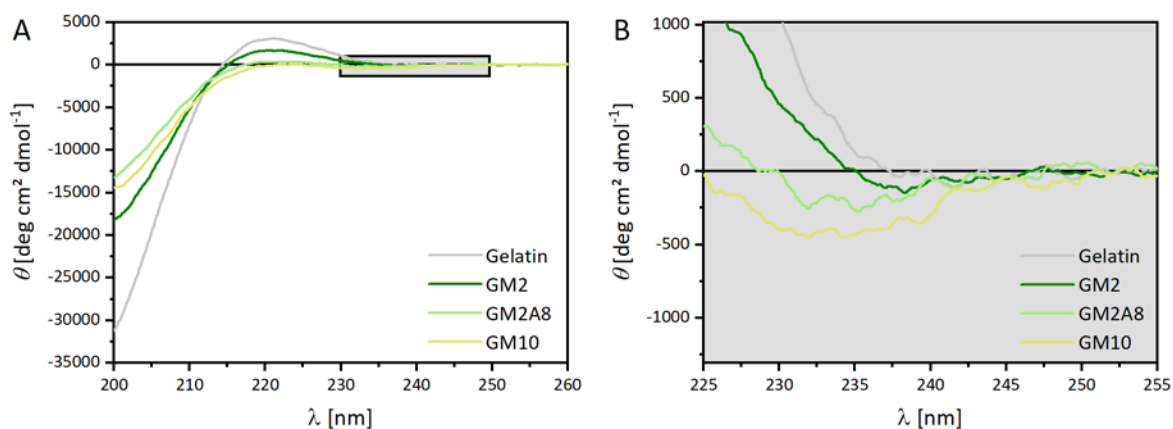


**Figure S 11:** Circular dichroism (CD) spectra of gelatin (derivatives) after cooling procedure (A) and a zoom-in of these CD spectra between 225-255 nm (B). The figure was created with Origin 2019b (<http://www.originlab.com/2019b>).

**Table S 10:** Chemical gelation delay time ( $t_{d,c}$ ) and final double bond conversion (DBC) in mmol g<sup>-1</sup> of GM2, GM2A8 and GM10 cross-linked with the classical method at 37 °C.

	$t_{d,c}$ [s]	DBC [mmol g <sup>-1</sup> ]
<b>GM2</b>	25.0±2.7	0.250±0.003
<b>GM2A8</b>	72.9±1.5	0.272±0.004
<b>GM10</b>	18.3±0.6	0.885±0.001

**Table S 11:** Chemical gelation delay time ( $t_{d,c}$ ) and final double bond conversion (DBC) in mmol g<sup>-1</sup> of GM2, GM2A8 and GM10 cross-linked with sequential cross-linking protocol (starting at 37 °C, cooling to 21 °C for 20 min followed by cooling to 4 °C for 40 min).

	$t_{d,c}$ [s]	DBC [mmol g <sup>-1</sup> ]
<b>GM2</b>	12.2±0.3	0.168±0.006
<b>GM2A8</b>	34.3±1.5	0.224±0.023
<b>GM10</b>	31.2±1.7	0.768±0.008

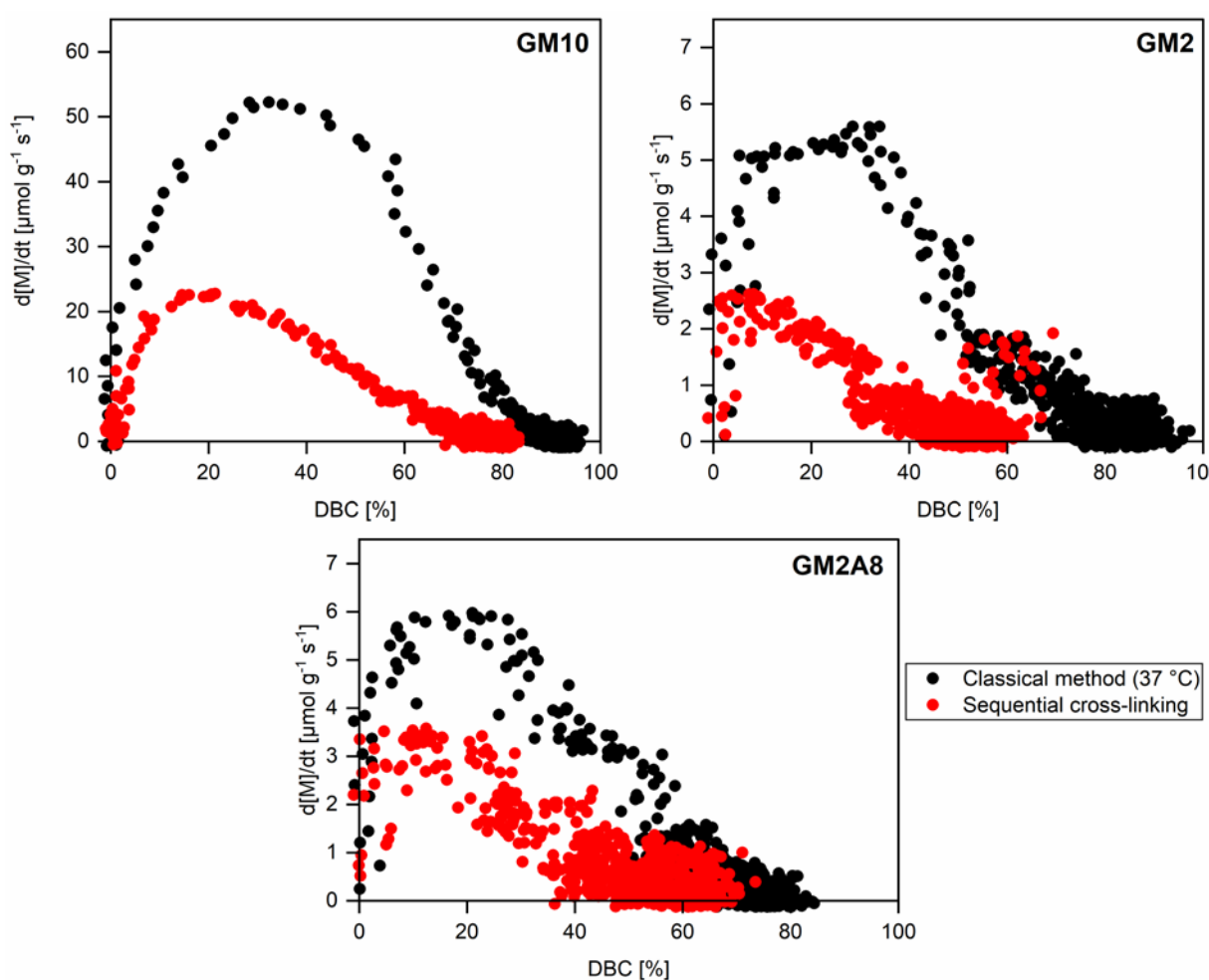


**Figure S 12:** Reaction rate of double bond conversion for GM10, GM2, and GM2A8. The figure was created with Origin 2019b (<http://www.originlab.com/2019b>).

5

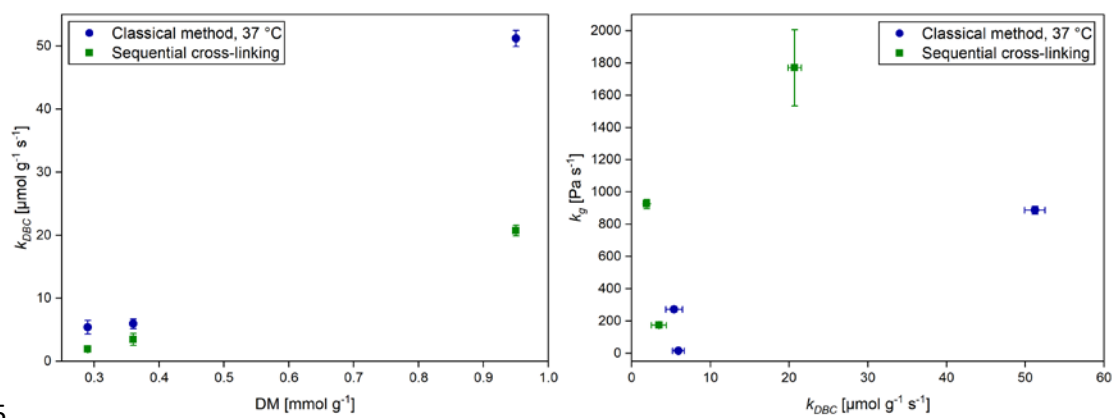


**Figure S 13:** Correlations between  $k_{DBC}$  and DM (left) as well as  $k_g$  and  $k_{DBC}$  (right). The figure was created with Origin 2019b (<http://www.originlab.com/2019b>).

## 6. Gelatine-Methacryloyl-Hydrogele mit einem Glykosaminoglykan-Gradienten als Biomaterial für das zonale Gelenkknorpel-*Tissue Engineering*

In diesem Kapitel werden die Ergebnisse und die Diskussion zu Hypothese 3 dargestellt. Die Untersuchungen wurden in dem Manuskript „*Biomimetic Hydrogel Compositions for Reconstruction of Zonal Articular Cartilage Structure*“ dargestellt und für die Veröffentlichung vorbereitet. In Kapitel 7.3 wird die Hypothese 3 zusammenfassend diskutiert.

Hinweis: Das Layout des Manuskripts wurde an das Layout der Abhandlung angepasst. Diese Überarbeitungen haben den Inhalt der Veröffentlichung nicht verändert.

### 6.0 Erklärung meiner selbstständigen Leistung

Ich habe die Studie zum größten Teil eigenständig konzipiert und ihre wissenschaftliche Methodik ausgearbeitet. Außerdem habe ich den Großteil der praktischen Arbeiten durchgeführt oder angeleitet, dies beinhaltet konkret:

- Die Synthese der meisten verwendeten methacryloylierten Biopolymer-Derivate (GM2 (5 von 6), HAM (3 von 5), CSM (3 von 4)). Die Synthesen der anderen 4 Biopolymer-Derivate erfolgten unter meiner Anleitung.
- Die quantitative Bestimmung des Methacryloylierungsgrades aller GM, HAM und CSM-Synthesen.
- Die Untersuchung der Zytotoxizität des Kühllens während der sequenziellen Vernetzung.
- Die Herstellung aller Hydrogele für die Charakterisierung mithilfe von Relaxationsversuchen unter Kompression sowie die Durchführung dieser Versuche wurden unter meiner Anleitung und meinen Vorgaben von Dominik Walz im Rahmen seiner von mir betreuten Masterarbeit durchgeführt. Die Messungen zonaler Hydrogele wurden von Sophia Regett an von ihr hergestellten Hydrogelen unter meiner Anleitung und im Rahmen ihrer von mir betreuten Masterarbeit durchgeführt.
- Die Herstellung aller Hydrogele für die Untersuchung der enzymatischen Degradation sowie die Durchführung dieser Versuche wurden unter meiner Anleitung und meinen Vorgaben von Sophia Regett im Rahmen ihrer von mir betreuten Masterarbeit durchgeführt.

- Die Verkapselung von Chondrozyten in Hydrogelen sowie die histologische Charakterisierung der zellhaltigen Hydrogele wurde von Sophia Regett unter meiner Anleitung und nach meinen Vorgaben im Rahmen ihrer von mir betreuten Masterarbeit durchgeführt.

Alle erhobenen Daten wurden von mir ausgewertet. Der weitaus größte Teil des *peer-reviewed* Fachartikels wurde von mir geschrieben, konkret habe ich den Original-Entwurf des Manuskripts konzipiert und geschrieben und federführend die Änderungsvorschläge meiner Co-Autoren harmonisiert und eingearbeitet.



## 6.1 Biomimetic Hydrogel Compositions and Zonal Structured Hydrogels for Reconstruction of Zonal Articular Cartilage Structure

Lisa Rebers<sup>1</sup>, Sophia Regett<sup>1,2</sup>, Dominik Walz<sup>1</sup>, Silke Keller<sup>1</sup>, Günter E. M. Tovar<sup>1,2,\*</sup>, Kirsten Borchers<sup>1,2</sup>,  
Alexander Southan<sup>1,\*</sup>

<sup>1</sup> Institute of Interfacial Process Engineering and Plasma Technology IGVP, University of Stuttgart, Nobelstraße 12, 70569 Stuttgart, Germany.

<sup>2</sup> Fraunhofer Institute for Interfacial Engineering and Biotechnology IGB, Nobelstraße 12, 70569 Stuttgart, Germany.

\*Corresponding Author: E-Mail: alexander.southan@igvp.uni-stuttgart.de, guenter.tovar@igvp.uni-stuttgart.de

**Vorbereitet für die Veröffentlichung in einer *peer-reviewed* Fachzeitschrift**

### 6.1.1 Abstract

Articular cartilage has a zonal structure regarding for instance its extracellular matrix (ECM), mechanical properties, chondrocyte distribution and density. However, biomaterials containing just one of these anisotropic properties are barely investigated. Thus, we aimed to prepare a cartilage-mimetic glycosaminoglycan-graded hydrogel in this study. We used methacryloylated derivatives of polymers occurring in the extracellular matrix of articular cartilage: Gelatin (as collagen hydrolysate, GM), hyaluronic acid (HAM) and chondroitin sulfate (CSM). We prepared sequentially cross-linked hydrogels out of GM, GM+HAM, GM+CSM and GM+HAM+CSM with a constant total biopolymer content of 10 % (w/w). Furthermore, we used a three-parted hydrogel mold to prepare hydrogels with three zones out of pure GM, GM+CSM and GM+HAM+CSM. We investigated mechanical properties of the different hydrogel compositions and showed that the E-Moduli of pure GM hydrogels was highest, followed by GM+CSM+HAM and GM+CSM. Zonal hydrogels compression characteristics were predominated by its composition with lowest E-moduli GM+CSM ( $E_{ini} \sim 230$  kPa,  $E_{eq} \sim 170$  kPa). We showed that the sequential cross-linking procedure with a cooling period up to 2 h was cytocompatible with chondrocytes. Furthermore, porcine chondrocytes encapsulated in pure GM and zonal hydrogels synthesized glycosaminoglycan- and collagen type II containing ECM after 28 d cultivation, thus redifferentiation was assumed. However, differences in ECM secretion neither between pure GM and zonal hydrogels nor between different zones of zonal hydrogel were observed.

### 6.1.2 Introduction

Articular cartilage has unique biomechanical properties, which are given by the composition and structure of its anisotropic extracellular matrix (ECM) [14, 367]. The ultra-structure of non-calcified articular cartilage includes the superficial, transitional and deep zone (listed from joint gap to bone). [2] These zones differ for example in mechanical properties, water content, ECM composition and structure as well as phenotype, density and organization of chondrocytes.

The main component of articular cartilage ECM is collagen type II (90-95 %) which lends its tensile strength. [2] Collagen type II is evenly distributed in all zones, however its alignment differs, which is described by the arcade-like structure [5]. The compressive strength of articular cartilage is generated by proteoglycans. [2] Disaccharide glycosaminoglycans (GAGs) are subunits of proteoglycans, whereby chondroitin sulfate and keratin sulfate are the most common ones. Sulfate and carboxylate groups of proteoglycans charge them negatively, increasing the osmolarity of articular cartilage and thereby giving the compressive strength. The concentration of proteoglycans increases with depth of articular cartilage.

Trauma or degenerative diseases destroy the zonal structure of articular cartilage. Surgical interventions are often needed to treat those defects, since articular cartilage has a limited self-repair capability. Autologous chondrocyte implantation (ACI) was developed in 1984 [368] and is utilized to treat cartilage defects [2]. However, follow-ups of ACI treated patients showed in most of the cases hyaline-like cartilage [28]. This is caused by the dedifferentiation process, which takes place when chondrocytes are isolated and cultured for expansion [26, 369]. During this dedifferentiation process chondrocytes change their morphology and ECM synthesis: Differentiated chondrocytes have a spherical shape, which changes to an elongated fibroblast-like morphology during two-dimensional (2D) expansion. Furthermore, chondrocytes secrete collagen type I instead of collagen type II [27]. Since the expansion of chondrocytes is needed to obtain sufficient amount of chondrocytes but differentiated chondrocytes are needed to build up articular cartilage-specific ECM, possibilities to redifferentiate dedifferentiated chondrocytes are investigated.

Three-dimensional (3D) cultivation of dedifferentiated chondrocytes is a relatively simple method for to induce their redifferentiation [27, 29, 30]. Hydrogels are promising candidates for this 3D cultivation of chondrocytes [370], since their high water and low polymer content resemble certain properties of articular cartilage [371]. Therefore, hydrogels out of natural polymers (derivatives) [45, 52, 177] and synthetic polymers [372-374] were investigated for cartilage tissue engineering (TE). However, the objective of cartilage TE changed over time: Whereas one first worked towards a homogenous TE construct mimicking the overall bulk properties of articular cartilage, zonal structured constructs are investigated currently [44]. It is hypothesized that mimicking the zonal structure of articular cartilage results in superior properties of biomaterial used for cartilage TE [48]. Since there are various zonal differences and gradients in native articular cartilage, there are many approaches to realize different structures and functions. Extensive reviews on zonal cartilage TE and zonal biomaterials can be found in [44, 57, 371, 375].

Zonal structured scaffolds out of two [376-378], three [56] or more [59, 379, 380] layers were investigated for cartilage TE. The manufacturing effort of these scaffold ranged from multi-layered photopolymerization [56] over additive methods (e.g. inkjet-printing [381]) to sophisticated methods combining two procedures (e.g. leaching and electrospinning [378]). Other studies investigated gradients in pore size [382], chondrocyte density [383], chondrocyte phenotype [57] and oxygen concentration [384]. Zonal differences in ECM synthesis, for example a higher GAG content in the lower part [376] and superficial zone protein in the upper part [57, 376, 378], were shown in some of the cell-containing zonal constructs. Furthermore, in some cases superior mechanical properties were found for zonal structured constructs [376, 385]. However, most of this zonal constructs consist out of

synthetic polymers [56, 59, 377, 378], blends [380, 386] or natural polymers not occurring in articular cartilage.

Levett *et al.* investigated hydrogels out of methacryloylated gelatin (GM), methacryloylated hyaluronic acid (HAM) and methacryloylated chondroitin sulfate (CSM). [52] They found that the incorporation of HAM had superior impact on mechanical properties and articular cartilage-specific ECM synthesis of chondrocytes. Incorporation of CSM had the same but less pronounced effect. Furthermore, no difference between chondrocytes isolated out of the superficial and the deep/middle zone was observed. However, they did not prepare zonal hydrogels.

In our study, we aimed to build up a zonal hydrogels containing three zones and a GAG gradient, in congruence with the non-calcified articular cartilage. Therefore, we prepared hydrogel compositions out of GM as substitute for collagen type II, HAM and CSM representing GAGs, as Levett *et al.* [52]. The total biopolymer content of hydrogels was kept constant, thus GM was replaced by CSM and HAM. We used sequential cross-linking procedure [95] to obtain further strengthened hydrogels and investigated the cytotoxicity of this cross-linking. We investigated the impact of zonal structure on compression characteristics, enzymatic degradability and redifferentiation potential of dedifferentiated chondrocytes of biopolymer-based hydrogels.

### 6.1.3 Materials and Methods

#### Materials

Dulbecco's phosphate buffered saline with  $MgCl_2$  and  $CaCl_2$  (PBS), methacrylic anhydride (MAAnh), hyaluronidase (from bovine testes) as well as sodium hydroxide (NaOH) was bought from Sigma Aldrich (Darmstadt, Germany). We purchased sodium 3-trimethylsilyl-propionate-2,2,3,3-d4 (TMSP) from Merck (Darmstadt, Germany). Other reagents were purchased from the following sources (given in parentheses): Deuterium oxide ( $D_2O$ ) (Deutero; Kastellaun, Germany), Gelatin (type B, Limes, bovine bone, 232 Bloom, standard viscosity = 4.5 mPa s; Gelita; Eberbach, Germany), dialysis membranes (MWCO 12 kDa–14 kDa) (Medicell International Ltd.; London, United Kingdom), collagenase type II for enzymatic degradation (Worthington Biochemical; Lakewood, United States of America), collagenase type II for chondrocyte isolation (NB4, Serva; Heidelberg, Germany), Roti-Histofix (Carl Roth; Karlsruhe, Germany), hyaluronic acid ( $5.1 \times 10^4$  Da; Lifecore Biomedicals, Chaska, United States of America), chondroitin sulfate (Bioiberica, Rheda-Wiedenbrück, Germany), Alcian Blue – Nucler Fast Red Staining Kit (Morphisto, Frankfurt a. M., Germany), Isomount (2000 Q Path®, VWR, Wien; Austria), ProLong™ Gold Antifade Mountant and Quant-iT™ PicoGreen™ dsDNA Assay Kit (ThermoFisher Scientific, Waltham; USA). Antibody diluent and target retrieval solution were purchased from Agilent Technologies (Santa Clara, USA). The photoinitiator lithium phenyl-2,4,6-

trimethylbenzoylphosphinate (LAP) was synthesized according to Fairbanks *et al.* [313].  $^1\text{H-NMR}$  spectroscopy (500 MHz,  $\text{D}_2\text{O}$ , d) proofed adequate shifts and integrals, i.e., 7.74 (m, 2H), 7.56 (m, 1H), 7.46 (m, 2H), 6.87 (2H, s), 2.22 (s, 3H), 2.04 (s, 6H).

### **Biopolymer Methacryloyl Synthesis Procedures**

GM was synthesized with a two-fold molecular excess of methacrylic anhydride (MAAnh) with regard to reported amino group content of gelatin ( $0.35 \text{ mmol g}^{-1}$ ) [42], as described previously (GM2) [94, 96]. In this study, six different GM2 synthesis (typical yield  $\sim 72\%$ ) with a degree of methacryloylation (DM), calculated as described by Claaßen *et al.* [94], of  $0.294 \pm 0.007 \text{ g mol}^{-1}$  were used. In the following, we do not use the suffix “2”, since we used just this GM derivative in this study.

We synthesized HAM with an equivalent molar amount of MAAnh with regard to a hydroxyl group content of  $5.19 \text{ mmol g}^{-1}$  as described in the following.  $0.521 \text{ g}$  hyaluronic acid was dissolved in  $100 \text{ mL}$  ultrapure water under stirring at  $21^\circ\text{C}$ . Afterwards,  $0.816 \text{ g}$  ( $0.529 \text{ mmol}$ ) of MAAnh was added dropwise, while the pH 7.3 was kept constant with an automatic titration device utilizing  $4 \text{ M NaOH}$ . The solution was stirred for  $5 \text{ h}$  at  $21^\circ\text{C}$ . Then, the solution was filtrated and stirred for  $16 \text{ h}$  at  $21^\circ\text{C}$  with pH adjustment (7.3). The pH was set to 8.5 with  $4 \text{ M NaOH}$  and the solution was transferred in dialysis membranes. Dialysis was done against ultrapure water for four days, whereby the water was changed twice per day. Subsequently, the pH of the dialysed solution was set to 8.5 and the solution was freeze dried for  $2 \text{ d}$ . This yielded in a foam-like white solid (typical yield  $\sim 82\%$ ), which was stored at  $21^\circ\text{C}$ . We used five different HAM synthesis in this study with a DM of  $0.308 \pm 0.139 \text{ mmol g}^{-1}$ , determined as mentioned before.

CSM was synthesized with a two-fold molar excess of MAAnh relative to hydroxyl group content ( $14.07 \text{ mmol g}^{-1}$ ). The synthesis procedure was the same as for HAM, whereby  $2.258 \text{ g}$  chondroitin sulfate were dissolved in  $100 \text{ mL}$  ultrapure water and  $4.32 \text{ g}$  ( $28.02 \text{ mmol}$ ) MAAnh was used. After freeze-drying, CSM was a white foam-like solid with a typical yield of  $\sim 75\%$  and was stored at  $21^\circ\text{C}$ . In this study, four synthesis were used with a mean DM of  $0.147 \pm 0.091 \text{ mmol g}^{-1}$  calculated as described before. Typical  $^1\text{H-NMR}$  spectra of methacryloylated biopolymers are shown in **Figure S 14** in the supporting information.

### **Porcine Chondrocyte Isolation**

We isolated porcine chondrocytes from knee cartilage of pigs (5-8 months, German Landrace) as described before [177]. In short, knee cartilage was cut into  $\sim 1 \text{ mm}^3$  pieces under sterile conditions. Afterwards, cartilage pieces were digested overnight by collagenase type II ( $3 \text{ U mL}^{-1}$ ) and washed with PBS. Cells were cultivated in DMEM/Ham's F12 containing  $10\%$  (v/v) fetal calf serum (FCS),  $1\%$  (v/v) penicillin/streptomycin, and  $50 \mu\text{g mL}^{-1}$  ascorbat-2-phosphate under standard cultivation conditions

(37 °C, humidified atmosphere, 5 % CO<sub>2</sub>). Cells were used in passage one and harvested by trypsinization.

### Hydrogel Preparation Procedure

Hydrogel precursor solutions consisted out of methacryloylated biopolymers, photoinitiator LAP and PBS. Firstly, methacryloylated biopolymers were dissolved in PBS for 2 h shaking at 37 °C. Secondly, a 1 % (w/w) LAP solution was prepared by dissolving the solid material in PBS at 37 °C for 30 min. Finally, LAP solution was added to methacryloylated biopolymer solution yielding in a 10 % (w/w) biopolymer concentration (for detailed compositions see **Table 7**) and 0.02 % (w/w) LAP concentration.

We used sequential hydrogel preparation procedure for all hydrogels. Therefore, all precursor solutions were cooled before chemical cross-linking. For preparation of hydrogels with one composition (without zonal structure), hydrogel precursor solution was filled in a cylindrical cast (5 mm depth and 25 mm diameter), covered with quartz glass plane and incubated for 2 h at 4 °C. Afterwards, chemical cross-linking was done for 2.5 min (12.1 mW cm<sup>-2</sup> at 365 nm). Cylindrical specimens with 8 mm diameter were cut out with a circle cutter and swollen shaking in PBS for at least 18 h.

**Table 7:** Composition of the four hydrogels with constant biopolymer content investigated in this study. (GM=gelatin methacryloyl, CSM=chondroitin sulphate methacryloyl, HAM=hyaluronic acid methacryloyl)

Hydrogel	Methacryloylated Biopolymer Content [% (w/w)]		
	GM	CSM	HAM
GM	10	-	-
GM+CSM	7.5	2.5	-
GM+HAM	7.5	-	2.5
GM+CSM+HAM	7.5	1.25	1.25

We manufactured a special three-part hydrogel mould for preparation of zonal hydrogels (see **Figure 16**). Zonal hydrogels consisted out of three different hydrogel precursor solutions (GM, GM+CSM and GM+HAM). The first hydrogel precursor solution (GM) was filled in the first aluminium mould (1 mm depth and 30 mm diameter), covered with a quartz glass plate and physically gelled at 4 °C for 10 min. Afterwards, the quartz glass plate was removed and a second aluminium plate (2 mm thick) with 30 mm diameter holes was placed on the first mould and fixed with a screw. The second hydrogel precursor solution (GM+CSM) was filled in the hole on top of the first already gelled hydrogel precursor solution. The two-part mould was incubated again at 4 °C for 10 min. For the third hydrogel precursor solution (GM+CSM+HAM) the procedure was repeated with another 2 mm thick aluminium plate, but the mould was incubated for 2 h at 4 °C. Afterwards, chemical cross-linking and swelling was done as described before for hydrogels with one composition.

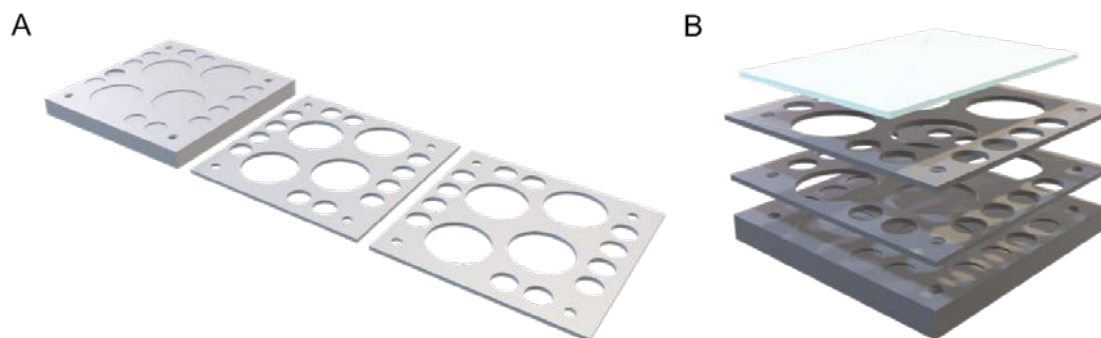


**Figure 16:** Three parts of hydrogel mold for preparation of zonal structured hydrogels.

For preparation of cell-containing hydrogels, hydrogel precursor solutions were prepared under sterile conditions. Furthermore, biopolymer derivatives were heat-sterilized by incubation for 8 h at 80 °C twice and instead of PBS cell culture media was used (DMEM/Ham's F12 containing 10 % (v/v) FCS, 1 % (v/v) penicillin/streptomycin, and 50  $\mu\text{g mL}^{-1}$  ascorbat-2-phosphate). Unlike insterile preparation, a 12.5 % (w/w) biopolymer derivative solution was mixed and diluted shortly before hydrogel casting by cell culture media containing chondrocytes ( $2.5 \times 10^6$  cells  $\text{mL}^{-1}$ ), yielding in a 10 % (w/w) biopolymer methacryloyl solution containing  $0.5 \times 10^6$  chondrocytes  $\text{mL}^{-1}$ . The rest of hydrogel preparation procedure remained unchanged. For cutting hydrogel samples (height 5 mm, diameter 8 mm), the disinfected circle cutter was used. Samples were cultured in a well plate in media (DMEM/Ham's F12 containing 10 % (v/v) FCS, 1 % (v/v) penicillin/streptomycin, and 50  $\mu\text{g mL}^{-1}$  ascorbat-2-phosphate), whereby media was changed twice a week.

We used at least three independently prepared hydrogels per hydrogel composition with different synthesis of biopolymer methacryloyls to display the deviation due to slightly different DM for hydrogel characterization. For cell encapsulation one synthesis, each biopolymer methacryloyl was used.

### Mechanical Testing

Rheological testing was done with 1 mm high hydrogels (8 mm diameter) and the Physica Modular Compact MCR301 (Anton Paar, Germany). Hydrogels were prepared as described before and were washed in PBS for 24 h. Since zonal hydrogels could only be realized with 5 mm height, it was not possible characterize their rheological behaviour. The measuring procedure was described before [96, 97]. A parallel-plate model (8 mm, 37 °C, 0.32 N load) was used and an oscillatory strain amplitude sweep ( $0.01 \% \leq \gamma \leq 100 \%$ ,  $1 \text{ s}^{-1}$ ) was done to determine storage and loss moduli ( $G'$ ,  $G''$ ) within the linear viscoelastic range. Furthermore, loss factor ( $\tan(\delta)$ , damping factor) was calculated according to Equation 6.

$$\tan \delta = \frac{G''}{G'} \quad (6)$$

Hydrogel samples were prepared with a circle cutter, resulting in nearly ideal cylinders (height 5 mm, diameter 8 mm), photos of hydrogel samples are shown in **Figure S 15**. Height and diameter of the cut sample was measured with a micrometer and deposited in the software (testXpert II) of the material testing machine (Allround-Line Z005 equipped with a 50 N load cell (Zwick, Ulm, Germany)). The measuring set-up for compression testing of hydrogels under physiological conditions (swollen in PBS, 37 °C) was extensively explained before [95].

In this study, we did unconfined compression testing. The measuring head was moved to a pre-load of 0.2 N with 0.5 mm s<sup>-1</sup>. The hydrogels were pre-conditioned by 8 cycles of 25 % strain ( $\epsilon$ ). Afterwards, the samples were gradually strain-controlled compressed in 5 % steps up to a maximal  $\epsilon$  of 25 %. A relaxation duration of 30 min was made between each compression step. We showed in preliminary studies that force change after 30 min relaxation was max. 0.02 N min<sup>-1</sup>, considered sufficient for determination of relaxation modulus in equilibrium. The initial stress ( $\sigma_{ini}$ ) to achieve the respective compression of hydrogels and the pressure after 30 min relaxation ( $\sigma_{eq}$ ) were used to calculate the relaxation moduli ( $E_{ini}$  and  $E_{eq}$ ) of the different hydrogel compositions as slope of the linear fitting calculated with Origin 2019b.

### Enzymatic Degradation

The enzymatic degradation of methacryloylated biopolymer hydrogels by collagenase (2.5 U mL<sup>-1</sup> in PBS), hyaluronidase (2.5 U mL<sup>-1</sup> in PBS) and a mixture of both (each 1.25 U mL<sup>-1</sup> in PBS) was investigated for 28 d. Hydrogels with one composition and zonal hydrogels were prepared as described above. After chemical cross-linking and cutting out cylindrical specimens, these specimens were quartered with a scalpel and each quarter was weighed before swelling ( $m_{cross-linked}$ ). After swelling, one specimen per composition was weighed ( $m_{swollen}$ ). The other specimens were transferred in enzymatic solutions or PBS as control and were incubated at 37 °C shaking. The remaining hydrogels were weighed after 1 d, 2 d, 3 d, 7 d, 14 d, 21 d, 28 d, 35 d and 42 d ( $m_{swollen}$ ). Furthermore, samples were dried at 60 °C for 18 h and weighed again ( $m_{dry}$ ).

$$gel\ yield\ [\%] = \frac{m_{dry}}{0.1 * m_{cross-linked}} * 100 \quad (7)$$

$$polymer\ content\ [\%] = \frac{m_{dry}}{m_{swollen}} * 100 \quad (8)$$

$$swelling\ capacity\ [\%] = \frac{m_{swollen}}{m_{dry}} * 100 \quad (9)$$

We calculated the gel yield using equation 7, whereby the initial dry weight of hydrogels was presumed to be 10 % of the respective wet weight, due to biopolymer content of 10 % (w/w). The gel yield is the percentage of remaining mass of original mass. The polymer content was calculated with equation 8 and corresponds to the percentage of dry weight in total weight. Furthermore, the swelling



capacity was calculated as reciprocal of polymer content with equation 9. Relative gel yield, polymer content and swelling capacity were calculated with respect to value of day 0.

### **Cytotoxicity of Sequential Hydrogel Preparation Procedure**

Chondrocyte containing GM hydrogels (1 mm high) for cytotoxicity investigations were prepared as described above. However, cooling at 4 °C before chemical cross-linking was varied between 0, 0.5, 1, 1.5 and 2 h. Viable cells were stained by fluorescence diacetate directly after hydrogel preparation and 24 h later. Fluorescence z-stacks were generated with a confocal laser scanning microscope (LSM 710, Carl Zeiss). Viable cells in full focus pictures were counted and compared relative to amount of viable cells in hydrogels prepared without cooling to 4 °C before chemical cross-linking. Chondrocytes of three donors and three GM synthesis were investigated per data point.

### **Histological Preparation and Staining**

Hydrogels were halved and fixed for 1 h in Bouin's fluid. After washing for 1 h in distilled water, samples were embedded in in paraffin, and sections of 3-9 µm were prepared using a rotary microtome. Sections were rehydrated by incubation at 60 °C for 30 min, followed by incubation at descending alcohol concentrations.

Alcian Blue-Nuclear Fast Red staining was done following the instructions of the staining kit. In short, after washing in distilled water after dewaxing, sections were pre-treated in 3 % acetic acid and for 3 min and stained for 30 min in Alcian Blue solution (1 %, pH 2.5). Samples were differentiated in acetic acid (3 %, 3 min), washed in distilled water for 2 min, stained in Nuclear Fast Red solution (0.1 %), washed again (distilled water, 1 min), dehydrated and mounted with Isomount.

For antibody stainings, silanized slides were used. Epitopes of samples were unmasked for 30 min in *Target Retrieval Solution* (pH 6), heated in a steam cooker for 30 min, cooled for 10 min in an ice-bath and washed for 2 min in washing buffer. Cell membranes were permeabilized by incubation in 0.1 % Triton-X-solution for 10 min followed by washing for 2 min. Afterwards, unspecific binding sites were blocked using 3 % BSA in PBS solution (30 min) and slides washed three times. Primary antibodies were diluted with *Antibody Diluent* (1:250) and incubated on slides for 1 h at room temperatures. After washing, diluted secondary antibodies (1:1000 (collagen type I) and 1:250 (collagen type II)) were added on the slide and incubated for 30 min in the dark at room temperature. Slides were washed again, stained with DAPI (1:1000 in PBS without calcium and magnesium) for 15 min, washed again and mounted with ProLong™ Gold.

Bright field pictures were taken with a fluorescence microscope (BZ-9000, Keyence) and fluorescence pictures with a confocal laser scanning microscope (LSM 710, Carl Zeiss).

### **Double stranded DNA Content in Cell-containing Hydrogels**

Content of dsDNA in cell containing hydrogels directly after encapsulation and after 28 d of static cultivation was investigated following the instructions of the Quant-iT™ PicoGreen™ dsDNA Assay Kit. Hydrogels were weighed, halved and weighed again before the assay was performed. The half of hydrogel was digested in 0.3 mL Proteinase-K-solution at 65 °C under shaking. Standard solutions were prepared as described in the instructions. The microtiter plate was loaded with 50 µL of sample or standard solution followed by 100 µL TE-buffer and 150 µL PicoGreen-solution. After 5 min incubation, the fluorescence emission at 480 nm was measured. With the assistance of standard curve, the dsDNA-concentration per mg hydrogel was calculated.

### Statistical Analysis

Each measurement, except cell encapsulation, was carried out in at least triplicates, whereby for each measurement replication different synthesis of methacryloylated biopolymers was used. In the following the mean and the standard deviation of each investigation is shown. For statistical analysis a two-sided Student *t*-test was used. Statistical significance was considered for *p*-values < 0.05.

## 6.1.4 Results

### Zonal Hydrogels

Zonal hydrogels were prepared by piling up three different hydrogel precursor solutions (GM, GM+CSM, GM+HAM+CSM). Thereby, a negative charge gradient within the zonal hydrogel was built up, associated with the methacryloylated GAGs CSM and HAM, whereby hyaluronic acid carries more negative charges than chondroitin sulfate. This gradient of methacryloylated GAGs was investigated utilizing Alcian Blue Staining (see **Figure S 16**).

Alcian Blue staining showed a clear border between the three zones and different staining colours of each zone. The upper zone, containing of GM2 was stained pink, the middle zone light blue and the bottom zone dark blue.

### Mechanical Testing

We determined  $G'$ ,  $G''$  and  $\tan(\delta)$  within the linear viscoelastic range of 1 mm high hydrogels utilizing rheology and their relaxation behavior under compression with up to 25 %  $\epsilon$ . Since zonal hydrogels could only be prepared with a height of 5 mm, no rheological data was taken. Results of rheological and relaxation studies are shown in **Figure 17** and **Figure 18**. The results of GM+HAM hydrogels are shown in **Figure S 17** and **Figure S 18**, respectively. Furthermore, the respective mean values and scales relative to GM hydrogels are given in **Table S 12** in the supporting information.

$G'$  of GM and GM+HAM+CSM were indistinguishable ( $p > 0.05$ ) and were ~60 kPa. GM+HAM and GM+CSM were had significantly lower  $G'$  than GM and GM+HAM+CSM hydrogels (GM+HAM: ~15 kPa,

$p < 0.001$ , GM+CSM:  $\sim 55$  kPa,  $p < 0.05$ ). Regarding  $\tan(\delta)$ , value of GM+HAM+CSM was lowest ( $\sim 0.010$ ), followed by GM and GM+CSM ( $\sim 0.015$ ) and GM+HAM ( $\sim 0.03$ ).  $\tan(\delta)$  of GM+HAM and GM+HAM+CSM was significantly different from GM ( $p < 0.05$ ).

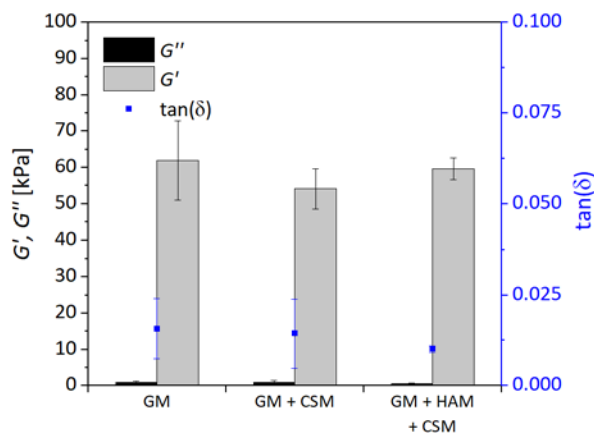


**Figure 17:** Storage, loss moduli ( $G'$ ,  $G''$ ) and loss factor ( $\tan(\delta)$ ) of GM, GM+CSM and GM+HAM+CSM hydrogels with 1 mm height and 8 mm diameter.  $G''$  and  $\tan(\delta)$  increased in parallel. Highest  $G'$  was found for GM and GM+HAM+CSM.

Relaxation tests of different hydrogel compositions were done with 5 % strain ( $\epsilon$ ) steps up to 25 %  $\epsilon$ . The compression was hold for 30 min between each compression step. The respective stresses ( $\sigma_{ini}$  and  $\sigma_{eq}$ ) and the calculated E-moduli ( $E_{ini}$  and  $E_{eq}$ ) are shown in **Figure 18** and the results of GM+HAM in **Figure S 18**. For all hydrogel compositions,  $\sigma_{ini}$  increased with  $\epsilon$ . Furthermore,  $\sigma_{eq}$  was lower compared to  $\sigma_{ini}$  for each strain and composition. Comparing all hydrogel compositions, the highest stress was needed to compress pure GM hydrogels, indicated by the highest relaxation moduli ( $E_{ini}=291.5$  kPa,  $E_{eq}=207.7$  kPa). For compression of hybrid hydrogels the highest stress was needed for GM+HAM+CSM hydrogels ( $E_{ini}=258.6$  kPa,  $E_{eq}=195.1$  kPa), followed by GM+CSM ( $E_{ini}=234.2$  kPa,  $E_{eq}=177.4$  kPa), zonal hydrogels ( $E_{ini}=229.7$  kPa,  $E_{eq}=166.5$  kPa) and GM+HAM ( $E_{ini}=148.7$  kPa,  $E_{eq}=109.8$  kPa). Consequently, the replacement of GM by methacryloylated GAGs yielded in lower E-moduli. However, E-moduli of GM+HAM+CSM hydrogels were close to the respective values of pure GM hydrogels.

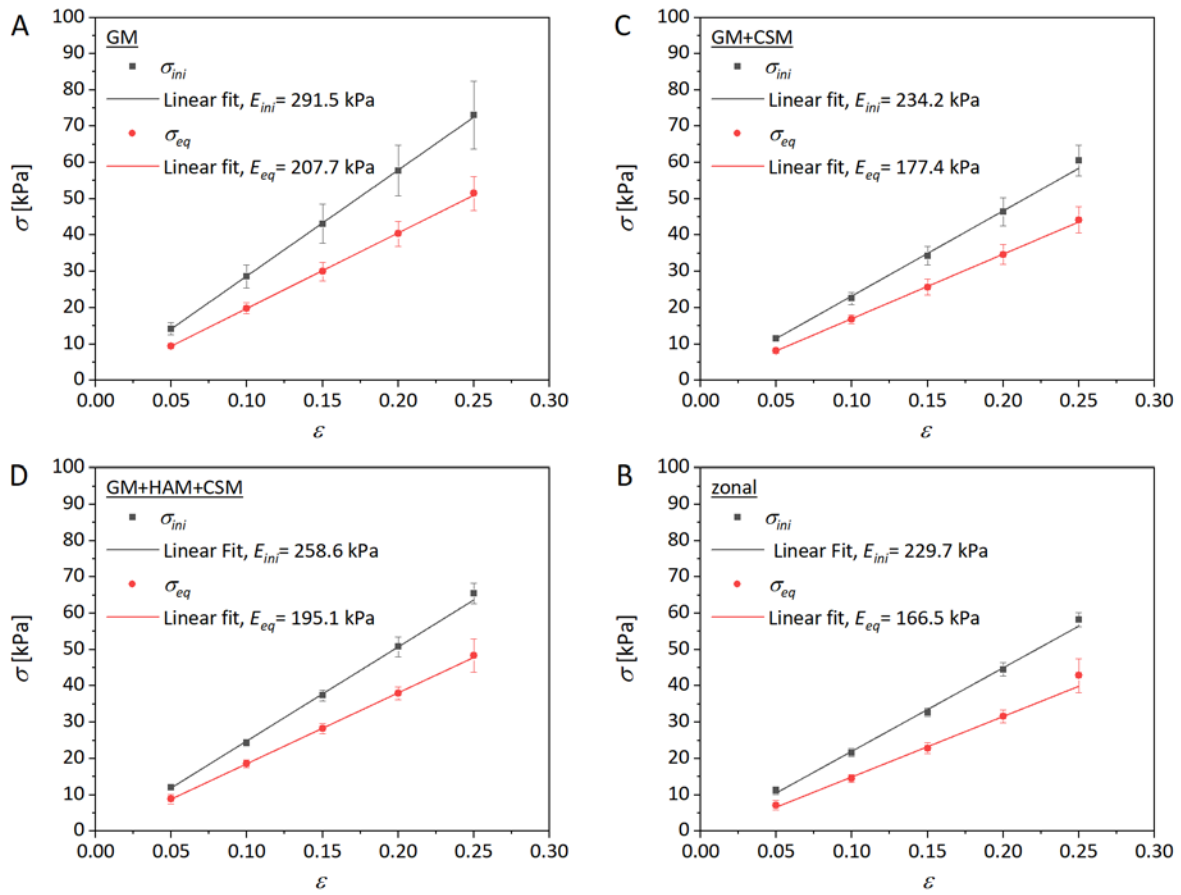


**Figure 18:** Relaxation testing of GM (A), GM+CSM (B), GM+HAM+CSM (C) and zonal (D) hydrogels. Black squares denote the initial stress ( $\sigma_{ini}$ ) to achieve the respective compression and red squares denote the remaining stress ( $\sigma_{eq}$ ) after 30 min holding the respective strain ( $\epsilon$ ). Furthermore, the linear fit of  $\sigma_{ini}$  and  $\sigma_{eq}$  are shown. The slopes of these linear fits were calculated as E-moduli ( $E_{ini}$ ,  $E_{eq}$ ). E-moduli of GM were highest, followed by GM+HAM+CSM. GM+HAM hydrogels had the lowest E-moduli.

## Enzymatic Degradation

We investigated the enzymatic degradation of the different hydrogel composition with collagenase type II (2.5 U mL<sup>-1</sup> in PBS), hyaluronidase (2.5 U mL<sup>-1</sup> in PBS) and a mixture of both (each 1.25 U mL<sup>-1</sup> in PBS) over 42 d. We used testicular-type hyaluronidase, which degrades hyaluronic acid and chondroitin sulfates [387], to target HAM and CSM. We incubated hydrogels in PBS to monitor hydrolytic degradation, too. The gel yields relative to the start of experiments during degradation studies are shown in **Figure 19**. Furthermore, the relative swelling capacity and relative polymer content of hydrogels can be found in **Figure S 19** and **Figure S 20** in the supporting information.

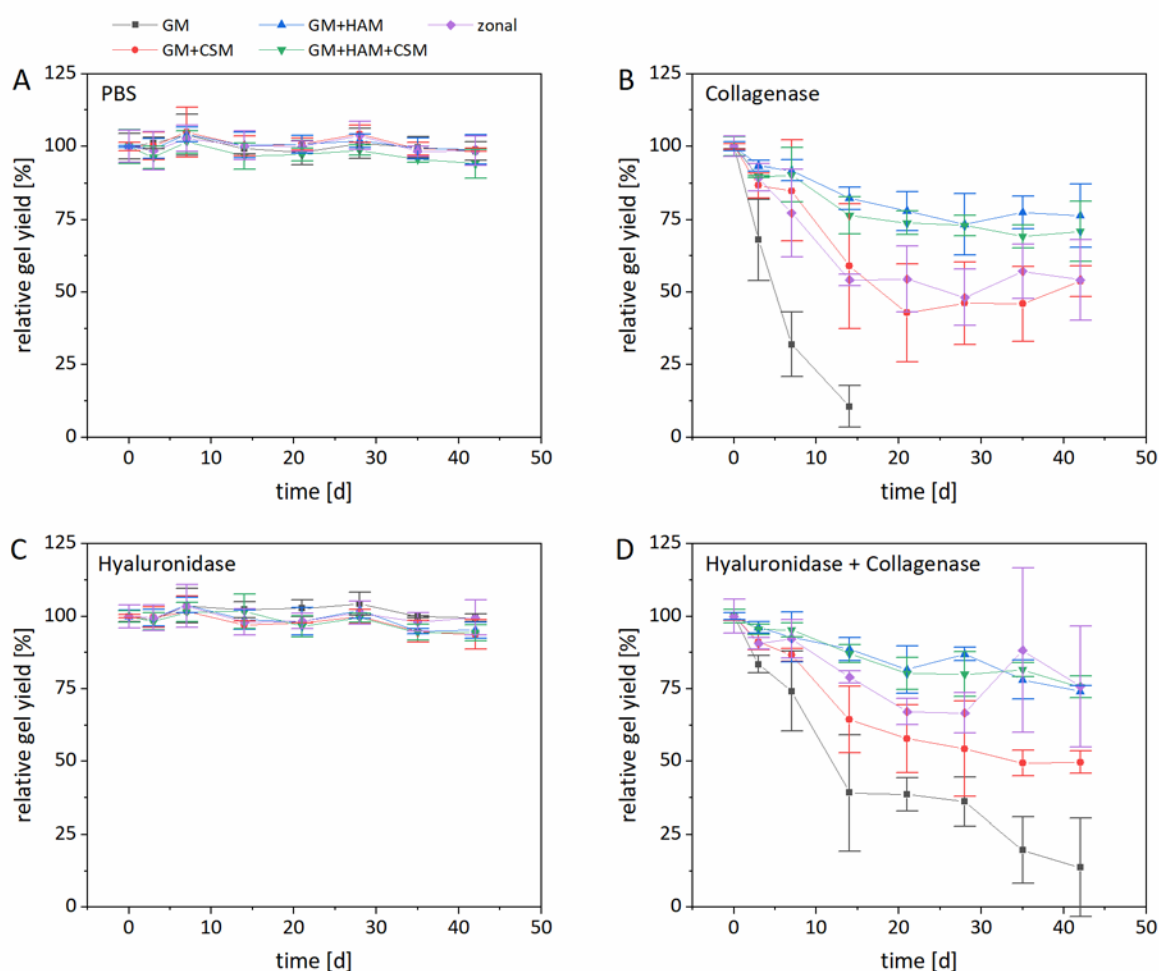


**Figure 19:** Relative gel yield of biopolymer hydrogels during degradation studies. Hydrogels consisted out of GM (10 % (w/w)), GM+CSM (7.5 % (w/w) GM + 2.5 % (w/w) CSM), GM+HAM (7.5 % (w/w) GM + 2.5 % (w/w) HAM), GM+CSM+HAM (7.5 % (w/w) GM + 1.25 % (w/w) CSM + 1.25 % (w/w) HAM) and zonal structured hydrogels. Hydrogels were incubated for 42 d in PBS (A), collagenase type II (B, 2.5 U mL<sup>-1</sup>), hyaluronidase (C, 2.5 U mL<sup>-1</sup>) and a mixture of collagenase and hyaluronidase (D, each 1.25 U mL<sup>-1</sup>). Collagenase reduced the gel yield over time for all hydrogels while PBS and hyaluronidase alone did not effect the gel yield.

Relative gel yield, polymer content and swelling capacity were indistinguishable over incubation in PBS for each hydrogel composition (~100 %). The same was observed for incubation in hyaluronidase solution (compare A-C of **Figure 19**, **Figure S 19** and **Figure S 20**). Incubation in collagenase solution lead to decreased polymer content and gel yield but increased degree of swelling. GM hydrogels were

completely degraded after 21 d. GM+CSM and zonal hydrogels had a remaining gel yield of ~55 %, GM+HAM of ~70 % and GM+CSM+HAM of ~75 % after 42 d. This was in accordance with polymer content results. Degradation kinetics of hyaluronidase-collagenase mixture were very similar to the kinetics of collagenase solution, except for pure GM hydrogels: After 42 d ~12 % relative gel yield remained.

### Cytotoxicity of Sequential Cross-Linking Procedure

The cytotoxicity of sequential cross-linking procedure was investigated taking 0 h, 0.5 h, 1 h, 1.5 h and 2 h of cooling before chemical cross-linking into account. The quantity of viable cells relative to chondrocyte-containing hydrogels prepared without cooling are shown in **Figure 20**: Relative amount of viable cells in GM-hydrogels relative to chondrocyte-containing hydrogels prepared without cooling (0 h). Duration of cooling did not affect the amount of viable cells in cell-containing hydrogels.. The number of viable chondrocytes in GM-hydrogels was not significantly affected by duration of cooling prior to chemical cross-linking. The lowest quantity of viable cells was found for 0.5 h incubation at 4 °C before chemical cross-linking (~75 %). All other time points had more than 80 % of viable cells relative to solely chemical cross-linked hydrogels. However, no significant differences were found due to relatively high standard deviation.

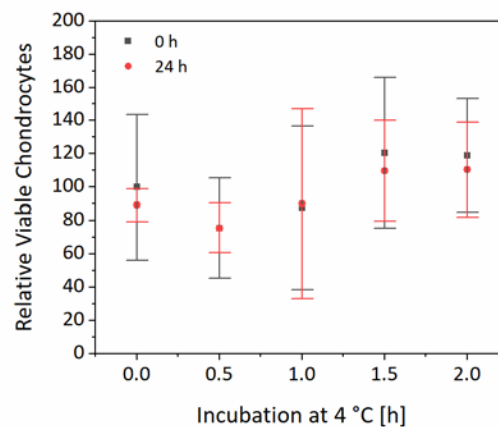


**Figure 20:** Relative amount of viable cells in GM-hydrogels relative to chondrocyte-containing hydrogels prepared without cooling (0 h). Duration of cooling did not affect the amount of viable cells in cell-containing hydrogels.

### Chondrocyte Encapsulation

Porcine chondrocytes were encapsulated in pure GM and zonal hydrogels (5 mm high, 8 mm diameter) and cultured statically for 28 d. Directly after encapsulation and at the end of cultivation samples were collected to investigate the dsDNA content and the ECM secretion of chondrocytes. Alcian Blue-Nuclear Red staining and antibody stainings against collagen type I and type II are shown in

**Figure 21** for pure GM hydrogels and in **Figure 22** for zonal hydrogels. dsDNA contents of different hydrogels are given in **Table 8**.

**Table 8:** Double stranded DNA content in cell-containing hydrogels (pure GM or zonal) directly after encapsulation and after 28 d of static cultivation. Furthermore, the relative reduction of DNA content is given. (GM=gelatin methacryloyl, dsDNA=double stranded deoxyribonucleic acid)

	dsDNA Content [ $\text{ng mg}^{-1}$ ]		Reduction [%]
	Day 0	Day 28	Day 28 : Day 0
GM	29.67±0.45	21.51±4.36	27.5
zonal	30.92±0.28	6.74±3.27	78.2

Regarding the background staining of Alcian Blue staining differences between hydrogel compositions were found. Pure GM hydrogels (**Figure 21-A,a** and **Figure 22-A,a**) were stained bright purple. GM+CSM hydrogels (**Figure 22-B,b**) had a bright blue background staining and GM+HAM+CSM hydrogels a dark blue staining (**Figure 22-C,c**). This was in accordance with Alcian Blue staining of cell-free hydrogels, see **Figure S 21**.

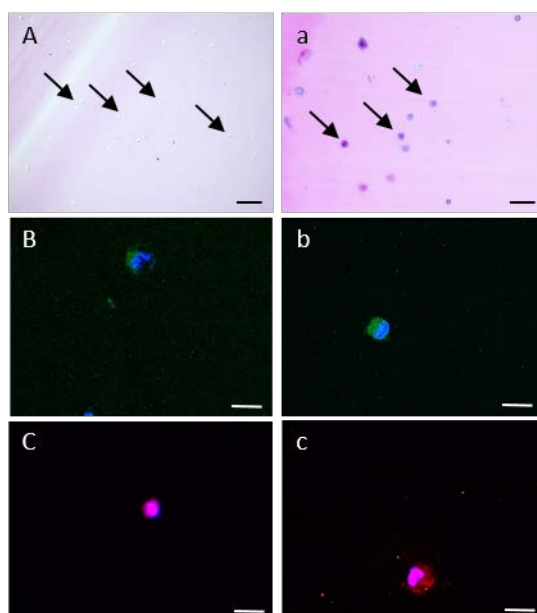


**Figure 21:** Staining of chondrocytes encapsulated in pure GM-hydrogels directly after encapsulation (A-C) and after 28 d of static cultivation (a-c). Alcian blue-nuclear fast red staining (A, a; scale=100  $\mu\text{m}$ ) showed alcian blue positive staining after 28 d cultivation, arrows mark encapsulated chondrocytes. Collagen type I (B, b; scale=10  $\mu\text{m}$ ) and collagen type II (C, c; scale=10  $\mu\text{m}$ ) was detected for both time points.

The dsDNA content of pure GM hydrogels and zonal hydrogels at the start of the experiment were indistinguishable ( $\sim 30 \text{ ng mg}^{-1}$ ). After 28 d of static cultivation, the dsDNA content was reduced by 27.5 % in GM ( $\sim 22 \text{ ng mg}^{-1}$ ) and by 78.2 % ( $\sim 7 \text{ ng mg}^{-1}$ ) in zonal hydrogels. Alcian Blue staining of hydrogels directly after encapsulation showed red stained cell nuclei and no blue stained ECM (see **Figure 21-A** and **(Figure 22-A-C)**). Furthermore, neither collagen type I nor collagen type II could be

determined qualitatively (see **Figure 21-B, C** and (**Figure 22-D, E**). After 28 d of static cultivation, Alcian Blue-positive staining and collagen type I and type II around cell nuclei were detected (**Figure 21-a-c** and **Figure 22-a-e**).

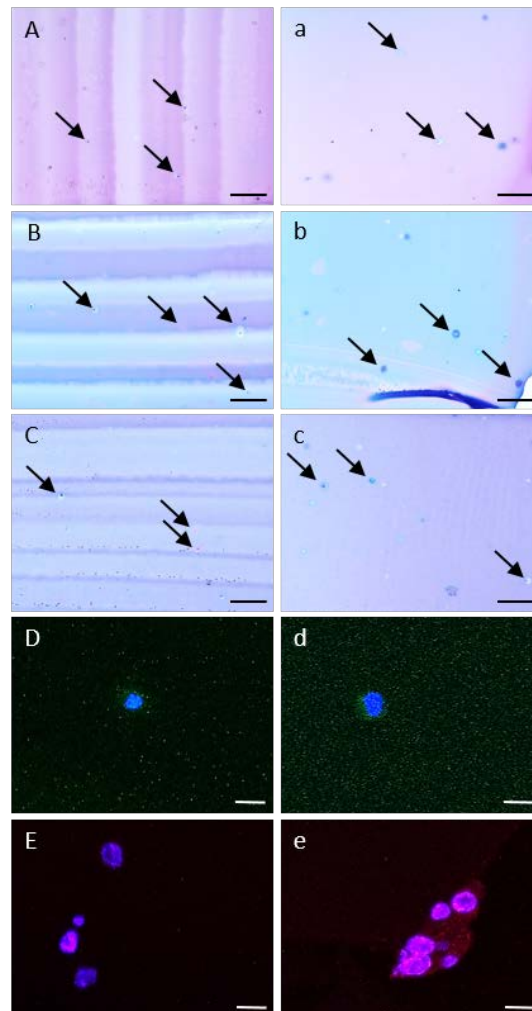


**Figure 22:** Staining of chondrocytes encapsulated in zonal-hydrogels directly after encapsulation (A-E) and after 28 d of static cultivation (a-e) in different zonal hydrogel compositions (A, a: GM; B, b: GM+CSM; C, c: GM+CSM+HAM). Alcian Blue-Nuclear Fast Red staining (A-C, a-c; scale=100  $\mu\text{m}$ ) showed Alcian Blue positive staining after 28 d cultivation, arrows mark encapsulated chondrocytes. Collagen type I (D, d; scale=10  $\mu\text{m}$ ) was scarcely detectable at both time points, collagen type II (E, e; scale=10  $\mu\text{m}$ ) was detected after 28 d cultivation.

### 6.1.5 Discussion

#### Zonal Hydrogel Preparation

Alcian Blue staining and Raman Spectroscopy proved the GAG-gradient of zonal hydrogels. Alcian Blue stains negatively charged GAGs blue, thus the color gradient from pink over light blue to dark blue indicated an increasing amount of negative charges with increasing hydrogel depth, see **Figure S 21**. The stability of zonal hydrogels was proved by incubating them for six weeks in PBS, see **Figure 19**. Concluding these results, the preparation of zonal hydrogels used in this study was suitable to prepare stable hydrogels with clearly defined zones.



## Mechanical Characterization

Articular cartilage has a non-linear stress-strain behavior [367, 388] and withstands up to 30 % strain [389]. This exceptional mechanical behavior arises from complex interaction between ECM structure, composition and high water content of the tissue and is overall described as viscoelastic [367, 390, 391]. We showed before, that our (sequential cross-linked) GM hydrogel had a non-linear stress-strain behavior [95]. In this study, we extended the mechanical characterization to investigate the viscoelastic properties of our biomimetic hydrogel compositions under shear and compression load to rank them with other hydrogels and articular cartilage.

Using rheology, we identified a nearly ideal solid-state behavior of all hydrogel compositions clarified by values close to zero of  $\tan(\delta)$  and low  $G''$  of all hydrogels (0.5-0.9 kPa), representing the viscous portion of their viscoelasticity, see **Figure 17**. The  $G'$  of sequential hydrogels presented in this study were significantly higher than those of solely chemically cross-linked hydrogels reported before: Chemically cross-linked GM2 hydrogels had a  $G'$  of  $\sim 15$  kPa [96], whereby sequentially cross-linked GM(2) hydrogels in this study had the triple  $G'$ . Even GM+HAM hydrogels with lowest  $G'$  in this study ( $\sim 20$  kPa) were twice as high as chemically cross-linked GM2, GM5 and GM10. These results were in congruence with our comparative study of compression studies with chemically and sequential cross-linked GM hydrogels [95]. In that study, the compressive stress at break of sequential GM2 hydrogels was twice as high as the compressive stress at break of solely chemically cross-linked GM2 hydrogels measured unconfined.

The compressive characteristics of all hydrogel compositions were investigated by relaxation testing with 5 % strain steps, which were hold for 30 min up to maximum strain of 25 %. E-moduli were calculated as linear fit of the initial and remaining stresses ( $E_{ini}$ ,  $E_{eq}$ ). Replacing GM by HAM or CSM resulted in lower E-moduli. However, a synergistic effect of GM+HAM+CSM combination was observed, since its E-moduli were higher than that of GM+CSM or GM+HAM. The layering of GM, GM+CSM and GM+HAM+CSM in zonal hydrogels resulted in E-moduli similar to those of the composition with the lowest E-moduli GM+CSM. Thus, the composition with lowest E-moduli predominated the compression characteristics of the zonal hydrogel in the investigated zonal hydrogel.

The replacement of GM by HAM and/or CSM resulted in lower  $G'$  and E-moduli, which was unexpected regarding the literature. Levett *et al.* replaced of 0.5 % GM in 10 % (w/v) hydrogels by HAM, which yielded in higher Young's moduli compared with pure 10 % (w/v) GM hydrogels.[52] Furthermore, the replacement by CSM did not affect the Young's modulus. Later, Levett *et al.* investigated different HAM concentrations in 10 % (w/v) hydrogels. [46] Their highest concentration of HAM was 2.0 % (w/v) and they showed that the Young's modulus was dependent on the HAM concentration and maximal for 1.0 % (65 kPa), 2.0 % HAM led to comparable Young's moduli as

hydrogels without or with 0.5 % HAM (40 kPa). However, the dynamic and equilibrium moduli of 2.0 % HAM hydrogels was highest ( $E_{ini}$ =150 kPa,  $E_{eq}$ =85 kPa). Considering the investigations of Levett *et al.*, the compression moduli of GM+HAM hydrogels could be increased by a lower HAM concentration or else by a higher molecular weight of the used hyaluronic acid; Levett *et al.* used a 0.86 MDa hyaluronic acid and we a 50 kDa one. However, the compression moduli of our investigated hydrogels were ~100 kDa stiffer than other biomimetic hydrogels containing HAM and/or CSM [46, 52].

Levett *et al.* assigned this strengthening effect of HAM to microscale phase separation. [52] It was hypothesized that the microscale phase separation supported a more interconnected and homogenous distributed ECM, thereby increasing the compressive modulus. In this study, a microscale separation was observed for GM+HAM hydrogels as well and not for all other investigated hydrogel compositions (see **Figure S 21**). However, since in our investigations the E-moduli of GM+HAM hydrogels were lowest, we hypothesize that the microscale separation leads to lower mechanical properties of hydrogels, since the hydrogel structure is less homogenous. According to our hypothesis Rizwan *et al.* showed that the hydrogel microstructure of sequentially cross-linked GM-hydrogels was more homogenous than that of solely chemical cross-linked hydrogels by X-ray diffraction and assigned this to the strengthening effect of sequential cross-linking [302].

We lack comparative results of GM hydrogels to benchmark our relaxation testing since the compressive elastic modulus or Young's modulus of GM hydrogels is determined typically [298]. Depending on the DM and cross-linking conditions Young's moduli varying between 2-15 kPa [109, 114, 115] and 30-50 kPa [45, 46, 127] were reported. However, this Young's modulus does not represent the complex behavior of viscoelastic properties [298]. One comparable study of Bartnikowski *et al.* [298] was found for sequential pure GM hydrogels. The E-moduli of their hydrogel were lower ( $E_{ini}$ ~110 kPa,  $E_{eq}$ ~70 kPa) than E-moduli of all hydrogel compositions investigated in this study.

However, the  $E_{ini}$  of articular cartilage is several times higher (1,750-2,250 kPa) compared with our hydrogels, but  $E_{eq}$  of articular cartilage is close to our values (200-400 kPa)[298]. The same was true for shear load: Temple *et al.* [392] reported a  $G'$  of ~32 MPa and  $G''$  of ~5 MPa for human articular cartilage for a frequency of 1 Hz, which is several magnitudes apart from hydrogels investigated in this study. But Levett *et al.* showed in their studies [46, 52] that the stiffness (compressive elastic modulus) of chondrocyte-containing GM (+HAM, +CSM, or +both) hydrogels increased with duration of cultivation. This implied that mechanical properties of cartilage does not need to be imitated since encapsulated chondrocytes strengthen hydrogels by their secreted ECM. However, scaffolds for cartilage TE should have a certain stability to avoid failure during physiological load.

We used sequential cross-linking procedure of hydrogels to mimic the dense network of collagen type II and proteoglycans of articular cartilage, which resulted in highest compressive moduli reported

so far. However, the water content of our hydrogels was between 89 % (GM+HAM) and 87 % (GM) and thereby higher than in articular cartilage (<80 %, wet weight) [367] and the biopolymer content in hydrogels (10 %) was lower (articular cartilage 19-29 %, wet weight) [367]. Thus, in subsequent investigations higher polymer contents should be investigated to mimic the lower water content and tighter biopolymer network resulting in higher compressive stiffness.

### **Enzymatic Degradation**

Biomaterials investigated as temporal scaffolds for TE applications must be degradable by enzymes to enable disassembling and remodelling by encapsulated cells. For cartilage TE proteases secreted by chondrocytes should be taken into account [393], e.g. collagenases [394], aggrecanases [395] and hyaluronidases [396]. We investigated the degradability of different hydrogel compositions by collagenase type II and hyaluronidase, see **Figure 19**, **Figure S 19** and **Figure S 20**. Hydrogels incubated in PBS showed constant relative gel yield, polymer content and swelling capacity over 42 d, thus no significant influence of hydrolysis during incubation in PBS for 42 d was detectable for the investigated hydrogel compositions.

Similar results as for PBS were observed for incubation in hyaluronidase solution. Thus, hyaluronidase was not able to break down any hydrogel network, containing HAM or not. This was in accordance with previous investigations showing that the bioactivity of hyaluronic acid is impaired due to (methacryloyl) modification [46, 397]: HAM was degraded slower than hyaluronic acid [46] and it seemed like it was dependent on degree of modification [397]. Furthermore, link protein did not recognize or bound less strong to HAM compared to hyaluronic acid [46]. The binding of link protein is crucial for building up of cartilage proteoglycan aggregates, it connects hyaluronic acid with aggrecan and versican through the G1 domain of their core protein [14].

Incubation in collagenase solutions lead to decreased polymer content and gel yield but increased degree of swelling. GM hydrogels were completely degraded after 21 d. GM+CSM and zonal hydrogels had a remaining gel yield of ~55 %, GM+HAM of ~70 % and GM+CSM+HAM of ~75 % after 42 d. This was in accordance with polymer content results. This correlation pointed out that the degradation led to biopolymer loss of the hydrogels. If biopolymers would remain in the network despite of partial degradation of the hydrogel network, the polymer content would be stable, the degree of swelling would increase and the gel yield would decrease due to increased water uptake.

Our results complied with various studies showing that collagenase type I [110, 111, 221, 295] and type II [97, 102, 109, 114, 177] are able to (partially) break down GM hydrogels. Hence, the methacryloylation of gelatin, unlike hyaluronic acid, did not alter the collagenase cleavage site (Pro-X-Gly-Pro, X=neutral amino acid), since free amino groups were mainly functionalized [35, 93, 221, 295]. We explained the differences between degradation profiles of collagenase and

collagenase+hyaluronidase by the halved collagenase concentration, since hyaluronidase alone did not degrade the hydrogels. This explanation was in congruence with other studies investigating the impact of collagenase concentration [102, 110, 111, 114]. These studies showed that increasing collagenase concentration was accompanied with faster degradation.

Zhu *et al.* made the presumption that the chemical cross-linking density has the highest impact on collagenase degradation rates of pure GM hydrogels, referring to their own study and results of others [295]. This presumption could be applicable to our hybrid hydrogels out of GM and methacryloylated GAG(s), too. Since we did not know the cross-linking density, we utilized the cross-linking capability of our hybrid hydrogel precursor solutions and found the correlation that high cross-linking capabilities lead to high relative gel yield after 42 d of enzymatic degradation and *visa versa*. The exact values of cross-linking capability and relative gel yield are given in **Table S 13** in the supporting information. Compared to pure GM hydrogels, the replacement of GM by methacryloylated GAGs (HAM or CSM) slowed the enzymatic degradation down. This effect was reported already for GM hydrogels containing CSM [177].

### **Chondrocyte Encapsulation**

In the concept of articular cartilage TE autologous chondrocytes are isolated and expanded [398]. Chondrocytes dedifferentiate during this 2D expansion culture [26, 369]. One possibility to redifferentiate chondrocytes is to encapsulate them in 3D biomaterials [29, 30]. A biomimetic biomaterial is aimed to create the most natural environment possible [32]. Thus, we investigated the suitability of sequential cross-linking for encapsulation of chondrocytes (**Figure 20**) and their redifferentiation qualitatively in pure GM and zonal hydrogels with GAG-gradient and investigated their redifferentiation (compare **Figure 21** and **Figure 22**).

The duration of cooling prior to chemical cross-linking did not influence the quantity of viable cells in GM hydrogels significantly ( $p>0.05$ ). Therefore, we concluded that our sequential cross-linking procedure is suitable for chondrocyte encapsulation. The utilized photoinitiator concentration we used was shown to be cytocompatible for chondrocytes before [97]. The dsDNA content of zonal and pure GM hydrogels was indistinguishable at the start of the experiment, which was expected since the same chondrocyte concentration was used for hydrogel preparation. However, the dsDNA content decreased significantly after 28 d of static culture for both investigated hydrogels (27.5 % for GM and 78.2 % for zonal hydrogels).

The investigated hydrogels were comparatively large for cell encapsulation (h=5 mm, d=8 mm). This dimension was necessary to manufacture and characterize zonal hydrogels with our presented method. Luo *et al.* calculated the oxygen pressure in hydrogel (d=6 mm) constructs and showed that the oxygen pressure reduced from the surface to the core of 2 mm high agarose hydrogels drastically

to 5 % and in 4 mm high agarose hydrogels to 1.2 %. [384] Furthermore, they modeled the glucose distribution and found a sufficient (22 mM) and homogenous distribution with no difference between 2 mm and 4 mm high hydrogels. Since our hydrogel dimensions were bigger, an insufficient oxygen supply for encapsulated chondrocytes especially in the center of hydrogels, can be assumed by the reported calculations for 4 mm high hydrogels [384]. This insufficient oxygen pressure is believed to result in more common cell death and thereby decreased dsDNA content. However, the three times greater reduction in zonal hydrogels compared with GM hydrogels in this study was inexplicable. Dynamic cultivation utilizing bioreactors is a common strategy to enhance viability of TE constructs and to apply biomechanical forces [399] and could improve the viability of our biomimetic hydrogels. Especially for articular cartilage TE dynamic cultivation is a biomimetic approach, since articular cartilage is supplied by synovial fluid which is exchanged by load during motion [400-402].

(Re)differentiated chondrocytes maintain and remodel specialized articular cartilage. We investigated the secreted ECM of encapsulated chondrocytes with respect to collagen type I, type II and GAGs. Directly after cell encapsulation no chondrocyte-specific ECM was detected, compare **Figure 21-A-C** and **Figure 22-A-E**. This was expected, since the chondrocytes were harvested from two-dimensional cultivation during encapsulation process and thereby parted from their ECM. After 28 d cultivation, Alcian Blue positive staining around the cell nuclei was detected, which was interpreted as GAGs. Furthermore, a slight coloring in antibody stainings proofed evidence for collagen type I and collagen type II (**Figure 21-a-c** and **Figure 22-a-e**).

The positive evidence of cartilage-specific ECM secretion (GAGs and collagen type II) of chondrocytes lead us to the conclusion that encapsulated chondrocytes redifferentiated during three-dimensional cultivation in pure GM and zonal hydrogels. Qualitative difference in cartilage-specific ECM secretion between pure GM and zonal hydrogels was not be observed. Furthermore, no obvious difference of ECM secretion between three zones of zonal hydrogels were found (compare **Figure 22-a-c**). This might be due to the relatively small amounts of detected ECM, which could in turn caused by low cell density and short cultivation duration. Other studies investigating zonal biomaterial models used typical cell densities between  $5 \times 10^6$  and  $2 \times 10^7$  cells per mL [55, 56, 381, 383, 384, 386] and cultured up to 16 weeks [55]. Ren *et al.* investigated the impact of chondrocyte density and chondrocyte distribution on ECM synthesis and found a positive correlation between cell density and ECM synthesis. [383] Furthermore, they bioprinted hydrogels with biomimetic density gradient and found an additional correlation between cell distribution and ECM synthesis. Thus, ECM accumulation in our hydrogels could be increased by encapsulation of higher chondrocyte densities and/or install a cell gradient in zonal structure, thereby revealing possible differences between pure GM and zonal hydrogels.

For further quantitative ranking of redifferentiation in our investigated biomimetic hydrogels quantitative investigations, such as reverse transcriptase polymerase chain reaction (RT-PCR), should be done in future experiments to make reliable statements on potential differences between hydrogel compositions and structures. Furthermore, in these investigations zone-specific proteins such as superficial zone protein (or known as proteoglycan 4) [18] and clusterin [19], both specific for superficial zone, cartilage oligomeric matrix protein (COMP) [20] and cartilage intermediate layer protein (CILP) [21], both specific for middle and deep zone could be examined.

There are three previous studies investigating biomimetic hydrogel compositions containing GM and chemical cross-linkable hyaluronic acid and chondroitin sulfate [52, 403]. Levett *et al.* found a more pronounced promoting chondrogenic effect for GM hydrogels containing HAM (GM+HAM, GM+HAM+CSM) compared with GM+CSM hydrogels. [52] However, the replacement of GM by both, HAM and CSM, resulted in higher redifferentiation levels of encapsulated chondrocytes. Constantini *et al.* found differentiated bone-marrow derived human mesenchymal stem cells (BM-MSCs) in bioprinted alginate+GM+CS-AEMA (vinyl-modified CS) hydrogels and hypertrophic BM-MSCs for alginate+GM+HAM+CS-AEMA hydrogels [403]. In both studies [52, 403] HAM concentration of 0.5 % were utilized, thus the known effect of dose-dependent influence of HA on chondrogenesis, whereby low concentration yield in chondrogenic effects [46, 52, 404-406], cannot be considered as explanation. Furthermore, Hoch *et al.* showed that the replacement of GM by CSM stabilized the round morphology of differentiated chondrocytes [177].

We hypothesizes that the molecular weight of the used HA plays a critical role. Levett *et al.* used a 0.86 MDa HA [52], while Constantini *et al.* used a 200 kPa HA [403], as already discussed above for compression moduli. The molecular weight of HA influences their solubility and the microscale phase separation is more pronounced in high molecular weight HA which was assigned to higher compressive moduli, which is contrary to our hypothesis for explanation of relatively low E-moduli of GM+HAM hydrogels, and more interconnected and distributed ECM in hydrogels [52]. However, both studies showed a redifferentiation effect of GM+CS(M,-AEMA) and GM+HAM+ CS(M,-AEMA) hydrogels, which is in congruence with our findings.

In this study, we presented a methacryloylated biopolymer-hydrogel structured in three zones, differing in biopolymer composition and mimicking the gradient of negative charges with tissue depth in articular cartilage. However, the zonal structure of articular cartilage is more complex including different chondrocyte phenotypes, chondrocyte density gradient, collagen fiber orientation and differing mechanical properties (compression and tensile). These aspects were addressed by other zonal cartilage TE methods [44] and could be combined with our approach: Matrix-based approach encapsulates zonal chondrocyte phenotypes in multilayered hydrogels out of one composition [55, 56, 377]. Scaffold- and matrix free zonal cartilage TE cultivates zonal phenotypes in high density

culture [57]. However, the isolation and expansion of zonal chondrocytes is highly complex [407] and an additional benefit of their use is incongruent [377], thus their use is critically discussed [48]. Scaffold-based approaches used pore-size gradient [382], fiber and porous zone [378], multi-layered polymer nanocomposite scaffolds [59] and unidirectional freeze casting combined with lyophilization [379] to mimic the complex ECM architecture of articular cartilage. Hybrid strategy is the last approach, combining different chondrocyte phenotypes and zonal structured biomaterials [44].

### 6.1.6 Conclusion

The anisotropy of articular cartilage is essential for its mechanical and biological function. However, only a few studies investigated zonal structured biomaterials and even less utilized natural polymers out of the articular cartilage extracellular matrix (ECM). In this study, we described a simple method for preparation of stable zonal structured sequentially cross-linked hydrogels using a three-part mold. Furthermore, we used methacryloylated biopolymers occurring in the articular cartilage ECM (gelatin as collagen hydrolysate (GM), hyaluronic acid (HAM) and chondroitin sulfate (CSM)) for hydrogel preparation. Relaxation testing and rheological investigations of GM, GM+HAM, GM+CSM, GM+HAM+CSM and zonal hydrogels showed that the replacement of GM by HAM decreased mechanical properties. All other hydrogels showed comparable properties and the compressive characteristics of zonal hydrogels were predominated by the hydrogel composition with the lowest E-modulus. Furthermore, the sequential hydrogel preparation procedure was shown to be cytocompatible for porcine chondrocytes. All hydrogels were (partly) degradable by enzymes occurring in articular cartilage (collagenase and hyaluronidase), making them to suitable candidates for application in cartilage TE. Additionally, porcine chondrocytes encapsulated in pure GM and zonal hydrogels redifferentiated, evidenced by collagen type II and GAG synthesis, without utilizing special growth factors or cell culture media. Our presented method and hydrogel compositions open up further investigations taking longer cultivation duration and mechanical stimulation into account to maximise ECM synthesis and creation of ECM differences between zones and thereby further strengthening the hydrogels.

### 6.1.7 Acknowledgements

L.R. thanks the Evonik Stiftung (Essen, Germany) for funding of PhD scholarship. The authors thank the ministry of science research and art Baden-Württemberg (Stuttgart, Germany) for financial support within the project ZEK (7533-7-11.10-13) in the funding program biotechnology and the Fraunhofer Gesellschaft for financial support within the project Dyna-Implant. We thank Veronika Schönhaar (Fraunhofer Institute for Interfacial Engineering and Biotechnology IGB) for photoinitiator synthesis,

Peter Loskill for the opportunity to carry out cell culture experiments in his MicroOrganoLab (Fraunhofer Institute for Interfacial Engineering and Biotechnology IGB), Gabriele Vacun (Fraunhofer Institute for Interfacial Engineering and Biotechnology IGB) for help with the cytotoxicity investigations and IGVP workshop for hydrogel mold manufacturing.



## 6.1.8 Supporting Information

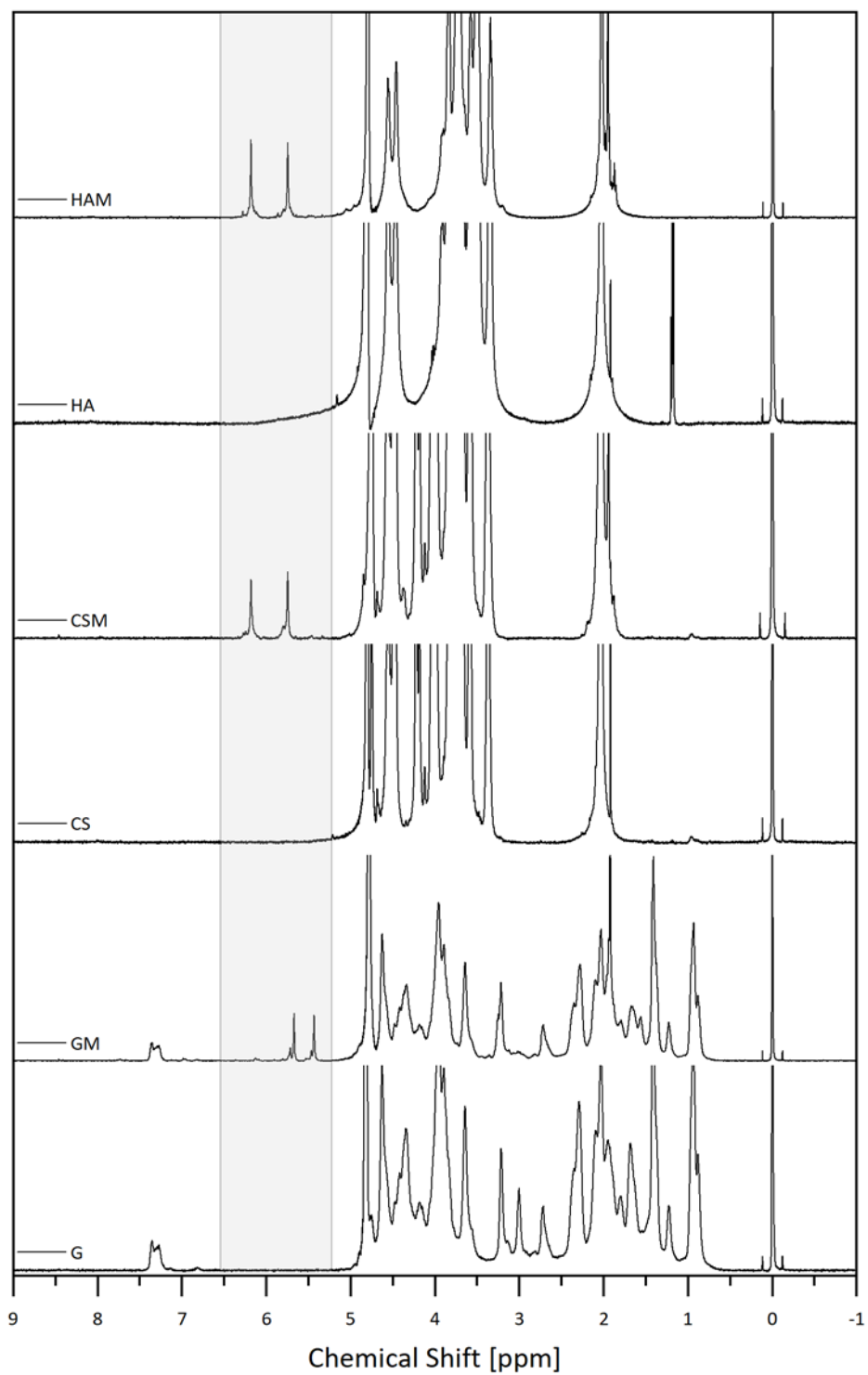


**Figure S 14:**  $^1\text{H-NMR}$  spectra of unmodified biopolymers gelatin (G), chondroitin sulfate (CS), hyaluronic acid (HA) and biopolymer derivatives gelatin methacryloyl (GM), chondroitin sulfate methacryloyl (CSM) and hyaluronic acid methacryloyl (HAM). Acrylic protons of methacryloyl groups were highlighted grey.

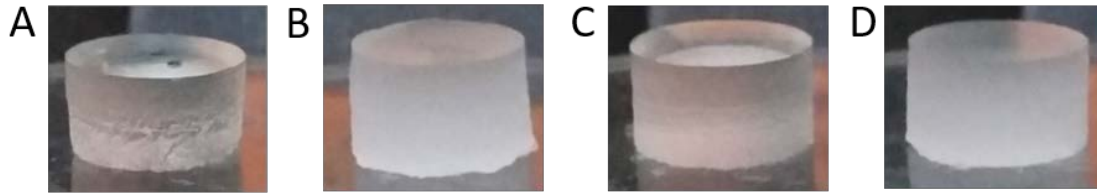


**Figure S 15:** Photos of hydrogel samples cut with a circle cutter for compression testing and cell encapsulation (height 5 mm, diameter 8 mm). Pictures show different hydrogel compositions: GM (A), GM+HAM (B), GM+CSM (C) and GM+HAM+CSM (D). Hydrogels containing HAM were cloudy, the others nearly transparent.

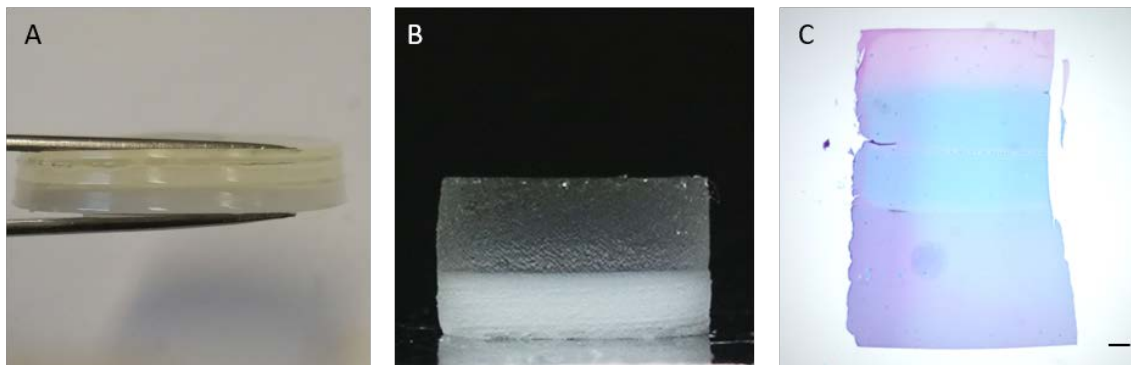


**Figure S 16:** Zonal hydrogels directly after preparation in the mold (A, height 5 mm, diameter 30 mm), cut sample for compression testing and cell encapsulation (B, height 5 mm, diameter 8 mm). In A and B the hyaluronic acid methacryloyl containing layer were opaque, while the other two layers were nearly transparent. A representative Alcian Blue-Nuclear Fast Red stained slice of zonal hydrogels is shown in C (scale bar = 500  $\mu$ m). The three layers could be differentiated by different staining, from top to bottom: GM (pink), GM+CSM (light blue) and GM+HAM+CSM (dark blue to purple).

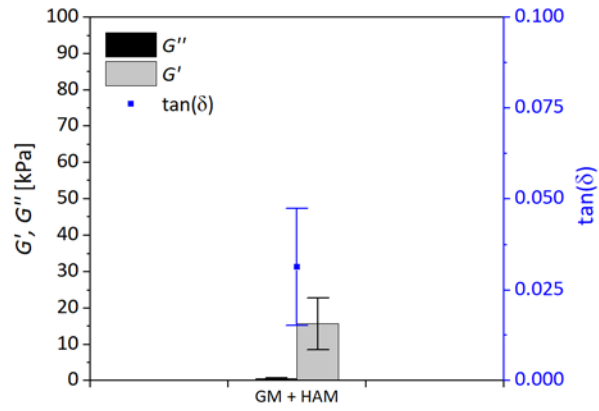


**Figure S 17:** Storage, loss moduli ( $G'$ ,  $G''$ ) and loss factor ( $\tan(\delta)$ ) of GM+HAM hydrogels with 1 mm height and 8 mm diameter.

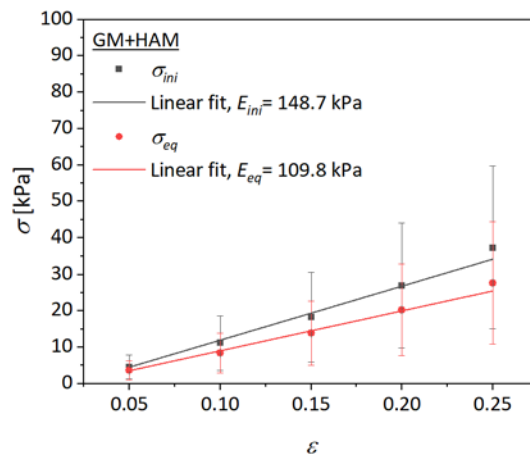


**Figure S 18:** Relaxation testing of GM+HAM hydrogels. Black squares denote the initial stress ( $\sigma_{ini}$ ) to achieve the respective compression and red squares denote the remaining stress ( $\sigma_{eq}$ ) after 30 min holding the respective strain ( $\epsilon$ ). Furthermore, the linear fit of  $\sigma_{ini}$  and  $\sigma_{eq}$  are shown. The slopes of these linear fits were calculated as E-moduli ( $E_{ini}$ ,  $E_{eq}$ ). E-moduli of GM were highest, followed by GM+HAM+CSM. GM+HAM hydrogels had the lowest E-moduli.

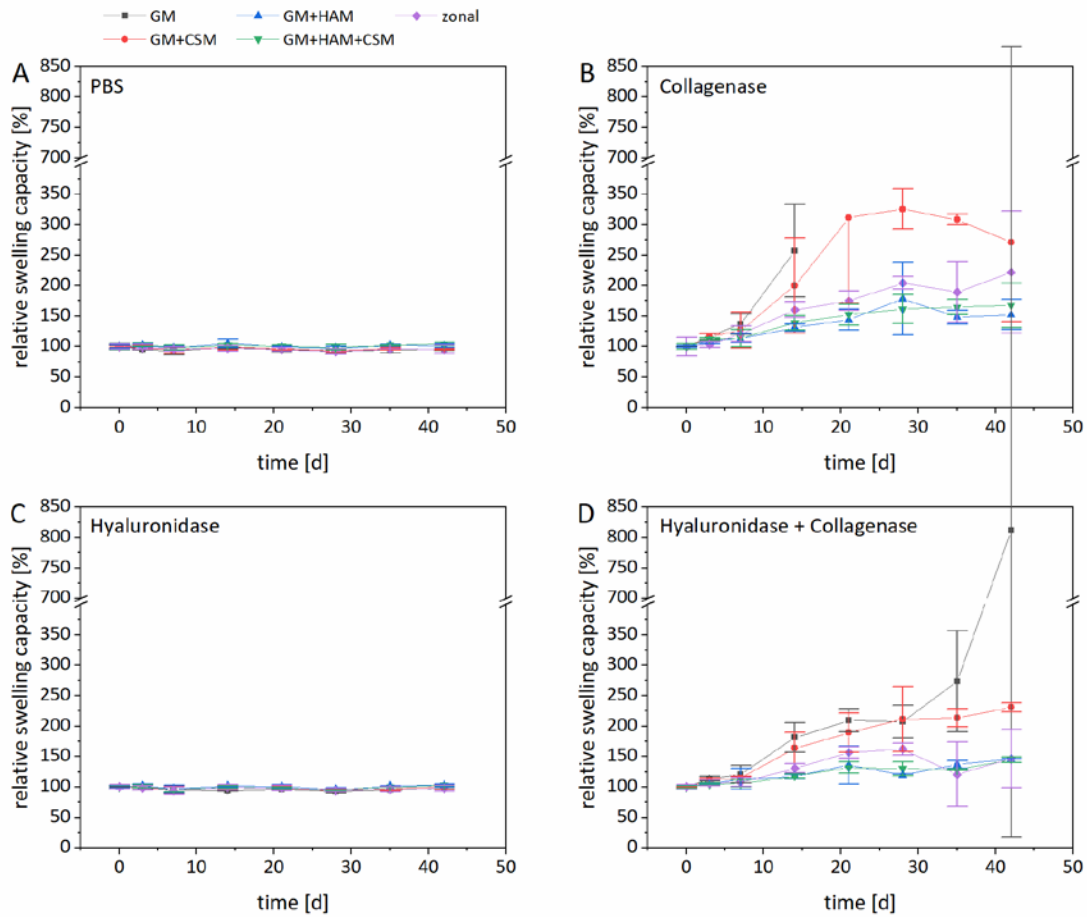


**Figure S 19:** Relative swelling capability of biopolymer hydrogels during degradation studies. Hydrogels consisted out of GM (10 % (w/w)), GM+CSM (7.5 % (w/w) GM + 2.5 % (w/w) CSM), GM+HAM (7.5 % (w/w) GM + 2.5 % (w/w) HAM), GM+CSM+HAM (7.5 % (w/w) GM + 1.25 % (w/w) CSM + 1.25 % (w/w) HAM) and zonal structured hydrogels. Hydrogels were incubated for 42 d in PBS (A), collagenase type II (B, 2.5 U mL<sup>-1</sup>), hyaluronidase (C, 2.5 U mL<sup>-1</sup>) and a mixture of collagenase and hyaluronidase (D, each 1.25 U mL<sup>-1</sup>). Collagenase increased the swelling capacity over time for all hydrogels while PBS and hyaluronidase alone did not effect it.

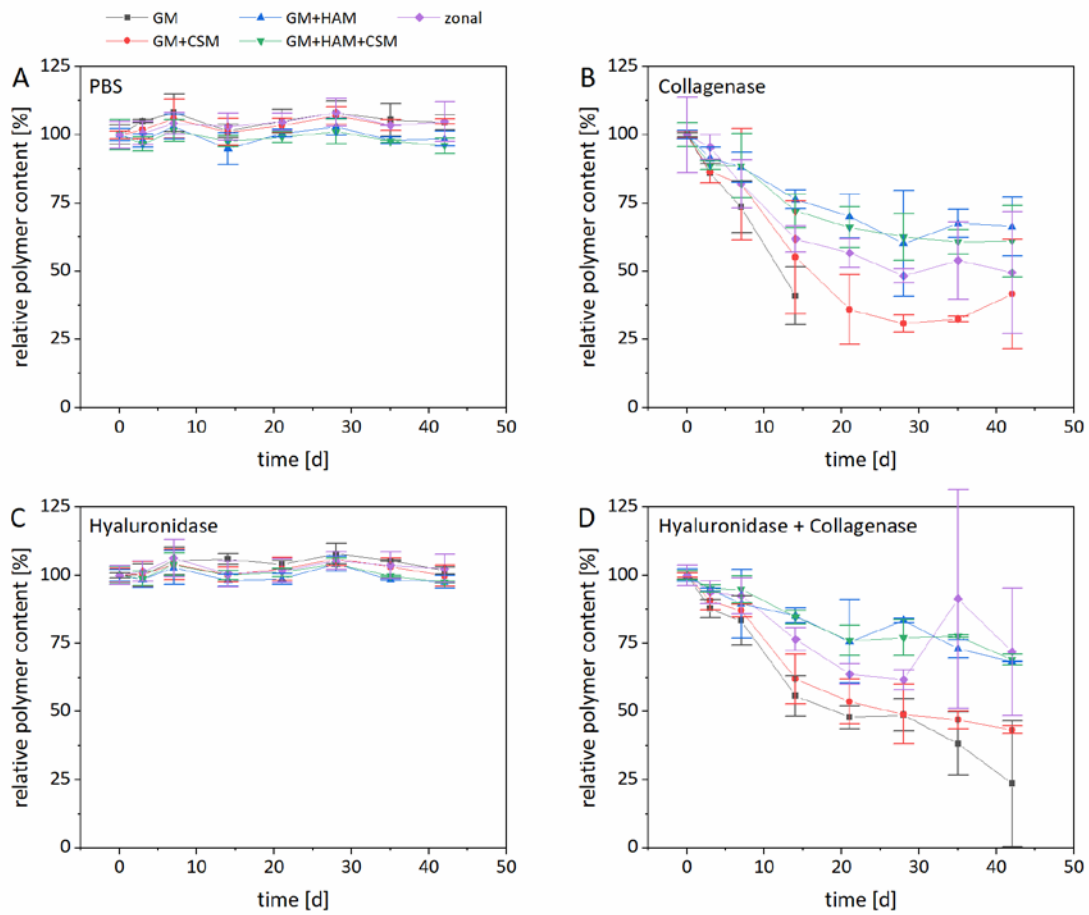


**Figure S 20:** Relative polymer content of biopolymer hydrogels during degradation studies. Hydrogels consisted out of GM (10 % (w/w)), GM+CSM (7.5 % (w/w) GM + 2.5 % (w/w) CSM), GM+HAM (7.5 % (w/w) GM + 2.5 % (w/w) HAM), GM+CSM+HAM (7.5 % (w/w) GM + 1.25 % (w/w) CSM + 1.25 % (w/w) HAM) and zonal structured hydrogels. Hydrogels were incubated for 42 d in PBS (A), collagenase type II (B, 2.5 U mL<sup>-1</sup>), hyaluronidase (C, 2.5 U mL<sup>-1</sup>) and a mixture of collagenase and hyaluronidase (D, each 1.25 U mL<sup>-1</sup>). Collagenase reduced the polymer content over time for all hydrogels while PBS and hyaluronidase alone did not effect the polymer content.

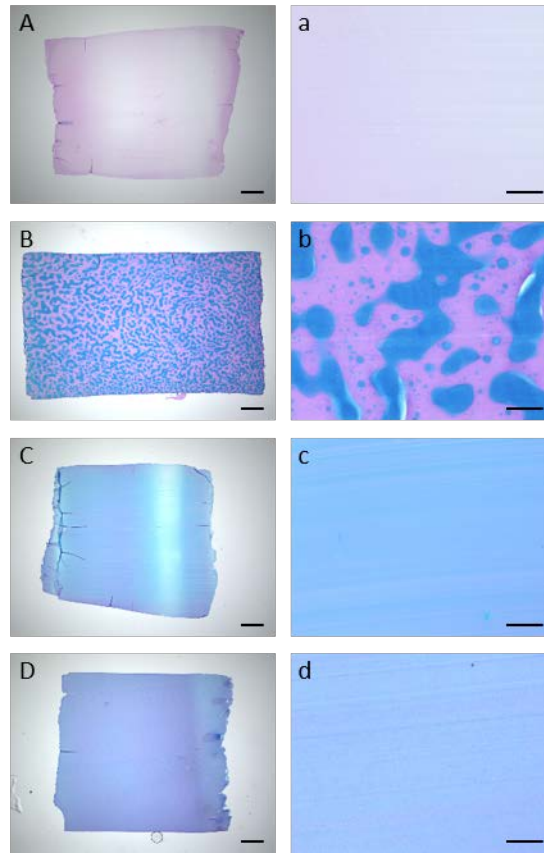


**Figure S 21:** Alcian Blue-Nuclear Fast Red staining of cell free hydrogels. Representative overview pictures (A-D, 2x magnification, scale = 500  $\mu\text{m}$ ) and detail pictures (a-d, 20x magnification, scale = 100  $\mu\text{m}$ ) of different hydrogel compositions (A, a: GM, B, b: GM+HAM, C, c: GM+CSM, D, d: GM+HAM+CSM) are shown.

**Table S 12:** Storage modulus ( $G'$ ), loss modulus ( $G''$ ), loss factor ( $\tan(\delta)$ ), initial E-modulus ( $E_{ini}$ ) and equilibrium E-modulus ( $E_{eq}$ ) of biomimetic hydrogel compositions and their scale relative to GM hydrogels. Zonal hydrogels could only be made with a height of 5 mm, thus no rheological data was available for them.

	$G'$	scale	$G''$	scale	$\tan(\delta)$	scale	$E_{ini}$	scale	$E_{eq}$	scale
	[kPa]	[-]	[kPa]	[-]	[-]	[-]	[kPa]	[-]	[kPa]	[-]
GM	61.9	1.00	0.92	1.00	0.016	1.00	291.5	1.00	207.7	1.00
GM+ HAM	15.7	0.25	0.53	0.58	0.031	1.99	148.7	0.51	109.8	0.53
GM+ CSM	54.1	0.88	0.87	0.94	0.014	0.92	234.4	0.80	177.4	0.85
GM+ HAM +CSM	59.6	0.96	0.63	0.69	0.010	0.64	258.6	0.89	195.8	0.94
zonal	-	-	-	-	-	-	229.9	-	166.5	-

**Table S 13:** Cross-linking capabilities of hydrogel precursor solutions (10 % (w/w)) and relative gel yields after enzymatic degradation with collagenase for 42 days of all investigated hydrogel compositions.

Hydrogel Composition	Cross-Linking Capability [mmol g <sup>-1</sup> ]	Relative Gel Yield [%]
GM	0.0294	0
GM+HAM	0.0314	76.3
GM+CSM	0.0247	53.8
GM+HAM+CSM	0.0280	70.9
Zonal	0.0266	54.2

## 7. Diskussion

Die in dieser Dissertation erzeugten Ergebnisse sind in den Kapiteln 4, 5 und 6 in Form von Veröffentlichungen bzw. Manuskripten, die für die Veröffentlichung in *peer-reviewed* Fachzeitschriften vorbereitet wurden, dargestellt und ausführlich diskutiert worden. In diesem Kapitel werden nun die Ergebnisse zu den in Kapitel 3 aufgestellten Hypothesen zusammengefasst und diskutiert und die Hypothesen abschließend bewertet.

### 7.1 Hypothese 1

Gelatine wird aus Kollagen hergestellt, dabei werden kommerziell zwei Verfahren verwendet: Der saure und der basische Aufschluss. Der saure Aufschluss führt zu Gelatine Typ A ( $G_A$ ) und der basische Aufschluss zu Gelatine Typ B ( $G_B$ ). In Kapitel 2.2.1 dieser Arbeit werden die Unterschiede der Konditionierungsprozesse und der Gelatine-Typen ausführlich beschrieben. Zusammengefasst lässt sich sagen, dass sich  $G_A$  und  $G_B$  in ihrer Aminosäurezusammensetzung, ihrem isoelektrischen Punkt (IEP) und ihrer Molekulargewichtsverteilung unterscheiden. Des Weiteren werden beispielsweise die Standardviskosität und der Bloom Wert durch den Gelatine-Herstellungsprozess bestimmt, weshalb eine ausführliche Standardcharakterisierung für jede Gelatine von den Gelatine-Herstellern durchgeführt wird (siehe 2.2.3).

Die Eigenschaften der Gelatine, die für die Synthese von Gelatine-Methacryloyl (GM) verwendet wird, sind also abhängig vom Gelatine-Typ und dem Herstellungsprozess. Dieser Einfluss der Eigenschaften des Rohmaterials auf die Eigenschaften der GM sowie auf GM-Lösungen und -Hydrogele wurde bisher jedoch kaum betrachtet. Solche Untersuchungen wären jedoch wichtig um die Reproduzierbarkeit von Ergebnissen im Zusammenhang mit GM, beispielsweise für die Anwendung als Biomaterial, zu ermöglichen. Bisher wurden in vielen Veröffentlichungen keine Angaben zum Rohmaterial wie beispielsweise der tierische Ursprung, Gelatine-Typ und Bloom-Wert gemacht, vergleiche Kapitel 2.3.1 dieser Arbeit. Deshalb wurde im Rahmen dieser Arbeit die folgende Hypothese aufgestellt und untersucht:

*Die Wahl des Gelatine-Rohmaterials und der Modifizierungsgrad beeinflussen die physikochemischen Eigenschaften von Gelatine Methacryloyl und den resultierenden Hydrogelen.*

Zur Untersuchung wurden je fünf Gelatine-Methacryloyl(-Acetyl) (GM(A))-Derivate aus  $G_A$  und  $G_B$  mit dem gleichen Vorgehen hergestellt. Dabei besaßen die gewählten  $G_A$ - und  $G_B$ -Rohmaterialien nahezu identische Bloom-Werte ( $G_A$ : 233 g Bloom,  $G_B$ : 232 g Bloom), unterschieden sich jedoch in ihrer



Standard-Viskosität ( $G_A$ : 2,8 mPa s,  $G_B$ : 4,5 mPa s). Außerdem konnte gezeigt werden, dass der Aminogruppen-Gehalt (Lysin- und Hydroxylysin-Gehalt) der Rohmaterialien  $G_A$  und  $G_B$  nicht unterscheidbar war.

Es wurde der Methacryloylierungsgrad (DM), der Gesamtmodifizierungsgrad (DMA), die Molekulargewichtsverteilung, der IEP, die Viskosität, das Gelier- und Schmelzverhalten, sowie der Speichermodul ( $G'$ ) und der Quellbarkeit (englisch *equilibrium degree of swelling*, EDS) der 10 Gew.-% Hydrogele der Derivate (GM2, GM5, GM10, GM2A8, GM5A5) untersucht. Die Ergebnisse sind in 4.1.4 dargestellt.

Es konnte gezeigt werden, dass mit dem verwendeten GM-Synthese-Vorgehen der DM und DMA unabhängig von dem eingesetzten Gelatine-Typ war. Dieses Ergebnis wurde erwartet, da sich der Aminogruppengehalt der zwei untersuchten Gelatine-Typen nicht signifikant unterschied und mehr Hydroxylgruppen zur Verfügung standen als methacryloyliert wurden. Darüber hinaus konnte gezeigt werden, dass der DM mit dem eingesetzten Überschuss an Methacrylsäureanhydrid und der DMA mit dem verwendeten Überschuss an Essigsäureanhydrid steigt (siehe **Figure 1**).

Lee *et al.* stellten in einer vorherigen Studie Unterschiede zwischen dem DM von  $G_A$ M und  $G_B$ M mit deren Synthesevorgehen fest. [300] Allerdings wurden in deren Studie niedrigere DMs erzeugt als in unseren Untersuchungen und die verwendeten Gelatine-Rohmaterialien unterschieden sich in ihren Bloom-Werten ( $G_A$ : 175 g Bloom,  $G_B$ : 225 g Bloom). Ein höherer Bloom-Wert könnte während der GM-Synthese zu einer höheren Viskosität der Gelatine-Lösung führen, die wiederum die Methacryloylierung beeinflussen könnte, insbesondere, wenn nur wenig Methacrylsäureanhydrid verwendet wird. Der DM des am höchsten modifizierte GM-Derivats der Studie war mit der von uns untersuchten GM2 vergleichbar und zwischen  $G_A$  und  $G_B$  nicht unterscheidbar. Für dieses Derivat stimmten somit unsere Ergebnisse mit denen von Lee *et al.* überein.

Der IEP der eingesetzten Rohmaterialien wurde ermittelt und lag bei pH 8,8 ( $G_A$ ) und pH 4,9 ( $G_B$ ), was jeweils ein typischer Wert für den Gelatine-Typ ist [64]. Nach Modifizierung lagen die IEPs aller  $G_A$ M-Derivate bei 4,5 und die IEPs von  $G_B$ M-Derivate bei 4,1 (siehe **Figure 2-B**). Da bei allen untersuchten GM-Derivaten alle zugänglichen basischen Aminogruppen methacryloyliert wurden [94], fehlten der GM im Vergleich zum verwendeten Rohmaterial positive Ladungen und der IEP der GM sank. Außerdem spiegelten die Ergebnisse die Unterschiede in dem Carboxylgruppen-Gehalt von  $G_A$  und  $G_B$  wieder: Saure Carboxylgruppen tragen zur negativen Ladung und somit zu einem geringeren IEP bei. Da  $G_B$  mehr saure Carboxylgruppen besitzt als  $G_A$  (vergleiche 2.2.1) und diese bei den Modifizierungsreaktionen nicht umgesetzt wurden, war der IEP der  $G_B$ M-Derivate erwartungsgemäß niedriger als der der  $G_A$ M-Derivate.

Der hydrodynamische Radius der Gelatinen und GM-Derivate wurde mittels Gel-Permeations-Chromatographie untersucht (**Figure 3**). Dabei werden Moleküle mit einem großen hydrodynamischen Radius zuerst eluiert und Moleküle mit kleinem hydrodynamischen Radius später eluiert. Es konnte für  $G_A$  und  $G_B$  gezeigt werden, dass das Rohmaterial und GM2 zu einem ähnlichen Zeitpunkt eluiert wurden und GM-Derivate mit steigendem DM später. Noch später, mit steigendem Acetylierungsgrad, wurden GMA-Derivate eluiert.

Da die Reaktionsbedingungen während der Modifizierung mild waren wurde im Gegensatz zu Van Hoorick *et al.* [303] geschlussfolgert, dass die Verschiebung der Elugramme nicht durch die Hydrolyse der GM-Derivate zustande kommt, sondern durch einen verringerten hydrodynamischen Radius. Denn durch die Methacryloylierung und Acetylierung wurden die physikalischen Wechselwirkungen eingeschränkt, sodass die Polymerknäule kleiner wurden und der hydrodynamische Radius sank. Dass die physikalischen Wechselwirkungen mit steigendem Modifizierungsgrad sinken, wurde in einer unserer späteren Studien mittels Circular dichroismus-Spektroskopie gezeigt, siehe **Figure 11**.

Die dynamische Viskosität der wässrigen GM-Lösungen nahm mit zunehmendem DMA ab, wobei die dynamische Viskosität von GM5, GM10, GM2A8 und GM10 nicht voneinander unterscheidbar waren. Jedoch wurde ein signifikanter Unterschied ( $p < 0,05$ ) zwischen  $G_A$ ,  $G_{AM2}$ ,  $G_{AM5}$  und  $G_B$ ,  $G_{BM2}$ ,  $G_{BM5}$  beobachtet. Die dynamische Viskosität von  $G_A$  und ihren zwei Derivaten war geringer als die von  $G_B$  und deren Derivaten. Dies spiegelte die unterschiedliche Standard-Viskosität der zwei Rohmaterialien wieder und diese beeinflussten somit auch die Viskositäten der GM-Derivaten mit einem geringen DM, das heißt einem DM geringer  $0,9 \text{ mmol g}^{-1}$ .

Die Gelier- und der Schmelzpunkte hingen, wie die Viskosität, von dem DMA der GM-Derivate ab, wobei für die hoch-modifizierten GM(A)-Derivate GM10, GM2A8 und GM5A5 keine Schmelz- und Gelierpunkt zwischen  $10 \text{ }^\circ\text{C}$  und  $40 \text{ }^\circ\text{C}$  gemessen werden konnten. Der Gelier- und Schmelzpunkt sank mit zunehmendem DM für GM2 und GM5. In dieser Charakteristik unterschieden sich die  $G_{AM}$ - und  $G_{BM}$ -Derivate nicht voneinander (vergleiche **Table 1**). Spätere Untersuchungen, die bis  $4 \text{ }^\circ\text{C}$  kühlten zeigten, dass 10 Gew.-%  $G_{BM2A8}$ - und  $G_{BM10}$ -Lösungen bei Temperaturen unterhalb von  $10 \text{ }^\circ\text{C}$  gelierten, siehe **Figure S 6**.

Der Speichermodul der GM-Hydrogele, die mit 10 Gew.-% GM hergestellt und gequollen wurden, unterschied sich jeweils nicht zwischen GM2, GM5 und GM10, jedoch zwischen den verwendeten Rohmaterialien (siehe **Figure 5-A**). Die Speichermoduln von GM2A8 und GM5A5 von  $G_A$  und  $G_B$  waren jedoch nicht unterscheidbar. Diese Ergebnisse widersprachen vorherigen Ergebnissen in denen Hydrogele aus GMs mit einem niedrigeren DM untersucht wurden und gezeigt wurde, dass der DM mit dem Speichermodul korreliert [42, 300]. Außerdem hatten die Hydrogele aus  $G_{AM}$  und  $G_{BM}$  unterschiedliche Speichermoduln, obwohl sie nicht unterscheidbare DMs besaßen. Der *EDS* aller

Hydrogele, bis auf GM2A8, waren trotz unterschiedlicher Speichermoduln zwischen  $G_A$  und  $G_B$  nicht unterscheidbar.

Diese unerwarteten Ergebnisse wurden auf die Eigenschaften der Rohmaterialien zurückgeführt. Es wurde vermutet, dass die Hydrogele aus GM2 und GM5 nach der chemischen Vernetzung durch physikalische Wechselwirkungen (die sie noch ausbilden können, siehe Daten zu Viskosität, Gelier- und Schmelzpunkt) verstärkt wurden. Die höhere Quellbarkeit der  $G_B$ MA-Hydrogele, verglichen mit den  $G_A$ MA-Hydrogele, wurde auf den höheren Carboxylgruppen-Gehalt des  $G_B$ -Rohmaterials zurückgeführt. Dass physikalische Wechselwirkungen chemisch vernetzte GM-Hydrogele verfestigen könnte wurde in Untersuchungen der sequenziellen Vernetzung gezeigt, siehe **Figure 7** und **Figure 8**.

In dieser Untersuchung konnte gezeigt werden, dass GM(A)-Derivate aus  $G_A$  und  $G_B$  mit vergleichbarem DM(A) synthetisiert werden können. Allerdings beeinflusste der DM(A) der GM(A)-Derivate nicht allein die physikochemischen Eigenschaften der GM(A), ihrer Lösungen und Hydrogele. Beispielsweise beeinflusste die Aminosäuren-Zusammensetzung, den IEP und die Quellbarkeit der GM(A)-Hydrogele. Außerdem beeinflusste der IEP des Rohmaterials den der GM(A) und die physikalischen Wechselwirkungen, die die Standard-Viskosität bestimmten, beeinflussten die Viskosität sowie den Gelier- und Schmelzpunkt von GM(A)-Lösungen und den Speichermodul von GM(A)-Hydrogelen.

Somit konnte die erste Hypothese dieser Dissertation bestätigt werden. Die Untersuchungen machten außerdem die Notwendigkeit einer möglichst vollständigen GM(A)-Charakterisierung deutlich. Diese Angaben sollten zusammen mit Angaben zu den Rohmaterial-Eigenschaften dargestellt werden um Ergebnisse miteinander vergleichen und reproduzieren zu können und die potenzielle Anwendung von GM als Biomaterial voranzutreiben.

## 7.2 Hypothese 2

Die Ergebnisse der Bearbeitung von Hypothese 1 haben gezeigt, dass chemisch vernetzte GM2-Hydrogele durch physikalische Wechselwirkungen verstärkt werden, sodass die Speichermoduln nicht von GM10-Hydrogelen, wobei der DM von GM10 etwa dreimal so hoch ist wie der von GM2, unterschieden werden konnten. Dieses Ergebnis stimmte mit Ergebnissen der sequenziellen GM-Vernetzung anderer Autoren überein [45, 298, 302]. Wie in Kapitel 2.3.3 beschrieben wurde, wird bei der sequenziellen Vernetzung die Hydrogelvorläuferlösung zunächst gekühlt, sodass ein physikalisches Hydrogel entsteht und anschließend chemisch vernetzt. Diese physikalische und chemische Vernetzung führt dann im Vergleich zu rein chemisch vernetzten Hydrogelen zu verfestigten GM-Hydrogelen.

Bisher wurde allerdings nur in einer Veröffentlichung der Einfluss der sequenziellen Vernetzung auf Hydrogelen mit einem hohen DM ( $\sim 1 \text{ mmol g}^{-1}$ ) untersucht [303]. Um weitere Daten zur sequenziellen

Vernetzung von hoch-modifizierten GM(A)-Derivaten zu erzeugen sollten sequenzielle GM2A8- und GM10-Hydrogele untersucht werden. Durch den Vergleich mit GM2-Hydrogelen wurde versucht Rückschlüsse auf die chemische und physikalische Vernetzung zu ziehen, da die chemische Vernetzbarkeit (der DM) von GM2 und GM2A8 nicht unterscheidbar war, die physikalische Gelierfähigkeit aber von GM2A8 und GM10 vergleichbar war. Die folgende Hypothese wurde aufgestellt und untersucht:

*Die sequenzielle Vernetzung von hoch-modifizierten GM(A) Derivaten, für die kein Gelpunkt oberhalb von 10 °C gemessen wurde, verfestigt die resultierenden Hydrogele im Vergleich zu rein chemisch vernetzten Hydrogelen nicht. Die Verfestigung der sequenziellen Vernetzung kann durch den Vergleich von GM2, GM10 und GM2A8-Hydrogelen aufgeklärt werden.*

Für die Untersuchung dieser Hypothese wurden rein chemisch vernetzte GM(A)-Hydrogele und sequenzielle GM(A)-Hydrogele hergestellt und mit Kompressionsversuchen charakterisiert. Bei der sequenziellen Hydrogelherstellung wurde die Hydrogelvorläuferlösung vor der chemischen Vernetzung 20 min bei 21 °C und anschließend für 40 min bei 4 °C gelagert. Es wurden *confined* Kompressionsversuche durchgeführt, bei denen der Prüfkörper seitlich begrenzt war, und *unconfined* Messungen, bei denen keine seitliche Begrenzung verwendet wurde. Es wurde die maximale Spannung und Dehnung bis zur Zerstörung des Prüfkörpers betrachtet. Außerdem wurde die physikalische Gelierung während der Kühlprotokolls der sequenziellen Hydrogelherstellung rheologisch untersucht.

Die Ergebnisse der *confined*- und *unconfined*-Messungen führten zu unterschiedlichen absoluten Messwerten, allerdings waren die beobachteten Effekte gleich (vergleiche **Figure 7** und **Figure 8**). Die sequenziellen Hydrogele waren im Vergleich zu den rein chemischen Hydrogelen weniger dehnbar, und um die sequenziellen Hydrogele gleich stark zu deformieren wie die chemischen Hydrogele musste eine signifikant höhere Spannung ( $p < 0,01$ ) ausgeübt werden. Dieses Verhalten wurde für alle untersuchten Derivate beobachtet.

Es wurde überprüft, ob es in den untersuchten Hydrogelvorläuferlösungen, anders als erwartet und bisher gezeigt (siehe **Table 1**), zu einer Gelierung kam, da alle sequenziellen Hydrogele, auch die aus GM2A8 und GM10, eine höhere Druckspannung besaßen als die chemischen Hydrogele. Wie in **Table 3** und **Figure S 6** zu sehen ist, wurde für GM10 eine Gelierung gemessen und für GM2A8 auch in einer von drei unabhängigen Messungen. Diese Ergebnisse deuteten darauf hin, dass es auch in den hoch-modifizierten Hydrogelvorläuferlösungen aus GM2A8 und GM10 während der Kühlung zu physikalischen Wechselwirkungen kam. Dies wurde in der anschließenden Untersuchung mittels Dynamischer Differenzkalorimetrie und Circular dichroismus-Spektroskopie nachgewiesen, siehe **Figure 11** und **Figure 12**.

Für alle untersuchten GM(A)-Lösungen konnte mittels Circular dichroismus-Spektroskopie gezeigt werden, dass es während der Kühlung vor der chemischen Vernetzung zu einer Konformationsänderung kam (siehe **Figure 11**). Für GM2 konnte eine eindeutig positive Bande bei ~220 nm der Ausbildung von Tripel-Helices zugeordnet werden, vergleiche 2.2.2. Diese Bande war für GM2A8 nur leicht positiv und für GM10 sogar leicht negativ. Jedoch wurde die negative Bande ~200 nm bei allen GM(A)s durch die Kühlung ausgeprägter. Diese negative Bande bei ~200 nm kann der zufälligen Polypeptidketten-Konformation und den Tripelhelices zugewiesen werden. Darüber hinaus wurden Hinweise darauf gefunden, dass es bei der Kühlung von GM10-Hydrogelvorläuferlösungen zur Ausbildung von Einzel-Helices kommt. Die Ergebnisse der dynamischen Differenzkalorimetrie stimmten mit denen der Circular dichroismus-Spektroskopie überein, für GM2 und GM2A8 konnten Schmelztemperaturen detektiert werden, vergleiche **Figure 12** und **Table 4**. Somit wurde eine Konformationsänderung durch die Kühlung der Hydrogelvorläuferlösungen, die zu einer höheren Ordnung der Polymere führte, nachgewiesen.

Kollegen von der Universität Wien führten Echtzeit-Nahinfrarot-Spektroskopie-Photorheologie-Messungen während der (sequenziellen) GM-Vernetzung durch und konnten somit den C=C-Doppelbindungsumsatz *in situ* während der chemischen Vernetzung messen. Darüber hinaus konnte die Gelierung während der Kühlphase gemessen werden. Auch die rheologischen Messungen während der Kühlphase (**Figure 13**) konnten die Ergebnisse der Circular dichroismus-Spektroskopie und dynamischen Differenzkalorimetrie unterstützen: Während der Kühlung stieg der Speichermodul der GM2- und GM2A8-Lösungen an, was auf eine physikalische Gelierung der Lösungen hindeutet.

Die Untersuchung der Kinetik der chemischen Vernetzung sowie des C=C-Doppelbindungsumsatzes nach der chemischen Vernetzung mittels Echtzeit-Nahinfrarot-Spektroskopie-Photorheologie zeigte, dass der Doppelbindungsumsatz in sequenziellen GM(A)-Hydrogelen geringer war als in rein chemisch vernetzten GM(A)-Hydrogelen (siehe **Figure 14** und **Figure 15**). Dieses Ergebnis widerlegt die Hypothese, dass die chemische Vernetzungseffizienz in sequenziellen Hydrogelen höher ist sowie die Fourier-Transform-Infrarotspektrometrische Untersuchungen von Rizwan *et al.*, die erste Hinweise auf einen höheren C=C-Doppelbindungsumsatz in sequenziellen Hydrogelen zeigten [302]. Außerdem war für die Vernetzung zu einem Hydrogel bei der sequenziellen Vernetzung weniger chemische Vernetzungen notwendig als bei der rein chemischen Vernetzung.

Somit wurde der erste Teil von Hypothese 2 widerlegt, da auch für sequenziell vernetzte GM10- und GM2A8-Hydrogele ein verfestigender Effekt im Vergleich zu rein chemisch vernetzten GM-Hydrogelen beobachtet wurde. Es wurde für alle GM(A)-Derivate eine Konformationsänderung während des Kühlens nachgewiesen. Da der Doppelbindungsumsatz in sequenziellen Hydrogelen geringer war als in chemischen Hydrogelen, scheint diese Konformationsänderung in allen Hydrogelvorläuferlösungen

unabhängig von dem Modifizierungsgrad der GM, die Ursache der Verfestigung der sequenziellen Hydrogele gewesen zu sein. Somit wurde der zweite Teil der Hypothese 2 bestätigt.

### 7.3 Hypothese 3

GM-Hydrogele werden als *Scaffold* für den Aufbau künstlicher Gewebe untersucht. Allerdings sind alle Gewebe komplex aufgebaut und besitzen nur selten eine homogene Zusammensetzung, wie es bei GM-Hydrogelen der Fall ist. Ein Beispiel für so ein komplexes, aber einfach wirkendes Gewebe ist der Gelenkknorpel, vergleiche 2.1.1. Der Gelenkknorpel besteht scheinbar nur aus Chondrozyten und der sie umgebenden extrazellulären Matrix (EZM). Jedoch ist der Gelenkknorpel auf vielen Ebenen zonal strukturiert.

GM-Hydrogele werden aufgrund des kollagenen Ursprungs des Rohmaterials und der damit verbundenen Biomimetik häufig als Gerüststruktur für das Gelenkknorpel-*Tissue Engineering* untersucht. Um den zonalen Aufbau des Gelenkknorpels zu imitieren werden zonale Gelenkknorpel-*Tissue Engineering*-Ansätze untersucht, siehe Kapitel 2.1.4. Ziel dieser Arbeit war es unter anderem ein zonales GM-basiertes Hydrogel mit einem Glykosaminoglykan (GAG)-Gradienten für das zonale Gelenkknorpel-*Tissue Engineering* darzustellen. Es wurde folgende Hypothese untersucht:

*Ein zonal strukturiertes GM-basiertes, sequenziell vernetztes Hydrogel aus drei unterschiedlichen Zusammensetzungen ist als Scaffold für das Gelenkknorpel-Tissue-Engineering geeignet.*

Die sequenzielle Hydrogelherstellung ermöglichte die Herstellung zonal strukturierter Hydrogele mittels Gießen, indem jede Hydrogelschicht physikalisch gelierte bevor die nächste Schicht aufpipettiert wurde und erst nach der Kühlung alle Schichten zusammen chemisch vernetzt wurden.

Es wurden vier unterschiedliche Hydrogelzusammensetzungen untersucht (GM, GM+HAM, GM+CSM, GM+CSM+HAM) deren Polymergehalt der Hydrogelvorläuferlösung immer 10 Gew.-% war. Hydrogele aus GM und GAGs bestanden zu 7,5 Gew.-% aus GM und 2,5 Gew.-% GAG, siehe **Table 7**. Die Hydrogelvorläuferlösungen wurden sequenziell vernetzt und ihr Speichermodul sowie der initiale und relaxierte Elastizitätsmodul gemessen. Es wurde gezeigt, dass die Hydrogele aus GM+HAM den geringsten Speicher- und Elastizitätsmodul besaßen.

Dies widersprach Studien von Levett *et al.*, die zeigten, dass das Ersetzen von GM durch HAM zu höheren E-Moduln führte [46, 52]. Eine Möglichkeit für diesen Widerspruch könnten die unterschiedlichen Molekulargewichte der verwendeten Hyaluronsäuren sein. Alcianblau-Färbungen zeigten, dass es zu einer Phasenseparation zwischen GM und HAM kam. Es wurde die Hypothese aufgestellt, dass diese Inhomogenität die geringeren E-Moduln der GM+HAM-Hydrogele verursachte.

Trotzdem waren die gemessenen E-Moduln der sequenziell vernetzten, GM-basierten Hydrogele die höchsten bisher berichteten E-Moduln für GM-Hydrogele. Das macht sie besonders geeignet für die Herstellung von künstlichen Last-tragenden Geweben wie beispielsweise Knorpelgewebe. Es wurden deshalb zonale Hydrogele aus GM, GM+CSM und GM+CSM+HAM dargestellt, siehe **Figure S 21**. Die zonale Struktur der zonalen Hydrogele konnte mittels Alcianblau-Färbung nachgewiesen werden (**Figure S 16**). Darüber hinaus waren die zonalen Hydrogele, wie alle anderen untersuchten Hydrogelzusammensetzungen, über den beobachteten Zeitraum von 42 Tagen stabil, siehe **Figure 19**.

Im nächsten Schritt wurde der Einfluss der Kühlung während der sequenziellen Vernetzung auf die Vitalität der in den GM2-Hydrogelvorläuferlösungen verkapselten Chondrozyten untersucht. Die Dauer der Kühlung bei 4 °C wurde zwischen 0 h und 2 h variiert. Es wurde direkt nach der Hydrogelherstellung sowie 24 h danach kein signifikanter Einfluss der Kühlung bei 4 °C auf die Vitalität der verkapselten Chondrozyten nachgewiesen, siehe **Figure 20**. Da die Zytokompatibilität des Photoinitiators LAP bereits nachgewiesen wurde [319, 320] wurde die Zytokompatibilität der sequenziellen Vernetzung von GM-Hydrogelen für Chondrozyten geschlussfolgert.

Alle GM+GAG-Hydrogele, auch die zonalen Hydrogele, konnten teilweise durch Kollagenase Typ II abgebaut werden, reine GM-Hydrogele wurden nach 14 Tagen vollständig durch Kollagenase Typ II abgebaut, vergleiche **Figure 19**, **Figure S 19** und **Figure S 20**. Ein Abbau durch Hyaluronidase wurde nicht beobachtet. Dies entsprach den Ergebnissen in der Literatur, dass HAM durch die Methacryloylierung nicht mehr durch Hyaluronidase degradiert wird [46, 397]. Diese Ergebnisse zeigten, dass die sequenziellen Hydrogele von Chondrozyten abgebaut und somit remodelliert werden könnten, da die Chondrozyten Kollagenase sekretieren.

Es wurden dedifferenzierte Chondrozyten in reinen GM- und in zonale Hydrogele verkapselt, über 28 Tage kultiviert, und die synthetisierte EZM untersucht. Mithilfe von Alcianblau-Färbungen konnte gezeigt werden, dass die verkapselten Chondrozyten in beiden untersuchten Hydrogelen Alcianblau-positive EZM synthetisieren, siehe **Figure 21** und **Figure 22**. Des Weiteren wurde Kollagen Typ I und Kollagen Typ II mithilfe von Antikörper-Färbungen nachgewiesen. Zusammen mit der sphärischen Morphologie der Chondrozyten wurde deshalb geschlussfolgert, dass die Chondrozyten während der 28-tägigen Kultivierung in beiden untersuchten Hydrogelen (GM2- und zonale Hydrogele) redifferenzierten. Ein Einfluss der zonalen Strukturierung auf die EZM-Synthese der Chondrozyten wurde nicht beobachtet. Dies könnte an der verhältnismäßig kurzen Dauer der dreidimensionalen Kultivierung liegen.

Somit konnte die Hypothese 3 bestätigt werden: Es wurde unter zytokompatiblen Bedingungen mithilfe der sequenziellen Vernetzung zonal strukturierte GM-basierte Hydrogele erzeugt, die aus drei Zusammensetzung bestanden (GM, GM+CSM, GM+CSM+HAM). Die gemessenen E-Moduln waren die

höchsten bisher für GM-Hydrogele berichteten, was sie besonders geeignet für das Gelenkknorpel-*Tissue Engineering* macht. Der Ersatz von GM durch HAM oder CSM führte zu geringeren E-Moduln. Alle untersuchten Hydrogelzusammensetzungen waren teilweise oder vollständig durch Kollagenase degradierbar. Die in reinen GM- und zonalen Hydrogelen verkapselten dedifferenzierten Chondrozyten redifferenzierten über einen Zeitraum von 28 Tagen, in Bezug auf die EZM-Synthese.



## 8. Schlussfolgerungen

Die Ergebnisse dieser Dissertation demonstrieren die Notwendigkeit, das verwendete Gelatine-Rohmaterial in Veröffentlichungen zu benennen und mindestens den Methacryloylierungsgrad der verwendeten GM zu quantifizieren. Nur mit diesen Angaben ist es möglich zu überprüfen, ob Ergebnisse vergleichbar sind und somit die Erforschung von GM als Biomaterial zielorientiert zu verfolgen. Die Ergebnisse der Untersuchung in dieser Arbeit zeigten, dass die Eigenschaften des verwendeten Gelatine-Rohmaterials einen signifikanten Einfluss auf die resultierenden Eigenschaften der GM, sowie der GM-Lösungen und -Hydrogele haben. So wurde beispielsweise gezeigt, dass die Standard-Viskosität des Rohmaterials die Viskosität wässriger GM-Lösungen und den Speichermodul von GM-Hydrogelen beeinflusst. Darüber hinaus wurde gezeigt, dass sich die GM-Materialeigenschaften mit dem Methacryloylierungsgrad verändern, dabei sinkt zum Beispiel die Gelier- und Schmelztemperatur sowie die dynamische Viskosität von wässrigen GM-Lösungen mit steigendem Methacryloylierungsgrad.

Außerdem wurde im Rahmen dieser Arbeit gezeigt, dass es durch das Abkühlen von GM-Hydrogelvorläuferlösungen vor der chemischen Vernetzung zu Konformationsänderungen kam. Diese Konformationsänderung und die damit einhergehende Ordnung der Polymere in der GM-Hydrogelvorläuferlösung schienen die Ursache der Verfestigung von sequenziellen Hydrogelen zu sein. Dieses Ergebnis verdeutlicht einerseits, wie wichtig es ist, die Temperatur der Hydrogelvorläuferlösung vor und während der chemischen Vernetzung zu kontrollieren, da diese einen signifikanten Einfluss auf die Hydrogeleigenschaften hatte. Andererseits zeigt die Studie das Potenzial der sequenziellen Vernetzung zur Erzeugung von GM-Hydrogelen mit hohen Elastizitätsmoduln und somit für den Einsatz als *Scaffold* im Gelenkknorpel-*Tissue Engineering* geeignet sein könnten. Es wurde gezeigt, dass die sequenzielle Vernetzung den Speichermodul und die Druckspannung von allen untersuchten Hydrogelen erhöhte, unabhängig davon, ob die Hydrogelvorläuferlösungen während des Kühlens gelierten oder nicht. Die Untersuchung der physikalischen Interaktionen in den Hydrogelvorläuferlösungen während des Kühlens der sequenziellen Vernetzung zeigte Konformationsänderungen für alle untersuchten GM-Derivate. Allerdings waren diese Konformationsänderungen abhängig von dem Modifizierungsgrad der GM-Derivate. GM-Derivate, deren Aminogruppen vollständig modifiziert wurden, zeigten eine Tripel-Helix-Ausbildung während des Kühlens, was mit dem Gelieren der Hydrogelvorläuferlösung übereinstimmte. Hydrogelvorläuferlösungen aus einem GM-Acetyl (GMA)-Derivat, bei dem auch alle zugänglichen Aminogruppen methacryloyliert und zusätzlich Hydroxylgruppen acetyliert wurden, zeigten einen geringeren Gehalt an Triple-Helices. Für das hoch-methacryloylierte GM-Derivat konnten keine Triple-

Helices, aber dafür Einzel-Helices nachgewiesen werden. Außerdem wurde gezeigt, dass, anders als bisher vermutet, der Doppelbindungsumsatz in sequenziell vernetzten GM-Hydrogelen geringer ist als in rein chemisch vernetzten GM-Hydrogelen. Somit konnte die Verfestigung der sequenziellen GM-Hydrogele, anders als bisher vermutet, nicht mit einem höheren Doppelbindungsumsatz erklärt werden. Die Konformationsänderungen in den Hydrogelvorläuferlösungen während des Kühlens und die damit einhergehende Ordnung der Polymere scheint die Ursache der Verfestigung von sequenziellen Hydrogelen zu gewesen sein.

Mithilfe der sequenziellen Vernetzung konnten in dieser Arbeit zonal strukturierte GM-basierte Hydrogele aus drei Zusammensetzungen zytokompatibel dargestellt werden. Darüber hinaus wurde so ein Glykosaminoglykan-Gradient in dem zonalen Hydrogel aufgebaut, der mittels Acianblau-Färbung nachgewiesen werden konnte. Die materialwissenschaftlichen Untersuchungen zeigten, dass die Hydrogele belastbar und enzymatisch degradierbar waren. Erste Zellverkapselungs-Versuche zeigten, dass dedifferenzierte Chondrozyten nach 28 Tagen Kultivierung Kollagen Typ II und Glykosaminoglykan-reiche EZM sekretierten. Dieses Materialsystem liefert die Grundlage für die Erforschung zonal strukturierter GM-Hydrogele für das Gelenkknorpel-*Tissue Engineering*.

## 9. Ausblick

Die in dieser Arbeit durchgeführte Untersuchung zum Einfluss des verwendeten Gelatine-Rohmaterials auf die Eigenschaften des resultierenden Gelatine-Methacryloyls (GM), siehe Kapitel 4, betrachtete den Einfluss des Bloom-Wertes nicht, da die verwendeten Gelatine Typ A und Gelatine Typ B einen nahezu identischen Bloom-Wert besaßen. Da der Bloom-Wert die Gelierkraft des Rohmaterials beeinflusst, wird er wahrscheinlich auch die Ausbildung von Tripel-Helices der GM und somit weitere Eigenschaften der GM-Hydrogele beeinflussen. Deshalb wäre eine Untersuchung des Einflusses des Bloom-Wertes auf die GM-Materialeigenschaften sinnvoll, um die GM-Charakterisierung, ähnlich wie Standard-Charakterisierung von Gelatine, zu vervollständigen.

Erste vorläufige Ergebnisse zu dem Einfluss des Bloom-Wertes auf den Methacryloylierungsgrad und den Speichermodul der GM-Hydrogele wurden im Rahmen dieser Arbeit erzeugt. Es wurden GM2- und GM10-Derivate mit einer Gelatine Typ B aus Rinderknochen der Firma Gelita mit einem Bloom-Wert von 270 g Bloom synthetisiert (GM<sub>270 g Bloom</sub>). Der Methacryloylierungsgrad wurde wie in 4.1.3 beschrieben bestimmt und war nicht unterscheidbar von den Methacryloylierungsgraden der GMs, die aus einer Gelatine Typ B aus Rinderknochen mit einem Bloom-Wert von 235 g Bloom hergestellt wurden. Der Methacryloylierungsgrad der GM<sub>270 g Bloom</sub> lag bei  $0,26 \pm 0,04 \text{ mmol g}^{-1}$  und der von GM<sub>10 270 g Bloom</sub> bei  $0,92 \pm 0,1 \text{ mmol g}^{-1}$ .

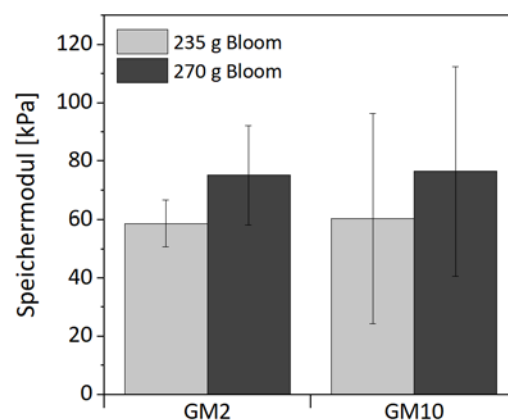


**Abbildung 9:** Speichermodul von 10 Gew.-% GM2- und GM10-Hydrogelen. Als Gelatine-Rohmaterial wurden eine Gelatine mit einem Bloom-Wert von 235 g Bloom verwendet (helle Balken) und eine Gelatine mit 270 g Bloom (dunkle Balken). Die Hydrogele, deren GM aus Gelatine mit 270 g Bloom zeigten tendenziell höhere Speichermoduln als die Hydrogele, deren GM aus 235 g Bloom Gelatine.

Außerdem wurden sequenzielle 10 Gew.-% GM<sub>270 g Bloom</sub>-Hydrogele hergestellt und deren Speichermodul bestimmt. Zum Vergleich wurden sequenzielle GM-Hydrogele hergestellt, für deren GM-Synthese 235 g Bloom Gelatine verwendet wurde (GM<sub>235 g Bloom</sub>). Die Ergebnisse sind in **Abbildung 9** dargestellt. Die Ergebnisse zeigten, dass die GM<sub>270 g Bloom</sub>-Hydrogele einen tendenziell höheren

Speichermodul besaßen als die GM<sub>235 g Bloom</sub>-Hydrogele, jedoch waren die Speichermoduln nicht signifikant unterschiedlich. Dies könnte daran liegen, dass die verglichenen Bloom-Werte im gleichen Größenbereich lagen. In Zukunft sollten also Rohmaterialien mit einem deutlich geringeren oder höheren Bloom-Wert, beispielsweise 100 g Bloom oder 300 g Bloom, untersucht werden. Solche GM-Derivate, für deren Synthese ein Rohmaterial mit einem höheren Bloom-Wert, beispielsweise 300 g Bloom, verwendet wurde, wären auch für die Erzeugung sequenzieller GM-Hydrogele interessant, denn wahrscheinlich wäre der Tripel-Helix-Gehalt in solchen Hydrogelen höher und würde zu einer ausgeprägten Strukturierung und Verfestigung der Gele führen.

Um eine andere Art der physikalischen Wechselwirkung als die Ausbildung von Tripel-Helices in der sequenziellen Vernetzung zu untersuchen könnten kationische GM-Derivate verwendet werden. Solche Derivate wurden von Claassen *et al.* [408] beschrieben und ein Teil der Charakterisierung im Rahmen dieser Dissertation durchgeführt. In einer Mischung aus solchen kationischen GM- und den in dieser Arbeit untersuchten anionischen GM-Derivaten kommt es wahrscheinlich zu Wechselwirkungen der Ladungen bei neutralem pH. Diese Wechselwirkungen könnten zum Gelieren und bzw. oder der Verfestigung der resultierenden Hydrogele führen.

Sollten weitere Arbeiten mit dem in dieser Arbeit erzeugten zonalen GM-basierten Hydrogel vielversprechend sein, könnte das zonale Hydrogel durch eine zusätzliche Schicht, die den subchondralen Knochen repräsentiert, erweitert werden und so ein vollständigeres Gewebeäquivalent entwickelt werden. Im Knochen-*Tissue Engineering* werden oft poröse Materialien untersucht, um die Knochen-Struktur zu imitieren. Im Rahmen dieser Dissertation wurde an der Erforschung von GM-Hydrogelschäumen mitgearbeitet [409]. Diese könnten als Gerüststruktur für die Kultivierung von Knochenzellen geeignet sein und somit das in dieser Arbeit zonale Hydrogel ergänzen. Arbeiten von Wenz *et al.* [304, 305, 320] zeigten zudem, dass beispielsweise Hydroxylapatit verwendet werden kann um GM-Hydrogele Knochen-mimetischer zu gestalten.



# I. Anhang

## I.I. Erklärung über die Eigenständigkeit der Dissertation

Ich versichere, dass ich die vorliegende Arbeit mit dem Titel

*Physikalische und chemische Wechselwirkungen in Gelatine-Methacryloyl-Lösungen und deren Vernetzung zu Hydrogelen als Trägerstruktur für Gelenknorpel-Äquivalente*

selbstständig verfasst und keine anderen als die angegebenen Quellen und Hilfsmittel benutzt habe; aus fremden Quellen entnommene Passagen und Gedanken sind als solche kenntlich gemacht. Diese Dissertation wurde zu keiner Zeit in derselben oder substantiell ähnlichen Version bei einem anderen Prüfungsamt eingereicht.

Lisa Rebers

### I.III. Veröffentlichungen

#### I.III.I. Veröffentlichungen in *peer-reviewed* Fachzeitschriften

Christiane Claaßen\*, Lisa Sewald\*, Günter E. M. Tovar and Kirsten Borchers; Controlled Release of Vascular Endothelial Growth Factor from Heparin-Functionalized Gelatin Type A and Albumin Hydrogels. *Gels* **3**(4): 35. (2017) (\* contributed equally) DOI: <https://doi.org/10.3390/gels3040035>.

Christiane Claaßen, Marc H. Claaßen, Vincent Truffault, Lisa Sewald, Günter E. M. Tovar, Kirsten Borchers and Alexander Southan; Quantification of Substitution of Gelatin Methacryloyl: Best Practice and Current Pitfalls. *Biomacromolecules* **19**(1): 42 (2018) DOI: <https://doi.org/10.1021/acs.biomac.7b01221>.

Lisa Sewald, Christiane Claaßen, Tobias Götz, Marc H. Claaßen, Vincent Truffault, Günter E. M. Tovar, Alexander Southan and Kirsten Borchers; Beyond the Modification Degree: Impact of Raw Material on Physicochemical Properties of Gelatin Type A and Type B. *Macromolecular Bioscience* **18**(12):1800167-1800178. (2018) DOI: <https://doi.org/10.1002/mabi.201800168>.

Lisa Rebers, Tobias Granse, Günter E. M. Tovar, Alexander Southan and Kirsten Borchers; Physical Interactions Strengthen Chemical Gelatin Methacryloyl Gels. *Gels* **5**(1):4. (2019) DOI: <https://doi.org/10.3390/gels5010004>.

Sandra Stier\*, Lisa Rebers\*, Veronika Schönhaar, Eva Hoch and Kirsten Borchers; Advanced Formulation of Methacryl- and Acetyl-Modified Biomolecules to Achieve Independent Control of Swelling and Stiffness in Printable Hydrogels. *Journal of Materials Science: Materials in Medicine* **30**(3): 35. (2019) (\* contributed equally) DOI: <https://doi.org/10.1007/s10856-019-6231-0>.

Christiane Claaßen, Lisa Rebers, Marc H. Claaßen, Kirsten Borchers, Günter E. M. Tovar and Alexander Southan; Expanding the Range of Available Isoelectric Points of Highly Methacryloylated Gelatin. *Macromolecular Chemistry and Physics* **220**(14):1900097. (2019) DOI: <https://doi.org/10.1002/macp.201900097>.

Friederike Dehli, Lisa Rebers, Cosima Stubenrauch and Alexander Southan; Highly Ordered Gelatin Methacryloyl Hydrogel Foams with Tunable Pore Size. *Biomacromolecules* **20**(7):2666. (2019) DOI: <https://doi.org/10.1021/acs.biomac.9b00433>.

Silke Keller, Tomke Bakker, Benjamin Kimmel, Lisa Rebers, Tobias Götz, Günter E. M. Tovar, Peter J. Kluger and Alexander Southan; Azido-Functionalized Gelatin via Direct Conversion of Lysine Amino Groups by Diazo Transfer as a Building Block for Biofunctional Hydrogels. *Journal of Biomedical Materials Research Part A* **109**:77. (2021) DOI: <https://doi.org/10.1002/jbm.a.37008>.

Lisa Rebers\*, Raffael Reichsöllner\*, Sophia Regett, Günter E. M. Tovar, Kirsten Borchers, Stefan Baudis and Alexander Southan; Differentiation of Physical and Chemical Cross-Linking in Gelatin Methacryloyl Hydrogels. *Scientific Reports* **11**:3256. (2021) DOI: <https://doi.org/10.1038/s41598-021-82393-z> (\* contributed equally).

Lisa Rebers, Sophia Regett, Dominik Walz, Silke Keller, Günter E. M. Tovar, Kirsten Borchers and Alexander Southan; Biomimetic Hydrogel Compositions for Reconstruction of Zonal Articular Cartilage Structure. **Prepared for Submission.**

### I.III.II. Vorträge auf Fachkonferenzen

Der vortragende Autor wurde im Folgenden durch Unterstreichen kenntlich gemacht.

Christiane Claaßen, Lisa Sewald, Günter E. M. Tovar, Boris V. Stanzel and Kirsten Borchers; Annual Meeting & Exposition of the Controlled Release Society, Seattle (United States of America), July 2016: Novel Bio-Based Heparin-Functionalized Hydrogels for Controlled VEGF Release.

Lisa Sewald, Christiane Claaßen, Maria-E. Kotzampasi, Günter E. M. Tovar, Boris V. Stanzel and Kirsten Borchers; Annual Meeting of the German Society of Biomaterials, Aachen (Germany), September 2016: Novel Bio-Based Heparin-Functionalized Hydrogels for Controlled VEGF Release I – EDC-Based Cross-linking.

Eva Hoch, Annika Wenz, Lisa Sewald, Christiane Claaßen, Petra J. Kluger, Achim Weber and Kirsten Borchers; 4<sup>th</sup> Fraunhofer Direct Digital Manufacturing Conference, Berlin (Germany), March 2018: Bioink Development and Bioprinting Bio-Based Matrices.

Eva Hoch, Annika Wenz, Lisa Sewald, Christiane Claaßen, Achim Weber and Kirsten Borchers; MRAS Material Research Society Spring Meeting & Exhibits, Phoenix (United States of America), April 2018: Bio-Based Inks with Adjustable Viscosities for Bioprinting.

Kirsten Borchers, Eva Hoch, Annika Wenz, Birgit Huber, Sandra Stier, Christiane Claaßen, Lisa Sewald, Peter J. Kluger and Achim Weber, 34<sup>th</sup> International Conference on Digital Printing Technologies, Dresden (Germany), September 2018: Bioink Development and Bioprinting Bio-Based Matrices.

Kirsten Borchers, Eva Hoch, Annika Wenz, Birgit Huber, Sandra Stier, Christiane Claaßen, Lisa Sewald, Peter J. Kluger and Achim Weber, 3<sup>rd</sup> Annual 3D Printing & Bio-Printing in Healthcare Conference, Brussel (Belgium), October 2018: Bio-Based Bioinks for Printing of Tissue-Specific Matrices.

Lisa Sewald, Tobias Granse, Günter E. M. Tovar, Alexander Southan and Kirsten Borchers; Annual Meeting of the German Society of Biomaterials, Braunschweig (Germany), November 2018: Physical



Gelling of Gelatin Methacryloyl Influences the Mechanical Characteristics of their Respective Chemically Cross-Linked Hydrogels.

Lisa Rebers, Eva Hoch, Sandra Stier, Veronika Schönhaar, Kirsten Borchers and Achim Weber; Werkstoffwoche, Dresden (Germany), September 2019: Gedruckte Biomaterialien am Beispiel von Hydrogelen mit zonal unterschiedlichen Quellbarkeiten.

Lisa Rebers, Kirsten Borchers, Eva Hoch, Sandra Stier, Veronika Schönhaar and Achim Weber; Printing for Fabrication, San Francisco (United States of America), September 2019: Printable Glycosaminoglycan Graded Gelatin Methacryloyl Acetyl Hydrogels.

### I.III.III. Poster-Präsentationen auf Fachkonferenzen

Der präsentierende Autor wurde im Folgenden durch Unterstreichen kenntlich gemacht.

Lisa Sewald, Alexander Southan, Günter E. M. Tovar and Kirsten Borchers; NanoBioMater International Conference, Bad Herrenalb (Germany), June 2017: Adjustable Synthesis of Biopolymer Methacryloyls.

Lisa Böhler, Lisa Sewald, Günter E. M. Tovar and Kirsten Borchers; NanoBioMater International Conference, Bad Herrenalb (Germany), June 2017: Isolation of Zonal Chondrocyte Phenotypes and their Culture in Bio-Based Hydrogels.

Christiane Claaßen, Lisa Sewald, Sabrina Erthle, Günter E. M. Tovar and Kirsten Borchers; 44<sup>th</sup> Annual Meeting & Exposition of the Controlled Release Society, Boston (United States of America), June 2017: Controlled Release of VEGF from Bio-Based Heparin-Functionalized Hydrogels: EDC-Mediated Cross-Linking.

Lisa Sewald, Alexander Southan, Eva Hoch, Sandra Stier, Günter E. M. Tovar and Kirsten Borchers; 28<sup>th</sup> Annual Meeting of the European Society of Biomaterials, Athens (Greece), September 2017: Design of Biopolymer-Based Hydrogels for Zonal Cartilage Tissue Engineering.

Christiane Claaßen, Maria-E. Kotzampasi, Lisa Sewald, Günter E. M. Tovar, and Kirsten Borchers; 28<sup>th</sup> Annual Meeting of the European Society of Biomaterials, Athens (Greece), September 2017: Heparin-Functionalized Gelatin Coatings on PET Membranes for the Controlled Release of VEGF.

Michael Walz, Lisa Sewald, Patrick Erwied and Achim Weber; 28<sup>th</sup> Annual Meeting of the European Society of Biomaterials, Athens (Greece), September 2017: Cytotoxic Investigations of Inulin Derivatives for Drug Delivery Applications.

Lisa Sewald, Tobias Granse, Günter E. M. Tovar, Alexander Southan and Kirsten Borchers; Annual Meeting of the European Society of Biomaterials, Maastricht (The Netherlands), September 2018:

Process of Physical Gelling Influences the Mechanical Characteristics of Chemically Cross-Linked Gelatin Methacryloyl Hydrogels.

Lisa Sewald, Christiane Claaßen, Tobias Götz, Marc H. Claaßen, Vincent Truffault, Günter E. M. Tovar, Alexander Southan and Kirsten Borchers; 29<sup>th</sup> Annual Meeting of the European Society of Biomaterials, Maastricht (The Netherlands), September 2018: Impact of Conditioning Process Related Properties on Material Properties of Methacryloylated Type A and Type B Gelatin.

Günter E. M. Tovar, Christiane Claaßen, Lisa Sewald, Achim Weber, Alexander Southan and Kirsten Borchers; Annual Meeting of ProcessNet 2018 and 33<sup>rd</sup> DECHEMA Annual Meeting of Biotechnologists, Aachen (Germany), September 2019: Biofunktionale Tinten mit einstellbaren Eigenschaften für Bioprinting und additive Fertigungsverfahren.

Lisa Sewald, Christiane Claaßen, Tobias Götz, Marc H. Claaßen, Vincent Truffault, Günter E. M. Tovar, Alexander Southan and Kirsten Borchers; 29<sup>th</sup> Annual Meeting of the German Society of Biomaterials, Braunschweig (Germany), November 2018: Physico-Chemical Properties of Gelatin Type A and Type B Methacryloyls Depend on their Raw Materials.

Lena Spindler, Lisa Rebers, Eva Hoch, Jessica Braun, Tobias Granse, Alexander Southan, Günter E. M. Tovar, Kirsten Borchers and Achim Weber; Annual Meeting & Exposition of Controlled Release Society, Valencia (Spain), July 2019: Cross-linkable Gelatin Derivatives with High Degrees of Modification and Low Solution Viscosities for Simplified Processing by Spray-Drying and Inkjet-Printing.

Friederike Dehli, Lisa Rebers, Cosima Stubenrauch and Alexander Southan; Conference of the European Colloid and Interface Society, Leuven (Belgium), September 2019: Highly Ordered Gelatin Methacryloyl Hydrogel Foams with Tunable Pore Size.

## II. Abbildungsverzeichnis

<b>Abbildung 1:</b> Zonale Struktur des Gelenkknorpels. Der nicht-kalzifizierte Knorpel wird von der Gelenkoberfläche Richtung Knochen in die Zonen I, II und III unterteilt. Die Zone III wird durch die Tidemark von Zone IV getrennt, die wiederum an den subchondralen Knochen anschließt. Nachdruck mit Genehmigung von Springer Nature: Springer-Verlag, Knorpelregeneration und Knorpelersatz, M. Rudert und C. J. Wirth, © 1998. [4].....	9
<b>Abbildung 2:</b> Arkaden-Modell der Kollagen-Organisation im Gelenkknorpel von Benninghoff [5]. Nachdruck mit Genehmigung von Elsevier: Elsevier Ltd., Stresses in the local collagen network of articular cartilage: a poroviscoelastic fibril-reinforced finite element study, W. Wilson <i>et al.</i> , © 2004. [13] Anmerkung: Die Beschriftungen in der Abbildung wurden übersetzt und die Bezeichnung der Zonen verändert.....	10
<b>Abbildung 3:</b> Extrazelluläre Matrix des Knorpelgewebes. Die Proteoglykan-Aggregate sind im Kollagenetzwerk immobilisiert. Die Aggregate bestehen aus einer Hyaluronsäure, an die über das Link-Protein Proteoglykane gebunden sind. Diese Proteoglykane haben einen Flaschenbürsten-artige Struktur und bestehen aus einem zentralen Kernprotein, an das Glykosaminoglykane gebunden sind. Nachdruck mit Genehmigung von Springer Nature: Springer-Verlag, Knorpelregeneration und Knorpelersatz, M. Rudert und C. J. Wirth, © 1998. [4].....	11
<b>Abbildung 4:</b> Prinzip der autologen Chondrozyten Transplantation. Außerhalb der Knorpelläsion wird ein Stück gesunder Knorpel entnommen und enzymatisch verdaut um die Chondrozyten zu isolieren. Die Chondrozyten werden zur Expansion zweidimensional kultiviert. Nach der Expansion wird eine Chondrozyten-Suspension in die Läsion injiziert und mit einem Stück Knochenhaut verschlossen. Nachdruck mit Genehmigung von Elsevier: Elsevier Ltd., An educational review of cartilage repair: precepts & practice – myths & misconceptions – progress & prospects, E. B. Hunziker <i>et al.</i> , © 2015. [25] Anmerkung: Die Beschriftungen in der Abbildung wurden übersetzt.....	13
<b>Abbildung 5:</b> Strategien des zonalen Gelenkknorpel- <i>Tissue Engineerings</i> . <b>A</b> Bei der <i>Scaffold</i> - und Matrix-freien Strategie werden die Chondrozyten aus den Zonen I, II und III getrennt und ohne <i>Scaffold</i> verwendet, und produzieren ihre eigene Matrix. <b>B</b> Bei der Matrix-basierten Strategie werden Hydrogele aufeinander geschichtet die jeweils einen zonalen Chondrozyten Phänotyp der Zonen I-III beinhalten. <b>C</b> Im <i>Scaffold</i> -basierten Ansatz wird eine Mischpopulation aus Chondrozyten der Zonen I-III auf eine zonal strukturierte Gerüststruktur gesät. <b>D</b> Für den Hybrid-Ansatz wird mit zellhaltigen Materialien mittels additiver Fertigungsverfahren eine zonale Struktur aufgebaut. Nachdruck mit Genehmigung von Mary Ann Liebert: Mary Ann Liebert, Inc., Tissue Engineering of Articular Cartilage with Biomimetic Zones, T. J. Klein <i>et al.</i> , © 2009. [44] Anmerkung: Die Beschriftungen in der Abbildung wurden übersetzt und die Bezeichnung der Zonen verändert.....	17

**Abbildung 6:** Präparation von Knorpelgewebe für die Isolierung der zonalen Phänotypen aus Zone I, II und III (A). Nur die oberen, mittleren und unteren 10 % des Knorpels wurden für die Isolierung verwendet (B). Nachdruck mit Genehmigung von Elsevier: Elsevier Ltd., Experimental Model for Cartilage Tissue Engineering to Regenerate the Zonal Organization of Articular Cartilage, T.-K. Kim *et al.*, © 2003. [56] ..... 18

**Abbildung 7:** Kumulative Darstellung der Publikationen, die zwischen 2000 und Juni 2019 veröffentlicht, GM synthetisiert wurde und die Publikation von Van den Bulcke *et al.* [42] zitiert wurde [35, 42, 45-47, 49-53, 94, 98-309]. ..... 27

**Abbildung 8:** Oben: Chemische Struktur und Spaltung der zwei Photoinitiatoren 1-[4-(2-Hydroxyethoxy)-phenyl]-2-hydroxy-2-methyl-1-propanon (I2959) und Lithiumphenyl-2,4,6-trimethylbenzoylphosphinat (LAP). Unten: Molare Absorption der Photoinitiatoren (durchgezogene Linie) und deren Spaltungsprodukten (gestrichelte Linie). Nachdruck mit Genehmigung von Elsevier: Elsevier Ltd., Photoinitiated polymerization of PEG-diacrylate with lithium phenyl-2,4,6-trimethylbenzoylphosphinate: polymerization rate and cytocompatibility, B. D. Fairbanks *et al.*, © 2009. [313] Anmerkung: Die Beschriftungen in der Abbildung wurden übersetzt. .... 30

**Abbildung 9:** Speichermodul von 10 Gew.-% GM2- und GM10-Hydrogelen. Als Gelatine-Rohmaterial wurden eine Gelatine mit einem Bloom-Wert von 235 g Bloom verwendet (helle Balken) und eine Gelatine mit 270 g Bloom (dunkle Balken). Die Hydrogele, deren GM aus Gelatine mit 270 g Bloom zeigten tendenziell höhere Speichermoduln als die Hydrogele, deren GM aus 235 g Bloom Gelatine. .... 152

**Figure 1 A)** DM, broken down to methacrylate (filled bars) and methacrylamide (criss-crossed upper bars) in  $\text{mmol g}^{-1}$  of  $G_A$  and  $G_B$  derivatives determined by integration of  $^1\text{H-NMR}$ -spectra with the TMSP-method.[37] The particular DMs were indistinguishable for  $G_A$  and  $G_B$ . The DM increased with the molar excess of MAAnh used. **B)** DMA in  $\text{mmol g}^{-1}$  for derivatives prepared with tenfold excess of anhydride, broken down to methacryloyl and acetyl modification. All corresponding values and statistical analysis results of two-sided Student t-tests are given in **Table S 3** and **Table S 3**, 4.1.7 Supporting Information. The data for  $G_A$  derivatives were published in ref. [37] before. .... 45

**Figure 2: A)** Solutions of deionized gelatin derivatives. Gelatin derivatives precipitated following the deionization process. **B)** IEP of  $G_A$  (8.8),  $G_B$  (4.9), and derivatives  $G_{AM}(A)$  ( $\approx 4.5$ ),  $G_{BM}(A)$  ( $\approx 4.1$ ). The IEP of modified gelatins were different compared to the respective unmodified gelatin. Additionally, the IEPs of  $G_A$  derivatives were higher compared to the corresponding  $G_B$  derivatives. Significant differences were calculated using a two-sided Student t-test, and significance levels were marked as follows:  $**p < 0.01$ ,  $***p < 0.001$ . .... 47

**Figure 3: A)** SEC elugrams of  $G_A$  and its derivatives **B)** as well as of  $G_B$  and its derivatives. GMs were eluted at higher elution volumes compared to the raw materials. Increasing DMs lead to increasing elution volumes. GMAs were eluted at even higher elution volumes, which further increased with the DA. Elution volumes smaller than 7.5 mL and greater than 10.5 mL were outside the separation range of the used SEC column. .... 48

**Figure 4:** Dynamic viscosity of 10 % (w/w)  $G_A$  and  $G_B$  (derivative) solutions determined at  $50\text{ s}^{-1}$ , pH 7.4, and  $37\text{ }^\circ\text{C}$ . All corresponding values are entitled in **Table S 4**, 4.1.7 Supporting Information. The viscosity of unmodified  $G_B$  was significantly higher compared to unmodified  $G_A$ . This was also true for relatively low methacryloylated derivatives GM2 and GM5. Viscosities of highly modified derivatives GM10, GM5A5, and GM2A8 were indistinguishable. Significant differences were determined using a two-sided Student t-test, and significance levels were marked as follows:  $*p<0.05$ ;  $***p<0.001$ . .... 51

**Figure 5: A)**  $G'_{LVER}$  (at  $37\text{ }^\circ\text{C}$ ) and **B)** EDS of GM(A) hydrogels prepared from 10 % (w/w) solutions.  $G'_{LVER}$  of GM-hydrogels were higher compared to GMA hydrogels with identical DM, and  $G_B$ M hydrogels had higher  $G'_{LVER}$  than  $G_A$ M hydrogels. All corresponding values and statistical analysis results of two-sided Student t-tests are given in and **Table S 7**, 4.1.7 Supporting Information). EDSs of hydrogels were approximately the same for all derivatives (700–800 %), except for GM2A8 which possessed significantly higher EDS and significant differences between  $G_A$  and  $G_B$ . Significant differences were calculated using a two-sided Student t-test, and significance levels were marked as follows:  $**p<0.01$ ;  $***p<0.001$ . .... 53

**Figure 6:** Schematic presentation of different gelatin derivatives used in this study. The suffix denotes the molar excess of anhydrides (MAAnh and AcAnh) used during synthesis procedure. Methacryloyl groups are marked green and acetyl groups blue. Furthermore, the degree of methacryloylation (DM), the total degree of modification (DMA, i.e., DM + degree of acetylation) and the capability to form physical gels [96] are given. .... 70

**Figure 7:** Stress-strain diagrams of gelatin methacryloyl acetyl (GM(A)) hydrogels made without (–) **(A,B)** and with cooling **(C,D)** cross-linking and measured in confined **(A,C)** and unconfined **(B,D)** set-up. The utilized the gels to different extents; therefore we determined the respective deformation and added it to the measured strains, which shifted the curves to the right to the corrected, effectively applied overall strains, resulting in different initial strains for the various specimens. Material failure resulted in complete drop of stress in the unconfined set-up **(B,D)**. In the confined set-up the first drop of stress was interpreted to indicate material failure and curves are only displayed up to the corresponding strain **(A,C)**. .... 71

**Figure 8:** Compressive strains at break ( $\epsilon_b$ ) measured in the confined **(A)** or unconfined **(B)** set-up and the respective compressive stresses at break ( $\sigma_b$ ) **(C,D)**. Hydrogels were prepared with (+) or without (–) cooling. The 25<sup>th</sup> and 75<sup>th</sup> percentiles of all specimen determine the boxes. The whiskers mark the inner fence (1.5-fold interquartile range). Data points beyond the inner fence are outliers and shown

as black diamonds. The line in the box represents the median and the center of the square the mean. Significant differences are marked as follows: \*\* $p < 0.01$ , \*\*\* $p < 0.001$ . ..... 72

**Figure 9:** Experimental set-up for compression tests of hydrogels in a swollen state at 37 °C. The measuring chamber was flushed with 37 °C warm PBS+ throughout the measurements. The PBS+ was warmed on a magnetic stirrer/hotplate and pumped in a closed circuit through the measuring chamber by the hose pump. .... 79

**Figure 10:** Technical drawing of the measurement components for unconfined (a–c) and confined (d–f) measurements: (a/d) Self-designed measuring head for the material testing machine Z005, consisting of an adapter and the measuring head. The diameter was 15 mm (a) and 8 mm (d). (b/e) Technical drawing of the inlet of the measuring chamber. Due to the perforation of the inlet the exchange of the PBS+ surrounding the hydrogel was ensured. For confined testing a chamber with a filter disk ensuring PBS+ exchange was utilized. (c/f) Transverse section of the measuring chamber..... 80

**Figure 11:** Molar ellipticity  $\theta$  of unmodified gelatin, GM2, GM2A8, and GM10. The spectra were recorded at 37 °C (A) or after the temperature protocol, whereby the 37 °C warm solution was cooled to 21 °C for 20 min followed by cooling to 4 °C for 40 min (B, Cooling). For gelatin and GM2 a clear positive signal around 220 nm was detected after cooling, which suggested the presence of alpha helices. The signal was absent for all solutions measured at 37 °C, and the negative molar ellipticity of all solutions around 200 nm emphasized the presence of random coil structures. The figure was created with Origin 2019b (<http://www.originlab.com/2019b>)..... 92

**Figure 12:** Differential scanning calorimetry (DSC) curves of unmodified gelatin, GM2, GM2A8, and GM10. Vertical dotted lines indicate the melting temperatures. The figure was created with Origin 2019b (<http://www.originlab.com/2019b>)..... 93

**Figure 13:** Evolution of storage modulus  $G'$  during the initial cooling protocol of the sequential cross-linking procedure for the tested gelatin derivatives and the raw material gelatin (G). Note that the data on the subsequently performed chemical cross-linking of the samples shown here is depicted in **Figure 14** and discussed in the next section. The figure was created with Origin 2019b (<http://www.originlab.com/2019b>)..... 95

**Figure 14:** Real time-near infrared spectroscopy-photorheology data of GM2, GM2A8 and GM10 solutions. The storage moduli ( $G'$ ) and double bond conversions (DBC) measured for chemical cross-linking at 37 °C (classical method) are shown in (A, B).  $G'$  and DBC measured during the sequential cross-linking procedure (cooling) are shown in (C, D), respectively. Note that the data in (C, D) were obtained directly after physical cross-linking shown in **Figure 13** using the same samples. The time axes in this figure therefore refer to the chemical cross-linking period only. Sequential cross-linking resulted in higher  $G'$  after chemical cross-linking and lower DBCs for all three gelatin derivatives. The grey dotted line indicates the start of UV-initiated cross-linking. The figure was created with Origin 2019b (<http://www.originlab.com/2019b>)..... 97

**Figure 15:** Increase of storage modulus  $G'$  with the double bond conversion ( $DBC$ ) for the three gelatin derivatives GM2, GM2A8, and GM10 using the classical or the sequential cross-linking procedure, respectively. Note that the light blue triangles representing the data obtained for GM2A8 with the classical cross-linking procedure are visible close to the abscissa at  $DBC$ s below  $0.3 \text{ mmol g}^{-1}$ . The figure was created with Origin 2019b (<http://www.originlab.com/2019b>)..... 100

**Figure 16:** Three parts of hydrogel mold for preparation of zonal structured hydrogels. .... 116

**Figure 17:** Storage, loss moduli ( $G'$ ,  $G''$ ) and loss factor ( $\tan(\delta)$ ) of GM, GM+CSM and GM+HAM+CSM hydrogels with 1 mm height and 8 mm diameter.  $G''$  and  $\tan(\delta)$  increased in parallel. Highest  $G'$  was found for GM and GM+HAM+CSM. .... 120

**Figure 18:** Relaxation testing of GM (A), GM+CSM (B), GM+HAM+CSM (C) and zonal (D) hydrogels. Black squares denote the initial stress ( $\sigma_{ini}$ ) to achieve the respective compression and red squares denote the remaining stress ( $\sigma_{eq}$ ) after 30 min holding the respective strain ( $\epsilon$ ). Furthermore, the linear fit of  $\sigma_{ini}$  and  $\sigma_{eq}$  are shown. The slopes of these linear fits were calculated as E-moduli ( $E_{ini}$ ,  $E_{eq}$ ). E-moduli of GM were highest, followed by GM+HAM+CSM. GM+HAM hydrogels had the lowest E-moduli..... 121

**Figure 19:** Relative gel yield of biopolymer hydrogels during degradation studies. Hydrogels consisted out of GM (10 % (w/w)), GM+CSM (7.5 % (w/w) GM + 2.5 % (w/w) CSM), GM+HAM (7.5 % (w/w) GM + 2.5 % (w/w) HAM), GM+CSM+HAM (7.5 % (w/w) GM + 1.25 % (w/w) CSM + 1.25 % (w/w) HAM) and zonal structured hydrogels. Hydrogels were incubated for 42 d in PBS (A), collagenase type II (B,  $2.5 \text{ U mL}^{-1}$ ), hyaluronidase (C,  $2.5 \text{ U mL}^{-1}$ ) and a mixture of collagenase and hyaluronidase (D, each  $1.25 \text{ U mL}^{-1}$ ). Collagenase reduced the gel yield over time for all hydrogels while PBS and hyaluronidase alone did not effect the gel yield. .... 122

**Figure 20:** Relative amount of viable cells in GM-hydrogels relative to chondrocyte-containing hydrogels prepared without cooling (0 h). Duration of cooling did not affect the amount of viable cells in cell-containing hydrogels. .... 123

**Figure 21:** Staining of chondrocytes encapsulated in pure GM-hydrogels directly after encapsulation (A-C) and after 28 d of static cultivation (a-c). Alcian blue-nuclear fast red staining (A, a; scale= $100 \mu\text{m}$ ) showed alcian blue positive staining after 28 d cultivation, arrows mark encapsulated chondrocytes. Collagen type I (B, b; scale= $10 \mu\text{m}$ ) and collagen type II (C, c; scale= $10 \mu\text{m}$ ) was detected for both time points..... 124

**Figure 22:** Staining of chondrocytes encapsulated in zonal-hydrogels directly after encapsulation (A-E) and after 28 d of static cultivation (a-e) in different zonal hydrogel compositions (A, a: GM; B, b: GM+CSM; C, c: GM+CSM+HAM). Alcian Blue-Nuclear Fast Red staining (A-C, a-c; scale= $100 \mu\text{m}$ ) showed Alcian Blue positive staining after 28 d cultivation, arrows mark encapsulated chondrocytes. Collagen type I (D, d; scale= $10 \mu\text{m}$ ) was scarcely detectable at both time points, collagen type II (E, e; scale= $10 \mu\text{m}$ ) was detected after 28 d cultivation. .... 125

<b>Figure S 1:</b> <sup>1</sup> H-NMR of G <sub>B</sub> and its derivatives. Acrylic protons of methacryl groups were highlighted light grey, non-modified lysine residues criss-crossed light grey, methyl protons of acetyl groups criss-crossed dark grey and methyl protons of methacryl groups dark grey. ....	56
<b>Figure S 2:</b> Calculated isoelectric points of G <sub>A</sub> regarding different degrees of derivatization of amino groups (method see main manuscript). ....	58
<b>Figure S 3:</b> SEC elograms of G <sub>A</sub> and G <sub>B</sub> <b>(A)</b> and derivatives <b>(B-F)</b> . ....	59
<b>Figure S 4:</b> Gelling behavior of G <sub>A</sub> <b>(A)</b> and its derivatives G <sub>AM2</sub> <b>(B)</b> , G <sub>AM5</sub> <b>(C)</b> , G <sub>AM10</sub> <b>(D)</b> , G <sub>AM2A8</sub> <b>(E)</b> , G <sub>AM5A5</sub> <b>(F)</b> in terms of $G'$ and $G''$ . ....	60
<b>Figure S 5:</b> Gelling behavior of G <sub>B</sub> <b>(A)</b> and its derivatives G <sub>BM2</sub> <b>(B)</b> , G <sub>BM5</sub> <b>(C)</b> , G <sub>BM10</sub> <b>(D)</b> , G <sub>BM2A8</sub> <b>(E)</b> , G <sub>BM5A5</sub> <b>(F)</b> in terms of $G'$ and $G''$ . ....	61
<b>Figure S 6:</b> Rheological evaluation of GM(A) gelling behavior during the chosen thermal protocol: <b>(A)</b> Storage moduli ( $G'$ ) and <b>(B)</b> loss moduli ( $G''$ ). Note the interruption of the y-axis the associated change of scales. Due to this interruption the curves of GM10 and GM2A8 both end at 200 Pa and start again at 800 Pa. ....	83
<b>Figure S 7:</b> <sup>1</sup> H-NMR spectra of gelatin used for methacryloylation (GM) (and acetylation (GMA)) and its derivatives. Unmodified lysine groups, only present in the spectrum of the unmodified gelatin, were highlighted in dark grey, acrylic protons of methacryloyl groups in light grey. The figure was created with Origin 2019b ( <a href="http://www.originlab.com/2019b">http://www.originlab.com/2019b</a> ). ....	104
<b>Figure S 8:</b> Utilized temperature profile for physical gelation prior to chemical cross-linking. The 37 °C warm GM-solutions were cooled for 20 min to 21 °C followed by cooling to 4 °C 40 min (green dotted lines). Afterwards, infrared spectroscopy (IR) acquisition was started (orange dotted line) and the UV light was turned on 5 s later (blue dotted line). The figure was created with Origin 2019b ( <a href="http://www.originlab.com/2019b">http://www.originlab.com/2019b</a> ). ....	104
Figure S 9. ....	105
<b>Figure S 10:</b> Circular dichroism (CD) spectra of gelatin <b>(A)</b> , GM2 <b>(B)</b> , GM2A8 <b>(C)</b> and GM10 <b>(D)</b> . CD spectra were recorded at 37 °C or after cooling procedure (37 °C to 21 °C for 20 min followed by cooling to 4 °C for 40 min). The figure was created with Origin 2019b ( <a href="http://www.originlab.com/2019b">http://www.originlab.com/2019b</a> ). ..	105
<b>Figure S 11:</b> Circular dichroism (CD) spectra of gelatin (derivatives) after cooling procedure <b>(A)</b> and a zoom-in of these CD spectra between 225-255 nm <b>(B)</b> . The figure was created with Origin 2019b ( <a href="http://www.originlab.com/2019b">http://www.originlab.com/2019b</a> ). ....	105
<b>Figure S 12:</b> Reaction rate of double bond conversion for GM10, GM2, and GM2A8. The figure was created with Origin 2019b ( <a href="http://www.originlab.com/2019b">http://www.originlab.com/2019b</a> ). ....	106
<b>Figure S 13:</b> Correlations between $k_{DBC}$ and DM (left) as well as $k_g$ and $k_{DBC}$ (right). The figure was created with Origin 2019b ( <a href="http://www.originlab.com/2019b">http://www.originlab.com/2019b</a> ). ....	107
<b>Figure S 14:</b> <sup>1</sup> H-NMR spectra of unmodified biopolymers gelatin (G), chondroitin sulfate (CS), hyaluronic acid (HA) and biopolymer derivatives gelatin methacryloyl (GM), chondroitin sulfate methacryloyl	



(CSM) and hyaluronic acid methacryloyl (HAM). Acrylic protons of methacryloyl groups were highlighted grey..... 134

**Figure S 15:** Photos of hydrogel samples cut with a circle cutter for compression testing and cell encapsulation (height 5 mm, diameter 8 mm). Pictures show different hydrogel compositions: GM (A), GM+HAM (B), GM+CSM (C) and GM+HAM+CSM (D). Hydrogels containing HAM were cloudy, the others nearly transparent..... 135

**Figure S 16:** Zonal hydrogels directly after preparation in the mold (A, height 5 mm, diameter 30 mm), cut sample for compression testing and cell encapsulation (B, height 5 mm, diameter 8 mm). In A and B the hyaluronic acid methacryloyl containing layer were opaque, while the other two layers were nearly transparent. A representative Alcian Blue-Nuclear Fast Red stained slice of zonal hydrogels is shown in C (scale bar = 500  $\mu$ m). The three layers could be differentiated by different staining, from top to bottom: GM (pink), GM+CSM (light blue) and GM+HAM+CSM (dark blue to purple). ..... 135

**Figure S 17:** Storage, loss moduli ( $G'$ ,  $G''$ ) and loss factor ( $\tan(\delta)$ ) of GM+HAM hydrogels with 1 mm height and 8 mm diameter..... 136

**Figure S 18:** Relaxation testing of GM+HAM hydrogels. Black squares denote the initial stress ( $\sigma_{ini}$ ) to achieve the respective compression and red squares denote the remaining stress ( $\sigma_{eq}$ ) after 30 min holding the respective strain ( $\epsilon$ ). Furthermore, the linear fit of  $\sigma_{ini}$  and  $\sigma_{eq}$  are shown. The slopes of these linear fits were calculated as E-moduli ( $E_{ini}$ ,  $E_{eq}$ ). E-moduli of GM were highest, followed by GM+HAM+CSM. GM+HAM hydrogels had the lowest E-moduli. .... 136

**Figure S 19:** Relative swelling capability of biopolymer hydrogels during degradation studies. Hydrogels consisted out of GM (10 % (w/w)), GM+CSM (7.5 % (w/w) GM + 2.5 % (w/w) CSM), GM+HAM (7.5 % (w/w) GM + 2.5 % (w/w) HAM), GM+CSM+HAM (7.5 % (w/w) GM + 1.25 % (w/w) CSM + 1.25 % (w/w) HAM) and zonal structured hydrogels. Hydrogels were incubated for 42 d in PBS (A), collagenase type II (B, 2.5 U mL<sup>-1</sup>), hyaluronidase (C, 2.5 U mL<sup>-1</sup>) and a mixture of collagenase and hyaluronidase (D, each 1.25 U mL<sup>-1</sup>). Collagenase increased the swelling capacity over time for all hydrogels while PBS and hyaluronidase alone did not effect it. .... 137

**Figure S 20:** Relative polymer content of biopolymer hydrogels during degradation studies. Hydrogels consisted out of GM (10 % (w/w)), GM+CSM (7.5 % (w/w) GM + 2.5 % (w/w) CSM), GM+HAM (7.5 % (w/w) GM + 2.5 % (w/w) HAM), GM+CSM+HAM (7.5 % (w/w) GM + 1.25 % (w/w) CSM + 1.25 % (w/w) HAM) and zonal structured hydrogels. Hydrogels were incubated for 42 d in PBS (A), collagenase type II (B, 2.5 U mL<sup>-1</sup>), hyaluronidase (C, 2.5 U mL<sup>-1</sup>) and a mixture of collagenase and hyaluronidase (D, each 1.25 U mL<sup>-1</sup>). Collagenase reduced the polymer content over time for all hydrogels while PBS and hyaluronidase alone did not effect the polymer content. .... 138

**Figure S 21:** Alcian Blue-Nuclear Fast Red staining of cell free hydrogels. Representative overview pictures (A-D, 2x magnification, scale = 500  $\mu$ m) and detail pictures (a-d, 20x magnification, scale =

100  $\mu\text{m}$ ) of different hydrogel compositions (A, a: GM, B, b: GM+HAM, C, c: GM+CSM, D, d: GM+HAM+CSM) are shown. .... 139

### III. Tabellenverzeichnis

**Tabelle 1:** Gegebene Information über Gelatine-Typ und tierischen Ursprung der für die GM-Synthese verwendeten Gelatine von 2000 bis Juni 2019 publizierten Studien, in denen GM synthetisiert wurde und in denen die Publikation von Van den Bulcke *et al.* [42] zitiert wurde [35, 42, 45-47, 49-53, 94, 98-309]. In den berücksichtigten 223 Veröffentlichungen wurden 231 GM-Synthesen beschrieben..... 28

**Table 1:** Gelation temperatures ( $T_{gel}$ ) and melting temperatures ( $T_{melt}$ ) of solutions (10 % w/w, pH 7.4) of unmodified  $G_A$ ,  $G_B$  and derivatives thereof.  $T_{gel}$  and  $T_{melt}$  of the raw materials decreased after chemical modification. No  $T_{gel}$  and  $T_{melt}$  could be determined (CND) for derivatives with high degrees of modification (GM10, GM5A5, GM2A8) above 10 °C GM10. No significant differences between sol-gel points of  $G_A$  and  $G_B$  as well as their respective derivatives were detected. .... 50

**Table 2:** Compressive strain at break ( $\epsilon_b$ ) and the respective compressive stresses at break ( $\sigma_b$ ) of GM(A) hydrogels measured in a confined or an unconfined setting. Each GM(A) hydrogel was investigated without cooling (-) and with cooling (+) before chemical cross-linking. .... 73

**Table 3:** Rheological analysis of GM(A) solutions (10% (w/w)) during cooling (20 min 21°C + 40 min 4°C). Gelation was determined when the storage modulus  $G'$  became larger than the loss modulus  $G''$  ( $G' \geq G''$ ). Furthermore, the storage moduli of the physical hydrogels measured at the end of the thermal protocol (after 60 min), before chemical cross-linking, is given ( $G'$ ). The loss factor of physical hydrogels is determined as ratio of  $G''$  and  $G'$  ( $\tan\delta$ ). .... 75

**Table 4:** Melting temperatures  $T_m$  and melting enthalpies  $\Delta H_m$  obtained from the DSC curves shown in **Figure 12** as well as renaturation levels  $X_{DSC}$  calculated from DSC measurements. GM10 did not show any signal in the DSC measurements or the signal was too shallow to be analysed, so no values were found (n.f.). The measured melting enthalpies were significantly different from each other [ $p < 0.05$  (gelatin, GM2),  $p < 0.001$  (gelatin, GM2A8; GM2, GM2A8)]. .... 94

**Table 5:** Parameters describing the physical gelation of gelatin derivative solutions using the sequential cross-linking protocol: physical gelation delay time  $t_{d,p}$ , initial increase rate  $k_{g,p}$  of storage modulus  $G'$  upon cooling, and  $G'$  after cooling to 21 °C for 20 min and 4 °C for 40 min, respectively..... 96

**Table 6:** Parameters describing the chemical cross-linking of gelatin derivative solutions with the classical method at 37°C or with the sequential cross-linking method: Initial increases  $k_{g,c}$  and  $k_{DBC}$  of  $G'$  and  $DBC$ , respectively, chemical gelation delay time  $t_{d,c}$  upon UV irradiation, final storage modulus  $G'$ , and final  $DBC$ . The data given in % are relative to the degree of methacryloylation (DM) of the respective gelatin derivative..... 98

<b>Table 7:</b> Composition of the four hydrogels with constant biopolymer content investigated in this study. (GM=gelatin methacryloyl, CSM=chondroitin sulphate methacryloyl, HAM=hyaluronic acid methacryloyl) .....	115
<b>Table 8:</b> Double stranded DNA content in cell-containing hydrogels (pure GM or zonal) directly after encapsulation and after 28 d of static cultivation. Furthermore, the relative reduction of DNA content is given. (GM=gelatin methacryloyl, dsDNA=double stranded deoxyribonucleic acid) .....	124
<b>Table S 1:</b> Amino acid composition of non-modified $G_A$ and $G_B$ . The results from the amino acid analysis and information given in [64] were used to perform the theoretical IEP estimation for $G_A$ . (Source: Encyclopedia of Polymer Science and Engineering, Volume 3, p. 488–513 (1987). Copyright Wiley & Sons. Reproduced with permission from John Wiley & Sons Ltd. Data taken from [64]: “Gelatin Handbook: Theory and Industrial Practice” Reinhard Schrieber, Herbert Gareis, ISBN: 978-3-527-31548-2. Reproduced with permission.) .....	55
<b>Table S 2:</b> Degree of methacryloylation (DM) of $G_A$ and $G_B$ derivatives in $\text{mmol g}^{-1}$ split up in methacrylamide and methacrylate .....	57
<b>Table S 3:</b> Entitled differences of degree of methacryloylation (DM) of $G_A$ and $G_B$ derivatives. Significances are tagged as follows: $*=p<0.05$ , $**=p<0.01$ , $***=p<0.001$ , n. s. = not significant.....	57
<b>Table S 4:</b> Dynamic viscosity of $G_A$ and $G_B$ derivatives’ solutions (10 % (w/w) in PBS) in Pa s. ....	62
<b>Table S 5:</b> Entitled differences of viscosity of 10 % (w/w) solutions. Significances are tagged as follows: $*=p<0.05$ , $**=p<0.01$ , $***=p<0.001$ , n. s. = not significant.....	62
<b>Table S 6:</b> Storage modulus in the linear viscoelastic range ( $G'_{LVER}$ in kPa) and equilibrium degree of swelling ( $EDS$ in % of the polymer dry mass applied) of GM(A) hydrogels (10 % (w/w)). ....	63
<b>Table S 7:</b> Entitled differences of $G'_{LVER}$ of hydrogels from utilized gelatin derivatives. Significances are tagged as follows: $*=p<0.05$ , $**=p<0.01$ , $***=p<0.001$ , n. s. = not significant.....	63
<b>Table S 8:</b> Entitled differences of $EDS$ of hydrogels from utilized gelatin derivatives. Significances are tagged as follows: $*=p<0.05$ , $**=p<0.01$ , $***=p<0.001$ , n. s. = not significant.....	64
<b>Table S 9:</b> Degree of modification of gelatin derivatives. The mean distance of two chemically modified amino acids was calculated as the reciprocal of the degree of modification. The amount of amino acids between the two chemically modified amino acids was estimated assuming an average molecular weight of amino acids of $122 \text{ g mol}^{-1}$ calculated out of the amino acid composition of the used gelatin type B (composition can be found in ref. [96]). ....	83
<b>Table S 10:</b> Chemical gelation delay time ( $t_{d,c}$ ) and final double bond conversion ( $DBC$ ) in $\text{mmol g}^{-1}$ of GM2, GM2A8 and GM10 cross-linked with the classical method at $37 \text{ }^\circ\text{C}$ . ....	106

**Table S 11:** Chemical gelation delay time ( $t_{d,c}$ ) and final double bond conversion ( $DBC$ ) in  $\text{mmol g}^{-1}$  of GM2, GM2A8 and GM10 cross-linked with sequential cross-linking protocol (starting at 37 °C, cooling to 21 °C for 20 min followed by cooling to 4 °C for 40 min). ..... 106

**Table S 12:** Storage modulus ( $G'$ ), loss modulus ( $G''$ ), loss factor ( $\tan(\delta)$ ), initial E-modulus ( $E_{ini}$ ) and equilibrium E-modulus ( $E_{eq}$ ) of biomimetic hydrogel compositions and their scale relative to GM hydrogels. Zonal hydrogels could only made with a height of 5 mm, thus no rheological data was available for them. .... 139

**Table S 13:** Cross-linking capabilities of hydrogel precursor solutions (10 % (w/w)) and relative gel yields after enzymatic degradation with collagenase for 42 days of all investigated hydrogel compositions. .... 140

## IV. Literaturverzeichnis

1. Martel-Pelletier, J., et al., *Cartilage in Normal and Osteoarthritis Conditions*. Best Practice & Research Clinical Rheumatology, 2008. **22**(2): p. 351-384.
2. Bhosale, A.M. and J.B. Richardson, *Articular Cartilage: Structure, Injuries and Review of Management*. British Medical Bulletin, 2008. **87**(1): p. 77-95.
3. Muir, H., *The Chondrocyte, Architect of Cartilage. Biomechanics, Structure, Function and Molecular Biology of Cartilage Matrix Macromolecules*. Bioessays, 1995. **17**(12): p. 1039-1048.
4. Rudert, M. and C.J. Wirth, *Knorpelregeneration und Knorpelersatz*. Der Orthopäde, 1998. **27**(5): p. 309-321.
5. Benninghoff, A., *Form und Bau der Gelenkknorpel in ihren Beziehungen zur Funktion*. Zeitschrift für Zellforschung und Mikroskopische Anatomie, 1925. **2**(5): p. 783-862.
6. Cohen, N.P., R.J. Foster, and V.C. Mow, *Composition and Dynamics of Articular Cartilage: Structure, Function, and Maintaining Healthy State*. Journal of Orthopaedic & Sports Physical Therapy, 1998. **28**(4): p. 203-215.
7. Burgeson, R.E. and M.E. Nimni, *Collagen Types. Molecular Structure and Tissue Distribution*. Clinical Orthopaedics and Related Research, 1992. **282**: p. 250-272.
8. Bruckner, P. and M. van der Rest, *Structure and Function of Cartilage Collagens*. Microscopy Research and Technique, 1994. **28**(5): p. 378-384.
9. Fleischmajer, R., et al., *Immunoelectron Microscopy of Type III Collagen in Normal and Scleroderma Skin*. Journal of Investigative Dermatology, 1980. **75**(2): p. 189-191.
10. Miller, E.J., *Biochemical Characteristics and Biological Significance of the Genetically-Distinct Collagens*. Molecular and Cellular Biochemistry, 1976. **13**(3): p. 165-192.
11. Grynblas, M.D., D.R. Eyre, and D.A. Kirschner, *Collagen Type II Differs from Type I in Native Molecular Packing*. Biochimica et Biophysica Acta (BBA)-Protein Structure, 1980. **626**(2): p. 346-355.
12. Nimni, M.E. *Collagen: Its Structure and Function in Normal and Pathological Connective Tissues*. in *Seminars in Arthritis and Rheumatism*. 1974. Elsevier.
13. Wilson, W., et al., *Stresses in the Local Collagen Network of Articular Cartilage: a Poroviscoelastic Fibril-Reinforced Finite Element Study*. Journal of Biomechanics, 2004. **37**(3): p. 357-366.
14. Aspberg, A., *Cartilage Proteoglycans*, in *Cartilage: Volume 1: Physiology and Development*, S. Grässel and A. Aszódi, Editors. 2016, Springer International Publishing. p. 1-22.
15. Kiani, C., et al., *Structure and Function of Aggrecan*. Cell Research, 2002. **12**(1): p. 19-32.
16. Athanasiou, K., et al., *Interspecies Comparisons of In Situ Intrinsic Mechanical Properties of Distal Femoral Cartilage*. Journal of Orthopaedic Research, 1991. **9**(3): p. 330-340.
17. O'Hara, B., J. Urban, and A. Maroudas, *Influence of Cyclic Loading on the Nutrition of Articular Cartilage*. Annals of the Rheumatic Diseases, 1990. **49**(7): p. 536-539.
18. Schumacher, B.L., et al., *A Novel Proteoglycan Synthesized and Secreted by Chondrocytes of the Superficial Zone of Articular Cartilage*. Archives of Biochemistry and Biophysics, 1994. **311**(1): p. 144-152.
19. Khan, I.M., et al., *Expression of Clusterin in the Superficial Zone of Bovine Articular Cartilage*. Arthritis & Rheumatism, 2001. **44**(8): p. 1795-1799.
20. DiCesare, P.E., et al., *Cartilage Oligomeric Matrix Protein: Isolation and Characterization from Human Articular Cartilage*. Journal of Orthopaedic Research, 1995. **13**(3): p. 422-428.
21. Lorenzo, P., M.T. Bayliss, and D. Heinegård, *A Novel Cartilage Protein (CILP) Present in the Mid-Zone of Human Articular Cartilage Increases with Age*. Journal of Biological Chemistry, 1998. **273**(36): p. 23463-23468.
22. Keenan, A.m., et al., *Impact of Multiple Joint Problems on Daily Living Tasks in People in the Community Over Age Fifty-Five*. Arthritis Care & Research: Official Journal of the American College of Rheumatology, 2006. **55**(5): p. 757-764.

23. Fuchs, J. and F. Prütz, *Prävalenz von Gelenkschmerzen in Deutschland*. Journal of Health Monitoring, 2017. **2**(3): p. 66-71.
24. Rabenberg, M., *Arthrose*. Gesundheitsberichterstattung des Bundes, ed. M. Rabenberg. Vol. 54. 2013, Berlin: Robert Koch-Institut.
25. Hunziker, E.B., et al., *An Educational Review of Cartilage Repair: Precepts & Practice—Myths & Misconceptions—Progress & Prospects*. Osteoarthritis and Cartilage, 2015. **23**(3): p. 334-350.
26. Parreno, J., et al., *Interplay Between Cytoskeletal Polymerization and the Chondrogenic Phenotype in Chondrocytes Passaged in Monolayer Culture*. Journal of Anatomy, 2017. **230**(2): p. 234-248.
27. Benya, P.D. and J.D. Shaffer, *Dedifferentiated Chondrocytes Reexpress the Differentiated Collagen Phenotype when Cultured in Agarose Gels*. Cell, 1982. **30**(1): p. 215-224.
28. Brittberg, M., et al., *Treatment of Deep Cartilage Defects in the Knee with Autologous Chondrocyte Transplantation*. New England Journal of Medicine, 1994. **331**(14): p. 889-895.
29. Kudva, A.K., F.P. Luyten, and J. Patterson, *Initiating Human Articular Chondrocyte Redifferentiation in a 3D System After 2D Expansion*. Journal of Materials Science: Materials in Medicine, 2017. **28**(10): p. 156.
30. Schuh, E., et al., *Chondrocyte Redifferentiation in 3D: the Effect of Adhesion Site Density and Substrate Elasticity*. Journal of Biomedical Materials Research Part A, 2012. **100**(1): p. 38-47.
31. Jones, C., et al., *Matrix-Induced Autologous Chondrocyte Implantation in Sheep: Objective Assessments Including Confocal Arthroscopy*. Journal of Orthopaedic Research, 2008. **26**(3): p. 292-303.
32. Balakrishnan, B. and R. Banerjee, *Biopolymer-Based Hydrogels for Cartilage Tissue Engineering*. Chemical Reviews, 2011. **111**(8): p. 4453-4474.
33. IUPAC, I.U.o.P.a.A.C., *Compendium of Chemical Terminology (the "Gold Book")* 2nd ed, ed. A.D. McNaught and A. Wilkinson. Vol. 1669. 1997: Blackwell Science Oxford.
34. Murphy, G., et al., *Purification and Characterization of a Bone Metalloproteinase that Degrades Gelatin and Types IV and V Collagen*. Biochimica et Biophysica Acta (BBA)-Protein Structure and Molecular Enzymology, 1985. **831**(1): p. 49-58.
35. Yue, K., et al., *Synthesis, Properties, and Biomedical Applications of Gelatin Methacryloyl (GelMA) Hydrogels*. Biomaterials, 2015. **73**: p. 254-271.
36. Kuijpers, A.J., et al., *Cross-Linking and Characterisation of Gelatin Matrices for Biomedical Applications*. Journal of Biomaterials Science, Polymer Edition, 2000. **11**(3): p. 225-243.
37. Tomihata, K. and Y. Ikada, *Cross-Linking of Gelatin with Carbodiimides*. Tissue Engineering, 1996. **2**(4): p. 307-313.
38. Azarikia, F., et al., *Stabilization of Biopolymer Microgels Formed by Electrostatic Complexation: Influence of Enzyme (laccase) Cross-Linking on pH, Thermal, and Mechanical Stability*. Food Research International, 2015. **78**: p. 18-26.
39. Zeeb, B., L. Fischer, and J. Weiss, *Cross-Linking of Interfacial Layers Affects the Salt and Temperature Stability of Multilayered Emulsions Consisting of Fish Gelatin and Sugar Beet Pectin*. Journal of Agricultural and Food Chemistry, 2011. **59**(19): p. 10546-10555.
40. Han, Y.-P. and X.-H. Zhao, *Properties of Bovine Gelatin Cross-Linked by a Mixture of Two Oxidases (Horseradish Peroxidase and Glucose Oxidase) and Glucose*. CyTA-Journal of Food, 2016. **14**(3): p. 457-464.
41. Nazarova, O.V., et al., *Methacryloyl Derivatives of Gelatin and Copolymers Based on Them*, in *Russian Journal of Applied Chemistry*. 1994. p. 623-624.
42. Van Den Bulcke, A.I., et al., *Structural and Rheological Properties of Methacrylamide Modified Gelatin Hydrogels*. Biomacromolecules, 2000. **1**(1): p. 31-38.
43. Sun, M., et al., *Synthesis and Properties of Gelatin Methacryloyl (GelMA) Hydrogels and Their Recent Applications in Load-Bearing Tissue*. Polymers, 2018. **10**(11): p. 1290.
44. Klein, T.J., et al., *Tissue Engineering of Articular Cartilage with Biomimetic Zones*. Tissue Engineering Part B: Reviews, 2009. **15**(2): p. 143-157.
45. Schuurman, W., et al., *Gelatin-Methacrylamide Hydrogels as Potential Biomaterials for Fabrication of Tissue-Engineered Cartilage Constructs*. Macromolecular Bioscience, 2013. **13**(5): p. 551-561.

46. Levett, P.A., et al., *Hyaluronic Acid Enhances the Mechanical Properties of Tissue-Engineered Cartilage Constructs*. PLOS ONE 2014. **9**(12): p. e113216-ee11339.
47. Bas, O., et al., *Enhancing Structural Integrity of Hydrogels by Using Highly Organised Melt Electrospun Fibre Constructs*. European Polymer Journal, 2015. **72**: p. 451-463.
48. Schuurman, W., et al., *Cartilage Regeneration Using Zonal Chondrocyte Subpopulations: a Promising Approach or an Overcomplicated Strategy?* Journal of Tissue Engineering and Regenerative Medicine, 2015. **9**(6): p. 669-678.
49. Loessner, D., et al., *Functionalization, Preparation and Use of Cell-Laden Gelatin Methacryloyl-Based Hydrogels as Modular Tissue Culture Platforms*. Nature Protocols, 2016. **11**(4): p. 727-746.
50. Yue, K., et al., *Structural Analysis of Photocrosslinkable Methacryloyl-Modified Protein Derivatives*. Biomaterials, 2017. **139**: p. 163-171.
51. Pahoff, S., et al., *Effect of Gelatin Source and Photoinitiator Type on Chondrocyte Redifferentiation in Gelatin Methacryloyl-Based Tissue-Engineered Cartilage Constructs*. Journal of Materials Chemistry B, 2019. **7**(10): p. 1761-1772.
52. Levett, P.A., et al., *A Biomimetic Extracellular Matrix for Cartilage Tissue Engineering Centered on Photocurable Gelatin, Hyaluronic Acid and Chondroitin Sulfate*. Acta Biomaterialia, 2014. **10**(1): p. 214-223.
53. Levett, P.A., et al., *Chondrocyte Redifferentiation and Construct Mechanical Property Development in Single-Component Photocrosslinkable Hydrogels*. Journal of Biomedical Materials Research Part A, 2014. **102**(8): p. 2544-2553.
54. Vunjak-Novakovic, G., et al., *Dynamic Cell Seeding of Polymer Scaffolds for Cartilage Tissue Engineering*. Biotechnology Progress, 1998. **14**(2): p. 193-202.
55. Kim, M., et al., *Enhanced Nutrient Transport Improves the Depth-Dependent Properties of Tri-Layered Engineered Cartilage Constructs with Zonal Co-Culture of Chondrocytes and MSCs*. Acta Biomaterialia, 2017. **58**: p. 1-11.
56. Kim, T.K., et al., *Experimental Model for Cartilage Tissue Engineering to Regenerate the Zonal Organization of Articular Cartilage*. Osteoarthritis and Cartilage, 2003. **11**(9): p. 653-664.
57. Klein, T., et al., *Tissue Engineering of Stratified Articular Cartilage from Chondrocyte Subpopulations*. Osteoarthritis and Cartilage, 2003. **11**(8): p. 595-602.
58. Hutmacher, D.W., *Scaffolds in Tissue Engineering Bone and Cartilage*. Biomaterials, 2000. **21**(24): p. 2529-2543.
59. Camarero-Espinosa, S., et al., *Directed Cell Growth in Multi-Zonal Scaffolds for Cartilage Tissue Engineering*. Biomaterials, 2016. **74**: p. 42-52.
60. Cohen, D.L., et al., *Direct Freeform Fabrication of Seeded Hydrogels in Arbitrary Geometries*. Tissue Engineering, 2006. **12**(5): p. 1325-1335.
61. Veis, A., *The Macromolecular Chemistry of Gelatin*. 1964: Academic Press
62. Ward, A.G. and A. Courts, *Science and Technology of Gelatin*. 1977: Academic press.
63. Veit, G., et al., *Collagen XXVIII, a Novel von Willebrand Factor A Domain-Containing Protein with Many Imperfections in the Collagenous Domain*. Journal of Biological Chemistry, 2006. **281**(6): p. 3494-3504.
64. Schrieber, R. and H. Gareis, *Gelatine Handbook: Theory and Industrial Practice*. 2007: John Wiley & Sons.
65. Liu, D., et al., *Collagen and Gelatin*. Annual Review of Food Science and Technology, 2015. **6**: p. 527-557.
66. Ramachandran, G. and G. Kartha, *Structure of Collagen*. Nature, 1954. **174**(4423): p. 269-270.
67. Ramachandran, G. and G. Kartha. *Studies on Collagen*. in *Proceedings of the Indian Academy of Sciences-Section A*. 1955. Springer.
68. Ramachandran, G. and G. Kartha, *Structure of Collagen*. Nature, 1955. **176**(4482): p. 593-595.
69. Engel, J., *Investigation of the Denaturation and Renaturation of Soluble Collagen by Light Scattering*. Archives of Biochemistry and Biophysics, 1962. **97**(1): p. 150-158.
70. Ames, W.M., *The Conversion of Collagen to Gelatin and their Molecular Structures*. Journal of the Science of Food and Agriculture, 1952. **3**(10): p. 454-463.



71. Tiffany, M.L. and S. Krimm, *Circular Dichroism of the "Random" Polypeptide Chain*. *Biopolymers: Original Research on Biomolecules*, 1969. **8**(3): p. 347-359.
72. Gardi, A., H. Nitschmann, and K. Rieder, *Comparative Optical Studies on Modified Gelatins and Calf Skin Collagen-Influence of Modification on Conformational Behavior*. *Chimia*, 1973. **27**(2): p. 116-121.
73. Nishio, T. and R. Hayashi, *Regeneration of a Collagen-Like Circular Dichroism Spectrum from Industrial Gelatin*. *Agricultural and Biological Chemistry*, 1985. **49**(6): p. 1675-1682.
74. Wetzel, R., et al., *Conformations of Different Gelatins in Solutions and in Films an Analysis of Circular Dichroism (CD) Measurements*. *Colloid and Polymer Science*, 1987. **265**(12): p. 1036-1045.
75. Ohsaku, M., J. Izumi, and A. Imamura, *Electronic Structures of Collagen Model Polymers:(Gly-Pro) n,(Gly-Hyp) n,(Ala-Pro) n,(Ala-Hyp) n,(Gly-Pro-Gly) n,(Gly-Hyp-Gly) n,(Gly-Pro-Pro) n, and (Gly-Pro-Hyp) n*. *International Journal of Biological Macromolecules*, 1984. **6**(5): p. 234-240.
76. Brandts, J.F., H.R. Halvorson, and M. Brennan, *Consideration of the Possibility that the Slow Step in Protein Denaturation Reactions is due to Cis-Trans Isomerism of Proline Residues*. *Biochemistry*, 1975. **14**(22): p. 4953-4963.
77. *Physical Networks - Polymers and Gels*. 1990: Springer Netherlands. 418.
78. Djabourov, M., J. Leblond, and P. Papon, *Gelation of Aqueous Gelatin Solutions. I. Structural Investigation*. *Journal de Physique*, 1988. **49**(2): p. 319-332.
79. Djabourov, M., J. Leblond, and P. Papon, *Gelation of Aqueous Gelatin Solutions. II. Rheology of the Sol-Gel Transition*. *Journal de Physique*, 1988. **49**(2): p. 333-343.
80. Bohidar, H.B. and S.S. Jena, *Kinetics of Sol-Gel Transition in Thermoreversible Gelation of Gelatin*. *The Journal of Chemical Physics*, 1993. **98**(11): p. 8970-8977.
81. Godard, P., et al., *Crystallization and Melting of Aqueous Gelatin*. *Journal of Polymer Science: Polymer Physics Edition*, 1978. **16**(10): p. 1817-1828.
82. Emery, J., J. Chatellier, and D. Durand, *Application des Techniques Ultrasonores à l'Etude de la Transition Pelote-Hélice dans les Solutions Aqueuses de Gélatine*. *Journal de Physique*, 1986. **47**(6): p. 921-925.
83. Michon, C., G. Cuvelier, and B. Launay, *Concentration Dependence of the Critical Viscoelastic Properties of Gelatin at the Gel Point*. *Rheologica Acta*, 1993. **32**(1): p. 94-103.
84. Macsuga, D., *Thermal Transitions in Gelatin: Optical Rotation and Enthalpy Changes*. *Biopolymers: Original Research on Biomolecules*, 1972. **11**(12): p. 2521-2532.
85. Petrie, S. and R. Becker, *Thermal Behavior of Aqueous Gelatin Solutions*, in *Analytical Calorimetry*. 1970, Springer. p. 225-238.
86. Borchard, W., et al., *Thermodynamische Eigenschaften des Systems Gelatine—Wasser*, in *Kolloidchemie Heute II*. 1976, Springer. p. 120-129.
87. Bloom, O.T., *Machine for Testing Jelly Strength of Glues, Gelatins and the Like*. 1923.
88. *Wichtige Kennzahlen von Gelatine*. 2020 [cited 2020 19.06.2020]; Available from: <http://www.parmentier.de/gpfneu/gelatine/deutsch/kennzahl.php>.
89. Janus, J., A. Kenchington, and A. Ward, *A Rapid Method for the Determination of the Isoelectric Point of Gelatin Using Mixed Bed Deionization*. *Research*, 1951. **4**: p. 247-248.
90. Côté, M.-F., et al., *Denatured Collagen as Support for a FGF-2 Delivery System: Physicochemical Characterizations and In Vitro Release Kinetics and Bioactivity*. *Biomaterials*, 2004. **25**(17): p. 3761-3772.
91. [cited 2018 2018-04-22]; Available from: [https://web.expasy.org/compute\\_pi/pi\\_tool-doc.html](https://web.expasy.org/compute_pi/pi_tool-doc.html)[https://web.expasy.org/compute\\_pi/pi\\_tool-doc.html](https://web.expasy.org/compute_pi/pi_tool-doc.html).
92. Kock, L.M., et al., *RGD-Dependent Integrins are Mechanotransducers in Dynamically Compressed Tissue-Engineered Cartilage Constructs*. *Journal of Biomechanics*, 2009. **42**(13): p. 2177-2182.
93. Klotz, B.J., et al., *Gelatin-Methacryloyl Hydrogels: Towards Biofabrication-Based Tissue Repair*. *Trends in Biotechnology*, 2016. **34**(5): p. 394-407.
94. Claaßen, C., et al., *Quantification of Substitution of Gelatin Methacryloyl: Best Practice and Current Pitfalls*. *Biomacromolecules*, 2018. **19**(1): p. 42-52.

95. Rebers, L., et al., *Physical Interactions Strengthen Chemical Gelatin Methacryloyl Gels*. *Gels*, 2019. **5**(1): p. 4-16.
96. Sewald, L., et al., *Beyond the Modification Degree: Impact of Raw Material on Physicochemical Properties of Gelatin Type A and Type B Methacryloyls*. *Macromolecular Bioscience*, 2018. **18**(12): p. 1800168-1800177.
97. Stier, S., et al., *Advanced Formulation of Methacryl- and Acetyl-Modified Biomolecules to Achieve Independent Control of Swelling and Stiffness in Printable Hydrogels*. *Journal of Materials Science: Materials in Medicine*, 2019. **30**(3): p. 35-44.
98. Barbetta, A., et al., *Scaffolds Based on Biopolymeric Foams*. *Advanced Functional Materials*, 2005. **15**(1): p. 118-124.
99. Dubrue, P., et al., *Porous Gelatin Hydrogels: 2. In Vitro Cell Interaction Study*. *Biomacromolecules*, 2007. **8**(2): p. 338-344.
100. Sutter, M., et al., *Recombinant Gelatin Hydrogels for the Sustained Release of Proteins*. *Journal of Controlled Release*, 2007. **119**(3): p. 301-312.
101. Van Vlierberghe, S., et al., *Toward Modulating the Architecture of Hydrogel Scaffolds: Curtains Versus Channels*. *Journal of Materials Science: Materials in Medicine*, 2008. **19**(4): p. 1459-1466.
102. Benton, J.A., et al., *Photocrosslinking of Gelatin Macromers to Synthesize Porous Hydrogels That Promote Valvular Interstitial Cell Function*. *Tissue Engineering Part A*, 2009. **15**(11): p. 3221-3230.
103. Peters, K., et al., *A New Approach for Adipose Tissue Regeneration Based on Human Mesenchymal Stem Cells in Contact to Hydrogels-an In Vitro Study*. *Advanced Engineering Materials*, 2009. **11**(10): p. B155-B161.
104. Aubin, H., et al., *Directed 3D Cell Alignment and Elongation in Microengineered Hydrogels*. *Biomaterials*, 2010. **31**(27): p. 6941-6951.
105. Liu, Y.X. and M.B. Chan-Park, *A Biomimetic Hydrogel Based on Methacrylated Dextran-Graft-Lysine and Gelatin for 3D Smooth Muscle Cell Culture*. *Biomaterials*, 2010. **31**(6): p. 1158-1170.
106. Nichol, J.W., et al., *Cell-Laden Microengineered Gelatin Methacrylate Hydrogels*. *Biomaterials*, 2010. **31**(21): p. 5536-5544.
107. Qi, H., et al., *Patterned Differentiation of Individual Embryoid Bodies in Spatially Organized 3D Hybrid Microgels*. *Advanced Materials*, 2010. **22**(46): p. 5276-5281.
108. Engelhardt, S., et al., *Fabrication of 2D Protein Microstructures and 3D Polymer-Protein Hybrid Microstructures by Two-Photon Polymerization*. *Biofabrication*, 2011. **3**(2): p. 025003-025011.
109. Hutson, C.B., et al., *Synthesis and Characterization of Tunable Poly(ethylene glycol): Gelatin Methacrylate Composite Hydrogels*. *Tissue Engineering Part A*, 2011. **17**(13-14): p. 1713-1723.
110. Ovsianikov, A., et al., *Laser Fabrication of Three-Dimensional CAD Scaffolds from Photosensitive Gelatin for Applications in Tissue Engineering*. *Biomacromolecules*, 2011. **12**(4): p. 851-858.
111. Ovsianikov, A., et al., *Laser Fabrication of 3D Gelatin Scaffolds for the Generation of Bioartificial Tissues*. *Materials*, 2011. **4**(1): p. 288-299.
112. Van Vlierberghe, S., S.K. Samal, and P. Dubrue, *Development of Mechanically Tailored Gelatin-Chondroitin Sulphate Hydrogel Films*. *Macromolecular Symposia*, 2011. **309-310**(1): p. 173-181.
113. Van Vlierberghe, S., et al., *Gelatin Functionalization of Biomaterial Surfaces: Strategies for Immobilization and Visualization*. *Polymers*, 2011. **3**(1): p. 114-130.
114. Xiao, W., et al., *Synthesis and Characterization of Photocrosslinkable Gelatin and Silk Fibroin Interpenetrating Polymer Network Hydrogels*. *Acta Biomaterialia*, 2011. **7**(6): p. 2384-2393.
115. Chen, Y.-C., et al., *Functional Human Vascular Network Generated in Photocrosslinkable Gelatin Methacrylate Hydrogels*. *Advanced Functional Materials*, 2012. **22**(10): p. 2027-2039.
116. De Cock, L.J., et al., *Engineered (hep/pARG)(2) Polyelectrolyte Capsules for Sustained Release of Bioactive TGF-beta 1*. *Soft Matter*, 2012. **8**(4): p. 1146-1154.
117. Dragusin, D.M., et al., *Novel Gelatin-PHEMA Porous Scaffolds for Tissue Engineering Applications*. *Soft Matter*, 2012. **8**(37): p. 9589-9602.
118. Fan, Y.T., et al., *Single Neuron Capture and Axonal Development in Three-Dimensional Microscale Hydrogels*. *Lab on a Chip*, 2012. **12**(22): p. 4724-4731.

119. Gauvin, R., et al., *Microfabrication of Complex Porous Tissue Engineering Scaffolds Using 3D Projection Stereolithography*. *Biomaterials*, 2012. **33**(15): p. 3824-3834.
120. Hoch, E., et al., *Stiff Gelatin Hydrogels Can be Photo-Chemically Synthesized from Low Viscous Gelatin Solutions Using Molecularly Functionalized Gelatin with a High Degree of Methacrylation*. *Journal of Materials Science: Materials in Medicine*, 2012. **23**(11): p. 2607-2617.
121. Nikkhah, M., et al., *Directed Endothelial Cell Morphogenesis in Micropatterned Gelatin Methacrylate Hydrogels*. *Biomaterials*, 2012. **33**(35): p. 9009-9018.
122. Ramón-Azcón, J., et al., *Gelatin Methacrylate as a Promising Hydrogel for 3D Microscale Organization and Proliferation of Dielectrophoretically Patterned Cells*. *Lab On a Chip*, 2012. **12**(16): p. 2959-2969.
123. Shin, H., B.D. Olsen, and A. Khademhosseini, *The Mechanical Properties and Cytotoxicity of Cell-Laden Double-Network Hydrogels Based on Photocrosslinkable Gelatin and Gellan Gum Biomacromolecules*. *Biomaterials*, 2012. **33**(11): p. 3143-3152.
124. Billiet, T., et al., *Quantitative Contrasts in the Photopolymerization of Acrylamide and Methacrylamide-Functionalized Gelatin Hydrogel Building Blocks*. *Macromolecular Bioscience*, 2013. **13**(11): p. 1531-1545.
125. Hoch, E., et al., *Chemical Tailoring of Gelatin to Adjust its Chemical and Physical Properties for Functional Bioprinting*. *Journal of Materials Chemistry B*, 2013. **1**(41): p. 5675-5685.
126. Lin, R.Z., et al., *Transdermal Regulation of Vascular Network Bioengineering Using a Photopolymerizable Methacrylated Gelatin Hydrogel*. *Biomaterials*, 2013. **34**(28): p. 6785-6796.
127. Pedron, S. and B. Harley, *Impact of the Biophysical Features of a 3D Gelatin Microenvironment on Glioblastoma Malignancy*. *Journal of Biomedical Materials Research Part A*, 2013. **101**(12): p. 3404-3415.
128. Shin, S.R., et al., *Carbon-Nanotube-Embedded Hydrogel Sheets for Engineering Cardiac Constructs and Bioactuators*. *ACS Nano*, 2013. **7**(3): p. 2369-2380.
129. Soman, P., et al., *Digital Microfabrication of User-Defined 3D Microstructures in Cell-Laden Hydrogels*. *Biotechnology and Bioengineering*, 2013. **110**(11): p. 3038-3047.
130. Tan, G.X., et al., *Biomimetically-Mineralized Composite Coatings on Titanium Functionalized with Gelatin Methacrylate Hydrogels*. *Applied Surface Science*, 2013. **279**: p. 293-299.
131. Ahadian, S., et al., *Facile and Rapid Generation of 3D Chemical Gradients within Hydrogels for High-Throughput Drug Screening Applications*. *Biosensors and Bioelectronics*, 2014. **59**: p. 166-173.
132. Billiet, T., et al., *The 3D Printing of Gelatin Methacrylamide Cell-Laden Tissue-Engineered Constructs with High Cell Viability*. *Biomaterials*, 2014. **35**(1): p. 49-62.
133. Boere, K.W.M., et al., *Covalent Attachment of a Three-Dimensionally Printed Thermoplastic to a Gelatin Hydrogel for Mechanically Enhanced Cartilage Constructs*. *Acta Biomaterialia*, 2014. **10**(6): p. 2602-2611.
134. Chan, K.M.C., et al., *Functionalizable Hydrogel Microparticles of Tunable Size and Stiffness for Soft-Tissue Filler Applications*. *Acta Biomaterialia*, 2014. **10**(6): p. 2563-2573.
135. Coimbra, P., M.H. Gil, and M. Figueiredo, *Tailoring the Properties of Gelatin Films for Drug Delivery Applications: Influence of the Chemical Cross-Linking Method*. *International Journal of Biological Macromolecules*, 2014. **70**: p. 10-19.
136. Daniele, M.A., et al., *Interpenetrating Networks Based on Gelatin Methacrylamide and PEG Formed Using Concurrent Thiol Click Chemistries for Hydrogel Tissue Engineering Scaffolds*. *Biomaterials*, 2014. **35**(6): p. 1845-1856.
137. Fathi, A., et al., *Enhancing the Mechanical Properties and Physical Stability of Biomimetic Polymer Hydrogels for Micro-Patterning and Tissue Engineering Applications*. *European Polymer Journal*, 2014. **59**: p. 161-170.
138. Gevaert, E., et al., *Galactose-Functionalized Gelatin Hydrogels Improve the Functionality of Encapsulated Hepg2 Cells*. *Macromolecular Bioscience*, 2014. **14**(3): p. 419-427.
139. Heo, D.N., et al., *Enhanced Bone Regeneration with a Gold Nanoparticle-Hydrogel Complex*. *Journal of Materials Chemistry B*, 2014. **2**(11): p. 1584-1593.

140. Jung, J. and J. Oh, *Cell-Induced Flow-Focusing Instability in Gelatin Methacrylate Microdroplet Generation*. *Biomicrofluidics*, 2014. **8**(3): p. 036503-036509.
141. Kaemmerer, E., et al., *Gelatin Methacrylamide-Based Hydrogels: An Alternative Three-Dimensional Cancer Cell Culture System*. *Acta Biomaterialia*, 2014. **10**(6): p. 2551-2562.
142. Kim, J., et al., *Cell-Friendly Inverse Opal-Like Hydrogels for a Spatially Separated Co-Culture System*. *Macromolecular Rapid Communications*, 2014. **35**(18): p. 1578-1586.
143. Kolesky, D.B., et al., *3D Bioprinting of Vascularized, Heterogeneous Cell-Laden Tissue Constructs*. *Advanced Materials*, 2014. **26**(19): p. 3124-3130.
144. Lin, H., et al., *Cartilage Tissue Engineering Application of Injectable Gelatin Hydrogel with In Situ Visible-Light-Activated Gelation Capability in Both Air and Aqueous Solution*. *Tissue Engineering Part A*, 2014. **20**(17-18): p. 2402-2411.
145. Lin, H., et al., *Stem Cell-Based Microphysiological Osteochondral System to Model Tissue Response to Interleukin-1 beta*. *Molecular Pharmaceutics*, 2014. **11**(7): p. 2203-2212.
146. Melchels, F.P.W., et al., *Development and Characterisation of a New Biopink for Additive Tissue Manufacturing*. *Journal of Materials Chemistry B*, 2014. **2**(16): p. 2282-2289.
147. Nemeth, C.L., et al., *Enhanced Chondrogenic Differentiation of Dental Pulp Stem Cells Using Nanopatterned PEG-GelMA-HA Hydrogels*. *Tissue Engineering Part A*, 2014. **20**(21-22): p. 2817-2829.
148. Ovsianikov, A., et al., *Laser Photofabrication of Cell-Containing Hydrogel Constructs*. *Langmuir*, 2014. **30**(13): p. 3787-3794.
149. Serafim, A., et al., *One-Pot Synthesis of Superabsorbent Hybrid Hydrogels Based on Methacrylamide Gelatin and Polyacrylamide. Effortless Control of Hydrogel Properties Through Composition Design*. *New Journal of Chemistry*, 2014. **38**(7): p. 3112-3126.
150. Sirova, M., et al., *Immunocompatibility Evaluation of Hydrogel-Coated Polyimide Implants for Applications in Regenerative Medicine*. *Journal of Biomedical Materials Research Part A*, 2014. **102**(6): p. 1982-1990.
151. Zhou, L., et al., *Biomimetic Mineralization of Anionic Gelatin Hydrogels: Effect of Degree of Methacrylation*. *RSC Advances*, 2014. **4**(42): p. 21997-22008.
152. Chen, Y., et al., *A Universal and Facile Approach for the Formation of a Protein Hydrogel for 3D Cell Encapsulation*. *Advanced Functional Materials*, 2015. **25**(39): p. 6189-6198.
153. Gao, G.F., et al., *Improved Properties of Bone and Cartilage Tissue from 3D Inkjet-Bioprinted Human Mesenchymal Stem Cells by Simultaneous Deposition and Photocrosslinking in PEG-GelMA*. *Biotechnology Letters*, 2015. **37**(11): p. 2349-2355.
154. Graulus, G.J., et al., *Cross-Linkable Alginate-Graft-Gelatin Copolymers for Tissue Engineering Applications*. *European Polymer Journal*, 2015. **72**: p. 494-506.
155. Hasan, A., et al., *A Multilayered Microfluidic Blood Vessel-Like Structure*. *Biomedical Microdevices*, 2015. **17**(5): p. 88-30.
156. Jeon, O., D.W. Wolfson, and E. Alsberg, *In-Situ Formation of Growth-Factor-Loaded Coacervate Microparticle-Embedded Hydrogels for Directing Encapsulated Stem Cell Fate*. *Advanced Materials*, 2015. **27**(13): p. 2216-2223.
157. Lee, B.H., et al., *Efficient and Controllable Synthesis of Highly Substituted Gelatin Methacrylamide for Mechanically Stiff Hydrogels*. *RSC Advances*, 2015. **5**(128): p. 106094-106097.
158. Sadat-Shojai, M., M.T. Khorasani, and A. Jamshidi, *3-Dimensional Cell-Laden Nano-Hydroxyapatite/Protein Hydrogels for Bone Regeneration Applications*. *Materials Science & Engineering C: Materials for Biological Applications*, 2015. **49**: p. 835-843.
159. Saini, H., et al., *3D Cardiac Microtissues Encapsulated with the Co-Culture of Cardiomyocytes and Cardiac Fibroblasts*. *Advanced Healthcare Materials*, 2015. **4**(13): p. 1961-1971.
160. Saraiva, S.M., et al., *Synthesis and Characterization of a Photocrosslinkable Chitosan-Gelatin Hydrogel Aimed for Tissue Regeneration*. *RSC Advances*, 2015. **5**(78): p. 63478-63488.
161. Shi, X., et al., *Microfluidic Spinning of Cell-Responsive Grooved Microfibers*. *Advanced Functional Materials*, 2015. **25**(15): p. 2250-2259.

162. Suo, H.R., K.D. Xu, and X.X. Zheng, *Using Glucosamine to Improve the Properties of Photocrosslinked Gelatin Scaffolds*. Journal of Biomaterials Applications, 2015. **29**(7): p. 977-987.
163. Van Hoorick, J., et al., *Indirect Additive Manufacturing as an Elegant Tool for the Production of Self-Supporting Low Density Gelatin Scaffolds*. Journal of Materials Science: Materials in Medicine, 2015. **26**(10): p. 247-256.
164. Van Nieuwenhove, I., et al., *Photo-Crosslinkable Biopolymers Targeting Stem Cell Adhesion and Proliferation: the Case Study of Gelatin and Starch-Based IPNs*. Journal of Materials Science: Materials in Medicine, 2015. **26**(2): p. 104-111.
165. Visser, J., et al., *Endochondral Bone Formation in Gelatin Methacrylamide Hydrogel with Embedded Cartilage-Derived Matrix Particles*. Biomaterials, 2015. **37**: p. 174-182.
166. Wei, D., et al., *A Biocompatible Hydrogel with Improved Stiffness and Hydrophilicity for Modular Tissue Engineering Assembly*. Journal of Materials Chemistry B, 2015. **3**(14): p. 2753-2763.
167. Albrecht, L.D., S.W. Sawyer, and P. Soman, *Developing 3D Scaffolds in the Field of Tissue Engineering to Treat Complex Bone Defects*. 3D Printing and Additive Manufacturing, 2016. **3**(2): p. 106-112.
168. Arya, A.D., et al., *Gelatin Methacrylate Hydrogels as Biomimetic Three-Dimensional Matrixes for Modeling Breast Cancer Invasion and Chemoresponse in Vitro*. ACS Applied Materials & Interfaces, 2016. **8**(34): p. 22005-22017.
169. Barati, D., et al., *Spatiotemporal Release of BMP-2 and VEGF Enhances Osteogenic and Vasculogenic Differentiation of Human Mesenchymal Stem Cells and Endothelial Colony-Forming Cells Co-Encapsulated in a Patterned Hydrogel*. Journal of Controlled Release, 2016. **223**: p. 126-136.
170. Bartnikowski, M., et al., *A Hydrogel Model Incorporating 3D-Plotted Hydroxyapatite for Osteochondral Tissue*. Materials, 2016. **9**(4): p. 285-301.
171. Chen, H., et al., *Quickly Promoting Angiogenesis by using a DFO-Loaded Photo-Crosslinked Gelatin Hydrogel for Diabetic Skin Regeneration*. Journal of Materials Chemistry B, 2016. **4**(21): p. 3770-3781.
172. Chen, P.F., et al., *Intra-Articular Delivery of Sinomenium Encapsulated by Chitosan Microspheres and Photo-Crosslinked GelMA Hydrogel Ameliorates Osteoarthritis by Effectively Regulating Autophagy*. Biomaterials, 2016. **81**: p. 1-13.
173. Correia, T.R., et al., *Development of UV Cross-Linked Gelatin Coated Electrospun Poly(caprolactone) Fibrous Scaffolds for Tissue Engineering*. International Journal of Biological Macromolecules, 2016. **93**: p. 1539-1548.
174. Daly, A.C., et al., *3D Bioprinting of Developmentally Inspired Templates for Whole Bone Organ Engineering*. Advanced Healthcare Materials, 2016. **5**(18): p. 2353-2362.
175. Fang, X.X., et al., *Biomimetic Gelatin Methacrylamide Hydrogel Scaffolds for Bone Tissue Engineering*. Journal of Materials Chemistry B, 2016. **4**(6): p. 1070-1080.
176. Feng, Q., et al., *Mechanically Resilient, Injectable, and Bioadhesive Supramolecular Gelatin Hydrogels Crosslinked by Weak Host-Guest Interactions Assist Cell Infiltration and In Situ Tissue Regeneration*. Biomaterials, 2016. **101**: p. 217-228.
177. Hoch, E., G.E. Tovar, and K. Borchers, *Biopolymer-Based Hydrogels for Cartilage Tissue Engineering*. Bioinspired Biomimetic and Nanobiomaterials, 2016. **5**(2): p. 51-66.
178. Houben, A., et al., *Indirect Solid Freeform Fabrication of an Initiator-Free Photocrosslinkable Hydrogel Precursor for the Creation of Porous Scaffolds*. Macromolecular Bioscience, 2016. **16**(12): p. 1883-1894.
179. Kadri, R., et al., *Preparation and Characterization of Nanofunctionalized Alginate/Methacrylated Gelatin Hybrid Hydrogels*. RSC Advances, 2016. **6**(33): p. 27879-27884.
180. Kim, J., et al., *Skin Penetration-Inducing Gelatin Methacryloyl Nanogels for Transdermal Macromolecule Delivery*. Macromolecular Research, 2016. **24**(12): p. 1115-1125.
181. Knowlton, S., et al., *3D-Printed Microfluidic Chips with Patterned, Cell-Laden Hydrogel Constructs*. Biofabrication, 2016. **8**(2): p. 025019.

182. Kuo, C.Y., et al., *Development of a 3D Printed, Bioengineered Placenta Model to Evaluate the Role of Trophoblast Migration in Preeclampsia*. ACS Biomaterials Science & Engineering, 2016. **2**(10): p. 1817-1826.
183. Kuo, Y.C. and Y.C. Chen, *Regeneration of Neurite-Like Cells from Induced Pluripotent Stem Cells in Self-Assembled Hyaluronic Acid-Gelatin Microhydrogel*. Journal of the Taiwan Institute of Chemical Engineers, 2016. **67**: p. 74-87.
184. Li, C., C. Mu, and W. Lin, *Novel Hemocompatible Nanocomposite Hydrogels Crosslinked with Methacrylated Gelatin*. RSC Advances 2016. **6**(49): p. 43663-43671.
185. Li, X., et al., *3D Culture of Chondrocytes in Gelatin Hydrogels with Different Stiffness*. Polymers, 2016. **8**(8): p. 269.
186. Lim, K.S., et al., *New Visible-Light Photoinitiating System for Improved Print Fidelity in Gelatin-Based Bioinks*. ACS Biomaterials Science & Engineering, 2016. **2**(10): p. 1752-1762.
187. Lin, C.H., et al., *Antioxidant N-Acetylcysteine and Glutathione Increase the Viability and Proliferation of MG63 Cells Encapsulated in the Gelatin Methacrylate/VA-086/Blue Light Hydrogel System*. Tissue Engineering Part C: Methods, 2016. **22**(8): p. 792-800.
188. Navaei, A., et al., *Gold Nanorod-Incorporated Gelatin-Based Conductive Hydrogels for Engineering Cardiac Tissue Constructs*. Acta Biomaterialia, 2016. **41**: p. 133-146.
189. O'Connell, C.D., et al., *Development of the Biopen: a Handheld Device for Surgical Printing of Adipose Stem Cells at a Chondral Wound Site*. Biofabrication, 2016. **8**(1): p. 015019.
190. Peela, N., et al., *A Three Dimensional Micropatterned Tumor Model for Breast Cancer Cell Migration Studies*. Biomaterials, 2016. **81**: p. 72-83.
191. Sadat-Shojai, M., M.T. Khorasani, and A. Jamshidi, *A New Strategy for Fabrication of Bone Scaffolds Using Electrospun Nano-HAp/PHB Fibers and Protein Hydrogels*. Chemical Engineering Journal, 2016. **289**: p. 38-47.
192. Samorezov, J.E., et al., *Sustained Presentation of BMP-2 Enhances Osteogenic Differentiation of Human Adipose-Derived Stem Cells in Gelatin Hydrogels*. Journal of Biomedical Materials Research Part A, 2016. **104**(6): p. 1387-1397.
193. Sawyer, S., et al., *Behavior of Encapsulated Saos-2 Cells within Gelatin Methacrylate Hydrogels*. Journal of Tissue Science & Engineering, 2016. **7**(2): p. 1000173-1000179.
194. Shirahama, H., et al., *Precise Tuning of Facile One-Pot Gelatin Methacryloyl (GelMA) Synthesis*. Scientific Reports, 2016. **6**: p. 1-11.
195. Shirazi, A.N., et al., *A Novel Strategy for Softening Gelatin-Bioactive-Glass Hybrids*. ACS Applied Materials & Interfaces, 2016. **8**(3): p. 1676-1686.
196. Steyaert, I., et al., *Gelatin Nanofibers: Analysis of Triple Helix Dissociation Temperature and Cold-Water-Solubility*. Food Hydrocolloids, 2016. **57**: p. 200-208.
197. Van Nieuwenhove, I., et al., *Gelatin- and Starch-Based Hydrogels. Part A: Hydrogel Development, Characterization and Coating*. Carbohydrate Polymers, 2016. **152**: p. 129-139.
198. Van Vlierberghe, S., *Crosslinking Strategies for Porous Gelatin Scaffolds*. Journal of Materials Science, 2016. **51**(9): p. 4349-4357.
199. Waters, R., et al., *Stem Cell Secretome-Rich Nanoclay Hydrogel: a Dual Action Therapy for Cardiovascular Regeneration*. Nanoscale, 2016. **8**(14): p. 7371-7376.
200. Wu, W., et al., *Fabrication of a Photo-Crosslinked Gelatin Hydrogel for Preventing Abdominal Adhesion*. RSC Advances, 2016. **6**(95): p. 92449-92453.
201. Wu, Y., et al., *Fabrication of Conductive Gelatin Methacrylate-Polyaniline Hydrogels*. Acta Biomaterialia, 2016. **33**: p. 122-130.
202. Yoon, H.J., et al., *Cold Water Fish Gelatin Methacryloyl Hydrogel for Tissue Engineering Application*. PLOS ONE, 2016. **11**(10): p. e0163902.
203. Zhao, X., et al., *Photocrosslinkable Gelatin Hydrogel for Epidermal Tissue Engineering*. Advanced Healthcare Materials, 2016. **5**(1): p. 108-118.
204. Zhao, X., et al., *Injectable Stem Cell-Laden Photocrosslinkable Microspheres Fabricated Using Microfluidics for Rapid Generation of Osteogenic Tissue Constructs*. Advanced Functional Materials, 2016. **26**(17): p. 2809-2819.
205. Zhou, X., et al., *3D Bioprinting a Cell-Laden Bone Matrix for Breast Cancer Metastasis Study*. ACS Applied Materials & Interfaces, 2016. **8**(44): p. 30017-30026.

206. Zhuang, H., et al., *Gelatin-Methacrylamide Gel Loaded with Microspheres to Deliver GDNF in Bilayer Collagen Conduit Promoting Sciatic Nerve Growth*. International Journal of Nanomedicine, 2016. **11**: p. 1383-1394.
207. Aldana, A.A., et al., *Temperature-Sensitive Biocompatible IPN Hydrogels Based on Poly (NIPA-PEGd<sub>ma</sub>) and Photocrosslinkable Gelatin Methacrylate*. Soft Materials, 2017. **15**(4): p. 341-349.
208. Bertlein, S., et al., *Thiol-Ene Clickable Gelatin: A Platform Bioink for Multiple 3D Biofabrication Technologies*. Advanced Materials, 2017. **29**(44): p. 173404.
209. Brigo, L., et al., *3D High-Resolution Two-Photon Crosslinked Hydrogel Structures for Biological Studies*. Acta Biomaterialia, 2017. **55**: p. 373-384.
210. Brown, G.C.J., et al., *Covalent Incorporation of Heparin Improves Chondrogenesis in Photocurable Gelatin-Methacryloyl Hydrogels*. Macromolecular Bioscience, 2017. **17**(12).
211. Cha, B.H., et al., *Integrin-Mediated Interactions Control Macrophage Polarization in 3D Hydrogels*. Advanced Healthcare Materials, 2017. **6**(21).
212. Chen, P.F., et al., *The Amelioration of Cartilage Degeneration by Photo-Crosslinked GelHA Hydrogel and Crizotinib Encapsulated Chitosan Microspheres*. Oncotarget, 2017. **8**(18): p. 30235-30251.
213. Costantini, M., et al., *Engineering Muscle Networks in 3D Gelatin Methacryloyl Hydrogels: Influence of Mechanical Stiffness and Geometrical Confinement*. Frontiers in Bioengineering and Biotechnology, 2017. **5**: p. 22.
214. Duchi, S., et al., *Handheld co-axial bioprinting: application to in situ surgical cartilage repair*. Scientific reports, 2017. **7**(1): p. 1-12.
215. Giustina, G.D., et al., *Hydrogel with Orthogonal Reactive Units: 2D and 3D Cross-Linking Modulation*. Macromolecular Rapid Communications, 2017. **38**(1): p. 1600570.
216. Han, L., et al., *Biohybrid Methacrylated Gelatin/Polyacrylamide Hydrogels for Cartilage Repair*. Journal of Materials Chemistry B, 2017. **5**(4): p. 731-741.
217. Htwe, S.S., et al., *Role of Rho-Associated Coiled-Coil Forming Kinase Isoforms in Regulation of Stiffness-Induced Myofibroblast Differentiation in Lung Fibrosis*. American Journal of Respiratory Cell and Molecular Biology, 2017. **56**(6): p. 772-783.
218. Kerscher, P., et al., *Direct Production of Human Cardiac Tissues by Pluripotent Stem Cell Encapsulation in Gelatin Methacryloyl*. ACS Biomaterials Science & Engineering, 2017. **3**(8): p. 1499-1509.
219. Kessler, L., et al., *Methacrylated Gelatin/Hyaluronan-Based Hydrogels for Soft Tissue Engineering*. Journal of Tissue Engineering, 2017. **8**: p. 1-14.
220. Kim, J.W., et al., *Fabrication of Bi-Layer Scaffold of Keratin Nanofiber and Gelatin-Methacrylate Hydrogel: Implications for Skin Graft*. International Journal of Biological Macromolecules, 2017. **105**: p. 541-548.
221. Lee, B.H., et al., *Colloidal Templating of Highly Ordered Gelatin Methacryloyl-Based Hydrogel Platforms for Three-Dimensional Tissue Analogues*. NPG Asia Materials, 2017. **9**(7): p. e412-e412.
222. McBeth, C., et al., *3D Bioprinting of GelMA Scaffolds Triggers Mineral Deposition by Primary Human Osteoblasts*. Biofabrication, 2017. **9**(1).
223. Mistry, P., et al., *Bioprinting Using Mechanically Robust Core-Shell Cell-Laden Hydrogel Strands*. Macromolecular Bioscience, 2017. **17**(6).
224. Ouyang, L.L., et al., *A Generalizable Strategy for the 3D Bioprinting of Hydrogels from Nonviscous Photo-Crosslinkable Inks*. Advanced Materials, 2017. **29**(8).
225. Pacelli, S., et al., *Controlling Adult Stem Cell Behavior Using Nanodiamond-Reinforced Hydrogel: Implication in Bone Regeneration Therapy*. Scientific Reports, 2017. **7**: p. 1-15.
226. Puckert, C., et al., *Electro-Mechano Responsive Properties of Gelatin Methacrylate (GelMA) Hydrogel on Conducting Polymer Electrodes Quantified Using Atomic Force Microscopy*. Soft Matter, 2017. **13**(27): p. 4761-4772.
227. Rahali, K., et al., *Synthesis and Characterization of Nanofunctionalized Gelatin Methacrylate Hydrogels*. International Journal of Molecular Sciences, 2017. **18**(12): p. 2675-2689.

228. Resmi, R., et al., *Synthesis and Characterization of Silver Nanoparticle Incorporated Gelatin-Hydroxypropyl Methacrylate Hydrogels for Wound Dressing Applications*. Journal of Applied Polymer Science, 2017. **134**(10): p. 44529-44537.
229. Stratesteffen, H., et al., *GelMA-Collagen Blends Enable Drop-On-Demand 3D Printability and Promote Angiogenesis*. Biofabrication, 2017. **9**(4): p. 045002.
230. Wang, Z.J., et al., *Comparative Study of Gelatin Methacrylate Hydrogels from Different Sources for Biofabrication Applications*. Biofabrication, 2017. **9**(4): p. 044101.
231. Wilkens, C.A., et al., *Layer-by-Layer Approach for a Uniformed Fabrication of a Cell Patterned Vessel-Like Construct*. Biofabrication, 2017. **9**(1).
232. Wu, B.Z., et al., *Microencapsulation of 1-Hexadecanol as a Phase Change Material with Reversible Thermochromic Properties*. RSC Advances, 2017. **7**(67): p. 42129-42137.
233. Xin, T.W., et al., *Inorganic Strengthened Hydrogel Membrane as Regenerative Periosteum*. ACS Applied Materials & Interfaces, 2017. **9**(47): p. 41168-41180.
234. Bektas, C.K. and V. Hasirci, *Mimicking Corneal Stroma Using Keratocyte-Loaded Photopolymerizable Methacrylated Gelatin Hydrogels*. Journal of Tissue Engineering and Regenerative Medicine, 2018. **12**(4): p. e1899-e1910.
235. Chakravarti, A.R., et al., *Pre-Conditioning Stem Cells in a Biomimetic Environment for Enhanced Cardiac Tissue Repair: In Vitro and In Vivo Analysis*. Cellular and Molecular Bioengineering, 2018. **11**(5): p. 321-336.
236. Chen, C.S., et al., *Three-Dimensionally Printed Silk-Sericin-Based Hydrogel Scaffold: A Promising Visualized Dressing Material for Real-Time Monitoring of Wounds*. ACS Applied Materials & Interfaces, 2018. **10**(40): p. 33879-33890.
237. Donaldson, A.R., et al., *Photocrosslinkable Gelatin Hydrogels Modulate the Production of the Major Pro-inflammatory Cytokine, TNF-alpha, by Human Mononuclear Cells*. Frontiers in Bioengineering and Biotechnology, 2018. **6**: p. 116.
238. Fan, L., et al., *Directing Induced Pluripotent Stem Cell Derived Neural Stem Cell Fate with a Three-Dimensional Biomimetic Hydrogel for Spinal Cord Injury Repair*. ACS Applied Materials & Interfaces, 2018. **10**(21): p. 17742-17755.
239. Frey, L., et al., *A Dual-Layered Microfluidic System for Long-Term Controlled In Situ Delivery of Multiple Anti-Inflammatory Factors for Chronic Neural Applications*. Advanced Functional Materials, 2018. **28**(12): p. 1702009.
240. García-Lizarriar, A., et al., *Composite Biomaterials as Long-Lasting Scaffolds for 3D Bioprinting of Highly Aligned Muscle Tissue*. Macromolecular Bioscience, 2018. **18**(10): p. 1800167.
241. Grix, T., et al., *Bioprinting Perfusion-Enabled Liver Equivalents for Advanced Organ-on-a-Chip Applications*. Genes, 2018. **9**(4): p. 176.
242. Huang, Z., et al., *Injectable Polyphosphazene/Gelatin Hybrid Hydrogel for Biomedical Applications*. Materials & Design, 2018. **160**: p. 1137-1147.
243. Klotz, B.J., et al., *Engineering of a Complex Bone Tissue Model with Endothelialised Channels and Capillary-Like Networks* European Cells & Materials, 2018. **35**: p. 335-349.
244. Kuo, C.Y., et al., *Placental Basement Membrane Proteins are Required for Effective Cytotrophoblast Invasion in a Three-Dimensional Bioprinted Placenta Model*. Journal of Biomedical Materials Research Part A, 2018. **106**(6): p. 1476-1487.
245. Lin, C.H., et al., *Stiffness Modification of Photopolymerizable Gelatin-Methacrylate Hydrogels Influences Endothelial Differentiation of Human Mesenchymal Stem Cells*. Journal of Tissue Engineering and Regenerative Medicine, 2018. **12**(10): p. 2099-2111.
246. Liu, B.C., et al., *Hydrogen Bonds Autonomously Powered Gelatin Methacrylate Hydrogels with Super-Elasticity, Self-Heal and Underwater Self-Adhesion for Sutureless Skin and Stomach Surgery and E-Skin*. Biomaterials, 2018. **171**: p. 83-96.
247. Liu, L., et al., *Injectable Alendronate-Functionalized GelMA Hydrogels for Mineralization and Osteogenesis*. RSC Advances, 2018. **8**(40): p. 22764-22776.
248. Ma, C., et al., *Bio-Inspired Micropatterned Platforms Recapitulate 3D Physiological Morphologies of Bone and Dentinal Cells*. Advanced Science, 2018. **5**(12): p. 1801037.
249. Meinert, C., et al., *A Method for Prostate and Breast Cancer Cell Spheroid Cultures Using Gelatin Methacryloyl-Based Hydrogels*, in *Prostate Cancer*. 2018, Springer. p. 175-194.



250. Miri, A.K., et al., *Permeability Mapping of Gelatin Methacryloyl Hydrogels*. *Acta Biomaterialia*, 2018. **77**: p. 38-47.
251. Modaresifar, K., A. Hadjizadeh, and H. Niknejad, *Design and Fabrication of GelMA/Chitosan Nanoparticles Composite Hydrogel for Angiogenic Growth Factor Delivery*. *Artificial Cells Nanomedicine and Biotechnology*, 2018. **46**(8): p. 1799-1808.
252. O'Connell, C.D., et al., *Tailoring the Mechanical Properties of Gelatin Methacryloyl Hydrogels Through Manipulation of the Photocrosslinking Conditions*. *Soft Matter*, 2018. **14**(11): p. 2142-2151.
253. Onofrillo, C., et al., *Biofabrication of Human Articular Cartilage: a Path Towards the Development of a Clinical Treatment*. *Biofabrication*, 2018. **10**(4): p. 045006.
254. Pacelli, S., et al., *Fabrication of a Double-Cross-Linked Interpenetrating Polymeric Network (IPN) Hydrogel Surface Modified with Polydopamine to Modulate the Osteogenic Differentiation of Adipose-Derived Stem Cells*. *ACS Applied Materials & Interfaces*, 2018. **10**(30): p. 24955-24962.
255. Ruland, A., et al., *A Contactless Approach for Monitoring the Mechanical Properties of Swollen Hydrogels*. *Soft Matter*, 2018. **14**(35): p. 7228-7236.
256. Sasaki, H., et al., *In Vitro Repair of Meniscal Radial Tear With Hydrogels Seeded With Adipose Stem Cells and TGF-beta 3*. *American Journal of Sports Medicine*, 2018. **46**(10): p. 2402-2413.
257. Sawyer, S.W., et al., *Perfusion Directed 3D Mineral Formation within Cell-Laden Hydrogels*. *Biofabrication*, 2018. **10**(3): p. 035013.
258. Serafim, A., et al., *Bicomponent Hydrogels Based on Methacryloyl Derivatives of Gelatin and Mucin with Potential Wound Dressing Applications*. *Materiale Plastice*, 2018. **55**(1): p. 68-74.
259. Shrimali, P., et al., *Efficient in situ Gene Delivery via PEG Diacrylate Matrices*. *Biomaterials Science*, 2018. **6**(12): p. 3241-3250.
260. Soucy, J.R., et al., *Photocrosslinkable Gelatin/Tropoelastin Hydrogel Adhesives for Peripheral Nerve Repair*. *Tissue Engineering Part A*, 2018. **24**(17-18): p. 1393-1405.
261. Spencer, A.R., et al., *Electroconductive Gelatin Methacryloyl-PEDOT:PSS Composite Hydrogels: Design, Synthesis, and Properties*. *ACS Biomaterials Science & Engineering*, 2018. **4**(5): p. 1558-1567.
262. Tytgat, L., et al., *Synergistic Effect of Kappa-Carrageenan and Gelatin Blends Towards Adipose Tissue Engineering*. *Carbohydrate Polymers*, 2018. **189**: p. 1-9.
263. Van Hoorick, J., et al., *Highly Reactive Thiol-Norbornene Photo-Click Hydrogels: Toward Improved Processability*. *Macromolecular Rapid Communications*, 2018. **39**(14): p. 1800181.
264. Wang, J., et al., *Responsive Graphene Oxide Hydrogel Microcarriers for Controllable Cell Capture and Release*. *Science China Materials*, 2018. **61**(10): p. 1314-1324.
265. Wang, X.P., et al., *3D Printed Enzymatically Biodegradable Soft Helical Microswimmers*. *Advanced Functional Materials*, 2018. **28**(45).
266. Wang, Y.H., et al., *Development of a Photo-Crosslinking, Biodegradable GelMA/PEGDA Hydrogel for Guided Bone Regeneration Materials*. *Materials*, 2018. **11**(8): p. 1345.
267. Wu, Y.w., W.c. Zhang, and R.j. Yang, *Ultralight and Low Thermal Conductivity Polyimide-Polyhedral Oligomeric Silsesquioxanes Aerogels*. *Macromolecular Materials and Engineering*, 2018. **303**(2): p. 1700403.
268. Yin, J., et al., *3D Bioprinting of Low-Concentration Cell-Laden Gelatin Methacrylate (GelMA) Bioinks with a Two-Step Cross-linking Strategy*. *ACS Applied Materials & Interfaces*, 2018. **10**(8): p. 6849-6857.
269. Yoon, S., et al., *Inkjet-Spray Hybrid Printing for 3D Freeform Fabrication of Multilayered Hydrogel Structures*. *Advanced Healthcare Materials*, 2018. **7**(14): p. 1800050.
270. Zhao, Q., et al., *Programmed Shape-Morphing Scaffolds Enabling Facile 3D Endothelialization*. *Advanced Functional Materials*, 2018. **28**(29): p. 1801027.
271. Zheng, J., et al., *Hydrolytic Stability of Methacrylamide and Methacrylate in Gelatin Methacryloyl and Decoupling of Gelatin Methacrylamide from Gelatin Methacryloyl through Hydrolysis*. *Macromolecular Chemistry and Physics*, 2018. **219**(18): p. 1800266.
272. Zhu, W., et al., *3D Bioprinting Mesenchymal Stem Cell-Laden Construct with Core-Shell Nanospheres for Cartilage Tissue Engineering*. *Nanotechnology*, 2018. **29**(18): p. 185101.

273. Aldana, A.A., et al., *Fabrication of Gelatin Methacrylate (GelMA) Scaffolds with Nano-and Micro-Topographical and Morphological Features*. *Nanomaterials*, 2019. **9**(1): p. 120.
274. Anada, T., et al., *Vascularized Bone-Mimetic Hydrogel Constructs by 3D Bioprinting to Promote Osteogenesis and Angiogenesis*. *International Journal of Molecular Sciences*, 2019. **20**(5): p. 1096.
275. Bahcecioglu, G., et al., *A 3D Printed PCL/Hydrogel Construct with Zone-Specific Biochemical Composition Mimicking that of the Meniscus*. *Biofabrication*, 2019. **11**(2): p. 025002.
276. Celikkin, N., et al., *Enhancing X-Ray Attenuation of 3D Printed Gelatin Methacrylate (GelMA) Hydrogels Utilizing Gold Nanoparticles for Bone Tissue Engineering Applications*. *Polymers*, 2019. **11**(2): p. 367.
277. Chandrasekharan, A., et al., *In Situ Photocrosslinkable Hyaluronic Acid-Based Surgical Glue with Tunable Mechanical Properties and High Adhesive Strength*. *Journal of Polymer Science Part A: Polymer Chemistry*, 2019. **57**(4): p. 522-530.
278. Chen, P., et al., *Desktop-Stereolithography 3D Printing of a Radially Oriented Extracellular Matrix/Mesenchymal Stem Cell Exosome Bioink for Osteochondral Defect Regeneration*. *Theranostics*, 2019. **9**(9): p. 2439.
279. Chen, P.F., et al., *Photo-Crosslinked Gelatin-Hyaluronic Acid Methacrylate Hydrogel-Committed Nucleus Pulposus-Like Differentiation of Adipose Stromal Cells for Intervertebral Disc Repair*. *Journal of Tissue Engineering and Regenerative Medicine*, 2019. **13**(4): p. 682-693.
280. Gan, D., et al., *Mussel-Inspired Dopamine Oligomer Intercalated tough and Resilient Gelatin Methacryloyl (GelMA) Hydrogels for Cartilage Regeneration*. *Journal of Materials Chemistry B*, 2019. **7**(10): p. 1716-1725.
281. Gu, L., et al., *Hydroxyapatite Nanowire Compositated Gelatin Cryogel with Improved Mechanical Properties and Cell Migration for Bone Regeneration*. *Biomedical Materials*, 2019. **14**(4): p. 045001.
282. Irmak, G., T.T. Demirtas, and M. Gumusderelioglu, *Highly Methacrylated Gelatin Bioink for Bone Tissue Engineering*. *Acs Biomaterials Science & Engineering*, 2019. **5**(2): p. 831-845.
283. Kosik-Kozioł, A., et al., *3D Bioprinted Hydrogel Model Incorporating  $\beta$ -Tricalcium Phosphate for Calcified Cartilage Tissue Engineering*. *Biofabrication*, 2019. **11**(3): p. 035016.
284. Krishnamoorthy, S., Z.Y. Zhang, and C.X. Xu, *Biofabrication of Three-Dimensional Cellular Structures Based on Gelatin Methacrylate-Alginate Interpenetrating Network Hydrogel*. *Journal of Biomaterials Applications*, 2019. **33**(8): p. 1105-1117.
285. Lee, D., et al., *Injectable Biodegradable Gelatin-Methacrylate/ $\beta$ -Tricalcium Phosphate Composite for the Repair of Bone Defects*. *Chemical Engineering Journal*, 2019. **365**: p. 30-39.
286. Liang, J., et al., *Enhanced Mechanical and Cell Adhesive Properties of Photo-Crosslinked PEG Hydrogels by Incorporation of Gelatin in the Networks*. *Biomedical Materials*, 2019. **14**(2): p. 024102.
287. Navaei, A., et al., *The Influence of Electrically Conductive and Non-Conductive Nanocomposite Scaffolds on the Maturation and Excitability of Engineered Cardiac Tissues*. *Biomaterials Science*, 2019. **7**(2): p. 585-595.
288. O'Connell, C., et al., *Evaluation of Sterilisation Methods for Bio-Ink Components: Gelatin, Gelatin Methacryloyl, Hyaluronic Acid and Hyaluronic Acid Methacryloyl*. *Biofabrication*, 2019. **11**(3): p. 035003.
289. Suvarnapathaki, S., et al., *Synthesis and Characterization of Photocrosslinkable Hydrogels from Bovine Skin Gelatin*. *RSC Advances*, 2019. **9**(23): p. 13016-13025.
290. Wadnap, S., et al., *Biofabrication of 3D Cell-Encapsulated Tubular Constructs Using Dynamic Optical Projection Stereolithography*. *Journal of Materials Science: Materials in Medicine*, 2019. **30**(3): p. 36.
291. Wang, Z.F., et al., *3D-Printable Self-Healing and Mechanically Reinforced Hydrogels with Host-Guest Non-Covalent Interactions Integrated into Covalently Linked Networks*. *Materials Horizons*, 2019. **6**(4): p. 733-742.
292. Wu, Y.B., et al., *The Influence of the Stiffness of GelMA Substrate on the Outgrowth of PC12 Cells*. *Bioscience Reports*, 2019. **39**: p. BSR20181748.

293. Xu, W., et al., *On Low-Concentration Inks Formulated by Nanocellulose Assisted with Gelatin Methacrylate (GelMA) for 3D Printing Toward Wound Healing Application*. ACS Applied Materials & Interfaces, 2019. **11**(9): p. 8838-8848.
294. Zhou, M.M., et al., *Microbial Transglutaminase Induced Controlled Crosslinking of Gelatin Methacryloyl to Tailor Rheological Properties for 3D Printing*. Biofabrication, 2019. **11**(2): p. 025011.
295. Zhu, M., et al., *Gelatin Methacryloyl and its Hydrogels with an Exceptional Degree of Controllability and Batch-to-Batch Consistency*. Scientific Reports, 2019. **9**(1): p. 1-13.
296. Parthiban, S.P., et al., *Covalently Immobilized VEGF-Mimicking Peptide with Gelatin Methacrylate Enhances Microvascularization of Endothelial Cells*. Acta Biomaterialia, 2017. **51**: p. 330-340.
297. Bartnikowski, M., et al., *Protective Effects of Reactive Functional Groups on Chondrocytes in Photocrosslinkable Hydrogel Systems*. Acta Biomaterialia, 2015. **27**: p. 66-76.
298. Bartnikowski, M., et al., *Tailoring Hydrogel Viscoelasticity with Physical and Chemical Crosslinking*. Polymers, 2015. **7**(12): p. 2650-2669.
299. Nguyen, A.H., et al., *Gelatin Methacrylate Microspheres for Controlled Growth Factor Release*. Acta Biomaterialia, 2015. **13**: p. 101-110.
300. Lee, B.H., et al., *Synthesis and Characterization of Types A and B Gelatin Methacryloyl for Bioink Applications*. Materials, 2016. **9**(10): p. 797.
301. Mouser, V.H.M., et al., *Yield Stress Determines Bioprintability of Hydrogels Based on Gelatin-Methacryloyl and Gellan Gum for Cartilage Bioprinting*. Biofabrication, 2016. **8**(3): p. 035003.
302. Rizwan, M., et al., *Sequentially-Crosslinked Bioactive Hydrogels as Nano-Patterned Substrates with Customizable Stiffness and Degradation for Corneal Tissue Engineering Applications*. Biomaterials, 2017. **120**: p. 139-154.
303. Van Hoorick, J., et al., *Cross-Linkable Gelatins with Superior Mechanical Properties Through Carboxylic Acid Modification: Increasing the Two-Photon Polymerization Potential*. Biomacromolecules, 2017. **18**(10): p. 3260-3272.
304. Wenz, A., et al., *Bone Matrix Production in Hydroxyapatite-Modified Hydrogels Suitable for Bone Bioprinting*. Biofabrication, 2017. **9**(4): p. 044103.
305. Wenz, A., et al., *Improved Vasculogenesis and Bone Matrix Formation through Coculture of Endothelial Cells and Stem Cells in Tissue-Specific Methacryloyl Gelatin-Based Hydrogels*. Biotechnology and Bioengineering, 2018. **115**(10): p. 2643-2653.
306. Celikkin, N., et al., *Gelatin Methacrylate Scaffold for Bone Tissue Engineering: The Influence of Polymer Concentration*. Journal of Biomedical Materials Research Part A, 2018. **106**(1): p. 201-209.
307. Celikkin, N., et al., *3D Printing of Thermoresponsive Polyisocyanide (PIC) Hydrogels as Bioink and Fugitive Material for Tissue Engineering*. Polymers, 2018. **10**(5): p. 555.
308. Claaßen, C., et al., *Interactions of Methacryloylated Gelatin and Heparin Modulate Physico-Chemical Properties of Hydrogels and Release of Vascular Endothelial Growth Factor*. Biomedical Materials, 2018. **13**(5): p. 055008.
309. Erkoc, P., et al., *Gelatin Methacryloyl Hydrogels in the Absence of a Crosslinker as 3D Glioblastoma Multiforme (GBM)-Mimetic Microenvironment*. Macromolecular Bioscience, 2018. **18**(3): p. 1700369.
310. Claaßen, C., et al., *Controlled Release of Vascular Endothelial Growth Factor from Heparin-Functionalized Gelatin Type A and Albumin hydrogels*. Gels, 2017. **3**(4): p. 35.
311. Habeeb, A.S.A., *Determination of Free Amino Groups in Proteins by Trinitrobenzenesulfonic Acid*. Analytical Biochemistry, 1966. **14**(3): p. 328-336.
312. Bowman, C.N. and C.J. Kloxin, *Toward an Enhanced Understanding and Implementation of Photopolymerization Reactions*. AIChE Journal, 2008. **54**(11): p. 2775-2795.
313. Fairbanks, B.D., et al., *Photoinitiated Polymerization of PEG-Diacrylate with Lithium Phenyl-2,4,6-Trimethylbenzoylphosphinate: Polymerization Rate and Cytocompatibility*. Biomaterials, 2009. **30**(35): p. 6702-6707.

314. Fouassier, J.P., D. Burr, and F. Wieder, *Water-Soluble Photoinitiators: Primary Processes in Hydroxy Alkyl Phenyl Ketones*. *Journal of Polymer Science Part A: Polymer Chemistry*, 1991. **29**(9): p. 1319-1327.
315. Kielbassa, C., L. Roza, and B. Epe, *Wavelength Dependence of Oxidative DNA Damage Induced by UV and Visible Light*. *Carcinogenesis*, 1997. **18**(4): p. 811-816.
316. Jones, C.A., et al., *Mutagenesis and Cytotoxicity in Human Epithelial Cells by Far-and Near-Ultraviolet Radiations: Action Spectra*. *Radiation Research*, 1987. **110**(2): p. 244-254.
317. Kappes, U.P., et al., *Short-and Long-Wave UV Light (UVB and UVA) Induce Similar Mutations in Human Skin Cells*. *Journal of Investigative Dermatology*, 2006. **126**(3): p. 667-675.
318. Majima, T., W. Schnabel, and W. Weber, *Phenyl-2, 4, 6-Trimethylbenzoylphosphinates as Water-Soluble Photoinitiators. Generation and Reactivity of  $O^{\ominus}P(C_6H_5)(O^-)$  Radical Anions*. *Die Makromolekulare Chemie: Macromolecular Chemistry and Physics*, 1991. **192**(10): p. 2307-2315.
319. Huber, B., et al., *Methacrylated Gelatin and Mature Adipocytes are Promising Components for Adipose Tissue Engineering*. *Journal of Biomaterials Applications*, 2016. **30**(6): p. 699-710.
320. Wenz, A., et al., *Hydroxyapatite-Modified Gelatin Bioinks for Bone Bioprinting*. *BioNanoMaterials*, 2016. **17**(3-4): p. 179-184.
321. Rebers, L., et al., *Differentiation of Physical and Chemical Cross-Linking in Gelatin Methacryloyl Hydrogels*. *Scientific Reports*, 2021. **11**(1): p. 3256.
322. Gorgieva, S. and V. Kokol, *Collagen-vs. Gelatine-Based Biomaterials and their Biocompatibility: Review and Perspectives*. *Biomaterials Applications for Nanomedicine*, 2011. **2**: p. 17-52.
323. Babel, W., *Gelatine – ein vielseitiges Biopolymer*. *Chemie In Unserer Zeit*, 1996. **30**(2): p. 86-95.
324. Liu, W., et al., *Coaxial Extrusion Bioprinting of 3D Microfibrous Constructs with Cell-Favorable Gelatin Methacryloyl Microenvironments*. *Biofabrication*, 2018. **10**(2): p. 024102.
325. Liu, W., et al., *Extrusion Bioprinting of Shear-Thinning Gelatin Methacryloyl Bioinks*. *Advanced Healthcare Materials*, 2017. **6**(12): p. 1601451.
326. Zhu, K., et al., *Gold Nanocomposite Bioink for Printing 3D Cardiac Constructs*. *Advanced Functional Materials*, 2017. **27**(12): p. 1605352.
327. Lai, T., J. Yu, and W. Tsai, *Gelatin Methacrylate/Carboxybetaine Methacrylate Hydrogels with Tunable Crosslinking for Controlled Drug Release*. *Journal of Materials Chemistry B*, 2016. **4**(13): p. 2304-2313.
328. Egger, M., et al., *Gelatin Methacrylamide as Coating Material in Cell Culture*. *Biointerphases*, 2016. **11**(2): p. 021007.
329. Liu, Y. and M.B. Chan-Park, *Hydrogel Based on Interpenetrating Polymer Networks of Dextran and Gelatin for Vascular Tissue Engineering*. *Biomaterials*, 2009. **30**(2): p. 196-207.
330. Hattori, S., et al., *Alkali-Treated Collagen Retained the Triple Helical Conformation and the Ligand Activity for the Cell Adhesion via  $\alpha 2\beta 1$  Integrin*. *The Journal of Biochemistry*, 1999. **125**(4): p. 676-684.
331. Tabata, Y. and Y. Ikada, *Protein Release from Gelatin Matrices*. *Advanced Drug Delivery Reviews*, 1998. **31**(3): p. 287-301.
332. Kishan, A.P., et al., *Development of a Bi-Modal, in situ Crosslinking Method to Achieve Multi-Factor Release from Electrospun Gelatin*. *Journal of Biomedical Materials Research Part A*, 2018. **106**.
333. Radhika, M. and P. Sehgal, *Studies on the Desamidation of Bovine Collagen*. *Journal of Biomedical Materials Research Part A*, 1997. **35**(4): p. 497-503.
334. Malik, W. and S. Ashraf, *Viscometric Studies on the Interaction of Sodium Dodecyl Sulphate with Transfused Gelatin*. *Kolloid-Zeitschrift und Zeitschrift für Polymere*, 1970. **237**(2): p. 309-310.
335. Dreja, M., et al., *Rheological Study of the pH-Dependence of Interactions Between Gelatin and Anionic Surfactants: Flow Behaviour and Gelation*. *Colloid and Polymer Science*, 1996. **274**(11): p. 1044-1053.
336. GMIA, M.o.t., *Gelatin Handbook*. 2019, Gelatin Manufactureres Institute of America.
337. Te Nijenhuis, K., *Gelatin, in Thermoreversible Networks: Viscoelastic Properties and Structure of Gels*. 1997, Springer Berlin Heidelberg: Berlin, Heidelberg. p. 160-193.

338. Janus, J.W., B.E. Tabor, and R.L.R. Darlow, *The Setting of Gelatin Sols*. *Kolloid-Zeitschrift und Zeitschrift für Polymere*, 1965. **205**(2): p. 134-139.
339. Niehues, E. and M.G.N. Quadri, *Spinnability, Morphology and Mechanical Properties of Gelatins with Different Bloom Index*. *Brazilian Journal of Chemical Engineering*, 2017. **34**: p. 253-261.
340. De Gans, B.J. and U.S. Schubert, *Inkjet Printing of Polymer Micro-Arrays and Libraries: Instrumentation, Requirements, and Perspectives*. *Macromolecular Rapid Communications*, 2003. **24**(11): p. 659-666.
341. Chang, C.C., et al., *Direct-Write Bioprinting Three-Dimensional Biohybrid Systems for Future Regenerative Therapies*. *Journal of Biomedical Materials Research Part B, Applied Biomaterials*, 2011. **98**(1): p. 160-170.
342. Van Vlierberghe, S., P. Dubruel, and E. Schacht, *Biopolymer-Based Hydrogels as Scaffolds for Tissue Engineering Applications: a Review*. *Biomacromolecules*, 2011. **12**(5): p. 1387-1408.
343. Bode, F., et al., *Enzymatically Cross-Linked Tilapia Gelatin Hydrogels: Physical, Chemical, and Hybrid Networks*. *Biomacromolecules*, 2011. **12**(10): p. 3741-3752.
344. Bode, F., et al., *Hybrid Gelation Processes in Enzymatically Gelled Gelatin: Impact on Nanostructure, Macroscopic Properties and Cellular Response*. *Soft Matter*, 2013. **9**(29): p. 6986-6999.
345. Da Silva, M.A., et al., *Exploring the Kinetics of Gelation and Final Architecture of Enzymatically Cross-Linked Chitosan/Gelatin Gels*. *Biomacromolecules*, 2015. **16**(4): p. 1401-1409.
346. Hellio-Serughetti, D. and M. Djabourov, *Gelatin Hydrogels Cross-Linked with Bis(vinylsulfonyl)methane (BVSM): 1. The Chemical Networks*. *Langmuir*, 2006. **22**(20): p. 8509-8515.
347. Hellio-Serughetti, D. and M. Djabourov, *Gelatin Hydrogels Cross-Linked with Bisvinyl Sulfonemethyl. 2. The Physical and Chemical Networks*. *Langmuir*, 2006. **22**(20): p. 8516-8522.
348. Hiller, A., et al., *Impact of intermediate UV Curing and Yield Stress of 3D Printed Poly (ethylene glycol) Diacrylate Hydrogels on Interlayer Connectivity and Maximum Build Height*. *Additive Manufacturing*, 2017. **18**: p. 136-144.
349. Deiber, J.A., et al., *Characterization of Cross-Linked Polyampholytic Gelatin Hydrogels Through the Rubber Elasticity and Thermodynamic Swelling Theories*. *Polymer*, 2009. **50**(25): p. 6065-6075.
350. Schulz, G.E. and R.H. Schirmer, *Principles of Protein Structure*. 2013: Springer Science & Business Media.
351. Van Hoorick, J., et al., *(Photo-) Crosslinkable Gelatin Derivatives for Biofabrication Applications*. *Acta Biomaterialia*, 2019(97): p. 46-73.
352. Young, A.T., O.C. White, and M.A. Daniele, *Rheological Properties of Coordinated Physical Gelation and Chemical Crosslinking in Gelatin Methacryloyl (GelMA) Hydrogels*. *Macromolecular Bioscience*, 2020. **20**(12): p. 2000183.
353. Park, H.E., et al., *Effect of Temperature on Gelation and Cross-Linking of Gelatin Methacryloyl for Biomedical Applications*. *Physics of Fluids*, 2020. **32**(3): p. 033102.
354. Van Vlierberghe, S., et al., *Hydrogel Network Formation Revised: High-Resolution Magic Angle Spinning Nuclear Magnetic Resonance as a Powerful Tool for Measuring Absolute Hydrogel Cross-Link Efficiencies*. *Applied Spectroscopy*, 2010. **64**(10): p. 1176-1180.
355. Martin, S.R. and M.J. Schilstra, *Circular Dichroism and its Application to the Study of Biomolecules*. *Methods in Cell Biology*, 2008. **84**: p. 263-293.
356. Bigi, A., S. Panzavolta, and K. Rubini, *Relationship Between Triple-Helix Content and Mechanical Properties of Gelatin Films*. *Biomaterials*, 2004. **25**(25): p. 5675-5680.
357. Gorsche, C., et al., *Real Time-NIR/MIR-Photorheology: A Versatile Tool for the In Situ Characterization of Photopolymerization Reactions*. *Analytical Chemistry*, 2017. **89**(9): p. 4958-4968.
358. Gómez-Guillén, M.C., et al., *Structural and Physical Properties of Gelatin Extracted from Different Marine Species: A Comparative Study*. *Food Hydrocolloids*, 2002. **16**(1): p. 25-34.
359. Von Hippel, P., *Treatise on Collagen*. 1967, Academic Press, New York.
360. Horng, J.C. and R.T. Raines, *Stereoelectronic Effects on Polyproline Conformation*. *Protein Science*, 2006. **15**(1): p. 74-83.

361. Kakinoki, S., Y. Hirano, and M. Oka, *On the Stability of Polyproline-I and II Structures of Proline Oligopeptides*. *Polymer Bulletin*, 2005. **53**(2): p. 109-115.
362. Guo, L., et al., *Kinetics of Triple Helix Formation in Semidilute Gelatin Solutions*. *Macromolecules*, 2003. **36**(26): p. 9999-10008.
363. Achet, D. and X. He, *Determination of the renaturation level in gelatin films*. *Polymer*, 1995. **36**(4): p. 787-791.
364. Motooka, D., et al., *The Triple Helical Structure and Stability of Collagen Model Peptide with 4(s)-Hydroxyprolyl-Pro-Gly Units*. *Peptide Science*, 2012. **98**(2): p. 111-121.
365. Ma, S., et al., *Monodisperse Collagen–Gelatin Beads as Potential Platforms for 3D Cell Culturing*. *Journal of Materials Chemistry B*, 2013. **1**(38): p. 5128-5136.
366. Giraudier, S., et al., *Influence of Weak and Covalent Bonds on Formation and Hydrolysis of Gelatin Networks*. *Biomacromolecules*, 2004. **5**(5): p. 1662-1666.
367. Lu, X. and V. Mow, *Biomechanics of Articular Cartilage and Determination of Material Properties*. *Medicine+ Science in Sports+ Exercise*, 2008. **40**(2): p. 193.
368. Peterson, L., *Chondrocyte Transplantation. An Experimental Model in the Rabbit*. *Transactions from the 30th Annual Orthopaedic Research Society* 1984. **30**(9): p. 218.
369. Vaca-González, J., et al., *Cellular Automata Model for Human Articular Chondrocytes Migration, Proliferation and Cell Death: an in vitro Validation*. *In Silico Biology*, 2017. **12**(3-4): p. 83-93.
370. Vinatier, C., et al., *Cartilage and Bone Tissue Engineering Using Hydrogels*. *Bio-Medical Materials and Engineering*, 2006. **16**(4): p. S107-S113.
371. Irawan, D., D. Hutmacher, and T. Klein, *Matrices for Zonal Cartilage Tissue Engineering*, in *Handbook of Intelligent Scaffold for Tissue Engineering and Regenerative Medicine*. 2012, Pan Stanford Publishers. p. 733-756.
372. Sala, R.L., et al., *Thermosensitive Poly (N-vinylcaprolactam) Injectable Hydrogels for Cartilage Tissue Engineering*. *Tissue Engineering Part A*, 2017. **23**(17-18): p. 935-945.
373. Gao, G., et al., *Bioprinting Cartilage Tissue from Mesenchymal Stem Cells and PEG Hydrogel, in 3D Cell Culture*. 2017, Springer. p. 391-398.
374. Neumann, A.J., T. Quinn, and S.J. Bryant, *Nondestructive Evaluation of a New Hydrolytically Degradable and Photo-Clickable PEG Hydrogel for Cartilage Tissue Engineering*. *Acta Biomaterialia*, 2016. **39**: p. 1-11.
375. Lowen, J.M. and J.K. Leach, *Functionally Graded Biomaterials for Use as Model Systems and Replacement Tissues*. *Advanced Functional Materials*, 2020: p. 1909089.
376. Ng, K.W., G.A. Ateshian, and C.T. Hung, *Zonal Chondrocytes Seeded in a Layered Agarose Hydrogel Create Engineered Cartilage with Depth-Dependent Cellular and Mechanical Inhomogeneity*. *Tissue Engineering Part A*, 2009. **15**(9): p. 2315-2324.
377. Schuurman, W., et al., *Three-Dimensional Assembly of Tissue-Engineered Cartilage Constructs Results in Cartilaginous Tissue Formation without Retainment of Zonal Characteristics*. *Journal of Tissue Engineering and Regenerative Medicine*, 2016. **10**(4): p. 315-324.
378. Steele, J.A.M., et al., *Combinatorial Scaffold Morphologies for Zonal Articular Cartilage Engineering*. *Acta Biomaterialia*, 2014. **10**(5): p. 2065-2075.
379. Clearfield, D., A. Nguyen, and M. Wei, *Biomimetic Multidirectional Scaffolds for Zonal Osteochondral Tissue Engineering via a Lyophilization Bonding Approach*. *Journal of Biomedical Materials Research Part A*, 2018. **106**(4): p. 948-958.
380. Zhu, D., et al., *Mimicking Cartilage Tissue Zonal Organization by Engineering Tissue-Scale Gradient Hydrogels as 3D Cell Niche*. *Tissue Engineering Part A*, 2018. **24**(1-2): p. 1-10.
381. Cui, X., et al., *Direct Human Cartilage Repair Using Three-Dimensional Bioprinting Technology*. *Tissue Engineering Part A*, 2012. **18**(11-12): p. 1304-1312.
382. Woodfield, T., et al., *Polymer Scaffolds Fabricated with Pore-Size Gradients as a Model for Studying the Zonal Organization within Tissue-Engineered Cartilage Constructs*. *Tissue Engineering*, 2005. **11**(9-10): p. 1297-1311.
383. Ren, X., et al., *Engineering Zonal Cartilage Through Bioprinting Collagen Type II Hydrogel Constructs with Biomimetic Chondrocyte Density Gradient*. *BMC Musculoskeletal Disorders*, 2016. **17**(1): p. 301.

384. Luo, L., et al., *Engineering Zonal Cartilaginous Tissue by Modulating Oxygen Levels and Mechanical Cues Through the Depth of Infrapatellar Fat Pad Stem Cell Laden Hydrogels*. Journal of Tissue Engineering and Regenerative Medicine, 2017. **11**(9): p. 2613-2628.
385. Sharma, B., et al., *Designing Zonal Organization into Tissue-Engineered Cartilage*. Tissue Engineering, 2007. **13**(2): p. 405-414.
386. Hwang, N.S., et al., *Response of Zonal Chondrocytes to Extracellular Matrix-Hydrogels*. FEBS letters, 2007. **581**(22): p. 4172-4178.
387. Menzel, E.J. and C. Farr, *Hyaluronidase and its Substrate Hyaluronan: Biochemistry, Biological Activities and Therapeutic Uses*. Cancer Letters, 1998. **131**(1): p. 3-11.
388. Oloyede, A., R. Flachsmann, and N.D. Broom, *The Dramatic Influence of Loading Velocity on the Compressive Response of Articular Cartilage*. Connective Tissue Research, 1992. **27**(4): p. 211-224.
389. Bingham, J.T., et al., *In Vivo Cartilage Contact Deformation in the Healthy Human Tibiofemoral Joint*. Rheumatology, 2008. **47**(11): p. 1622-1627.
390. Guilak, F., D.L. Butler, and S.A. Goldstein, *Functional Tissue Engineering: The Role of Biomechanics in Articular Cartilage Repair*. Clinical Orthopaedics and Related Research, 2001. **391**: p. S295-S305.
391. Mansour, J.M., *Biomechanics of Cartilage*, in *Kinesiology: The Mechanics and Pathomechanics of Human Movement*. 2003. p. 69-83.
392. Temple, D.K., et al., *Viscoelastic Properties of Human and Bovine Articular Cartilage: a Comparison of Frequency-Dependent Trends*. BMC Musculoskeletal Disorders, 2016. **17**(1): p. 419.
393. Bleuel, J., et al., *Effects of Cyclic Tensile Strain on Chondrocyte Metabolism: A Systematic Review*. PLOS ONE, 2015. **10**(3): p. e0119816-e0119816.
394. Murphy, G., et al., *Matrix Metalloproteinases in Athritic Disease*. Arthritis Research, 2002. **4**(Suppl 3): p. S39-S49.
395. Nagase, H. and M. Kashiwagi, *Aggrecanases and Cartilage Matrix Degradation*. Arthritis Research & Therapy, 2003. **5**(2): p. 94-103.
396. Bastow, E.R., et al., *Hyaluronan Synthesis and Degradation in Cartilage and Bone*. Cellular and Molecular Life Sciences, 2008. **65**(3): p. 395-413.
397. Seidlits, S.K., et al., *The Effects of Hyaluronic Acid Hydrogels with Tunable Mechanical Properties on Neural Progenitor Cell Differentiation*. Biomaterials, 2010. **31**(14): p. 3930-3940.
398. Zhao, Z., et al., *Progress in Articular Cartilage Tissue Engineering: a Review on Therapeutic Cells and Macromolecular Scaffolds*. Macromolecular Bioscience, 2020. **20**(2): p. 1900278.
399. Schulz, R.M. and A. Bader, *Cartilage Tissue Engineering and Bioreactor Systems for the Cultivation and Stimulation of Chondrocytes*. European Biophysics Journal, 2007. **36**(4-5): p. 539-568.
400. Hodge, J., *The Nutrition of Mature and Immature Cartilage in Rabbits*. The Journal of Bone and Joint Surgery 1969. **51**: p. 140-147.
401. Honner, R. and R.C. Thompson, *The Nutritional Pathways of Articular Cartilage: An Autoradiographic Study in Rabbits using: <sup>35</sup>S Injected Intravenously* JBJS, 1971. **53**(4): p. 742-748.
402. Schünke, M., *Funktionelle Anatomie-Topographie und Funktion des Bewegungssystems*. 2000: Georg Thieme Verlag.
403. Costantini, M., et al., *3D Bioprinting of BM-MSCs-Loaded ECM Biomimetic Hydrogels for In Vitro Neocartilage Formation*. Biofabrication, 2016. **8**(3): p. 035002.
404. Callahan, L.A.S., et al., *ECM Production of Primary Human and Bovine Chondrocytes in Hybrid PEG Hydrogels Containing Type I Collagen and Hyaluronic Acid*. Biomacromolecules, 2012. **13**(5): p. 1625-1631.
405. Allemann, F., et al., *Effects of Hyaluronan on Engineered Articular Cartilage Extracellular Matrix Gene Expression in 3-Dimensional Collagen Scaffolds*. Journal of Biomedical Materials Research, 2001. **55**(1): p. 13-19.
406. Akmal, M., et al., *The Effects of Hyaluronic Acid on Articular Chondrocytes*. The Journal of Bone and Joint Surgery. British Volume, 2005. **87**(8): p. 1143-1149.

407. Schuurman, W., et al., *Zonal Chondrocyte Subpopulations Reacquire Zone-Specific Characteristics During in vitro Redifferentiation*. The American Journal of Sports Medicine, 2009. **37**(1\_suppl): p. 97-104.
408. Claaßen, C., et al., *Expanding the Range of Available Isoelectric Points of Highly Methacryloylated Gelatin*. Macromolecular Chemistry and Physics, 2019. **220**(14): p. 1900097.
409. Dehli, F., et al., *Highly Ordered Gelatin Methacryloyl Hydrogel Foams with Tunable Pore Size*. Biomacromolecules, 2019. **20**(7): p. 2666-2674.













